ETSI TR 138 901 V19.3.0 (2026-04)

TECHNICAL REPORT

5G;
Study on channel model for frequencies from 0.5 to 100 GHz
(3GPP TR 38.901 version 19.3.0 Release 19)

Reference
RTR/TSGR-0138901vj30

Keywords
5G

ETSI

650 Route des Lucioles
F-06921 Sophia Antipolis Cedex - FRANCE

Tel.: +33 4 92 94 42 00 Fax: +33 4 93 65 47 16

Siret N° 348 623 562 00017 - APE 7112B
Association à but non lucratif enregistrée à la
Sous-Préfecture de Grasse (06) N° w061004871

Important notice

The present document can be downloaded from the
ETSI Search & Browse Standards application.

The present document may be made available in electronic versions and/or in print. The content of any electronic and/or print versions of the present document shall not be modified without the prior written authorization of ETSI. In case of any existing or perceived difference in contents between such versions and/or in print, the prevailing version of an ETSI deliverable is the one made publicly available in PDF format on ETSI deliver repository.

Users should be aware that the present document may be revised or have its status changed, this information is available in the Milestones listing.

If you find errors in the present document, please send your comments to the relevant service listed under Committee Support Staff.

If you find a security vulnerability in the present document, please report it through our Coordinated Vulnerability Disclosure (CVD) program.

Notice of disclaimer & limitation of liability

The information provided in the present deliverable is directed solely to professionals who have the appropriate degree of experience to understand and interpret its content in accordance with generally accepted engineering or other professional standard and applicable regulations.
No recommendation as to products and services or vendors is made or should be implied.
No representation or warranty is made that this deliverable is technically accurate or sufficient or conforms to any law and/or governmental rule and/or regulation and further, no representation or warranty is made of merchantability or fitness for any particular purpose or against infringement of intellectual property rights.
In no event shall ETSI be held liable for loss of profits or any other incidental or consequential damages.

Any software contained in this deliverable is provided "AS IS" with no warranties, express or implied, including but not limited to, the warranties of merchantability, fitness for a particular purpose and non-infringement of intellectual property rights and ETSI shall not be held liable in any event for any damages whatsoever (including, without limitation, damages for loss of profits, business interruption, loss of information, or any other pecuniary loss) arising out of or related to the use of or inability to use the software.

Copyright Notification

No part may be reproduced or utilized in any form or by any means, electronic or mechanical, including photocopying and microfilm except as authorized by written permission of ETSI.
The content of the PDF version shall not be modified without the written authorization of ETSI.
The copyright and the foregoing restriction extend to reproduction in all media.

© ETSI 2026.
All rights reserved.

Intellectual Property Rights

Essential patents

IPRs essential or potentially essential to normative deliverables may have been declared to ETSI. The declarations pertaining to these essential IPRs, if any, are publicly available for **ETSI members and non-members**, and can be found in ETSI SR 000 314: *"Intellectual Property Rights (IPRs); Essential, or potentially Essential, IPRs notified to ETSI in respect of ETSI standards"*, which is available from the ETSI Secretariat. Latest updates are available on the ETSI IPR online database.

Pursuant to the ETSI Directives including the ETSI IPR Policy, no investigation regarding the essentiality of IPRs, including IPR searches, has been carried out by ETSI. No guarantee can be given as to the existence of other IPRs not referenced in ETSI SR 000 314 (or the updates on the ETSI Web server) which are, or may be, or may become, essential to the present document.

Trademarks

The present document may include trademarks and/or tradenames which are asserted and/or registered by their owners. ETSI claims no ownership of these except for any which are indicated as being the property of ETSI, and conveys no right to use or reproduce any trademark and/or tradename. Mention of those trademarks in the present document does not constitute an endorsement by ETSI of products, services or organizations associated with those trademarks.

DECT™, **PLUGTESTS™**, **UMTS™** and the ETSI logo are trademarks of ETSI registered for the benefit of its Members. **3GPP™**, **LTE™** and **5G™** logo are trademarks of ETSI registered for the benefit of its Members and of the 3GPP Organizational Partners. **oneM2M™** logo is a trademark of ETSI registered for the benefit of its Members and of the oneM2M Partners. **GSM**® and the GSM logo are trademarks registered and owned by the GSM Association.

Legal Notice

This Technical Specification (TS) has been produced by the ETSI 3rd Generation Partnership Project (3GPP).

The present document may refer to technical specifications or reports using their 3GPP identities. These shall be interpreted as being references to the corresponding ETSI deliverables.

The cross reference between 3GPP and ETSI identities can be found at 3GPP to ETSI numbering cross-referencing.

Modal verbs terminology

In the present document "**shall**", "**shall not**", "**should**", "**should not**", "**may**", "**need not**", "**will**", "**will not**", "**can**" and "**cannot**" are to be interpreted as described in clause 3.2 of the ETSI Drafting Rules (Verbal forms for the expression of provisions).

"**must**" and "**must not**" are **NOT** allowed in ETSI deliverables except when used in direct citation.

Contents

Intellectual Property Rights 2
Legal Notice 2
Modal verbs terminology 2
Foreword 6
1 Scope 8
2 References 8
3 Definitions, symbols and abbreviations 9
3.1 Definitions 9
3.2 Symbols 9
3.3 Abbreviations 10
4 Introduction 12
5 Void 13
6 Status/expectation of existing information on high frequencies 13
6.1 Channel modelling works outside of 3GPP 13
6.2 Scenarios of interest 15
6.3 Channel measurement capabilities 16
6.4 Modelling objectives 18
7 Channel model(s) for 0.5-100 GHz 18
7.1 Coordinate system 18
7.1.1 Definition 18
7.1.2 Local and global coordinate systems 19
7.1.3 Transformation from a LCS to a GCS 19
7.1.4 Transformation from an LCS to a GCS for downtilt angle only 23
7.2 Scenarios 24
7.3 Antenna modelling 28
7.3.0 Antenna array structure 28
7.3.1 Antenna port mapping 32
7.3.2 Polarized antenna modelling 32
7.4 Pathloss, LOS probability and penetration modelling 35
7.4.1 Pathloss 35
7.4.2 LOS probability 38
7.4.3 O2I penetration loss 39
7.4.3.1 O2I building penetration loss 39
7.4.3.2 O2I car penetration loss 41
7.4.4 Autocorrelation of shadow fading 41
7.5 Fast fading model 41
7.6 Additional modelling components 58
7.6.0 Introduction of additional modelling components 58
7.6.1 Oxygen absorption 58
7.6.2 Large bandwidth and large antenna array 59
7.6.2.1 Modelling of the propagation delay 59
7.6.2.2 Modelling of intra-cluster angular and delay spreads 60
7.6.3 Spatial consistency 61
7.6.3.1 Spatial consistency procedure 61
7.6.3.2 Spatially-consistent UT/BS mobility modelling 62
7.6.3.3 LOS/NLOS, indoor states and O2I parameters 66
7.6.3.4 Applicability of spatial consistency 67
7.6.4 Blockage 67
7.6.4.1 Blockage model A 68
7.6.4.2 Blockage model B 70
7.6.5 Correlation modelling for multi-frequency simulations 72
7.6.5.1 Alternative channel generation method 73

7.6.6 Time-varying Doppler shift 75
7.6.7 UT rotation 75
7.6.8 Explicit ground reflection model 75
7.6.9 Absolute time of arrival 78
7.6.10 Dual mobility 79
7.6.11 Sources of EM interference 79
7.6.12 Embedded devices 79
7.6.13 Near-field channel model 80
7.6.14 Spatial non-stationarity channel model 81
7.6.14.1 Spatial non-stationarity channel model at TRP side 81
7.6.14.1.1 Introduction 81
7.6.14.1.2 Physical blocker-based Model 82
7.6.14.1.3 Stochastic based Model 83
7.6.14.2 Spatial non-stationarity channel model at UT side 84
7.6.15 Number of cluster variability model 85
7.6.16 Polarization power variability model 85
7.7 Channel models for link-level evaluations 86
7.7.1 Clustered Delay Line (CDL) models 86
7.7.2 Tapped Delay Line (TDL) models 90
7.7.3 Scaling of delays 93
7.7.4 Spatial filter for generating TDL channel model 94
7.7.4.1 Exemplary filters/antenna patterns 94
7.7.4.2 Generation procedure 95
7.7.5 Extension for MIMO simulations 95
7.7.5.1 CDL extension: Scaling of angles 95
7.7.5.2 TDL extension: Applying a correlation matrix 97
7.7.6 K-factor for LOS channel models 97
7.8 Channel model calibration 98
7.8.1 Large scale calibration 98
7.8.2 Full calibration 100
7.8.3 Calibration of additional features 102
7.8.4 Calibration of the indoor factory scenario 110
7.9 Channel model(s) for ISAC 111
7.9.0 Introduction 111
7.9.1 Scenarios 112
7.9.2 Physical object model 117
7.9.2.0 Introduction 117
7.9.2.1 RCS of a sensing target 117
7.9.2.2 Cross-polarization matrix of a sensing target 119
7.9.3 Reference channel models and required updates 120
7.9.4 Fast fading model 125
7.9.4.0 Introduction 125
7.9.4.1 Target channel 127
7.9.4.2 Background channel 132
7.9.4.3 Combining target channel and background channel 134
7.9.5 Additional modelling components 134
7.9.5.0 Introduction 134
7.9.5.1 Spatial consistency 134
7.9.5.2 Type-2 environment object 136
7.9.5.3 Power normalization across target channel and background channel 139
7.9.5.4 Doppler of mobile scatterers 139
7.9.5.5 Lower power clusters 139
7.9.5.6 Blockage 140
7.9.6 Channel model calibration 140
7.9.6.1 Large scale calibration 140
7.9.6.2 Full calibration 145
7.9.6.3 Calibration of additional features 146

8 Map-based hybrid channel model (Alternative channel model methodology) 150
8.1 Coordinate system 150
8.2 Scenarios 150
8.3 Antenna modelling 150

8.4 Channel generation 150
Annex A: Further parameter definitions 161
A.1 Calculation of angular spread 161
A.2 Calculation of mean angle 161
A.3 Calculation of cluster angular spread 161
A.4 Calculation of cluster mean angle 161
A.5 Calculation of scaling factor for changing CDL model angular spread 161
Annex B: Change history 163
History 164

Foreword

This Technical Report has been produced by the 3rd Generation Partnership Project (3GPP).

The contents of the present document are subject to continuing work within the TSG and may change following formal TSG approval. Should the TSG modify the contents of the present document, it will be re-released by the TSG with an identifying change of release date and an increase in version number as follows:

Version x.y.z

where:

- x the first digit:
  - 1 presented to TSG for information;
  - 2 presented to TSG for approval;
  - 3 or greater indicates TSG approved document under change control.
- y the second digit is incremented for all changes of substance, i.e. technical enhancements, corrections, updates, etc.
- z the third digit is incremented when editorial only changes have been incorporated in the document.

In the present document, modal verbs have the following meanings:

shall indicates a mandatory requirement to do something

shall not indicates an interdiction (prohibition) to do something

The constructions "shall" and "shall not" are confined to the context of normative provisions, and do not appear in Technical Reports.

The constructions "must" and "must not" are not used as substitutes for "shall" and "shall not". Their use is avoided insofar as possible, and they are not used in a normative context except in a direct citation from an external, referenced, non-3GPP document, or so as to maintain continuity of style when extending or modifying the provisions of such a referenced document.

should indicates a recommendation to do something

should not indicates a recommendation not to do something

may indicates permission to do something

need not indicates permission not to do something

The construction "may not" is ambiguous and is not used in normative elements. The unambiguous constructions "might not" or "shall not" are used instead, depending upon the meaning intended.

can indicates that something is possible

cannot indicates that something is impossible

The constructions "can" and "cannot" are not substitutes for "may" and "need not".

will indicates that something is certain or expected to happen as a result of action taken by an agency the behaviour of which is outside the scope of the present document

will not indicates that something is certain or expected not to happen as a result of action taken by an agency the behaviour of which is outside the scope of the present document

might indicates a likelihood that something will happen as a result of action taken by some agency the behaviour of which is outside the scope of the present document

might not indicates a likelihood that something will not happen as a result of action taken by some agency the behaviour of which is outside the scope of the present document

In addition:

is (or any other verb in the indicative mood) indicates a statement of fact

is not (or any other negative verb in the indicative mood) indicates a statement of fact

The constructions "is" and "is not" do not indicate requirements.

1 Scope

The present document captures the findings of the study item, "Study on channel model for frequency spectrum above 6 GHz" [2] and from further findings of:

- the study item, "Study on New Radio Access Technology [22]",
- the study item "Study on Channel Modeling for Indoor Industrial Scenarios [23]",
- the study item "New SID: Study on channel modelling enhancements for 7-24GHz for NR [24]",
- and the study item "Study on channel modelling for Integrated Sensing And Communication (ISAC) for NR [26]".

The channel models in the present document address the frequency range 0.5-100 GHz. The purpose of this TR is to help TSG RAN WG1 to properly model and evaluate the performance of physical layer techniques using the appropriate channel model(s). Therefore, the TR will be kept up-to-date via CRs in the future.

This document relates to the 3GPP evaluation methodology and covers the modelling of the physical layer of both Mobile Equipment and Access Network of 3GPP systems.

This document is intended to capture the channel model(s) for frequencies from 0.5GHz up to 100GHz.

2 References

The following documents contain provisions which, through reference in this text, constitute provisions of the present document.

- References are either specific (identified by date of publication, edition number, version number, etc.) or non-specific.
- For a specific reference, subsequent revisions do not apply.
- For a non-specific reference, the latest version applies. In the case of a reference to a 3GPP document (including a GSM document), a non-specific reference implicitly refers to the latest version of that document *in the same Release as the present document*.

[1] 3GPP TR 21.905: "Vocabulary for 3GPP Specifications".

[2] 3GPP TD RP-151606: "Study on channel model for frequency spectrum above 6 GHz".

[3] 3GPP TR 36.873 (V12.2.0): "Study on 3D channel model for LTE".

[4] 3GPP RP-151847: "Report of RAN email discussion about >6GHz channel modelling", Samsung.

[5] 3GPP TD R1-163408: "Additional Considerations on Building Penetration Loss Modelling for 5G System Performance Evaluation", Straight Path Communications.

[6] ICT-317669-METIS/D1.4: "METIS channel model, METIS 2020, Feb, 2015".

[7] Glassner, A S: "An introduction to ray tracing. Elsevier, 1989".

[8] McKown, J. W., Hamilton, R. L.: "Ray tracing as a design tool for radio networks, Network, IEEE, 1991(6): 27-30".

[9] Kurner, T., Cichon, D. J., Wiesbeck, W.: "Concepts and results for 3D digital terrain-based wave propagation models: An overview", IEEE J.Select. Areas Commun., vol. 11, pp. 1002–1012, 1993.

[10] Born, M., Wolf, E.: "Principles of optics: electromagnetic theory of propagation, interference and diffraction of light", CUP Archive, 2000.

[11] Friis, H.: "A note on a simple transmission formula", proc. IRE, vol. 34, no. 5, pp. 254–256, 1946.

[12] Kouyoumjian, R.G., Pathak, P.H.: "A uniform geometrical theory of diffraction for an edge in a perfectly conducting surface" Proc. IEEE, vol. 62, pp. 1448–1461, Nov. 1974.

[13] Pathak, P.H., Burnside, W., Marhefka, R.: "A Uniform GTD Analysis of the Diffraction of Electromagnetic Waves by a Smooth Convex Surface", IEEE Transactions on Antennas and Propagation, vol. 28, no. 5, pp. 631–642, 1980.

[14] IST-WINNER II Deliverable 1.1.2 v.1.2, "WINNER II Channel Models", IST-WINNER2, Tech. Rep., 2007 (http://www.ist-winner.org/deliverables.html).

[15] 3GPP TR36.101: "User Equipment (UE) radio transmission and reception".

[16] 3GPP TR36.104: "Base Station (BS) radio transmission and reception".

[17] Asplund, H., Medbo, J., Göransson, B., Karlsson, J., Sköld, J.: "A simplified approach to applying the 3GPP spatial channel model", in Proc. of PIMRC 2006.

[18] ITU-R Rec. P.1816: "The prediction of the time and the spatial profile for broadband land mobile services using UHF and SHF bands".

[19] ITU-R Rec. P.2040-1: "Effects of building materials and structures on radiowave propagation above about 100 MHz", International Telecommunication Union Radiocommunication Sector ITU-R, 07/2015.

[20] ITU-R Rec. P.527-3: "Electrical characteristics of the surface of the earth", International Telecommunication Union Radiocommunication Sector ITU-R, 03/1992.

[21] Jordan, E.C., Balmain, K.G.: "Electromagnetic Waves and Radiating Systems", Prentice-Hall Inc., 1968.

[22] 3GPP TD RP-162469: "Study on New Radio (NR) Access Technology".

[23] 3GPP TD RP-182138: "SID on Channel Modeling for Indoor Industrial Scenarios".

[24] 3GPP TD RP-234018: "New SID: Study on channel modelling enhancements for 7-24GHz for NR"

[25] 3GPP TD R1-2504960: "Data source descriptions for 7 – 24 GHz SI".

[26] 3GPP TD RP-242348: "Study on channel modelling for Integrated Sensing And Communication (ISAC) for NR".

[27] 3GPP TD R1-2504948: "Information on validations for ISAC"

3 Definitions, symbols and abbreviations

3.1 Definitions

For the purposes of the present document, the terms and definitions given in TR 21.905 [1] apply.

3.2 Symbols

For the purposes of the present document, the following symbols apply:

A	antenna radiation power pattern
A_{max}	maximum attenuation
d_{2D}	2D distance between Tx and Rx
d_{3D}	3D distance between Tx and Rx

d_H antenna element spacing in horizontal direction

d_V antenna element spacing in vertical direction

f frequency

f_c center frequency / carrier frequency

$F_{\mathrm{rx,u,\theta}}$ Receive antenna element *u* field pattern in the direction of the spherical basis vector $\hat{\theta}$

$F_{\mathrm{rx,u,\phi}}$ Receive antenna element *u* field pattern in the direction of the spherical basis vector $\hat{\phi}$

$F_{\mathrm{tx,s,\theta}}$ Transmit antenna element *s* field pattern in the direction of the spherical basis vector $\hat{\theta}$

$F_{\mathrm{rx,s,\phi}}$ Transmit antenna element *s* field pattern in the direction of the spherical basis vector $\hat{\phi}$

h_{BS} antenna height for BS

h_{UT} antenna height for UT

$\hat{r}_{rx,n,m}$ spherical unit vector of cluster *n*, ray *m*, for receiver

$\hat{r}_{tx,n,m}$ spherical unit vector of cluster *n*, ray *m*, for transmitter

α bearing angle

β downtilt angle

γ slant angle

λ wavelength

κ cross-polarization power ratio in linear scale

μ_{lgASA} mean value of 10-base logarithm of azimuth angle spread of arrival

μ_{lgASD} mean value of 10-base logarithm of azimuth angle spread of departure

μ_{lgDS} mean value of 10-base logarithm of delay spread

μ_{lgZSA} mean value of 10-base logarithm of zenith angle spread of arrival

μ_{lgZSD} mean value of 10-base logarithm of zenith angle spread of departure

$\mathrm{Pr}_{\mathrm{LOS}}$ LOS probability

SLA_V side-lobe attenuation in vertical direction

σ_{lgASA} standard deviation of 10-base logarithm of azimuth angle spread of arrival

σ_{lgASD} standard deviation of 10-base logarithm of azimuth angle spread of departure

σ_{lgDS} standard deviation value of 10-base logarithm of delay spread

σ_{lgZSA} standard deviation of 10-base logarithm of zenith angle spread of arrival

σ_{lgZSD} standard deviation of 10-base logarithm of zenith angle spread of departure

σ_{SF} standard deviation of SF

ϕ azimuth angle

θ zenith angle

$\hat{\phi}$ spherical basis vector (unit vector) for GCS

$\hat{\phi}'$ spherical basis vector (unit vector) for LCS

ϕ_{3dB} horizontal 3 dB beamwidth of an antenna

$\hat{\theta}$ spherical basis vector (unit vector), orthogonal to $\hat{\phi}$, for GCS

$\hat{\theta}'$ spherical basis vector (unit vector), orthogonal to $\hat{\phi}'$, for LCS

θ_{etilt} electrical steering angle in vertical direction

θ_{3dB} vertical 3 dB beamwidth of an antenna

ψ Angular displacement between two pairs of unit vectors

3.3 Abbreviations

For the purposes of the present document, the abbreviations given in TR 21.905 [1] and the following apply. An abbreviation defined in the present document takes precedence over the definition of the same abbreviation, if any, in TR 21.905 [1].

2D two-dimensional

3D	three-dimensional
AGV	Automated Guided Vehicles
AOA	Azimuth angle Of Arrival
AOD	Azimuth angle Of Departure
AS	Angular Spread
ASA	Azimuth angle Spread of Arrival
ASD	Azimuth angle Spread of Departure
BF	Beamforming
BS	Base Station
BP	Breakpoint
BW	Beamwidth
CDF	Cumulative Distribution Function
CDL	Clustered Delay Line
CRS	Common Reference Signal
D2D	Device-to-Device
DFT	Discrete Fourier Transform
DS	Delay Spread
EO	Environment Object
GCS	Global Coordinate System
IID	Independent and identically distributed
InF	Indoor Factory
InF-SL	Indoor Factory with Sparse clutter and Low base station height (both Tx and Rx are below the average height of the clutter)
InF-DL	Indoor Factory with Dense clutter and Low base station height (both Tx and Rx are below the average height of the clutter)
InF-SH	Indoor Factory with Sparse clutter and High base station height (Tx or Rx elevated above the clutter)
InF-DH	Indoor Factory with Dense clutter and High base station height (Tx or Rx elevated above the clutter)
InF-HH	Indoor Factory with High Tx and High Rx (both elevated above the clutter)
InH	Indoor Hotspot
IRR	Infrared Reflecting
ISAC	Integrated Sensing and Communication
ISD	Intersite Distance
K	Ricean K factor
LCS	Local Coordinate System
LOS	Line Of Sight
MIMO	Multiple-Input-Multiple-Output
MPC	Multipath Component
NLOS	Non-LOS
O2I	Outdoor-to-Indoor
O2O	Outdoor-to-Outdoor
OFDM	Orthogonal Frequency-Division Multiplexing
PAS	Power angular spectrum
PL	Path Loss
PRB	Physical Resource Block
RCS	Radar cross-section
RMa	Rural Macro
RMS	Root Mean Square
RP	Reference Point
RSRP	Reference Signal Received Power
Rx	Receiver
SCM	Spatial Channel Model
SINR	Signal-to-Interference-plus-Noise Ratio
SIR	Signal-to-Interference Ratio
SSCM	Statistical Spatial Channel Model
SF	Shadow Fading
SLA	Sidelobe Attenuation
SPST	Scattering Point of a ST
SRX	Sensing Receiver
ST	Sensing Target
STX	Sensing Transmitter

TDL	Tapped Delay Line
TOA	Time Of Arrival
TRP	Transmission Reception Point
Tx	Transmitter
UAV	Unmanned Aerial Vehicle
UMa	Urban Macro
UMi	Urban Micro
UT	User Terminal
UTD	Uniform Theory of Diffraction
V2V	Vehicle-to-Vehicle
XPR	Cross-Polarization Ratio
ZOA	Zenith angle Of Arrival
ZOD	Zenith angle Of Departure
ZSA	Zenith angle Spread of Arrival
ZSD	Zenith angle Spread of Departure

4 Introduction

At TSG RAN #69 meeting the Study Item Description on "Study on channel model for frequency spectrum above 6 GHz" was approved [2]. This study item covers the identification of the status/expectation of existing information on high frequencies (e.g. spectrum allocation, scenarios of interest, measurements, etc), and the channel model(s) for frequencies up to 100 GHz. This technical report documents the channel model(s). The new channel model has to a large degree been aligned with earlier channel models for <6 GHz such as the 3D SCM model (TR 36.873) or IMT-Advanced (ITU-R M.2135). The new model supports comparisons across frequency bands over the range 0.5-100 GHz. The modelling methods defined in this technical report are generally applicable over the range 0.5-100 GHz, unless explicitly mentioned otherwise in this technical report for specific modelling method, involved parameters and/or scenario.

Subsequently, at the TSG RAN #81 meeting the Study Item Description "Study on Channel Modeling for Indoor Industrial Scenarios" was approved [23]. The findings from this study item is also captured in the present technical report. The Industrial channel model was developed by considering new measurements and information in the literature. An overview list of all such contributions and sources is available in tdoc R1-1909706.

Subsequently, at the TSG RAN #102 meeting the Study Item Description "Study on channel modelling enhancements for 7-24GHz for NR" was approved [24]. The findings from this study are also captured in the present technical report. Channel modeling was further updated by considering new measurements and information in the literature. An overview of the information sources is available in tdoc R1-2504960 [25].

At TSG RAN #102 meeting the Study Item Description “Study on channel modelling for Integrated Sensing And Communication (ISAC) for NR” was approved. The findings from this study item are captured in Clause 7.9. The ISAC channel model was developed considering new measurements and information in the literature. The RCS validation results are obtained based on certain object sizes. An overview list of the sources is available in [27].

The channel model is applicable for link and system level simulations in the following conditions:

- For system level simulations, supported scenarios are urban microcell street canyon, urban macrocell, indoor office, rural macrocell, indoor factory, and suburban macrocell.
- Bandwidth is supported up to 10% of the center frequency but no larger than 2GHz.
- Mobility of either one end of the link or both ends of the link is supported
- For the stochastic model, spatial consistency is supported by correlation of LSPs and SSPs as well as LOS/NLOS state.
- Large array support is based on far field assumption and stationary channel over the size of the array.
- Near field channel modeling (i.e., characteristics of spherical wavefront) and spatial non-stationarity (i.e., antenna element-wise power variation) are supported.

- The sensing target is assumed in the far field of the sensing transmitter/receiver for the channel model(s) for ISAC in Clause 7.9.

5 Void

6 Status/expectation of existing information on high frequencies

6.1 Channel modelling works outside of 3GPP

This clause summarizes the channel modelling work outside of 3GPP based on the input from companies.

Groups and projects with channel models:

- METIS (Mobile and wireless communications Enablers for the Twenty-twenty Information Society)
- MiWEBA (Millimetre-Wave Evolution for Backhaul and Access)
- ITU-R M
- COST2100
- IEEE 802.11
- NYU WIRELESS: interdisciplinary academic research center
- Fraunhofer HHI has developed the QuaDRiGa channel model, Matlab implementation is available at http://quadriga-channel-model.de

Groups and projects which intend to develop channel models:

- 5G mmWave Channel Model Alliance: NIST initiated, North America based
- mmMAGIC (Millimetre-Wave Based Mobile Radio Access Network for Fifth Generation Integrated Communications): Europe based
- IMT-2020 5G promotion association: China based

METIS Channel Models:

- Identified 5G requirements (e.g., wide frequency range, high bandwidth, massive MIMO, 3-D and accurate polarization modelling)
- Performed channel measurements at various bands between 2GHz and 60 GHz
- Provided different channel model methodologies (map-based model, stochastic model or hybrid model). For stochastic model, the proposed channel is focused on outdoor square, Indoor cafeteria and indoor shopping mall scenarios.

MiWEBA Channel Models:

- Addressed various challenges: Shadowing, spatial consistency, environment dynamics, spherical wave modelling, dual mobility Doppler model, ratio between diffuse and specular reflections, polarization
- Proposed Quasi-deterministic channel model
- Performed channel measurements at 60 GHz

- Focused on university campus, street canyon, hotel lobby, backhaul, and D2D scenarios.

ITU-R M Channel Models:

- Addressed the propagation loss and atmospheric loss on mmW
- Introduced enabling antenna array technology and semiconductor technology
- Proposed deployment scenarios, focused on dense urban environment for high data rate service: indoor shopping mall, indoor enterprise, in home, urban hotspot in a square/street, mobility in city.

COST2100 and COST IC1004 Channel Models:

- Geometry-based stochastic channel model that reproduce the stochastic properties of MIMO channels over time, frequency and space. It is a cluster-level model where the statistics of the large scale parameters are always guaranteed in each series of channel instances.

NYU WIRELESS Channel Models:

- Conducted many urban propagation measurements on 28/38/60/73 GHz bands for both outdoor and indoor channels, measurements are continuing.
- Proposed 3 areas for 5G mmWave channel modelling which are small modifications or extensions from 3GPP's current below 6GHz channel models
- 1) LOS/NLOS/blockage modelling (a squared exponential term); 2). Wideband power delay profiles (time clusters and spatial lobes for a simple extension to the existing 3GPP SSCM model); 3). Physics-based path loss model (using the existing 3GPP path loss equations, but simply replacing the "floating" optimization parameter with a deterministic 1 m "close-in" free space reference term in order to provide a standard and stable definition of "path loss exponent" across all different parties, scenarios, and frequencies).

802.11 ad/ay Channel Models:

- Conducted ray-tracing methodology on 60 GHz band indoor channels, including conference room, cubicle, living room scenarios
- Intra cluster parameters were proposed in terms of ray excess delay and ray power distribution
- Human blockage models were proposed in terms of blockage probability and blockage attenuation

5G mmWave Channel Model Alliance:

- Will provide a venue to promote fundamental research into measurement, analysis, identification of physical parameters, and statistical representations of mmWave propagation channels.
- Divided into six collaborative working groups that include a Steering Committee; Modelling Methodology Group; Measurement Methodology Group; and groups that focus on defining and parameterizing Indoor, Outdoor, and Emerging Usage Scenarios.
- Sponsored by Communications Technology Research Laboratory within the NIST.

mmMAGIC:

- Brings together major infrastructure vendors, major European operators, leading research institutes and universities, measurement equipment vendors and one SME.
- Will undertake extensive radio channel measurements in the 6-100 GHz range.
- Will develop and validate advanced channel models that will be used for rigorous validation and feasibility analysis of the proposed concepts and system, as well as for usage in regulatory and standards fora.

IMT-2020 5G promotion association

- Jointly established by three ministries of China based on the original IMT-Advanced promotion group
- Members including the main operators, vendors, universities and research institutes in China

- The major platform to promote 5G technology research in China and to facilitate international communication and cooperation

QuaDRiGa (Fraunhofer HHI)

- QuaDRiGa (QUAsi Deterministic RadIo channel GenerAtor) was developed at the Fraunhofer Heinrich Hertz Institute within the Wireless Communications and Networks Department to enable the modelling of MIMO radio channels for specific network configurations, such as indoor, satellite or heterogeneous configurations.

- Besides being a fully-fledged 3D geometry-based stochastic channel model (well aligned with TR36.873), QuaDRiGa contains a collection of features created in SCM(e) and WINNER channel models along with novel modelling approaches which provide features to enable quasi-deterministic multi-link tracking of users (receiver) movements in changing environments. QuaDRiGa supports Massive MIMO modelling enabled through a new multi-bounce scattering approach and spherical wave propagation. It will be continuously extended with features required by 5G and frequencies beyond 6 GHz. The QuaDRiGa model is supported by data from extensive channel measurement campaigns at 10 / 28 / 43 / 60 / 82 GHz performed by the same group.

ATIS Next G Alliance

- Published a report that includes a collection of results from several measurement campaigns relevant to deployment scenarios and use cases for 7-24 GHz channel modeling enhancements and channel modeling for integrated sensing and communications.

ETSI Industry specification group (ISG) Integrated sensing and communications (ISAC)

- ETSI ISG ISAC plans to publish Group Report (GR) /ISC-002 that provides information on advanced ISAC channel modeling concepts and their validation through measurement, in addition to information on evaluation methodology framework, deployment scenarios and the corresponding potentially suitable frequency bands.

6.2 Scenarios of interest

Brief description of the key scenarios of interest identified (see note):

(1) UMi (Street canyon, open area) with O2O and O2I: This is similar to 3D-UMi scenario, where the BSs are mounted below rooftop levels of surrounding buildings. UMi open area is intended to capture real-life scenarios such as a city or station square. The width of the typical open area is in the order of 50 to 100 m.

Example: [Tx height:10 m, Rx height with reference to floor height: 1.5 m, ISD: 200 m]

(2) UMa with O2O and O2I: This is similar to 3D-UMa scenario, where the BSs are mounted above rooftop levels of surrounding buildings.

Example: [Tx height:25 m, Rx height with reference to floor height: 1.5 m, ISD: 200 m, 500 m]

(3) Indoor: This scenario is intended to capture various typical indoor deployment scenarios, including office environments, and shopping malls. The typical office environment is comprised of open cubicle areas, walled offices, open areas, corridors etc. The BSs are mounted at a height of 2-3 m either on the ceilings or walls. The shopping malls are often 1-5 stories high and may include an open area (or "atrium") shared by several floors. The BSs are mounted at a height of approximately 3 m on the walls or ceilings of the corridors and shops.

Example: [Tx height: 2-3 m, Rx height: 1.5 m, area: 500 square meters]

(4) Backhaul, including outdoor above roof top backhaul in urban area and street canyon scenario where small cell BSs are placed at lamp posts.

(5) D2D/V2V. Device-to-device access in open area, street canyon, and indoor scenarios. V2V is a special case where the devices are mobile.

(6) Other scenarios such as Stadium (open-roof) and Gym (close-roof).

(7) Indoor industrial scenarios

(8) Suburban macro (SMa) scenarios: In suburban macro-cells base stations are located above the surrounding environment to allow wide area coverage, and mobile stations are outdoors at street level and within commercial and residential buildings.

Example: [Tx height: 35 m, Rx height with reference to floor height: 1.5 m, ISD: 1299 m, 1732 m]

(9) Integrated sensing and communication scenarios as described in Clause 7.9.1.

Note: The scenarios of interest are based on the plenary email discussion and different from the supported scenarios in clause 7. The indoor industrial scenarios were identified at a later stage in the TSG RAN #81 meeting. SMa scenarios were identified at a later stage as part of Study on channel modelling enhancements for 7-24GHz for NR. The integrated sensing and communication scenarios were identified at a later stage as part of Study on channel modelling for integrated sensing and communications for NR.

6.3 Channel measurement capabilities

The measurement capability as reported by each company is summarized in the following table.

Table 6.3-1: Channel measurement capabilities

	6 - 20 GHz	20 - 30 GHz	30 - 60 GHz	>60 GHz
Urban macro	CMCC Nokia/Aalborg Ericsson Vodafone BT Apple BUPT Spark NZ Ltd AT&T NTT Docomo Huawei	Nokia/Aalborg Ericsson	NYU Ericsson	
Urban micro	Aalto University CMCC Ericsson Intel/Fraunhofer HHI Nokia/Aalborg NTT DOCOMO Orange NYU/Sharp Apple BUPT Spark NZ Ltd AT&T Samsung Keysight Huawei Southeast University/ Purple Mountain Laboratories/China Telecom	AT&T Aalto University CMCC Huawei Intel/Fraunhofer HHI Nokia/Aalborg NTT DOCOMO NYU Qualcomm Samsung CATT KT ETRI ITRI/CCU ZTE Ericsson	AT&T Huawei Intel/Fraunhofer HHI NTT DOCOMO Qualcomm CATT ETRI ITRI/CCU ZTE Ericsson	AT&T Aalto University Huawei Intel/Fraunhofer HHI NYU
Suburban macro	AT&T Ericsson Vodafone Apple Huawei	Ericsson Nokia	Ericsson	
Indoor	Aalto University CMCC Ericsson Huawei vivo Intel/Fraunhofer HHI Nokia/Aalborg NTT DOCOMO Orange NYU/Sharp Apple Sony ZTE BUPT Spark NZ Ltd AT&T	AT&T Alcatel-Lucent Aalto University BUPT CMCC Huawei Intel/Fraunhofer HHI Nokia/Aalborg NTT DOCOMO NYU Qualcomm Samsung CATT KT ETRI ITRI/CCU ZTE	AT&T Ericsson Huawei Intel/Fraunhofer HHI NTT DOCOMO NYU Qualcomm CATT ETRI ITRI/CCU ZTE	AT&T Aalto University Huawei Intel/Fraunhofer HHI NYU
O2I	Ericsson Huawei vivo Intel/Fraunhofer HHI Nokia/Aalborg NTT DOCOMO Orange BT Vodafone	AT&T Alcatel-Lucent Ericsson Huawei Intel/Fraunhofer HHI NTT DOCOMO NYU Samsung KT Nokia	AT&T Ericsson Huawei Intel/Fraunhofer HHI NTT DOCOMO	AT&T Huawei Intel/Fraunhofer HHI

6.4 Modelling objectives

The requirements for channel modelling are as follows.

- Channel model SI should take into account the outcome of RAN-level discussion in the '5G' requirement study item.
- Complexity in terms of Description, Generating channel coefficients, development complexity and Simulation time should be considered.
- Support frequency range up to 100 GHz.
  - The critical path of the SI is 6 – 100 GHz.
  - Take care of mmW propagation aspects such as blocking and atmosphere attenuation.
- The model should be consistent in space, time and frequency.
- Support large channel bandwidths (up to 10% of carrier frequency).
- Aim for the channel model to cover a range of coupling loss considering current typical cell sizes, e.g. up to km-range macro cells. Note: This is to enable investigation of the relevance of the 5G system using higher frequency bands to existing deployments.
- Accommodate UT mobility
  - Mobile speed up to 500 km/h.
  - Develop a methodology considering that model extensions to D2D and V2V may be developed in future SI.
- Support large antenna arrays.
- Support near-field channel propagation (i.e., characteristics of spherical wavefront) and spatial non-stationarity (i.e. antenna element-wise power variation).
- Support integrated sensing and communications

7 Channel model(s) for 0.5-100 GHz

7.1 Coordinate system

7.1.1 Definition

A coordinate system is defined by the x, y, z axes, the spherical angles and the spherical unit vectors as shown in Figure 7.1.1. Figure 7.1.1 defines the zenith angle θ and the azimuth angle ϕ in a Cartesian coordinate system. Note that $\theta = 0$ points to the zenith and $\theta = 90^0$ points to the horizon. The field component in the direction of $\hat{\theta}$ is given by F_θ and the field component in the direction of $\hat{\phi}$ is given by F_ϕ.

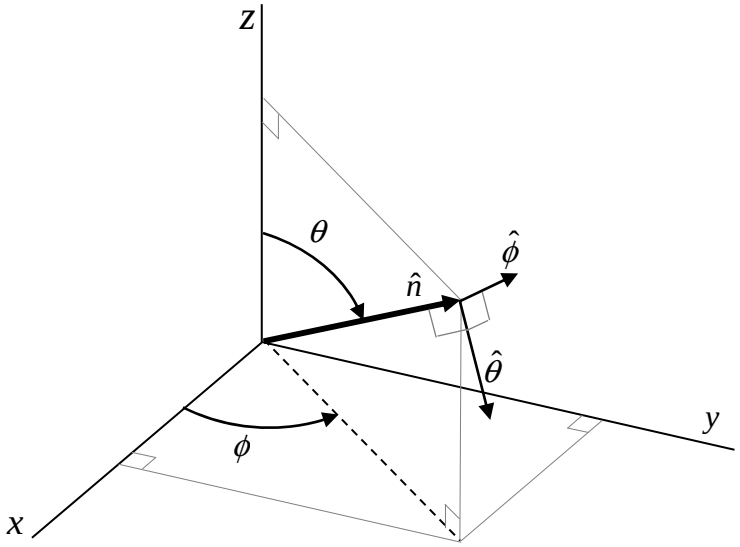

Figure 7.1.1: Definition of spherical angles and spherical unit vectors in a Cartesian coordinate system, where $\hat{n}$ is the given direction, $\hat{\theta}$ and $\hat{\phi}$ are the spherical basis vectors

7.1.2 Local and global coordinate systems

A Global Coordinate System (GCS) is defined for a system comprising multiple BSs and UTs. An array antenna for a BS or a UT can be defined in a Local Coordinate System (LCS). An LCS is used as a reference to define the vector far-field that is pattern and polarization, of each antenna element in an array. It is assumed that the far-field is known in the LCS by formulae. The placement of an array within the GCS is defined by the translation between the GCS and a LCS. The orientation of the array with respect to the GCS is defined in general by a sequence of rotations (described in clause 7.1.3). Since this orientation is in general different from the GCS orientation, it is necessary to map the vector fields of the array elements from the LCS to the GCS. This mapping depends only on the orientation of the array and is given by the equations in clause 7.1.3. Note that any arbitrary mechanical orientation of the array can be achieved by rotating the LCS with respect to the GCS.

7.1.3 Transformation from a LCS to a GCS

A GCS with coordinates (x, y, z, θ, ϕ) and unit vectors ($\hat{\theta}, \hat{\phi}$) and an LCS with "primed" coordinates ($x', y', z', \theta', \phi'$) and "primed" unit vectors ($\hat{\theta}', \hat{\phi}'$) are defined with a common origins in Figures 7.1.3-1 and 7.1.3-2. Figure 7.1.3-1 illustrates the sequence of rotations that relate the GCS (gray) and the LCS (blue). Figure 7.1.3-2 shows the coordinate direction and unit vectors of the GCS (gray) and the LCS (blue). Note that the vector fields of the array antenna elements are defined in the LCS. In Figure 7.1.3-1 we consider an arbitrary 3D-rotation of the LCS with respect to the GCS given by the angles α, β, γ. The set of angles α, β, γ can also be termed as the orientation of the array antenna with respect to the GCS.

Note that the transformation from a LCS to a GCS depends only on the angles α, β, γ. The angle α is called the bearing angle, β is called the downtilt angle and γ is called the slant angle.

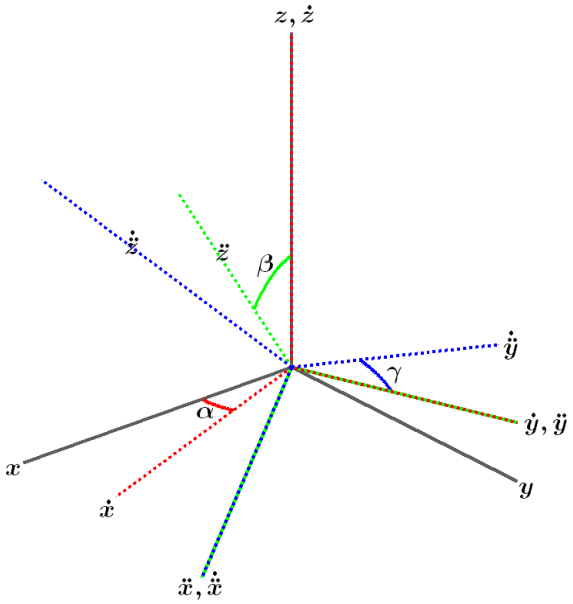

Figure 7.1.3-1: Orienting the LCS (blue) with respect to the GCS (gray) by a sequence of 3 rotations: α, β, γ.

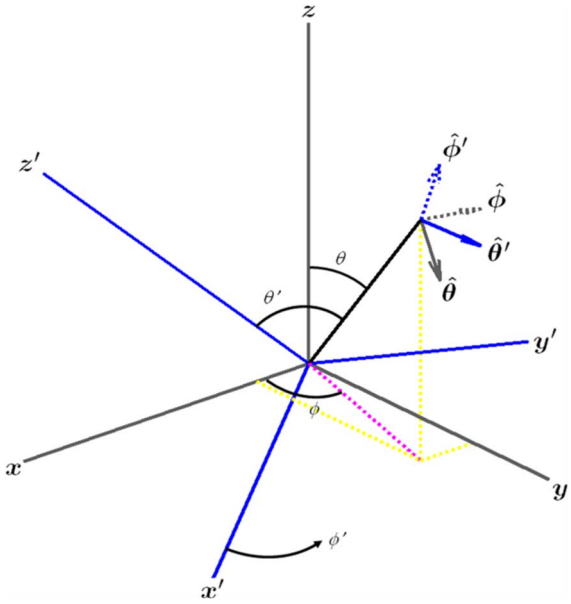

Figure 7.1.3-2: Definition of spherical coordinates and unit vectors in both the GCS and LCS.

Let $A'(\theta',\phi')$ denote an antenna element pattern in the LCS and $A(\theta,\phi)$ denote the same antenna element pattern in the GCS. Then the two are related simply by

$$A(\theta,\phi) = A'(\theta',\phi') \tag{7.1-1}$$

with θ' and ϕ' given by (7.1-7) and (7.1-8).

Let us denote the polarized field components in the LCS by $F'_{\theta'}(\theta',\phi')$, $F'_{\phi'}(\theta',\phi')$ and in the GCS by $F_{\theta}(\theta,\phi)$, $F_{\phi}(\theta,\phi)$. Then they are related by equation (7.1-11).

Any arbitrary 3D rotation can be specified by at most 3 elemental rotations, and following the framework of Figure 7.1.3-1, a series of rotations about the z, $\dot{y}$ and $\ddot{x}$ axes are assumed here, in that order. The dotted and double-dotted marks indicate that the rotations are intrinsic, which means that they are the result of one (·) or two (··) intermediate rotations. In other words, the $\dot{y}$ axis is the original y axis after the first rotation about z, and the $\ddot{x}$ axis is the original x axis after the first rotation about z and the second rotation about $\dot{y}$. A first rotation of α about *z* sets the antenna bearing angle (i.e. the sector pointing direction for a BS antenna element). The second rotation of β about $\dot{y}$ sets the antenna downtilt angle. Finally, the third rotation of γ about $\ddot{x}$ sets the antenna slant angle. The orientation of the *x*, *y* and *z* axes after all three rotations can be denoted as $\dddot{x}$, $\dddot{y}$ and $\dddot{z}$. These triple-dotted axes represents the final orientation of the LCS, and for notational purposes denoted as the *x′*, *y′* and *z′* axes (local or "primed" coordinate system).

In order to establish the equations for transformation of the coordinate system and the polarized antenna field patterns between the GCS and the LCS, it is necessary to determine the composite rotation matrix that describes the transformation of point (*x*, *y*, *z*) in the GCS into point (*x′*, *y′*, *z′*) in the LCS. This rotation matrix is computed as the product of three elemental rotation matrices. The matrix to describe rotations about the z, $\dot{y}$ and $\ddot{x}$ axes by the angles α, β and γ respectively and in that order is defined as

$$R = R_Z(\alpha)R_Y(\beta)R_X(\gamma) = \begin{pmatrix} +\cos\alpha & -\sin\alpha & 0 \\ +\sin\alpha & +\cos\alpha & 0 \\ 0 & 0 & 1 \end{pmatrix}\begin{pmatrix} +\cos\beta & 0 & +\sin\beta \\ 0 & 1 & 0 \\ -\sin\beta & 0 & +\cos\beta \end{pmatrix}\begin{pmatrix} 1 & 0 & 0 \\ 0 & +\cos\gamma & -\sin\gamma \\ 0 & +\sin\gamma & +\cos\gamma \end{pmatrix} \tag{7.1-2}$$

The reverse transformation is given by the inverse of *R*, which is also equal to the transpose of *R* since it is orthogonal.

$$R^{-1} = R_X(-\gamma)R_Y(-\beta)R_Z(-\alpha) = R^T \tag{7.1-3}$$

The simplified forward and reverse composite rotation matrices are given by

$$R = \begin{pmatrix} \cos\alpha\cos\beta & \cos\alpha\sin\beta\sin\gamma - \sin\alpha\cos\gamma & \cos\alpha\sin\beta\cos\gamma + \sin\alpha\sin\gamma \\ \sin\alpha\cos\beta & \sin\alpha\sin\beta\sin\gamma + \cos\alpha\cos\gamma & \sin\alpha\sin\beta\cos\gamma - \cos\alpha\sin\gamma \\ -\sin\beta & \cos\beta\sin\gamma & \cos\beta\cos\gamma \end{pmatrix} \tag{7.1-4}$$

and

$$R^{-1} = \begin{pmatrix} \cos\alpha\cos\beta & \sin\alpha\cos\beta & -\sin\beta \\ \cos\alpha\sin\beta\sin\gamma - \sin\alpha\cos\gamma & \sin\alpha\sin\beta\sin\gamma + \cos\alpha\cos\gamma & \cos\beta\sin\gamma \\ \cos\alpha\sin\beta\cos\gamma + \sin\alpha\sin\gamma & \sin\alpha\sin\beta\cos\gamma - \cos\alpha\sin\gamma & \cos\beta\cos\gamma \end{pmatrix} \tag{7.1-5}$$

These transformations can be used to derive the angular and polarization relationships between the two coordinate systems.

In order to establish the angular relationships, consider a point (*x*, *y*, *z*) on the unit sphere defined by the spherical coordinates (ρ=1, θ, ϕ), where ρ is the unit radius, θ is the zenith angle measured from the +*z*-axis, and ϕ is the azimuth angle measured from the +*x*-axis in the *x*-*y* plane. The Cartesian representation of that point is given by

$$\hat{\rho} = \begin{pmatrix} x \\ y \\ z \end{pmatrix} = \begin{pmatrix} \sin\theta\cos\phi \\ \sin\theta\sin\phi \\ \cos\theta \end{pmatrix} \tag{7.1-6}$$

The zenith angle is computed as $\arccos(\hat{\rho}\cdot\hat{z})$ and the azimuth angle as $\arg(\hat{x}\cdot\hat{\rho} + j\,\hat{y}\cdot\hat{\rho})$, where $\hat{x}$, $\hat{y}$ and $\hat{z}$ are the Cartesian unit vectors. If this point represents a location in the GCS defined by θ and ϕ, the corresponding position in the LCS is given by $R^{-1}\hat{\rho}$, from which local angles θ' and ϕ' can be computed. The results are given in equations (7.1-7) and (7.1-8).

$$\theta'(\alpha,\beta,\gamma;\theta,\phi) = \arccos\left(\begin{bmatrix}0\\0\\1\end{bmatrix}^T R^{-1}\hat{\rho}\right) = \text{acos}(\cos\beta\cos\gamma\cos\theta + (\sin\beta\cos\gamma\cos(\phi-\alpha) - \sin\gamma\sin(\phi-\alpha))\sin\theta) \tag{7.1-7}$$

$$\phi'(\alpha,\beta,\gamma;\theta,\phi) = \arg\left(\begin{bmatrix}1\\j\\0\end{bmatrix}^T R^{-1}\hat{\rho}\right) = \arg\begin{pmatrix}(\cos\beta\sin\theta\cos(\phi-\alpha) - \sin\beta\cos\theta) + \\ j(\cos\beta\sin\gamma\cos\theta + (\sin\beta\sin\gamma\cos(\phi-\alpha) + \cos\gamma\sin(\phi-\alpha))\sin\theta)\end{pmatrix} \tag{7.1-8}$$

These formulae relate the spherical angles (θ, ϕ) of the GCS to the spherical angles (θ', ϕ') of the LCS given the rotation operation defined by the angles (α, β, γ).

Let us denote the polarized field components $F_\theta(\theta,\phi)$, $F_\phi(\theta,\phi)$ in the GCS and $F'_{\theta'}(\theta',\phi')$, $F'_{\phi'}(\theta',\phi')$ in the LCS. These are related by

$$\begin{pmatrix} F_\theta(\theta,\phi) \\ F_\phi(\theta,\phi) \end{pmatrix} = \begin{pmatrix} \hat{\theta}(\theta,\phi)^T R\hat{\theta}'(\theta',\phi') & \hat{\theta}(\theta,\phi)^T R\hat{\phi}'(\theta',\phi') \\ \hat{\phi}(\theta,\phi)^T R\hat{\theta}'(\theta',\phi') & \hat{\phi}(\theta,\phi)^T R\hat{\phi}'(\theta',\phi') \end{pmatrix} \begin{pmatrix} F'_{\theta'}(\theta',\phi') \\ F'_{\phi'}(\theta',\phi') \end{pmatrix} \tag{7.1-9}$$

In this equation, $\hat{\theta}$ and $\hat{\phi}$ represent the spherical unit vectors of the GCS, and $\hat{\theta}'$ and $\hat{\phi}'$ are the representations in the LCS. The forward rotation matrix R transforms the LCS unit vectors into the GCS frame of reference. These pairs of unit vectors are orthogonal and can be represented as shown in Figure 7.1.3-3.

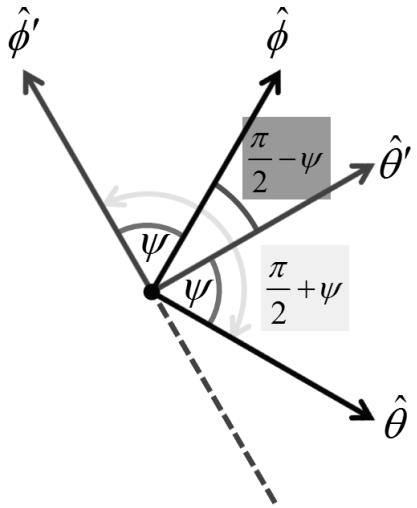

Figure 7.1.3-3: Rotation of the spherical basis vectors by an angle ψ due to the orientation of the LCS with respect to the GCS

Assuming an angular displacement of ψ between the two pairs of unit vectors, the rotation matrix of equation (7.1-9) can be further simplified as:

$$\begin{pmatrix} \hat{\theta}(\theta,\phi)^T R\hat{\theta}'(\theta',\phi') & \hat{\theta}(\theta,\phi)^T R\hat{\phi}'(\theta',\phi') \\ \hat{\phi}(\theta,\phi)^T R\hat{\theta}'(\theta',\phi') & \hat{\phi}(\theta,\phi)^T R\hat{\phi}'(\theta',\phi') \end{pmatrix} = \begin{pmatrix} \cos\psi & \cos(\pi/2+\psi) \\ \cos(\pi/2-\psi) & \cos\psi \end{pmatrix} = \begin{pmatrix} +\cos\psi & -\sin\psi \\ +\sin\psi & +\cos\psi \end{pmatrix} \quad (7.1\text{-}10)$$

and equation (7.1-9) can be written as:

$$\begin{pmatrix} F_\theta(\theta,\phi) \\ F_\phi(\theta,\phi) \end{pmatrix} = \begin{pmatrix} +\cos\psi & -\sin\psi \\ +\sin\psi & +\cos\psi \end{pmatrix} \begin{pmatrix} F'_{\theta'}(\theta',\phi') \\ F'_{\phi'}(\theta',\phi') \end{pmatrix} \quad (7.1\text{-}11)$$

The angle ψ can be computed in numerous ways from equation (7.1-10), with one such way approach being

$$\psi = \arg\left(\hat{\theta}(\theta,\phi)^T R\hat{\theta}'(\theta',\phi') + j\,\hat{\phi}(\theta,\phi)^T R\hat{\theta}'(\theta',\phi')\right) \quad (7.1\text{-}12)$$

The dot products are readily computed using the Cartesian representation of the spherical unit vectors. The general expressions for these unit vectors are given by

$$\hat{\theta} = \begin{pmatrix} \cos\theta\cos\phi \\ \cos\theta\sin\phi \\ -\sin\theta \end{pmatrix} \quad (7.1\text{-}13)$$

and

$$\hat{\phi} = \begin{pmatrix} -\sin\phi \\ +\cos\phi \\ 0 \end{pmatrix} \quad (7.1\text{-}14)$$

The angle ψ can be expressed as a function of mechanical orientation (α, β, γ) and spherical position (θ, ϕ), and is given by

$$\psi = \arg\begin{pmatrix} (\sin\gamma\cos\theta\sin(\phi-\alpha)+\cos\gamma(\cos\beta\sin\theta-\sin\beta\cos\theta\cos(\phi-\alpha)))+ \\ j(\sin\gamma\cos(\phi-\alpha)+\sin\beta\cos\gamma\sin(\phi-\alpha)) \end{pmatrix} \quad (7.1\text{-}15)$$

It can be shown that $\cos\psi$ and $\sin\psi$ can be expressed as:

$$\cos\psi = \frac{\cos\beta\cos\gamma\sin\theta-(\sin\beta\cos\gamma\cos(\phi-\alpha)-\sin\gamma\sin(\phi-\alpha))\cos\theta}{\sqrt{1-(\cos\beta\cos\gamma\cos\theta+(\sin\beta\cos\gamma\cos(\phi-\alpha)-\sin\gamma\sin(\phi-\alpha))\sin\theta)^2}} \quad (7.1\text{-}16)$$

$$\sin\psi = \frac{\sin\beta\cos\gamma\sin(\phi-\alpha)+\sin\gamma\cos(\phi-\alpha)}{\sqrt{1-(\cos\beta\cos\gamma\cos\theta+(\sin\beta\cos\gamma\cos(\phi-\alpha)-\sin\gamma\sin(\phi-\alpha))\sin\theta)^2}} \quad (7.1\text{-}17)$$

7.1.4 Transformation from an LCS to a GCS for downtilt angle only

In this clause equations are provided for the transformation from LCS to GCS assuming that the orientation of the LCS (with respect to the GCS) is such that the bearing angle α=0, the downtilt angle β is non-zero and the slant angle γ=0. In other words the *y'*-axis of the LCS is parallel to the *y*-axis of the GCS. Considering a BS antenna element the *x*-axis of the GCS is aligned with the pointing direction of the sector. Mechanical downtilt is modelled as a rotation of the LCS around the *y*-axis. For zero mechanical downtilt the LCS coincides with the GCS.

This transformation relates the spherical angles (θ , ϕ) in the global coordinate system to spherical angles (θ', ϕ') in the local (antenna-fixed) coordinate system and is defined as follows:

$$\theta' = \arccos(\cos\phi\sin\theta\sin\beta+\cos\theta\cos\beta) \quad (7.1\text{-}18)$$

$$\phi' = \arg(\cos\phi\sin\theta\cos\beta-\cos\theta\sin\beta+j\sin\phi\sin\theta) \quad (7.1\text{-}19)$$

where β is the mechanical tilt angle around the *y*-axis as defined in Figure 7.1.4. Note that the equations (7.1-7), (7.1-8) reduce to equations (7.1-18), (7.1-19) if both α and γ are zero.

The antenna element pattern $A(\theta,\phi)$ in the GCS is related to the antenna element pattern $A'(\theta',\phi')$ in the LCS by the relation

$$A(\theta,\phi) = A'(\theta',\phi') \quad (7.1\text{-}20)$$

with θ' and ϕ' given by (7.1-18) and (7.1-19).

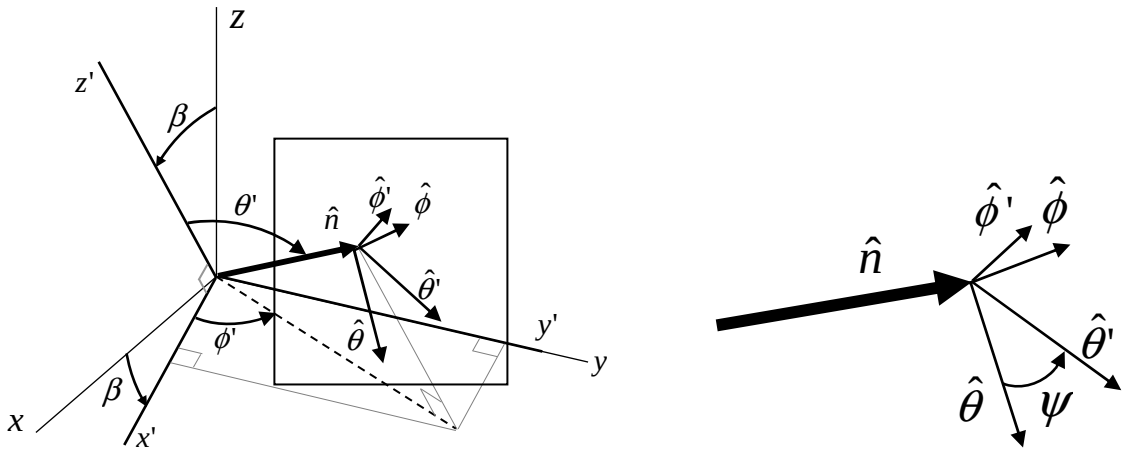

Figure 7.1.4: Definition of angles and unit vectors when the LCS has been rotated an angle β around the *y*-axis of the GCS

For a mechanical tilt angle β, the global coordinate system field components $F_\theta(\theta,\phi)$ and $F_\phi(\theta,\phi)$, are calculated from the field components $F'_{\theta'}(\theta',\phi')$ and $F'_{\phi'}(\theta',\phi')$ of the radiation pattern in the local (antenna-fixed) coordinate system as:

$$F_\theta(\theta,\phi) = F'_{\theta'}(\theta',\phi')\cos\psi - F'_{\phi'}(\theta',\phi')\sin\psi \quad (7.1\text{-}21)$$

$$F_\phi(\theta,\phi) = F'_{\theta'}(\theta',\phi')\sin\psi + F'_{\phi'}(\theta',\phi')\cos\psi \quad (7.1\text{-}22)$$

where θ' and ϕ' are defined as in (7.1-18) and (7.1-19), and ψ is defined as:

$$\psi = \arg\left(\sin\theta\cos\beta - \cos\phi\cos\theta\sin\beta + j\sin\phi\sin\beta\right). \quad (7.1\text{-}23)$$

Note that the equation (7.1-15) is reduced to equation (7.1-23) if both α and γ are zero.

As an example, in the horizontal cut, i.e., for $\theta = 90°$, equations (7.1-18), (7.1-19) and (7.1-23) become

$$\theta' = \arccos\left(\cos\phi\sin\beta\right) \quad (7.1\text{-}24)$$

$$\phi' = \arg\left(\cos\phi\cos\beta + j\sin\phi\right) \quad (7.1\text{-}25)$$

$$\psi = \arg\left(\cos\beta + j\sin\phi\sin\beta\right) \quad (7.1\text{-}26)$$

7.2 Scenarios

The detailed scenario description in this clause can be used for channel model calibration.

UMi-street canyon and UMa

Details on UMi-street canyon and UMa scenarios are listed in Table 7.2-1.

Table 7.2-1: Evaluation parameters for UMi-street canyon and UMa scenarios

Parameters		UMi - street canyon	UMa
Cell layout		Hexagonal grid, 19 micro sites, 3 sectors per site (ISD = 200 m)	Hexagonal grid, 19 macro sites, 3 sectors per site (ISD = 500 m, see note 1)
BS antenna height h_{BS}		10 m	25 m
UT location	Outdoor/indoor	Outdoor and indoor	Outdoor and indoor
	LOS/NLOS	LOS and NLOS	LOS and NLOS
	Height h_{UT}	Same as 3D-UMi in TR36.873	Same as 3D-UMa in TR36.873
Indoor UT ratio		80%	80%
UT mobility (horizontal plane only)		3 km/h	3 km/h
Min. BS - UT distance (2D)		10 m	35 m
UT distribution (horizontal)		Uniform	Uniform
NOTE 1: UMa scenarios with ISDs between 200-500m can be used for evaluations.			

Indoor-office

Details on indoor-office scenarios are listed in Table 7.2-2 and presented in Figure 7.2-1. More details, if necessary, can be added to Figure 7.2-1.

Table 7.2-2: Evaluation parameters for indoor-office scenarios

Parameters		Indoor - office open office	Indoor - office mixed office
Layout	Room size (W x L x H)	120 m x 50 m x 3 m	
	ISD	20 m	
BS antenna height h_{BS}		3 m (ceiling)	
UT location	LOS/NLOS	LOS and NLOS	
	Height h_{UT}	1 m	
UT mobility (horizontal plane only)		3 km/h	
Min. BS - UT distance (2D)		0	
UT distribution (horizontal)		Uniform	

Note: The only difference between the open office and mixed office models in this TR is the line of sight probability.

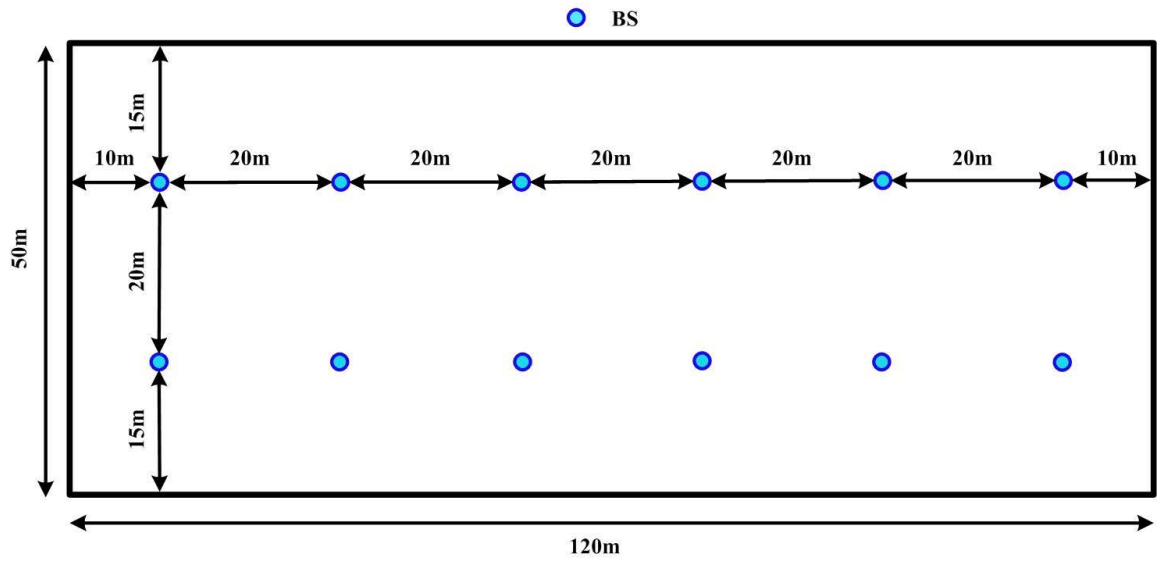

Figure 7.2-1: Layout of indoor office scenarios.

RMa

The rural deployment scenario focuses on larger and continuous coverage. The key characteristics of this scenario are continuous wide area coverage supporting high speed vehicles. This scenario will be noise-limited and/or interference-limited, using macro TRPs. Details of RMa scenario is described in Table 7.2-3.

Table 7.2-3: Evaluation parameters for RMa

Parameters	RMa
Carrier Frequency	Up to 7 GHz
BS height h_{BS}	35 m
Layout	Hexagonal grid, 19 Macro sites, 3 sectors per site, ISD = 1732 m or 5000 m
UT height h_{UT}	1.5 m
UT distribution	Uniform
Indoor/Outdoor	50% indoor and 50% in car
LOS/NLOS	LOS and NLOS
Min BS - UT distance(2D)	35 m

Indoor Factory (InF)

The indoor factory (InF) scenario focuses on factory halls of varying sizes and with varying levels of density of "clutter", e.g. machinery, assembly lines, storage shelves, etc. Details of the InF scenario are listed in Table 7.2-4.

Table 7.2-4: Evaluation parameters for InF

		InF				
Parameters		**InF-SL (sparse clutter, low BS)**	**InF-DL (dense clutter, low BS)**	**InF-SH (sparse clutter, high BS)**	**InF-DH (dense clutter, high BS)**	**InF-HH (high Tx, high Rx)**
Layout	Room size	Rectangular: 20-160000 m^2				
	Ceiling height	5-25 m	5-15 m	5-25 m	5-15 m	5-25 m
	Effective clutter height h_c	< Ceiling height, 0-10 m				

Parameters		InF				
		InF-SL (sparse clutter, low BS)	**InF-DL (dense clutter, low BS)**	**InF-SH (sparse clutter, high BS)**	**InF-DH (dense clutter, high BS)**	**InF-HH (high Tx, high Rx)**
	External wall and ceiling type	Concrete or metal walls and ceiling with metal-coated windows				
Clutter type		Big machineries composed of regular metallic surfaces. For example: several mixed production areas with open spaces and storage/commissioning areas	Small to medium metallic machinery and objects with irregular structure. For example: assembly and production lines surrounded by mixed small-sized machineries.	Big machineries composed of regular metallic surfaces. For example: several mixed production areas with open spaces and storage/commissioning areas	Small to medium metallic machinery and objects with irregular structure. For example: assembly and production lines surrounded by mixed small-sized machineries.	Any
Typical clutter size, $d_{clutter}$		10 m	2 m	10 m	2 m	Any
Clutter density r (percentage of surface area occupied by clutter)		Low clutter density (<40%)	High clutter density (≥40%)	Low clutter density (<40%)	High clutter density (≥40%)	Any
BS antenna height h_{BS}		Clutter-embedded, i.e. the BS antenna height is below the average clutter height		Above clutter		Above clutter
UT location	LOS/NLOS	LOS and NLOS				100% LOS
	Height h_{UT}	Clutter-embedded				Above clutter

SMa

In suburban macro-cells base stations are located above the surrounding environment to allow wide area coverage, and mobile stations are outdoors at street level and within commercial and residential buildings. Buildings are typically low residential detached houses with one or two floors, or blocks of apartments/condos or commercial buildings with a few floors. Occasional open areas such as parks or playgrounds between the houses make the environment rather open. Streets do not form urban-like regular strict grid structure. In suburban areas, vegetation is more prevalent than in urban areas with a high variability of foliage density across different suburban areas. Details on SMa scenarios are listed in Table 7.2-5.

Table 7.2-5: Evaluation parameters for SMa scenarios

Parameters		SMa
Cell layout		Hexagonal grid, 19 macro sites, 3 sectors per site (ISD = 1299 m and 1732 m, see note 1 and 2) Up to two floors for residential buildings, up to five floors for commercial buildings. Building distribution are 90% residential and 10% commercial buildings
BS antenna height h_{BS}		35 m
UT location	Outdoor/indoor	Outdoor and indoor
	LOS/NLOS	LOS and NLOS
	Height h_{UT}	1.5 m for outdoor, 1.5 or 4.5 m for residential buildings, 1.5/4.5/7.5/10.5/13.5 m for commercial buildings
Indoor UT ratio		80%
UT mobility (horizontal plane only)		Indoor UTs: 3 km/h Outdoor UTs (in car): 40 km/h
Min. BS - UT distance (2D)		35 m
UT distribution (horizontal)		Uniform
UT distribution (vertical)		Uniform distribution across all floors for a building type
NOTE 1: For evaluation in study items/work items, if needed, admission control policies may be considered in conjunction with the ISD choice to address out of coverage UEs NOTE 2: SMa scenarios with ISDs between 1200-1800m can be used for evaluations.		

7.3 Antenna modelling

7.3.0 Antenna array structure

This clause captures the antenna array structures considered in this SI for calibration.

BS antenna model:

The BS antenna is modelled by a uniform rectangular panel array, comprising $M_g N_g$ panels, as illustrated in Figure 7.3-1 with M_g being the number of panels in a column and N_g being the number of panels in a row. Furthermore the following properties apply:

- Antenna panels are uniformly spaced in the horizontal direction with a spacing of $d_{g,H}$ and in the vertical direction with a spacing of $d_{g,V}$.
- On each antenna panel, antenna elements are placed in the vertical and horizontal direction, where N is the number of columns, M is the number of antenna elements with the same polarization in each column.
  - Antenna numbering on the panel illustrated in Figure 7.3-1 assumes observation of the antenna array from the front (with x-axis pointing towards broad-side and increasing y-coordinate for increasing column number).
  - The antenna elements are uniformly spaced in the horizontal direction with a spacing of d_H and in the vertical direction with a spacing of d_V.
  - The antenna panel is either single polarized (P =1) or dual polarized (P =2).

The rectangular panel array antenna can be described by the following tuple (M_g, N_g, M, N, P).

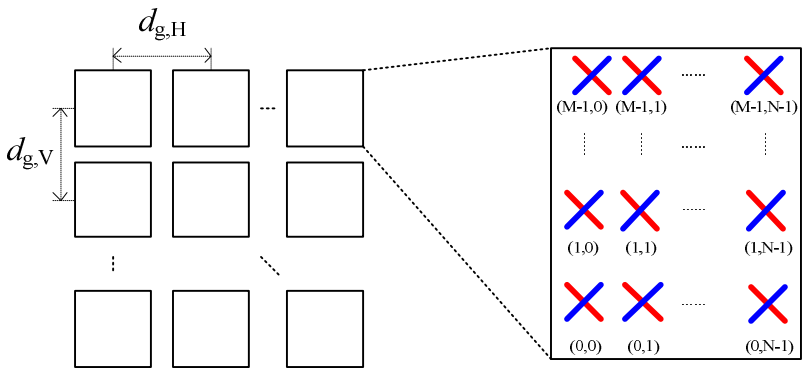

Figure 7.3-1: Cross-polarized panel array antenna model

The antenna radiation power pattern of each antenna element is generated according to Table 7.3-1.

Table 7.3-1: Radiation power pattern of a single antenna element

Parameter	Values
Vertical cut of the radiation power pattern (dB)	$A''_{\text{dB}}(\theta'', \phi'' = 0°) = -\min\left\{12\left(\frac{\theta'' - 90°}{\theta_{\text{3dB}}}\right)^2, SLA_V\right\}$ with $\theta_{\text{3dB}} = 65°, SLA_V = 30\,\text{dB}$ and $\theta'' \in [0°, 180°]$
Horizontal cut of the radiation power pattern (dB)	$A''_{\text{dB}}(\theta'' = 90°, \phi'') = -\min\left\{12\left(\frac{\phi''}{\phi_{\text{3dB}}}\right)^2, A_{\max}\right\}$ with $\phi_{\text{3dB}} = 65°, A_{\max} = 30\,\text{dB}$ and $\phi'' \in [-180°, 180°]$
3D radiation power pattern (dB)	$A''_{\text{dB}}(\theta'', \phi'') = -\min\{-(A''_{\text{dB}}(\theta'', \phi'' = 0°) + A''_{\text{dB}}(\theta'' = 90°, \phi'')), A_{\max}\}$
Maximum directional gain of an antenna element $G_{E,max}$	8 dBi

UT antenna model:

The UT antenna can be modelled by placing the antenna element/array at the placement candidate locations relative to the centre of the UT. The size of the device can be set to (X cm, Y cm, Z cm), in depth, width, and height respectively.

For handheld UT devices, the following additional properties apply:

- Four corners of the rectangle and the center of edges of the rectangle that reflect UT form factor are identified as potential locations of the UT antenna and potential locations are enumerated as illustrated in Figure 7.3-2.
- Each antenna is assumed to be oriented along the direction determined by the vector connecting the centre of the rectangle to the antenna location.
- Reference UT orientation vector of the handheld UT is perpendicular to the plane of the flat UT handheld device, and reference point for near field phase calculation of the UT is assumed to be the center of the plane of the UT handheld.
- Device dimensions for UT antenna modelling are (15 cm, 7 cm, 0 cm).

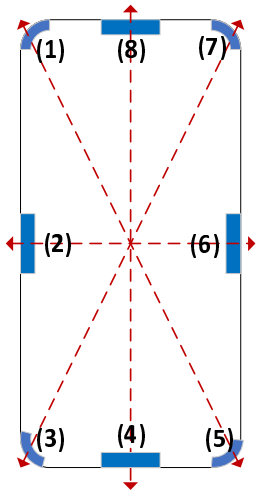

Figure 7.3-2: Handheld UT antenna placement candidate locations relative to centre of device (top down view)

- Reference handheld UT orientation is illustrated in Figure 7.3-3. The representation the handheld UT orientation will be same between GCS and UT LCS for $\Omega_{UT,\alpha}$ = 0 degrees, $\Omega_{UT,\beta}$ = 0 degrees, $\Omega_{UT,\gamma}$ = 0 degrees,

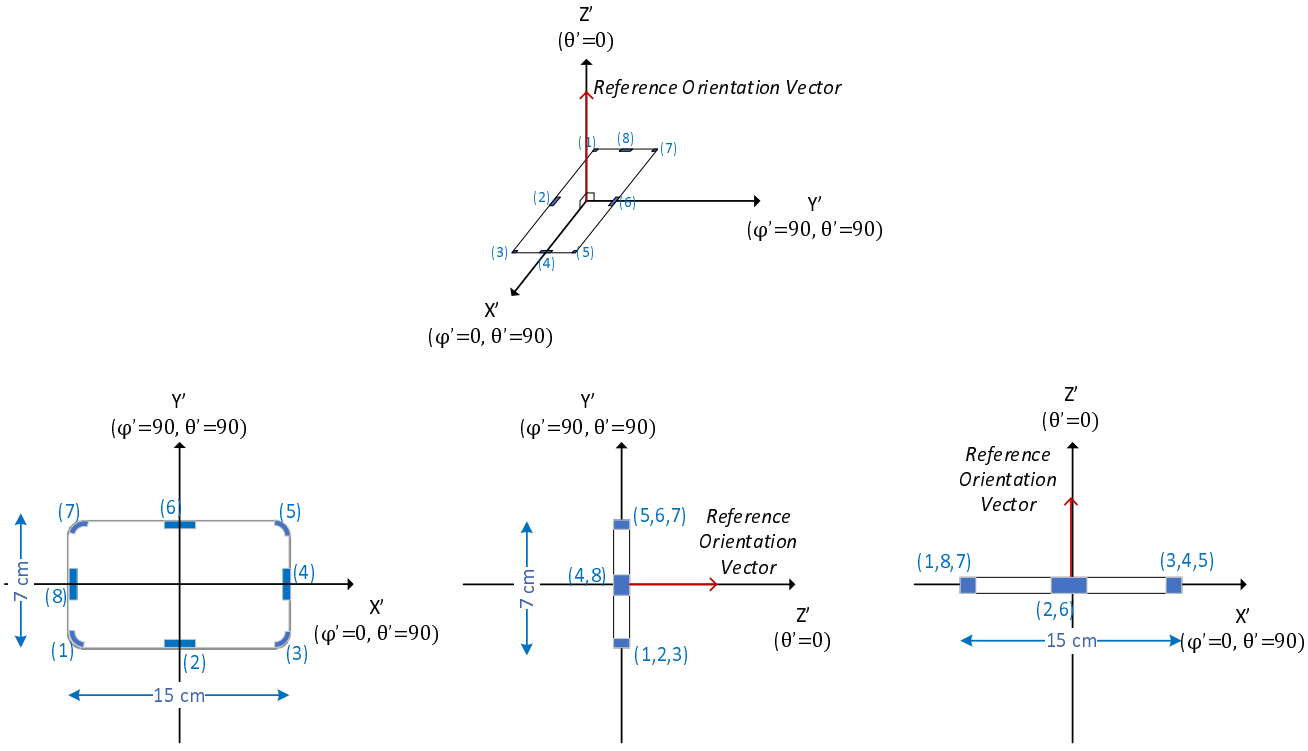

Figure 7.3-3: Illustration of reference handheld UT orientation in UT LCS

- For calibration of handheld UT, the following UT rotation based on reference UT orientation is assumed.
  - For calibration with spatial non-stationarity modelling:
    - For one-hand blockage, $\Omega_{UT,\alpha}$ = 0 – 360 degrees, $\Omega_{UT,\beta}$ = 45 degrees, $\Omega_{UT,\gamma}$ = 0 degrees,
    - For dual-hand blockage, $\Omega_{UT,\alpha}$ = 0 – 360 degrees, $\Omega_{UT,\beta}$ = 0 degrees, $\Omega_{UT,\gamma}$ = 45 degrees,
    - For hand and head blockage, $\Omega_{UT,\alpha}$ = 0 – 360 degrees, $\Omega_{UT,\beta}$ = 90 degrees, $\Omega_{UT,\gamma}$ = 0 degrees,
  - For all other cases:

- $\Omega_{UT,\alpha}$ = 0 – 360 degrees, $\Omega_{UT,\beta}$ = 45 degrees, $\Omega_{UT,\gamma}$ = 0 degrees,

- Example of UT rotations are illustrated in Figure 7.3-4 and 7.3-5.

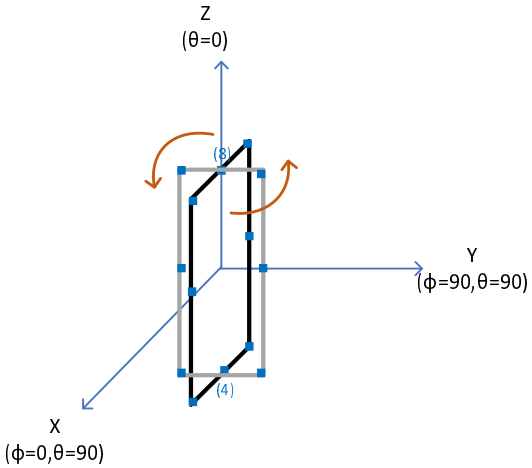

Figure 7.3-4: Example of UT rotation of $\Omega_{UT,\alpha}$ = 0 - 360 degrees, $\Omega_{UT,\beta}$ = 90 degrees, $\Omega_{UT,\gamma}$ = 0 degrees

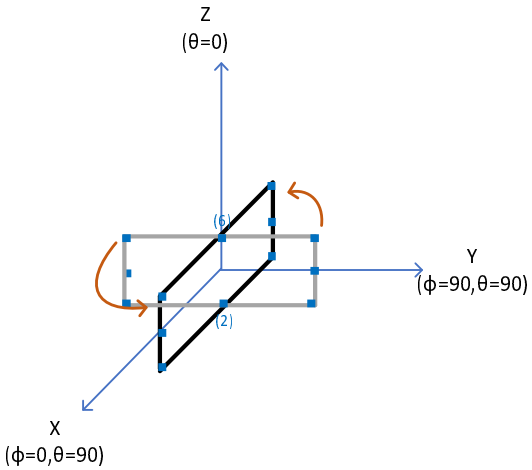

Figure 7.3-5: Example of UT rotation of $\Omega_{UT,\alpha}$ = 0 - 360 degrees, $\Omega_{UT,\beta}$ = 0 degrees, $\Omega_{UT,\gamma}$ = 90 degrees

- The antenna radiation power pattern of each antenna element for handheld UT is generated according to Table 7.3-2, which assumes antenna is oriented in $\theta'' = 90°$and $\phi'' = 0°$ direction.

Table 7.3-2: Radiation power pattern of a single antenna element for handheld UT

Parameter	Values
Vertical cut of the radiation power pattern (dB)	$A''_{\text{dB}}(\theta'',\ \phi''=0°) = -min\left\{12\left(\frac{\theta''-90°}{\theta_{\text{3dB}}}\right)^2, SLA_V\right\}$ with $\theta_{\text{3dB}}=125°, SLA_V=22.5$dB and $\theta'' \in [0°, 180°]$
Horizontal cut of the radiation power pattern (dB)	$A''_{\text{dB}}(\theta''=90°,\ \phi'') = -min\left\{12\left(\frac{\phi''}{\phi_{\text{3dB}}}\right)^2, A_{max}\right\}$ with $\phi_{\text{3dB}}=125°, A_{max}=22.5$ dB and $\phi'' \in$ [-180°, 180°]
3D radiation power pattern (dB)	$A''_{\text{dB}}(\theta'',\phi'') = -min\{-(A''_{\text{dB}}(\theta'',\ \phi''=0°) + A''_{\text{dB}}(\theta''=90°,\ \phi'')), A_{max}\}$
Maximum directional gain of an antenna element $G_{E,max}$	5.3 dBi
NOTE: For UT antenna modelling of handheld devices, optional antenna imbalance can be modelled. If modelled, randomized loss is applied per UT antenna port and randomized loss can be applied independently for the UL and DL directions. No imbalance is modelled by default.	

For consumer premise equipment (CPE) devices, the following properties apply:

- Total 9 candidate antenna locations in 4 corners of the vertical square plane, 4 center of the edges of the vertical square plane, and center of the vertical square plane. The figure below captures the side view on the device. Note that a candidate antenna location (e.g., 9) can be used for multiple antennas.
- Device dimensions for UT antenna modelling are (0 cm, 20 cm, 20 cm)

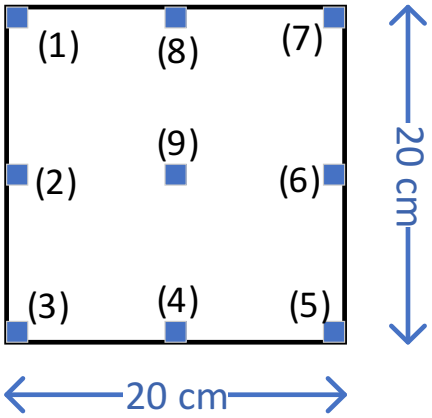

Figure 7.3-6: CPE UT antenna placement candidate locations relative to centre of device (side view)

7.3.1 Antenna port mapping

Legacy BS array antennas, i.e. uniform linear arrays with fix phase shifts between its *M* elements to obtain a beamtilt in vertical direction are modelled using complex weights

$$w_m = \frac{1}{\sqrt{M}} exp\left(-j\frac{2\pi}{\lambda}(m-1)d_V \cos\theta_{etilt}\right) \quad (7.3\text{-}1)$$

where *m=1, …, M*, θ_{etilt} is the electrical vertical steering angle defined between 0° and 180° (90° represents perpendicular to the array). λ denotes the wavelength and d_V the vertical element spacing.

7.3.2 Polarized antenna modelling

In general the relationship between radiation field and power pattern is given by:

$$A''(\theta'', \phi'') = \left|F''_{\theta''}(\theta'', \phi'')\right|^2 + \left|F''_{\phi''}(\theta'', \phi'')\right|^2. \quad (7.3\text{-}2)$$

The following two models represent two options on how to determine the radiation field patterns based on a defined radiation power pattern.

Model-1:

In case of polarized antenna elements assume ζ is the polarization slant angle where $\zeta = 0$ degrees corresponds to a purely vertically polarized antenna element and $\zeta = \pm 45$ degrees correspond to a pair of cross-polarized antenna elements. Then the antenna element field components in θ' and ϕ' direction are given by

$$\begin{pmatrix} F'_{\theta'}(\theta', \phi') \\ F'_{\phi'}(\theta', \phi') \end{pmatrix} = \begin{pmatrix} +\cos\psi & -\sin\psi \\ +\sin\psi & +\cos\psi \end{pmatrix} \begin{pmatrix} F''_{\theta''}(\theta'', \phi'') \\ F''_{\phi''}(\theta'', \phi'') \end{pmatrix}, \quad (7.3\text{-}3)$$

where

$$\cos\psi = \frac{\cos\zeta \sin\theta' + \sin\zeta \sin\phi' \cos\theta'}{\sqrt{1-(\cos\zeta \cos\theta' - \sin\zeta \sin\phi' \sin\theta')^2}}, \quad (7.3\text{-}3a)$$

$$\sin\psi = \frac{\sin\zeta \cos\phi'}{\sqrt{1-(\cos\zeta \cos\theta' - \sin\zeta \sin\phi' \sin\theta')^2}}. \quad (7.3\text{-}3b)$$

Note that the zenith and the azimuth field components $F'_{\theta'}(\theta', \phi')$, $F'_{\phi'}(\theta', \phi')$, $F''_{\theta''}(\theta'', \phi'')$ and $F''_{\phi''}(\theta'', \phi'')$ are defined in terms of the spherical basis vectors of an LCS as defined in Clause 7.1. The difference between the single-primed and the double-primed components is that the single-primed field components account for the polarization slant and the double-primed field components do not. For a single polarized antenna (purely vertically polarized antenna) we can write $F''_{\theta''}(\theta'', \phi'') = \sqrt{A''(\theta'', \phi'')}$, and $F''_{\phi''}(\theta'', \phi'') = 0$ where $A''(\theta'', \phi'')$, is the 3D antenna radiation power pattern as a function of azimuth angle ϕ'' and zenith angle θ'' in the LCS as defined in Table 7.3-1 converted into linear scale.

Model-2:

In case of polarized antennas, the polarization is modelled as angle-independent in both azimuth and elevation, in an LCS. For a linearly polarized antenna, the antenna element field pattern, in the vertical polarization and in the horizontal polarization, are given by

$$F'_{\theta'}(\theta', \phi') = \sqrt{A'(\theta', \phi')}\, cos(\zeta) \quad (7.3\text{-}4)$$

and

$$F'_{\phi'}(\theta', \phi') = \sqrt{A'(\theta', \phi')}\, sin(\zeta), \quad (7.3\text{-}5)$$

respectively, where ζ is the polarization slant angle and $A'(\theta', \phi')$ is the 3D antenna element power pattern as a function of azimuth angle, ϕ' and elevation angle, θ' in the LCS. Note that $\zeta = 0$ degrees correspond to a purely vertically polarized antenna element. The vertical and horizontal field directions are defined in terms of the spherical basis vectors, $\widehat{\theta'}$ and $\widehat{\phi'}$ respectively in the LCS as defined in Clause 7.1.2. Also $A'(\theta', \phi') = A''(\theta'', \phi'')$, $\theta' = \theta''$and $\phi' = \phi''$ as defined in Table 7.1-1.

Handheld UT Model:

For cases when a candidate antenna placement location is used for one antenna field pattern:

- Reference radiation pattern of the UT antenna model is vertically polarized with all the gain in the theta field component, $F''_{\theta''}(\theta'', \phi'') = \sqrt{A''(\theta'', \phi'')}$ and $F''_{\phi''}(\theta'', \phi'') = 0$, and referred to as the polarization direction along the Z'' axis.

For cases when a candidate antenna placement location is used for two distinct antenna polarization field patterns:

- Reference radiation pattern of the UT antenna model is,
  - For first antenna field pattern: $F''_{\theta''}(\theta'', \phi'') = \sqrt{A''(\theta'', \phi'')}$ and $F''_{\phi''}(\theta'', \phi'') = 0$.

- For second antenna field pattern: $F''_{\theta''}(\theta'', \phi'') = 0$ and $F''_{\phi''}(\theta'', \phi'') = \sqrt{A''(\theta'', \phi'')}$.

Each polarized field component of the reference radiation pattern $F''_{\theta''}(\theta'', \phi'')$ and $F''_{\phi''}(\theta'', \phi'')$ should be rotated according to the orientation and polarization direction of the each of UT antennae to get $F'_{u,\theta'}(\theta', \phi')$, $F'_{u,\phi'}(\theta', \phi')$ using equation

$$\begin{pmatrix} F'_{u,\theta'}(\theta', \phi') \\ F'_{u,\phi'}(\theta', \phi') \end{pmatrix} = \begin{pmatrix} +\cos\psi_u & -\sin\psi_u \\ +\sin\psi_u & +\cos\psi_u \end{pmatrix} \begin{pmatrix} F''_{\theta''}(\theta'', \phi'') \\ F''_{\phi''}(\theta'', \phi'') \end{pmatrix}, \quad (7.3\text{-}6)$$

$$\cos\psi_u = \frac{\cos\beta_u \cos\gamma_u \sin\theta' - (\sin\beta_u \cos\gamma_u \cos(\phi' - \alpha_u) - \sin\gamma_u \sin(\phi' - \alpha_u)) \cos\theta'}{\sqrt{1 - (\cos\beta_u \cos\gamma_u \cos\theta' + (\sin\beta_u \cos\gamma_u \cos(\phi' - \alpha_u) - \sin\gamma_u \sin(\phi' - \alpha_u)) \sin\theta')^2}}, \quad (7.3\text{-}7)$$

$$\sin\psi_u = \frac{\sin\beta_u \cos\gamma_u \sin(\phi' - \alpha_u) + \sin\gamma_u \cos(\phi' - \alpha_u)}{\sqrt{1 - (\cos\beta_u \cos\gamma_u \cos\theta' + (\sin\beta_u \cos\gamma_u \cos(\phi' - \alpha_u) - \sin\gamma_u \sin(\phi' - \alpha_u)) \sin\theta')^2}}, \quad (7.3\text{-}8)$$

where the 3D-rotation angles, α_u, β_u and γ_u, are obtained according to the orientation and polarization direction of each UT antenna u, the zenith and azimuth angles mapping between (θ', ϕ') and (θ'', ϕ'') are based on equations (7.1-7) and (7.1-8) using the same 3D-rotation angles, α_u, β_u and γ_u, and rotated based on the orientation of the UT in the global coordinate system to get $F_{u,\theta}(\theta, \phi)$ and $F_{u,\phi}(\theta, \phi)$ using Clause 7.1.3 equation (7.1-11).

Note: The angle ψ_u can be computed in numerous ways following equation (7.1-10) in Clause 7.1.3, also to avoid possible division by 0 in equations (7.3-7) and (7.3-8).

For cases when a candidate antenna placement location is used for one antenna field pattern (e.g., single polarization):

- The polarization direction is indicated by the arrow in Figure 7.3-7, which is parallel with the plane of the handheld UT and perpendicular to the direction from the UT center to the candidate antenna location.

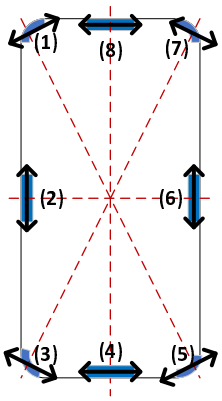

Figure 7.3-7: Handheld UT antenna polarization directions for one antenna field pattern (top down view)

For cases when a candidate antenna placement location is used for two antenna field patterns (e.g., dual polarization) (not intended for FR1):

- For the first antenna field pattern, the polarization direction is indicated by the arrows in Figure 7.3-7 but additionally rotated 45 degrees about the direction from the UT center to the candidate antenna location (i.e. rotated using the direction from the UT center to the candidate antenna location as the rotational axis).
- For the second antenna field pattern, the polarization direction is perpendicular to the polarization direction of the first filed pattern and perpendicular to the direction from the UT center to the candidate antenna location
- An example for candidate antenna location (6) is given in Figure 7.3-8.

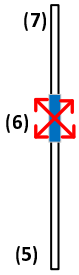

Figure 7.3-8: Handheld UT polarization direction for two antenna filed pattern (side view)

7.4 Pathloss, LOS probability and penetration modelling

7.4.1 Pathloss

The pathloss models are summarized in Table 7.4.1-1 and the distance definitions are indicated in Figure 7.4.1-1 and Figure 7.4.1-2. Note that the distribution of the shadow fading is log-normal, and its standard deviation for each scenario is given in Table 7.4.1-1.

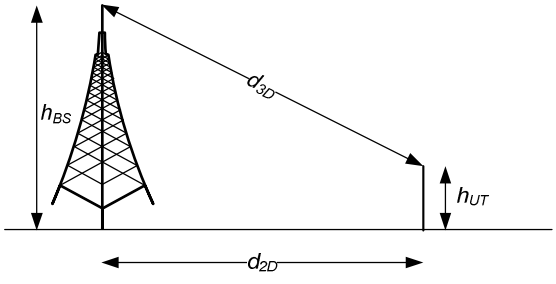

Figure7.4.1-1: Definition of d_{2D} and d_{3D} for outdoor UTs

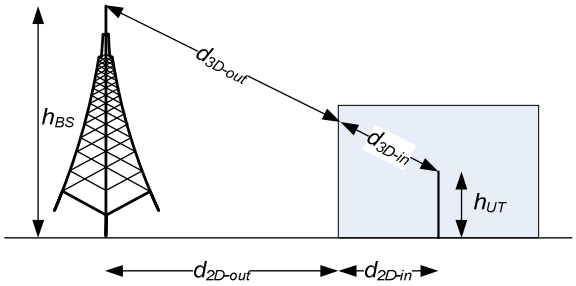

Figure 7.4.1-2: Definition of $d_{2D\text{-}out}$, $d_{2D\text{-}in}$ and $d_{3D\text{-}out}$, $d_{3D\text{-}in}$ for indoor UTs.

Note that

$$d_{\mathrm{3D-out}} + d_{\mathrm{3D-in}} = \sqrt{\left(d_{\mathrm{2D-out}} + d_{\mathrm{2D-in}}\right)^2 + \left(h_{\mathrm{BS}} - h_{\mathrm{UT}}\right)^2} \quad (7.4\text{-}1)$$

Table 7.4.1-1: Pathloss models

Scenario	LOS/NLOS	Pathloss [dB], f_c is in GHz and d is in meters, see note 6	Shadow fading std [dB]	Applicability range, antenna height default values
RMa	LOS	$PL_{\text{RMa-LOS}} = \begin{cases} PL_1 & 10m \le d_{\text{2D}} \le d_{\text{BP}} \\ PL_2 & d_{\text{BP}} \le d_{\text{2D}} \le 10\text{km} \end{cases}$, see note 5 $PL_1 = 20\log_{10}(40\pi d_{\text{3D}} f_c/3) + min(0.03h^{1.72}, 10)\log_{10}(d_{\text{3D}}) - min(0.044h^{1.72}, 14.77) + 0.002\log_{10}(h)d_{\text{3D}}$ $PL_2 = PL_1(d_{\text{BP}}) + 40\log_{10}(d_{\text{3D}}/d_{\text{BP}})$	For 10 m ≤ d_{2D} < d_{BP}, $\sigma_{SF} = 4$ For d_{BP} ≤ d_{2D} < 10 km, $\sigma_{SF} = 6$	$h_{\text{BS}} = 35\text{m}$ $h_{\text{UT}} = 1.5m$ $W = 20m$ $h = 5m$ h = avg. building height W = avg. street width The applicability ranges: $5m \le h \le 50m$ $5m \le W \le 50m$ $10\text{m} \le h_{\text{BS}} \le 150m$ $1m \le h_{\text{UT}} \le 10m$
	NLOS	$PL_{\text{RMa-NLOS}} = max(PL_{\text{RMa-LOS}}, PL'_{\text{RMa-NLOS}})$, for $10m \le d_{\text{2D}} \le 5\text{km}$ $PL'_{\text{RMa-NLOS}} = 161.04 - 7.1\log_{10}(W) + 7.5\log_{10}(h) - (24.37 - 3.7(h/h_{\text{BS}})^2)\log_{10}(h_{\text{BS}}) + (43.42 - 3.1\log_{10}(h_{\text{BS}}))(\log_{10}(d_{\text{3D}}) - 3) + 20\log_{10}(f_c) - (3.2(\log_{10}(11.75h_{\text{UT}}))^2 - 4.97)$	$\sigma_{\text{SF}} = 8$	
UMa	LOS	$PL_{\text{UMa-LOS}} = \begin{cases} PL_1 & 10m \le d_{\text{2D}} \le d'_{\text{BP}} \\ PL_2 & d'_{\text{BP}} \le d_{\text{2D}} \le 5\text{km} \end{cases}$, see note 1 $PL_1 = 28.0 + 22\log_{10}(d_{\text{3D}}) + 20\log_{10}(f_c)$ $PL_2 = 28.0 + 40\log_{10}(d_{\text{3D}}) + 20\log_{10}(f_c) - 9\log_{10}((d'_{\text{BP}})^2 + (h_{\text{BS}} - h_{\text{UT}})^2)$	$\sigma_{\text{SF}} = 4$	$1.5m \le h_{\text{UT}} \le 22.5m$ $h_{\text{BS}} = 25\text{m}$ See note 7
	NLOS	$PL_{\text{UMa-NLOS}} = max(PL_{\text{UMa-LOS}}, PL'_{\text{UMa-NLOS}})$, for $10m \le d_{\text{2D}} \le 5\text{km}$ $PL'_{\text{UMa-NLOS}} = 13.54 + 39.08\log_{10}(d_{\text{3D}}) + 20\log_{10}(f_c) - 0.6(h_{\text{UT}} - 1.5)$	$\sigma_{\text{SF}} = 6$	$1.5m \le h_{\text{UT}} \le 22.5m$ $h_{\text{BS}} = 25\text{m}$ Explanations: see note 3
		Optional $PL_{\text{UMa-NLOS}} = 32.4 + 20\log_{10}(f_c) + 30\log_{10}(d_{\text{3D}})$	$\sigma_{\text{SF}} = 7.8$	
UMi - Street Canyon	LOS	$PL_{\text{UMi-LOS}} = \begin{cases} PL_1 & 10m \le d_{\text{2D}} \le d'_{\text{BP}} \\ PL_2 & d'_{\text{BP}} \le d_{\text{2D}} \le 5\text{km} \end{cases}$, see note 1 $PL_1 = 32.4 + 21\log_{10}(d_{\text{3D}}) + 20\log_{10}(f_c)$ $PL_2 = 32.4 + 40\log_{10}(d_{\text{3D}}) + 20\log_{10}(f_c) - 9.5\log_{10}((d'_{\text{BP}})^2 + (h_{\text{BS}} - h_{\text{UT}})^2)$	$\sigma_{\text{SF}} = 4$	$1.5m \le h_{\text{UT}} \le 22.5m$ $h_{\text{BS}} = 10m$ See note 7
	NLOS	$PL_{\text{UMi-NLOS}} = max(PL_{\text{UMi-LOS}}, PL'_{\text{UMi-NLOS}})$, for $10m \le d_{\text{2D}} \le 5\text{km}$ $PL'_{\text{UMi-NLOS}} = 35.3\log_{10}(d_{\text{3D}}) + 22.4 + 21.3\log_{10}(f_c) - 0.3(h_{\text{UT}} - 1.5)$	$\sigma_{\text{SF}} = 7.82$	$1.5m \le h_{\text{UT}} \le 22.5m$ $h_{\text{BS}} = 10m$ Explanations: see note 4
		Optional $PL_{\text{UMi-NLOS}} = 32.4 + 20\log_{10}(f_c) + 31.9\log_{10}(d_{\text{3D}})$	$\sigma_{\text{SF}} = 8.2$	
InH - Office	LOS	$PL_{\text{InH-LOS}} = 32.4 + 17.3\log_{10}(d_{\text{3D}}) + 20\log_{10}(f_c)$	$\sigma_{\text{SF}} = 3$	$1m \le d_{\text{3D}} \le 150m$
	NLOS	$PL_{\text{InH-NLOS}} = max(PL_{\text{InH-LOS}}, PL'_{\text{InH-NLOS}})$ $PL'_{\text{InH-NLOS}} = 38.3\log_{10}(d_{\text{3D}}) + 17.30 + 24.9\log_{10}(f_c)$	$\sigma_{\text{SF}} = 8.03$	$1m \le d_{\text{3D}} \le 150m$
		Optional $PL'_{\text{InH-NLOS}} = 32.4 + 20\log_{10}(f_c) + 31.9\log_{10}(d_{\text{3D}})$	$\sigma_{\text{SF}} = 8.29$	$1m \le d_{\text{3D}} \le 150m$

Scenario	LOS/NLOS	Pathloss [dB], f_c is in GHz and d is in meters, see note 6	Shadow fading std [dB]	Applicability range, antenna height default values
InF	LOS	$PL_{LOS} = 31.84 + 21.50\log_{10}(d_{3D}) + 19.00\log_{10}(f_c)$	$\sigma_{SF} = 4.3$	$1 \le d_{3D} \le 600\ m$
	NLOS	InF-SL: $PL = 33 + 25.5\log_{10}(d_{3D}) + 20\log_{10}(f_c)$ $PL_{NLOS} = \max(PL, PL_{LOS})$	$\sigma_{SF} = 5.7$	
		InF-DL: $PL = 18.6 + 35.7\log_{10}(d_{3D}) + 20\log_{10}(f_c)$ $PL_{NLOS} = \max(PL, PL_{LOS}, PL_{InF-SL})$	$\sigma_{SF} = 7.2$	
		InF-SH: $PL = 32.4 + 23.0\log_{10}(d_{3D}) + 20\log_{10}(f_c)$ $PL_{NLOS} = \max(PL, PL_{LOS})$	$\sigma_{SF} = 5.9$	
		InF-DH: $PL = 33.63 + 21.9\log_{10}(d_{3D}) + 20\log_{10}(f_c)$ $PL_{NLOS} = \max(PL, PL_{LOS})$	$\sigma_{SF} = 4.0$	
SMa	LOS	$PL_{\text{SMa-LOS}} = \begin{cases} PL_1 & 10m \le d_{2D} < d_{BP} \\ PL_2 & d_{BP} \le d_{2D} \le 5\text{km'} \end{cases}$ $PL_1 = 20\log_{10}(40\pi d_{3D}\, f_c/3) + \min(0.03h^{1.72}, 10)\log_{10}(d_{3D}) - \min(0.044h^{1.72}, 14.77) + 0.002\log_{10}(h)d_{3D}$, see note 5 $PL_2 = PL_1(d_{BP}) + 40\log_{10}(d_{3D}/d_{BP})$, see note 5	For 10 m ≤ d_{2D} < d_{BP}, $\sigma_{SF} = 4$ For d_{BP} ≤ d_{2D} < 5000 m, $\sigma_{SF} = 6$	10 m ≤ d_{2D} < d_{BP} d_{BP} ≤ d_{2D} < 5000 m 25 m < h_{BS} < 35 m h = 10 m
	NLOS	$PL_{\text{SMa-NLOS}} = 161.04 - 7.1\log_{10}(W) + 7.5\log_{10}(h) - (24.37 - 3.7(h/h_{BS})^2)\log_{10}(h_{BS}) + (43.42 - 3.1\log_{10}(h_{BS}))(\log_{10}(d_{3D}) - 3) + 20\log_{10}(f_c) - (3.2(\log_{10}(11.75h_{UT}))^2 - 4.97)$	$\sigma_{SF} = 8$	10 m ≤ d_{2D} < 5000 m 1 m < h_{UT} < 14 m h = 10 m, W = 10 m

Scenario	LOS/NLOS	Pathloss [dB], f_c is in GHz and d is in meters, see note 6	Shadow fading std [dB]	Applicability range, antenna height default values

NOTE 1: Effective breakpoint distance $d'_{BP} = 4\,h'_{BS}\,h'_{UT}\,f_c/c$, where f_c is the centre frequency in Hz, $c = 3.0\times10^8$ m/s is the propagation velocity in free space, and h'_{BS} and h'_{UT} are the effective antenna heights at the BS and the UT, respectively. The effective antenna heights h'_{BS} and h'_{UT} are computed as follows: $h'_{BS} = h_{BS} - h_E$, $h'_{UT} = h_{UT} - h_E$, where h_{BS} and h_{UT} are the actual antenna heights, and h_E is the effective environment height. For UMi $h_E = 1.0$m. For UMa h_E=1m with a probability equal to 1/(1+C(d_{2D}, h_{UT})) and chosen from a discrete uniform distribution uniform(12,15,…,(h_{UT}-1.5)) otherwise. With C(d_{2D}, h_{UT}) given by

$$C(d_{2D}, h_{UT}) = \begin{cases} 0 & , h_{UT} < 13m \\ \left(\frac{h_{UT}-13}{10}\right)^{1.5} g(d_{2D}) & , 13m \le h_{UT} \le 23m \end{cases},$$

where

$$g(d_{2D}) = \begin{cases} 0 & , d_{2D} \le 18m \\ \frac{5}{4}\left(\frac{d_{2D}}{100}\right)^3 exp\left(\frac{-d_{2D}}{150}\right) & , 18m < d_{2D} \end{cases}.$$

Note that h_E depends on d_{2D} and h_{UT} and thus needs to be independently determined for every link between BS sites and UTs. A BS site may be a single BS or multiple co-located BSs.

NOTE 2: The applicable frequency range of the PL formula in this table is $0.5 < f_c < f_H$ GHz, where f_H = 30 GHz for RMa, f_H = 37 GHz for SMa, and f_H = 100 GHz for all the other scenarios. It is noted that RMa pathloss model for >7 GHz is validated based on a single measurement campaign conducted at 24 GHz.

NOTE 3: UMa NLOS pathloss is from TR36.873 with simplified format and $PL_{UMa\text{-}LOS}$ = Pathloss of UMa LOS outdoor scenario.

NOTE 4: $PL_{UMi\text{-}LOS}$ = Pathloss of UMi-Street Canyon LOS outdoor scenario.

NOTE 5: Break point distance $d_{BP} = 2\pi\, h_{BS}\, h_{UT}\, f_c/c$, where f_c is the centre frequency in Hz, $c = 3.0 \times 10^8$ m/s is the propagation velocity in free space, and h_{BS} and h_{UT} are the antenna heights at the BS and the UT, respectively.

NOTE 6: f_c denotes the center frequency normalized by 1GHz, all distance related values are normalized by 1m, unless it is stated otherwise.

NOTE 7: UMi and UMa pathloss formula converges for different frequencies when distances beyond the breakpoint distance is applied.

7.4.2 LOS probability

The Line-Of-Sight (LOS) probabilities are given in Table 7.4.2-1.

Table 7.4.2-1 LOS probability

Scenario	LOS probability (distance is in meters)
RMa	$\Pr_{LOS} = \begin{cases} 1 & , d_{2D\text{-}out} \le 10\text{m} \\ \exp\left(-\frac{d_{2D\text{-}out} - 10}{1000}\right) & , 10\text{m} < d_{2D\text{-}out} \end{cases}$
UMi - Street canyon	$\Pr_{LOS} = \begin{cases} 1 & , d_{2D\text{-}out} \le 18\text{m} \\ \frac{18}{d_{2D\text{-}out}} + \exp\left(-\frac{d_{2D\text{-}out}}{36}\right)\left(1 - \frac{18}{d_{2D\text{-}out}}\right) & , 18\text{m} < d_{2D\text{-}out} \end{cases}$
UMa	$\Pr_{LOS} = \begin{cases} 1 & , d_{2D\text{-}out} \le 18\text{m} \\ \left[\frac{18}{d_{2D\text{-}out}} + \exp\left(-\frac{d_{2D\text{-}out}}{63}\right)\left(1 - \frac{18}{d_{2D\text{-}out}}\right)\right]\left(1 + C'(h_{UT})\frac{5}{4}\left(\frac{d_{2D\text{-}out}}{100}\right)^3 \exp\left(-\frac{d_{2D\text{-}out}}{150}\right)\right) & , 18\text{m} < d_{2D\text{-}out} \end{cases}$ where $C'(h_{UT}) = \begin{cases} 0 & , h_{UT} \le 13\text{m} \\ \left(\frac{h_{UT} - 13}{10}\right)^{1.5} & , 13\text{m} < h_{UT} \le 23\text{m} \end{cases}$

Indoor - Mixed office	$\Pr_{\text{LOS}} = \begin{cases} 1 & ,d_{\text{2D-in}} \le 1.2\text{m} \\ \exp\left(-\frac{d_{\text{2D-in}} - 1.2}{4.7}\right) & ,1.2\text{m} < d_{\text{2D-in}} < 6.5\text{m} \\ \exp\left(-\frac{d_{\text{2D-in}} - 6.5}{32.6}\right) \cdot 0.32 & ,6.5\text{m} \le d_{\text{2D-in}} \end{cases}$
Indoor - Open office	$\Pr_{\text{LOS}} = \begin{cases} 1 & ,d_{\text{2D-in}} \le 5\text{m} \\ \exp\left(-\frac{d_{\text{2D-in}} - 5}{70.8}\right) & ,5\text{m} < d_{\text{2D-in}} \le 49\text{m} \\ \exp\left(-\frac{d_{\text{2D-in}} - 49}{211.7}\right) \cdot 0.54 & ,49\text{m} < d_{\text{2D-in}} \end{cases}$
InF-SL InF-SH InF-DL InF-DH	$\Pr_{\text{LOS,subsce}}(d_{\text{2D}}) = \exp\left(-\frac{d_{\text{2D}}}{k_{\text{subsce}}}\right)$ where $k_{subsce} = \begin{cases} -\frac{d_{clutter}}{\ln(1-r)} & \text{for InF-SL and InF-DL} \\ -\frac{d_{clutter}}{\ln(1-r)} \cdot \frac{h_{BS} - h_{UT}}{h_c - h_{UT}} & \text{for InF-SH and InF-DH} \end{cases}$ The parameters $d_{clutter}$, r, and h_c are defined in Table 7.2-4
InF-HH	$\Pr_{\text{LOS}} = 1$
SMa	$P_{\text{LOS}} = \begin{cases} 1, & d_{\text{2D-out}} \le 10\,m \\ \exp\left(-\frac{d_{\text{2D-out}}}{k_{\text{commercial}}}\right)\exp\left(-\frac{d_{\text{2D-out}}}{k_{\text{residential}}}\right)\exp\left(-\frac{d_{\text{2D-out}}}{k_{\text{vegetation}}}\right), & d_{\text{2D-out}} > 10\,m \end{cases}$ where $\frac{1}{\text{k}_{\text{commercial}}} = -\frac{\ln(1 - r_{\text{commericial}})}{d_{\text{clutter}}} \cdot \frac{h_{\text{commercial}} - h_{\text{UT}}}{h_{\text{BS}} - h_{\text{UT}}}$ $\frac{1}{k_{\text{residential}}} = -\frac{\ln(1 - r_{\text{residential}})}{d_{\text{clutter}}} \cdot \frac{\max(h_{\text{residential}} - h_{\text{UT}}, 0)}{h_{\text{BS}} - h_{\text{UT}}}$ $\frac{1}{k_{\text{vegetation}}} = -\frac{\ln(1 - r_{\text{vegetation}})}{d_{\text{clutter}}} \cdot \frac{h_{\text{vegetation}} - h_{\text{UT}}}{h_{\text{BS}} - h_{\text{UT}}}$ $d_{\text{clutter}} = 30\,m$, $h_{\text{commercial}}$ = 20 m, $h_{\text{residential}}$ = 8 m, $h_{\text{vegetation}}$ = 15 m $r_{\text{commericial}} = 2\%$, $r_{\text{residential}} = 18\%$, $r_{\text{vegetation}}$ =0% (no vegetation), 10% (sparse vegetation), or 20% (dense vegetation)
NOTE: The LOS probability is derived with assuming antenna heights of 3m for indoor, 10m for UMi, and 25m for UMa	

7.4.3 O2I penetration loss

7.4.3.1 O2I building penetration loss

The pathloss incorporating O2I building penetration loss is modelled as in the following:

$$\text{PL} = \text{PL}_b + \text{PL}_{\text{tw}} + \text{PL}_{\text{in}} + N(0, \sigma_P^2) \quad (7.4\text{-}2)$$

where PL_b is the basic outdoor path loss given in Clause 7.4.1, where d_{3D} is replaced by $d_{\text{3D-out}} + d_{\text{3D-in}}$. PL_{tw} is the building penetration loss through the external wall, PL_{in} is the inside loss dependent on the depth into the building, and σ_P is the standard deviation for the penetration loss.

PL_{tw} is characterized as:

$$PL_{tw} = PL_{npi} - 10\,log_{10}\sum_{i=1}^{N}\left(p_i \times 10^{\frac{L_{material_i}}{-10}}\right) \quad (7.4\text{-}3)$$

PL_{npi} is an additional loss is added to the external wall loss to account for non-perpendicular incidence; $L_{material_i} = a_{material_i} + b_{material_i} \cdot f$, is the penetration loss of material *i*, example values of which can be found in Table 7.4.3-1; p_i is proportion of *i*-th materials, where $\sum_{i=1}^{N} p_i = 1$; and *N* is the number of materials.

Table 7.4.3-1: Material penetration losses

Material	Penetration loss [dB]	Notes on Material
Standard multi-pane glass	$L_{\text{glass}} = 2 + 0.2f$	Reference thickness of 3 cm assumed
IRR glass	$L_{\text{IRRglass}} = 25.4 + 0.11f$, see note 2	Single coating is assumed
Concrete	$L_{\text{concrete}} = 5 + 4f$	Reference thickness of 23 cm assumed
Plywood	$L_{\text{plywood}} = 1.03 + 0.17f$	Reference thickness of 1.75 cm assumed
Wood	$L_{\text{wood}} = 4.85 + 0.12f$	Reference thickness of 3.3 cm assumed
NOTE 1: f is in GHz NOTE 2: Values marked with this note were updated as part of Release 19 Study on channel modelling enhancements for 7-24 GHz for NR.		

Table 7.4.3-2 gives PL_{tw}, PL_{in} and σ_P for two O2I penetration loss models. The O2I penetration is UT-specifically generated, and is added to the SF realization in the log domain.

Table 7.4.3-2: O2I building penetration loss model

	Path loss through external wall: PL_{tw} in [dB]	Indoor loss: PL_{in} in [dB]	Standard deviation: σ_P in [dB]
Low-loss model	$5 - 10\,log_{10}\left(0.3 \cdot 10^{\frac{-L_{\text{glass}}}{10}} + 0.7 \cdot 10^{\frac{-L_{\text{concrete}}}{10}}\right)$	0.5 d_{2D-in}	4.4
High-loss model	$5 - 10\,log_{10}\left(0.7 \cdot 10^{\frac{-L_{\text{IRRglass}}}{10}} + 0.3 \cdot 10^{\frac{-L_{\text{concrete}}}{10}}\right)$	0.5 d_{2D-in}	6.5
Low-loss A model	$5 - 10\log_{10}\left(0.3 \cdot 10^{\frac{-L_{\text{glass}}}{10}} + 0.7 \cdot 10^{\frac{-L_{\text{plywood}}}{10}}\right)$	0.5 d_{2D-in}	4.4

d_{2D-in} is minimum of two independently generated uniformly distributed variables between 0 and 25 m for UMa and UMi-Street Canyon, between 0 and 25 m for SMa UTs in commercials buildings, between 0 and 10 m for SMa UTs in residential buildings, and between 0 and 10 m for RMa. d_{2D-in} shall be UT-specifically generated.

Both low-loss and high-loss models are applicable to UMa and UMi-Street Canyon.

Only the low-loss model is applicable to RMa.

Only the high-loss model is applicable to InF.

Low-loss, high-loss, and low-loss A models are applicable to SMa.

The composition of low and high loss is a simulation parameter that should be determined by the user of the channel models, and is dependent on the use of metal-coated glass in buildings and the deployment scenarios. Such use is expected to differ in different markets and regions of the world and also may increase over years to new regulations and energy saving initiatives. Furthermore, the use of such high-loss glass currently appears to be more predominant in commercial buildings than in residential buildings in some regions of the world (see note).

Note: One example survey for the US market can be found in [5]. The survey does not necessarily be representative for all the scenarios. Other ratios outside of the survey should not be precluded.

For backwards compatibility with TR 36.873 [3], the following building penetration model should be used for UMa and UMi single-frequency simulations at frequencies below 6 GHz.

Table 7.4.3-3. O2I building penetration loss model for single-frequency simulations <6 GHz

Parameter	Value
PL_{tw}	20 dB
PL_{in}	0.5 d_{2D-in} with d_{2D-in} being *a single, link-specific,* uniformly distributed variable between 0 and 25 m
σ_P	0 dB
σ_{SF}	7 dB (note: replacing the respective value in Table 7.4.1-1)

7.4.3.2 O2I car penetration loss

The pathloss incorporating O2I car penetration loss is modelled as in the following:

$$\mathrm{PL} = \mathrm{PL}_{\mathrm{b}} + N\left(\mu, \sigma_P^2\right) \quad (7.4\text{-}4)$$

where PL_{b} is the basic outdoor path loss given in Clause 7.4.1. μ = 9, and σ_P = 5. The car penetration loss shall be UT-specifically generated. Optionally, for metallized car windows, μ = 20 can be used. The O2I car penetration loss models are applicable for at least 0.6-60 GHz.

7.4.4 Autocorrelation of shadow fading

The long-term (log-normal) fading in the logarithmic scale around the mean path loss *PL* (dB) is characterized by a Gaussian distribution with zero mean and standard deviation. Due to the slow fading process versus distance Δx (Δx is in the horizontal plane), adjacent fading values are correlated. Its normalized autocorrelation function $R(\Delta x)$ can be described with sufficient accuracy by the exponential function ITU-R Rec. P.1816 [18]

$$R(\Delta x) = \mathrm{e}^{-\frac{|\Delta x|}{d_{cor}}} \quad (7.4\text{-}5)$$

with the correlation length d_{cor} being dependent on the environment, see the correlation parameters for shadowing and other large scale parameters in Table 7.5-6 (Channel model parameters). In a spatial consistency procedure in Clause 7.6.3, the cluster specific random variables are also correlated following the exponential function with respect to correlation distances in the two dimensional horizontal plane.

7.5 Fast fading model

The radio channel realizations are created using the parameters listed in Table 7.5-1. The channel realizations are obtained by a step-wise procedure illustrated in Figure 7.5-1 and described below. It has to be noted that the geometric description covers arrival angles from the last bounce scatterers and respectively departure angles to the first scatterers interacted from the transmitting side. The propagation between the first and the last interaction is not defined. Thus, this approach can model also multiple interactions with the scattering media. This indicates also that e.g., the delay of a multipath component cannot be determined by the geometry. In the following steps, downlink is assumed. For uplink,it is assumed that BS receives with antenna element *s* and UT transmits with antenna element *u*. If UT transmits and receives with same antenna element *u* and BS transmits and receives with same antenna element *s*, use the downlink channel impulse response between transmit antenna element *s* and receive antenna element *u* for uplink, under ideal reciprocity condition.

Note: the channel generation in this clause is enough for at least the following cases.

- Case 1: For low complexity evaluations
- Case 2: To compare with earlier simulation results,
- Case 3: When none of the additional modelling components are turned on.

For other advanced simulations, e.g., spatially consistency, large bandwidth and arrays, oxygen absorption, blockage, absolute time of arrival, dual mobility, embedded devices, etc., some of the additional modelling components of Clause 7.6 should be considered.

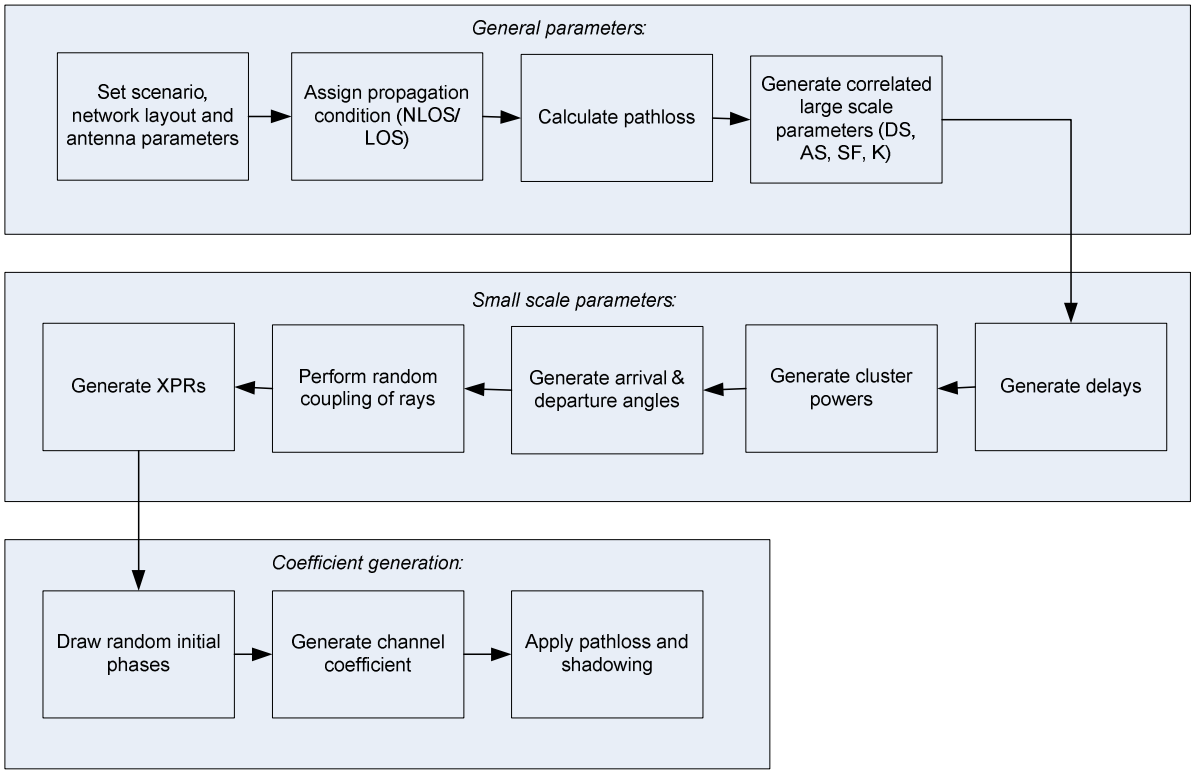

Figure 7.5-1 Channel coefficient generation procedure

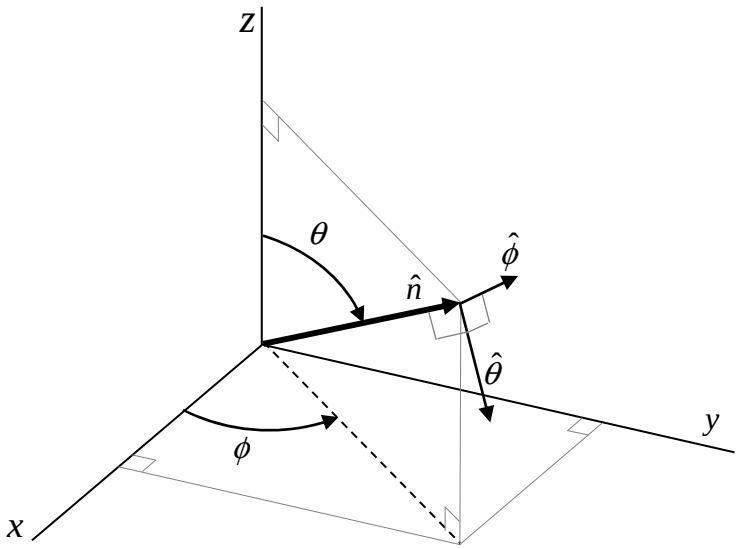

Figure 7.5-2: Definition of a global coordinate system showing the zenith angle θ and the azimuth angle ϕ. θ=0° points to zenith and θ=+90° points to the horizon.
The spherical basis vectors $\hat{\theta}$ and $\hat{\phi}$ shown above are defined based on the direction of propagation $\hat{n}$.

Table 7.5-1: Notations in the global coordinate system (GCS)

Parameter	Notation
LOS AOD	$\phi_{LOS,AOD}$
LOS AOA	$\phi_{LOS,AOA}$
LOS ZOD	$\theta_{LOS,ZOD}$
LOS ZOA	$\theta_{LOS,ZOA}$
AOA for cluster *n*	$\phi_{n,AOA}$
AOD for cluster *n*	$\phi_{n,AOD}$
AOA for ray *m* in cluster *n*	$\phi_{n,m,AOA}$
AOD for ray *m* in cluster *n*	$\phi_{n,m,AOD}$
ZOA for cluster *n*	$\theta_{n,ZOA}$
ZOD for cluster *n*	$\theta_{n,ZOD}$
ZOA for ray *m* in cluster *n*	$\theta_{n,m,ZOA}$
ZOD for ray *m* in cluster *n*	$\theta_{n,m,ZOD}$
Receive antenna element *u* field pattern in the direction of the spherical basis vector $\hat{\theta}$	$F_{rx,u,\theta}$
Receive antenna element *u* field pattern in the direction of the spherical basis vector $\hat{\phi}$	$F_{rx,u,\phi}$
Transmit antenna element *s* field pattern in the direction of the spherical basis vector $\hat{\theta}$	$F_{tx,s,\theta}$
Transmit antenna element *s* field pattern in the direction of the spherical basis vector $\hat{\phi}$	$F_{rx,s,\phi}$

Step 1: Set environment, network layout, and antenna array parameters

a) Choose one of the scenarios (e.g. UMa, UMi-Street Canyon, RMa, InH-Office or InF). Choose a global coordinate system and define zenith angle θ, azimuth angle ϕ, and spherical basis vectors $\hat{\theta}$, $\hat{\phi}$ as shown in Figure 7.5-2. Note: Scenario RMa is for up to 7GHz while others are for up to 100GHz

b) Give number of BS and UT

c) Give 3D locations of BS and UT, and determine LOS AOD ($\phi_{LOS,AOD}$), LOS ZOD ($\theta_{LOS,ZOD}$), LOS AOA ($\phi_{LOS,AOA}$), and LOS ZOA ($\theta_{LOS,ZOA}$) of each BS and UT in the global coordinate system

d) Give BS and UT antenna field patterns F_{rx} and F_{tx} in the global coordinate system and array geometries

e) Give BS and UT orientations with respect to the global coordinate system. BS array orientation is defined by three angles $\Omega_{BS,\alpha}$ (BS bearing angle), $\Omega_{BS,\beta}$ (BS downtilt angle) and $\Omega_{BS,\gamma}$ (BS slant angle). UT orientation is defined by three angles $\Omega_{UT,\alpha}$ (UT bearing angle), $\Omega_{UT,\beta}$ (UT downtilt angle) and $\Omega_{UT,\gamma}$ (UT slant angle).

f) Give speed and direction of motion of UT in the global coordinate system

g) Specify system centre frequency f_c and bandwidth B

Note: In case wrapping is used, each wrapping copy of a BS or site should be treated as a separate BS/site considering channel generation.

Large scale parameters:

Step 2: Assign propagation condition (LOS/NLOS) according to Table 7.4.2-1. The propagation conditions for different BS-UT links are uncorrelated.

Also, assign an indoor/outdoor state for each UT. It is noted that all the links from a UT have the same indoor/outdoor state.

Step 3: Calculate pathloss with formulas in Table 7.4.1-1 for each BS-UT link to be modelled.

Step 4: Generate large scale parameters, e.g. delay spread (DS), angular spreads (ASA, ASD, ZSA, ZSD), Ricean K factor (K) and shadow fading (SF) taking into account cross correlation according to Table 7.5-6 and using the procedure described in clause 3.3.1 of [14] with the square root matrix $\sqrt{C_{MxM}(0)}$ being generated using the Cholesky decomposition and the following order of the large scale parameter vector: $\mathbf{s}_M = [s_{SF}, s_K, s_{DS}, s_{ASD}, s_{ASA}, s_{ZSD}, s_{ZSA}]^T$.

These LSPs for different BS-UT links are uncorrelated, but the LSPs for links from co-sited sectors to a UT are the same. In addition, these LSPs for the links of UTs on different floors are uncorrelated.

Limit random RMS azimuth arrival and azimuth departure spread values to 104 degrees, i.e., ASA= min(ASA, 104°), ASD = min(ASD, 104°). Limit random RMS zenith arrival and zenith departure spread values to 52 degrees, i.e., ZSA = min(ZSA, 52°), ZSD = min(ZSD, 52°).

Small scale parameters:

Step 5: Generate cluster delays τ_n.

Delays are drawn randomly from the delay distribution defined in Table 7.5-6. With exponential delay distribution calculate

$$\tau_n' = -r_\tau \mathrm{DS} \ln(X_n), \tag{7.5-1}$$

Where r_τ is the delay distribution proportionality factor, $X_n \sim$ uniform(0,1), and cluster index $n = 1,\ldots,N$. With uniform delay distribution the delay values τ_n' are drawn from the corresponding range. Normalise the delays by subtracting the minimum delay and sort the normalised delays to ascending order:

$$\tau_n = \mathrm{sort}(\tau_n' - \min(\tau_n')). \tag{7.5-2}$$

In the case of LOS condition, additional scaling of delays is required to compensate for the effect of LOS peak addition to the delay spread. The heuristically determined Ricean K-factor dependent scaling constant is

$$C_\tau = 0.7705 - 0.0433K + 0.0002K^2 + 0.000017K^3, \tag{7.5-3}$$

where K [dB] is the Ricean K-factor as generated in Step 4. The scaled delays

$$\tau_n^{LOS} = \tau_n / C_\tau, \tag{7.5-4}$$

are **not** to be used in cluster power generation.

Step 6: Generate cluster powers P_n.

Cluster powers are calculated assuming a single slope exponential power delay profile. Power assignment depends on the delay distribution defined in Table 7.5-6. With exponential delay distribution the cluster powers are determined by

$$P_n' = \exp\left(-\tau_n \frac{r_\tau - 1}{r_\tau \mathrm{DS}}\right) \cdot 10^{\frac{-Z_n}{10}} \tag{7.5-5}$$

where $Z_n \sim N(0, \zeta^2)$ is the per cluster shadowing term in [dB]. Normalize the cluster powers so that the sum of all cluster powers is equal to one, i.e.,

$$P_n = \frac{P_n'}{\sum_{n=1}^{N} P_n'} \tag{7.5-6}$$

In the case of LOS condition an additional specular component is added to the first cluster. Power of the single LOS ray is:

$$P_{1,LOS} = \frac{K_R}{K_R + 1} \tag{7.5-7}$$

and the cluster powers are not normalized as in equation (7.5-6) , but:

$$P_n = \frac{1}{K_R + 1} \frac{P'_n}{\sum_{n=1}^{N} P'_n} + \delta(n-1) P_{1,LOS} \tag{7.5-8}$$

where δ(.) is Dirac's delta function and K_R is the Ricean *K*-factor as generated in Step 4 converted to linear scale. These power values are used *only* in equations (7.5-9) and (7.5-14), but *not* in equation (7.5-22).

Assign the power of each ray within a cluster as P_n / M, where M is the number of rays per cluster.

Remove clusters with less than -25 dB power compared to the maximum cluster power based on equation (7.5-6). The scaling factors need not be changed after cluster elimination.

Step 7: Generate arrival angles and departure angles for both azimuth and elevation.

The composite PAS in azimuth of all clusters is modelled as wrapped Gaussian. The AOAs are determined by applying the inverse Gaussian function (7.5-9) with input parameters P_n and RMS angle spread ASA

$$\phi'_{n,AOA} = \frac{2(\mathrm{ASA}/1.4)\sqrt{-\ln(P_n/\max(P_n))}}{C_\phi}, \tag{7.5-9}$$

with C_ϕ defined as

$$C_\phi = \begin{cases} C_\phi^{\mathrm{NLOS}} \cdot \left(1.1035 - 0.028K - 0.002K^2 + 0.0001K^3\right) & \text{, for LOS} \\ C_\phi^{\mathrm{NLOS}} & \text{, for NLOS} \end{cases}, \tag{7.5-10}$$

where C_ϕ^{NLOS} is defined as a scaling factor related to the total number of clusters and is given in Table 7.5-2:

Table 7.5-2: Scaling factors for AOA, AOD generation

# clusters	4	5	6	7	8		10	11	12
$C_\varphi^{\mathrm{NLOS}}$	0.779	0.860	0.921	0.973	1.018		1.090	1.123	1.146
# clusters		**14**	**15**	**16**			**19**	**20**	**25**
$C_\varphi^{\mathrm{NLOS}}$		1.190	1.211	1.226			1.273	1.289	1.358

In the LOS case, constant C_ϕ also depends on the Ricean K-factor *K* in [dB], as generated in Step 4. Additional scaling of the angles is required to compensate for the effect of LOS peak addition to the angle spread.

Assign positive or negative sign to the angles by multiplying with a random variable X_n with uniform distribution to the discrete set of {1,–1}, and add component $Y_n \sim N\left(0, (\mathrm{ASA}/7)^2\right)$ to introduce random variation

$$\phi_{n,AOA} = X_n \phi'_{n,AOA} + Y_n + \phi_{LOS,AOA}, \tag{7.5-11}$$

where $\phi_{LOS,AOA}$ is the LOS direction defined in the network layout description, see Step1c.

In the LOS case, substitute (7.5-11) by (7.5-12) to enforce the first cluster to the LOS direction $\phi_{LOS,\,AOA}$

$$\phi_{n,AOA} = \left(X_n \phi'_{n,AOA} + Y_n\right) - \left(X_1 \phi'_{1,AOA} + Y_1 - \phi_{LOS,AOA}\right) \tag{7.5-12}$$

Finally add offset angles α_m from Table 7.5-3 to the cluster angles

$$\phi_{n,m,AOA} = \phi_{n,AOA} + c_{ASA}\alpha_m\,, \tag{7.5-13}$$

where c_{ASA} is the cluster-wise rms azimuth spread of arrival angles (cluster ASA) in Table 7.5-6.

Table 7.5-3: Ray offset angles within a cluster, given for rms angle spread normalized to 1

Ray number *m*	Basis vector of offset angles α_m
1,2	± 0.0447
3,4	± 0.1413
5,6	± 0.2492
7,8	± 0.3715
9,10	± 0.5129
11,12	± 0.6797
13,14	± 0.8844
15,16	± 1.1481
17,18	± 1.5195
19,20	± 2.1551

The generation of AOD ($\phi_{n,m,AOD}$) follows a procedure similar to AOA as described above.

The generation of ZOA assumes that the composite PAS in the zenith dimension of all clusters is Laplacian (see Table 7.5-6). The ZOAs are determined by applying the inverse Laplacian function (7.5-14) with input parameters P_n and RMS angle spread ZSA

$$\theta'_{n,ZOA} = -\frac{\mathrm{ZSA}\ln\left(P_n/\max\left(P_n\right)\right)}{C_\theta}, \tag{7.5-14}$$

with C_θ defined as

$$C_\theta = \begin{cases} C_\theta^{\mathrm{NLOS}} \cdot \left(1.3086 + 0.0339K - 0.0077K^2 + 0.0002K^3\right) & \text{, for LOS} \\ C_\theta^{\mathrm{NLOS}} & \text{, for NLOS} \end{cases}, \tag{7.5-15}$$

Where C_θ^{NLOS} is a scaling factor related to the total number of clusters and is given in Table 7.5-4:

Table 7.5-4: Scaling factors for ZOA, ZOD generation

# clusters			**6**	**7**	**8**		**10**	**11**	**12**
C_θ^{NLOS}			0.788	0.847	0.889		0.957	1.031	1.104
# clusters		**14**	**15**	**16**			**19**	**20**	**25**
C_θ^{NLOS}		1.1072	1.1088	1.1276			1.184	1.178	1.282

In the LOS case, constant C_θ also depends on the Ricean K-factor *K* in [dB], as generated in Step 4. Additional scaling of the angles is required to compensate for the effect of LOS peak addition to the angle spread.

Assign positive or negative sign to the angles by multiplying with a random variable X_n with uniform distribution to the discrete set of {1,–1}, and add component $Y_n \sim N\left(0, \left(\mathrm{ZSA}/7\right)^2\right)$ to introduce random variation

$$\theta_{n,ZOA} = X_n\theta'_{n,ZOA} + Y_n + \bar{\theta}_{ZOA}\,, \tag{7.5-16}$$

where $\bar{\theta}_{ZOA} = 90°$ if the BS-UT link is O2I and $\bar{\theta}_{ZOA} = \theta_{LOS,ZOA}$ otherwise. The LOS direction is defined in the network layout description, see Step1c.

In the LOS case, substitute (7.5-16) by (7.5-17) to enforce the first cluster to the LOS direction $\theta_{LOS,ZOA}$

$$\theta_{n,ZOA} = \left(X_n\theta'_{n,ZOA} + Y_n\right) - \left(X_1\theta'_{1,ZOA} + Y_1 - \theta_{LOS,ZOA}\right). \tag{7.5-17}$$

Finally add offset angles α_m from Table 7.5-3 to the cluster angles

$$\theta_{n,m,ZOA} = \theta_{n,ZOA} + c_{ZSA}\alpha_m, \quad (7.5\text{-}18)$$

where c_{ZSA} is the cluster-wise rms spread of ZOA (cluster ZSA) in Table 7.5-6. Assuming that $\theta_{n,m,ZOA}$ is wrapped within [0, 360°], if $\theta_{n,m,ZOA} \in [180°, 360°]$, then $\theta_{n,m,ZOA}$ is set to $(360° - \theta_{n,m,ZOA})$.

The generation of ZOD follows the same procedure as ZOA described above except equation (7.5-16) is replaced by

$$\theta_{n,ZOD} = X_n\theta'_{n,ZOD} + Y_n + \theta_{LOS,ZOD} + \mu_{offset,ZOD}, \quad (7.5\text{-}19)$$

where variable X_n is with uniform distribution to the discrete set of {1,–1}, $Y_n \sim N\left(0, (\mathrm{ZSD}/7)^2\right)$, $\mu_{offset,ZOD}$ is given in Tables 7.5-6/7/8 and equation (7.5-18) is replaced by

$$\theta_{n,m,ZOD} = \theta_{n,ZOD} + (3/8)(10^{\mu_{\mathrm{lgZSD}}})\alpha_m \quad (7.5\text{-}20)$$

where μ_{lgZSD} is the mean of the ZSD log-normal distribution.

In the LOS case, the generation of ZOD follows the same procedure as ZOA described above using equation (7.5-17).

Step 8: Coupling of rays within a cluster for both azimuth and elevation

Couple randomly AOD angles $\phi_{n,m,AOD}$ to AOA angles $\phi_{n,m,AOA}$ within a cluster *n*, or within a sub-cluster in the case of two strongest clusters (see Step 11 and Table 7.5-3). Couple randomly ZOD angles $\theta_{n,m,ZOD}$ with ZOA angles $\theta_{n,m,ZOA}$ using the same procedure. Couple randomly AOD angles $\phi_{n,m,AOD}$ with ZOD angles $\theta_{n,m,ZOD}$ within a cluster *n* or within a sub-cluster in the case of two strongest clusters.

Step 9: Generate the cross polarization power ratios

Generate the cross polarization power ratios (XPR) κ for each ray *m* of each cluster *n*. XPR is log-Normal distributed. Draw XPR values as

$$\kappa_{n,m} = 10^{X_{n,m}/10}, \quad (7.5\text{-}21)$$

where $X_{n,m} \sim N(\mu_{\mathrm{XPR}}, \sigma^2_{\mathrm{XPR}})$ is Gaussian distributed with σ_{XPR} and μ_{XPR} from Table 7.5-6.

Note: $X_{n,m}$ is independently drawn for each ray and each cluster.

The outcome of Steps 1-9 shall be identical for all the links from co-sited sectors to a UT.

Coefficient generation:

Step 10: Draw initial random phases

Draw random initial phase $\left\{\Phi^{\theta\theta}_{n,m}, \Phi^{\theta\phi}_{n,m}, \Phi^{\phi\theta}_{n,m}, \Phi^{\phi\phi}_{n,m}\right\}$ for each ray *m* of each cluster *n* and for four different polarisation combinations ($\theta\theta$, $\theta\phi$, $\phi\theta$, $\phi\phi$). The distribution for initial phases is uniform within ($-\pi, \pi$).

Step 11: Generate channel coefficients for each cluster *n* and each receiver and transmitter element pair *u*, *s*.

The method described below is used at least for *drop-based evaluations* irrespective of UT speeds. Relevant cases for drop-based evaluations are:

- Case 1: For low complexity evaluations
- Case 2: To compare with earlier simulation results,
- Case 3: When none of the additional modelling components are turned on.
- Case 4: When spatial consistency and/or blockage is modeled for MU-MIMO simulations
- Other cases are not precluded

For the N – 2 weakest clusters, say n = 3, 4,…, N, the channel coefficients are given by:

$$H_{u,s,n}^{\mathrm{NLOS}}(t) = \sqrt{\frac{P_n}{M}} \sum_{m=1}^{M} \begin{bmatrix} F_{rx,u,\theta}\left(\theta_{n,m,ZOA}, \phi_{n,m,AOA}\right) \\ F_{rx,u,\phi}\left(\theta_{n,m,ZOA}, \phi_{n,m,AOA}\right) \end{bmatrix}^T \begin{bmatrix} \exp\left(j\Phi_{n,m}^{\theta\theta}\right) & \sqrt{\kappa_{n,m}^{-1}} \exp\left(j\Phi_{n,m}^{\theta\phi}\right) \\ \sqrt{\kappa_{n,m}^{-1}} \exp\left(j\Phi_{n,m}^{\phi\theta}\right) & \exp\left(j\Phi_{n,m}^{\phi\phi}\right) \end{bmatrix}$$
$$\begin{bmatrix} F_{tx,s,\theta}\left(\theta_{n,m,ZOD}, \phi_{n,m,AOD}\right) \\ F_{tx,s,\phi}\left(\theta_{n,m,ZOD}, \phi_{n,m,AOD}\right) \end{bmatrix} \exp\left(\frac{j2\pi\left(\hat{r}_{rx,n,m}^T . \bar{d}_{rx,u}\right)}{\lambda_0}\right) \exp\left(\frac{j2\pi\left(\hat{r}_{tx,n,m}^T . \bar{d}_{tx,s}\right)}{\lambda_0}\right) \exp\left(j2\pi \frac{\hat{r}_{rx,n,m}^T . \bar{v}}{\lambda_0} t\right) \quad (7.5\text{-}22)$$

where $F_{rx,u,\theta}$ and $F_{rx,u,\phi}$ are the field patterns of receive antenna element u according to (7.1-11) and in the direction of the spherical basis vectors, $\hat{\theta}$ and $\hat{\phi}$ respectively, $F_{tx,s,\theta}$ and $F_{tx,s,\phi}$ are the field patterns of transmit antenna element s in the direction of the spherical basis vectors, $\hat{\theta}$ and $\hat{\phi}$ respectively. Note that the patterns are given in the GCS and therefore include transformations with respect to antenna orientation as described in Clause 7.1. $\hat{r}_{rx,n,m}$ is the spherical unit vector with azimuth arrival angle $\phi_{n,m,AOA}$ and elevation arrival angle $\theta_{n,m,ZOA}$, given by

$$\hat{r}_{rx,n,m} = \begin{bmatrix} \sin\theta_{n,m,ZOA} \cos\phi_{n,m,AOA} \\ \sin\theta_{n,m,ZOA} \sin\phi_{n,m,AOA} \\ \cos\theta_{n,m,ZOA} \end{bmatrix}, \quad (7.5\text{-}23)$$

where n denotes a cluster and m denotes a ray within cluster n. $\hat{r}_{tx,n,m}$ is the spherical unit vector with azimuth departure angle $\phi_{n,m,AOD}$ and elevation departure angle $\theta_{n,m,ZOD}$, given by

$$\hat{r}_{tx,n,m} = \begin{bmatrix} \sin\theta_{n,m,ZOD} \cos\phi_{n,m,AOD} \\ \sin\theta_{n,m,ZOD} \sin\phi_{n,m,AOD} \\ \cos\theta_{n,m,ZOD} \end{bmatrix}, \quad (7.5\text{-}24)$$

where n denotes a cluster and m denotes a ray within cluster n. Also, $\bar{d}_{rx,u}$ is the location vector of receive antenna element u and $\bar{d}_{tx,s}$ is the location vector of transmit antenna element s, $\kappa_{n,m}$ is the cross polarisation power ratio in linear scale, and λ_0 is the wavelength of the carrier frequency. If polarisation is not considered, the 2x2 polarisation matrix can be replaced by the scalar $\exp\left(j\Phi_{n,m}\right)$ and only vertically polarised field patterns are applied.

The Doppler frequency component depends on the arrival angles (AOA, ZOA), and the UT velocity vector $\bar{v}$ with speed v, travel azimuth angle ϕ_v, elevation angle θ_v and is given by

$$v_{n,m} = \frac{\hat{r}_{rx,n,m}^T . \bar{v}}{\lambda_0}, \text{where } \bar{v} = v.\left[\sin\theta_v \cos\phi_v \quad \sin\theta_v \sin\phi_v \quad \cos\theta_v\right]^T. \quad (7.5\text{-}25)$$

For the two strongest clusters, say n = 1 and 2, rays are spread in delay to three sub-clusters (per cluster), with fixed delay offset. The delays of the sub-clusters are

$$\tau_{n,1} = \tau_n$$
$$\tau_{n,2} = \tau_n + 1.28\ c_{DS} \quad (7.5\text{-}26)$$
$$\tau_{n,3} = \tau_n + 2.56\ c_{DS}$$

where c_{DS} is cluster delay spread specified in Table 7.5-6. When intra-cluster delay spread is unspecified (i.e., N/A) the value 3.91 ns is used; it is noted that this value results in the legacy behaviour with 5 and 10 ns sub-cluster delays.

Twenty rays of a cluster are mapped to sub-clusters as presented in Table 7.5-5 below. The corresponding offset angles are taken from Table 7.5-3 with mapping of Table 7.5-5.

Table 7.5-5: Sub-cluster information for intra cluster delay spread clusters

sub-cluster # i	mapping to rays R_i	Power $\lvert R_i \rvert / M$	delay offset $\tau_{n,i} - \tau_n$
$i=1$	$R_1 = \{1,2,3,4,5,6,7,8,19,20\}$	10/20	0
$i=2$	$R_2 = \{9,10,11,12,17,18\}$	6/20	1.28 c_{DS}
$i=3$	$R_3 = \{13,14,15,16\}$	4/20	2.56 c_{DS}

Then, the channel impulse response is given by:

$$H_{u,s}^{\text{NLOS}}(\tau,t) = \sum_{n=1}^{2}\sum_{i=1}^{3}\sum_{m\in R_i} H_{u,s,n,m}^{\text{NLOS}}(t)\delta(\tau-\tau_{n,i}) + \sum_{n=3}^{N} H_{u,s,n}^{\text{NLOS}}(t)\delta(\tau-\tau_n) \quad (7.5\text{-}27)$$

where $H_{u,s,n}^{\text{NLOS}}(t)$ is given in (7.5-22) and $H_{u,s,n,m}^{\text{NLOS}}(t)$ defined as:

$$H_{u,s,n,m}^{\text{NLOS}}(t) = \sqrt{\frac{P_n}{M}} \begin{bmatrix} F_{rx,u,\theta}(\theta_{n,m,ZOA},\phi_{n,m,AOA}) \\ F_{rx,u,\phi}(\theta_{n,m,ZOA},\phi_{n,m,AOA}) \end{bmatrix}^T \begin{bmatrix} \exp(j\Phi_{n,m}^{\theta\theta}) & \sqrt{\kappa_{n,m}^{-1}}\exp(j\Phi_{n,m}^{\theta\phi}) \\ \sqrt{\kappa_{n,m}^{-1}}\exp(j\Phi_{n,m}^{\phi\theta}) & \exp(j\Phi_{n,m}^{\phi\phi}) \end{bmatrix} \quad (7.5\text{-}28)$$
$$\begin{bmatrix} F_{tx,s,\theta}(\theta_{n,m,ZOD},\phi_{n,m,AOD}) \\ F_{tx,s,\phi}(\theta_{n,m,ZOD},\phi_{n,m,AOD}) \end{bmatrix} \exp\left(j2\pi \frac{\hat{r}_{rx,n,m}^T . \bar{d}_{rx,u}}{\lambda_0}\right) \exp\left(j2\pi \frac{\hat{r}_{tx,n,m}^T . \bar{d}_{tx,s}}{\lambda_0}\right) \exp\left(j2\pi \frac{\hat{r}_{rx,n,m}^T . \bar{v}}{\lambda_0} t\right)$$

In the LOS case, determine the LOS channel coefficient by:

$$H_{u,s,1}^{\text{LOS}}(t) = \begin{bmatrix} F_{rx,u,\theta}(\theta_{LOS,ZOA},\phi_{LOS,AOA}) \\ F_{rx,u,\phi}(\theta_{LOS,ZOA},\phi_{LOS,AOA}) \end{bmatrix}^T \begin{bmatrix} 1 & 0 \\ 0 & -1 \end{bmatrix} \begin{bmatrix} F_{tx,s,\theta}(\theta_{LOS,ZOD},\phi_{LOS,AOD}) \\ F_{tx,s,\phi}(\theta_{LOS,ZOD},\phi_{LOS,AOD}) \end{bmatrix}$$
$$\cdot \exp\left(-j2\pi \frac{d_{3D}}{\lambda_0}\right) \exp\left(j2\pi \frac{\hat{r}_{rx,LOS}^T . \bar{d}_{rx,u}}{\lambda_0}\right) \exp\left(j2\pi \frac{\hat{r}_{tx,LOS}^T . \bar{d}_{tx,s}}{\lambda_0}\right) \exp\left(j2\pi \frac{\hat{r}_{rx,LOS}^T . \bar{v}}{\lambda_0} t\right) \quad (7.5\text{-}29)$$

where $\delta(\cdot)$ is the Dirac's delta function and K_R is the Ricean K-factor as generated in Step 4 converted to linear scale.

Then, the channel impulse response is given by adding the LOS channel coefficient to the NLOS channel impulse response and scaling both terms according to the desired K-factor K_R as

$$H_{u,s}^{\text{LOS}}(\tau,t) = \sqrt{\frac{1}{K_R+1}} H_{u,s}^{\text{NLOS}}(\tau,t) + \sqrt{\frac{K_R}{K_R+1}} H_{u,s,1}^{\text{LOS}}(t)\delta(\tau-\tau_1). \quad (7.5\text{-}30)$$

Step 12: Apply pathloss and shadowing for the channel coefficients.

Table 7.5-6 Part-1: Channel model parameters for UMi-Street Canyon and UMa

Scenarios		UMi - Street Canyon			UMa		
		LOS	NLOS	O2I	LOS	NLOS	O2I
Delay spread (DS) lgDS=$\log_{10}$(DS/1s)	μ_{lgDS}	-0.18 $\log_{10}(1+f_c)$ - 7.28, see note 8	-0.22 $\log_{10}(1+f_c)$ - 6.87, see note 8	-6.62	-7.067 - 0.0794 $\log_{10}(f_c)$, see note 8	-6.47 - 0.134 $\log_{10}(f_c)$, see note 8	-6.62
	σ_{lgDS}	0.39, see note 8	0.19 $\log_{10}(1+f_c)$ + 0.22, see note 8	0.32	0.57 + 0.026 $\log_{10}(f_c)$, see note 8	0.39 see note 9	0.32
AOD spread (ASD) lgASD=$\log_{10}$(ASD/1°)	μ_{lgASD}	-0.05 $\log_{10}(1+f_c)$ + 1.21 see note 9	-0.24 $\log_{10}(1+f_c)$ + 1.54 see note 8	1.25	0.92, see note 8	1.09, see note 8	0.58, see note 8
	σ_{lgASD}	0.08 $\log_{10}(1+f_c)$ + 0.29 see note 8	0.10 $\log_{10}(1+f_c)$ + 0.33 see note 8	0.42	0.31, see note 8	0.44, see note 8	0.7 see note 8
AOA spread (ASA) lgASA=$\log_{10}$(ASA/1°)	μ_{lgASA}	-0.07 $\log_{10}(1+f_c)$ + 1.66, see note 8	-0.07 $\log_{10}(1+f_c)$ + 1.76, see note 8	1.76	1.76, see note 8	2.04 - 0.25 $\log_{10}(f_c)$, see note 8	1.76
	σ_{lgASA}	0.021 $\log_{10}(1+f_c)$ + 0.26, see note 8	0.05 $\log_{10}(1+f_c)$ + 0.27, see note 8	0.16	0.19, see note 8	0.17 - 0.03 $\log_{10}(f_c)$, see note 8	0.16
ZOA spread (ZSA) lgZSA=$\log_{10}$(ZSA/1°)	μ_{lgZSA}	-0.11 $\log_{10}(1+f_c)$ + 0.81 see note 8	-0.03 $\log_{10}(1+f_c)$ + 0.92 see note 8	1.01	0.96 see note 8	-0.2856 $\log_{10}(f_c)$ + 1.445, see note 8	1.01
	σ_{lgZSA}	-0.03 $\log_{10}(1+f_c)$ + 0.29 see note 8	-0.05 $\log_{10}(1+f_c)$ + 0.35 see note 8	0.43	0.15 see note 8	0.17, see note 8	0.43
Shadow fading (*SF*) [dB]	σ_{SF}	See Table 7.4.1-1	See Table 7.4.1-1	7	See Table 7.4.1-1	See Table 7.4.1-1	7
K-factor (*K*) [dB]	μ_K	9	N/A	N/A	9	N/A	N/A
	σ_K	5	N/A	N/A	3.5	N/A	N/A
Cross-Correlations	*ASD* vs *DS*	0.5	0	0.4	0.4	0.4	0.4
	ASA vs *DS*	0.8	0.4	0.4	0.8	0.6	0.4
	ASA vs *SF*	-0.4	-0.4	0	-0.5	0	0
	ASD vs *SF*	-0.5	0	0.2	-0.5	-0.6	0.2
	DS vs *SF*	-0.4	-0.7	-0.5	-0.4	-0.4	-0.5
	ASD vs *ASA*	0.4	0	0	0	0.4	0
	ASD vs K	-0.2	N/A	N/A	0	N/A	N/A
	ASA vs K	-0.3	N/A	N/A	-0.2	N/A	N/A
	DS vs K	-0.7	N/A	N/A	-0.4	N/A	N/A
	SF vs K	0.5	N/A	N/A	0	N/A	N/A
Cross-Correlations [1)]	*ZSD* vs *SF*	0	0	0	0	0	0
	ZSA vs *SF*	0	0	0	-0.8	-0.4	0
	ZSD vs *K*	0	N/A	N/A	0	N/A	N/A
	ZSA vs *K*	0	N/A	N/A	0	N/A	N/A
	ZSD vs *DS*	0	-0.5	-0.6	-0.2	-0.5	-0.6
	ZSA vs *DS*	0.2	0	-0.2	0	0	-0.2
	ZSD vs *ASD*	0.5	0.5	-0.2	0.5	0.5	-0.2
	ZSA vs *ASD*	0.3	0.5	0	0	-0.1	0
	ZSD vs *ASA*	0	0	0	-0.3	0	0
	ZSA vs *ASA*	0	0.2	0.5	0.4	0	0.5

Scenarios		UMi - Street Canyon			UMa		
		LOS	NLOS	O2I	LOS	NLOS	O2I
	ZSD vs *ZSA*	0	0	0.5	0	0	0.5
Delay scaling parameter r_τ		3	2.1	2.2	2.5	2.3	2.2
XPR [dB]	μ_{XPR}	9	8.0	9	8	7	9
	σ_{XPR}	3	3	5	4	3	5
Number of clusters N		12	19	12	12	20	12
Number of rays per cluster M		20	20	20	20	20	20
Cluster *DS* (c_{DS}) in [ns]		5	11	11	max(0.25, 6.5622 -3.4084 $\log_{10}(f_c)$)	max(0.25, 6.5622 -3.4084 $\log_{10}(f_c)$)	11
Cluster *ASD* (c_{ASD}) in [deg]		3	10	5	3.58, see note 8	1.8, see note 8	1.8, see note 8
Cluster *ASA* (c_{ASA}) in [deg]		17	22	8	11	15	8
Cluster *ZSA* (c_{ZSA}) in [deg]		7	7	3	7	7	3
Per cluster shadowing std ζ [dB]		3	3	4	3	3	4
Correlation distance in the horizontal plane [m]	*DS*	7	10	10	30	40	10
	ASD	8	10	11	18	50	11
	ASA	8	9	17	15	50	17
	SF	10	13	7	37	50	7
	K	15	N/A	N/A	12	N/A	N/A
	ZSA	12	10	25	15	50	25
	ZSD	12	10	25	15	50	25

f_c is carrier frequency in GHz; d_{2D} is BS-UT distance in km.

NOTE 1: *DS* = rms delay spread, *ASD* = rms azimuth spread of departure angles, *ASA* = rms azimuth spread of arrival angles, *ZSD* = rms zenith spread of departure angles, *ZSA* = rms zenith spread of arrival angles, *SF* = shadow fading, and *K* = Ricean K-factor.

NOTE 2: The sign of the shadow fading is defined so that positive SF means more received power at UT than predicted by the path loss model.

NOTE 3: All large scale parameters are assumed to have no correlation between different floors.

NOTE 4: The following notation for mean ($\mu_{\lg X}$=mean{$\log_{10}$(X) }) and standard deviation ($\sigma_{\lg X}$=std{$\log_{10}$(X) }) is used for logarithmized parameters X.

NOTE 5: For all considered scenarios the AOD/AOA distributions are modelled by a wrapped Gaussian distribution, the ZOD/ZOA distributions are modelled by a Laplacian distribution and the delay distribution is modelled by an exponential distribution.

NOTE 6: For UMa and frequencies below 6 GHz, use f_c = 6 when determining the values of the frequency-dependent LSP values

NOTE 7: For UMi and frequencies below 2 GHz, use f_c = 2 when determining the values of the frequency-dependent LSP values

NOTE 8: Value(s) marked with this note were updated as part of Release 19 Study on channel modelling enhancements for 7-24 GHz for NR [25].

NOTE 9: Value(s) were unchanged even after the considering measurements as part of Release 19 Study on channel modelling enhancements for 7-24 GHz for NR [25].

Table 7.5-6 Part-2: Channel model parameters for RMa (up to 7GHz) and Indoor-Office

Scenarios		RMa			Indoor-Office	
		LOS	NLOS	O2I	LOS	NLOS
Delay spread (DS) lgDS=$\log_{10}$(DS/1s)	μ_{lgDS}	-7.49	-7.43	-7.47	-0.01 $\log_{10}(1+f_c)$ - 7.692	-0.28 $\log_{10}(1+f_c)$ - 7.173
	σ_{lgDS}	0.55	0.48	0.24	0.18	0.10 $\log_{10}(1+f_c)$ + 0.055

Scenarios		RMa			Indoor-Office	
		LOS	NLOS	O2I	LOS	NLOS
AOD spread (ASD) lgASD=$\log_{10}$(ASD/1°)	$\mu_{\lg ASD}$	0.90	0.95	0.67	1.60	1.62
	$\sigma_{\lg ASD}$	0.38	0.45	0.18	0.18	0.25
AOA spread (ASA) lgASA=$\log_{10}$(ASA/1°)	$\mu_{\lg ASA}$	1.52	1.52	1.66	-0.19 $\log_{10}(1+f_c)$ + 1.781	-0.11 $\log_{10}(1+f_c)$ + 1.863
	$\sigma_{\lg ASA}$	0.24	0.13	0.21	0.12 $\log_{10}(1+f_c)$ + 0.119	0.12 $\log_{10}(1+f_c)$ + 0.059
ZOA spread (ZSA) lgZSA=$\log_{10}$(ZSA/1°)	$\mu_{\lg ZSA}$	0.47	0.58	0.93	-0.26 $\log_{10}(1+f_c)$ + 1.44	-0.15 $\log_{10}(1+f_c)$ + 1.387
	$\sigma_{\lg ZSA}$	0.40	0.37	0.22	-0.04 $\log_{10}(1+f_c)$ + 0.264	-0.09 $\log_{10}(1+f_c)$ + 0.746
Shadow fading (SF) [dB]	σ_{SF}	See Table 7.4.1-1		8	See Table 7.4.1-1	
K-factor (*K*) [dB]	μ_K	7	N/A	N/A	7	N/A
	σ_K	4	N/A	N/A	4	N/A
Cross-Correlations	*ASD* vs *DS*	0	-0.4	0	0.6	0.4
	ASA vs *DS*	0	0	0	0.8	0
	ASA vs *SF*	0	0	0	–0.5	–0.4
	ASD vs *SF*	0	0.6	0	–0.4	0
	DS vs *SF*	-0.5	-0.5	0	–0.8	–0.5
	ASD vs *ASA*	0	0	-0.7	0.4	0
	ASD vs K	0	N/A	N/A	0	N/A
	ASA vs K	0	N/A	N/A	0	N/A
	DS vs K	0	N/A	N/A	-0.5	N/A
	SF vs K	0	N/A	N/A	0.5	N/A
Cross-Correlations [1)]	*ZSD* vs *SF*	0.01	-0.04	0	0.2	0
	ZSA vs *SF*	-0.17	-0.25	0	0.3	0
	ZSD vs *K*	0	N/A	N/A	0	N/A
	ZSA vs *K*	-0.02	N/A	N/A	0.1	N/A
	ZSD vs *DS*	-0.05	-0.10	0	0.1	-0.27
	ZSA vs *DS*	0.27	-0.40	0	0.2	-0.06
	ZSD vs *ASD*	0.73	0.42	0.66	0.5	0.35
	ZSA vs *ASD*	-0.14	-0.27	0.47	0	0.23
	ZSD vs *ASA*	-0.20	-0.18	-0.55	0	-0.08
	ZSA vs *ASA*	0.24	0.26	-0.22	0.5	0.43
	ZSD vs *ZSA*	-0.07	-0.27	0	0	0.42
Delay scaling parameter r_τ		3.8	1.7	1.7	3.6	3
XPR [dB]	μ_{XPR}	12	7	7	11	10
	σ_{XPR}	4	3	3	4	4
Number of clusters N		11	10	10	15	19
Number of rays per cluster M		20	20	20	20	20
Cluster *DS* (c_{DS}) in [ns]		N/A	N/A	N/A	N/A	N/A
Cluster *ASD* (c_{ASD}) in [deg]		2	2	2	5	5
Cluster *ASA* (c_{ASA}) in [deg]		3	3	3	8	11
Cluster *ZSA* (c_{ZSA}) in [deg]		3	3	3	9	9

Scenarios		RMa			Indoor-Office	
		LOS	NLOS	O2I	LOS	NLOS
Per cluster shadowing std ζ [dB]		3	3	3	6	3
Correlation distance in the horizontal plane [m]	*DS*	50	36	36	8	5
	ASD	25	30	30	7	3
	ASA	35	40	40	5	3
	SF	37	120	120	10	6
	K	40	N/A	N/A	4	N/A
	ZSA	15	50	50	4	4
	ZSD	15	50	50	4	4

f_c is carrier frequency in GHz; d_{2D} is BS-UT distance in km.

NOTE 1: *DS* = rms delay spread, *ASD* = rms azimuth spread of departure angles, *ASA* = rms azimuth spread of arrival angles, *ZSD* = rms zenith spread of departure angles, *ZSA* = rms zenith spread of arrival angles, *SF* = shadow fading, and *K* = Ricean K-factor.

NOTE 2: The sign of the shadow fading is defined so that positive SF means more received power at UT than predicted by the path loss model.

NOTE 3: The following notation for mean (μ_{lgX}=mean{$\log_{10}$(X) }) and standard deviation (σ_{lgX}=std{$\log_{10}$(X) }) is used for logarithmized parameters X.

NOTE 4: Void.

NOTE 5: For all considered scenarios the AOD/AOA distributions are modelled by a wrapped Gaussian distribution, the ZOD/ZOA distributions are modelled by a Laplacian distribution and the delay distribution is modelled by an exponential distribution.

NOTE 6: For InH and frequencies below 6 GHz, use f_c = 6 when determining the values of the frequency-dependent LSP values

Table 7.5-6 Part-3: Channel model parameters for InF

Scenarios		InF	
		LOS	NLOS
Delay spread (DS) lgDS=$\log_{10}$(DS/1s) [4)]	μ_{lgDS}	$\log_{10}$(26(V/S)+14)-9.35	$\log_{10}$(30(V/S)+32)-9.44
	σ_{lgDS}	0.15	0.19
AOD spread (ASD) lgASD=$\log_{10}$(ASD/1°)	μ_{lgASD}	1.56	1.57
	σ_{lgASD}	0.25	0.2
AOA spread (ASA) lgASA=$\log_{10}$(ASA/1°)	μ_{lgASA}	-0.18*log10(1+fc) + 1.78	1.72
	σ_{lgASA}	0.12*log10(1+fc) + 0.2	0.3
ZOA spread (ZSA) lgZSA=$\log_{10}$(ZSA/1°)	μ_{lgZSA}	-0.2*log10(1+fc) + 1.5	-0.13*log10(1+fc) + 1.45
	σ_{lgZSA}	0.35	0.45
Shadow fading (SF) [dB]	σ_{SF}	Specified as part of path loss models	
K-factor (*K*) [dB]	μ_K	7	N/A
	σ_K	8	N/A
Cross-Correlations	*ASD* vs *DS*	0	0
	ASA vs *DS*	0	0
	ASA vs *SF*	0	0
	ASD vs *SF*	0	0
	DS vs *SF*	0	0
	ASD vs *ASA*	0	0
	ASD vs K	-0.5	N/A
	ASA vs K	0	N/A
	DS vs K	-0.7	N/A
	SF vs K	0	N/A
Cross-Correlations [1)]	*ZSD* vs *SF*	0	0
	ZSA vs *SF*	0	0
	ZSD vs *K*	0	N/A
	ZSA vs *K*	0	N/A
	ZSD vs *DS*	0	0
	ZSA vs *DS*	0	0
	ZSD vs *ASD*	0	0
	ZSA vs *ASD*	0	0
	ZSD vs *ASA*	0	0
	ZSA vs *ASA*	0	0
	ZSD vs *ZSA*	0	0
Delay scaling parameter r_τ		2.7	3
XPR [dB]	μ_{XPR}	12	11
	σ_{XPR}	6	6
Number of clusters N		25	25
Number of rays per cluster M		20	20
Cluster *DS* (C_{DS}) in [ns]		N/A	N/A
Cluster *ASD* (C_{ASD}) in [deg]		5	5
Cluster *ASA* (C_{ASA}) in [deg]		8	8
Cluster *ZSA* (C_{ZSA}) in [deg]		9	9
Per cluster shadowing std ζ [dB]		4	3
Correlation distance in the horizontal plane [m] [5)]	*DS*	10	10
	ASD	10	10
	ASA	10	10
	SF	10	10
	K	10	N/A
	ZSA	10	10
	ZSD	10	10

f_c is carrier frequency in GHz; d_{2D} is BS-UT distance in km.
NOTE 1: *DS* = rms delay spread, *ASD* = rms azimuth spread of departure angles, *ASA* = rms azimuth spread of arrival angles, *ZSD* = rms zenith spread of departure angles, *ZSA* = rms zenith spread of arrival angles, *SF* = shadow fading, and *K* = Ricean K-factor.
NOTE 2: The sign of the shadow fading is defined so that positive SF means more received power at UT than predicted by the path loss model.
NOTE 3: The following notation for mean ($\mu_{\lg X}$=mean{$\log_{10}$(X) }) and standard deviation ($\sigma_{\lg X}$=std{$\log_{10}$(X) }) is used for logarithmized parameters X.
NOTE 4: V = hall volume in m^3, S = total surface area of hall in m^2 (walls+floor+ceiling)
NOTE 5: When the simulation scenario is small it is recommended to consider methods to improve the statistical confidence, such as using multiple random seeds in simulations.

Table 7.5-6 Part-4: Channel model parameters for SMa (up to 24 GHz)

Scenarios		SMa		
		LOS	**NLOS**	**O2I**
Delay spread (DS) lgDS=$\log_{10}$(DS/1s)	$\mu_{\lg DS}$	–7.42	-7.20	-7.20
	$\sigma_{\lg DS}$	0.60	0.58	0.58
AOD spread (ASD) lgASD=$\log_{10}$(ASD/1°)	$\mu_{\lg ASD}$	0.48	0.51	0.51
	$\sigma_{\lg ASD}$	0.27	0.33	0.33
AOA spread (ASA) lgASA=$\log_{10}$(ASA/1°)	$\mu_{\lg ASA}$	1.43	1.63	1.63
	$\sigma_{\lg ASA}$	0.12	0.26	0.26
ZOA spread (ZSA) lgZSA=$\log_{10}$(ZSA/1°)	$\mu_{\lg ZSA}$	1.18	1.16	1.16
	$\sigma_{\lg ZSA}$	0.05	0.14	0.14
Shadow fading (SF) [dB]	σ_{SF}	See Table 7.4.1-1	See Table 7.4.1-1	8
K-factor (*K*) [dB]	μ_K	9	N/A	N/A
	σ_K	7	N/A	N/A
Cross-Correlations	*ASD* vs *DS*	0.4	0	0
	ASA vs *DS*	0.8	0.7	0.7
	ASA vs *SF*	–0.5	0	0
	ASD vs *SF*	–0.5	-0.4	-0.4
	DS vs *SF*	–0.4	-0.13	-0.13
	ASD vs *ASA*	0	0	0
	ASD vs K	0	N/A	N/A
	ASA vs K	-0.2	N/A	N/A
	DS vs K	-0.4	N/A	N/A
	SF vs K	0	N/A	N/A
Cross-Correlations [1)]	*ZSD* vs *SF*	0	0	0
	ZSA vs *SF*	-0.8	-0.47	-0.47
	ZSD vs *K*	0	N/A	N/A
	ZSA vs *K*	0	N/A	N/A
	ZSD vs *DS*	-0.2	-0.5	-0.5
	ZSA vs *DS*	0	0	0
	ZSD vs *ASD*	0.5	0.5	0.5
	ZSA vs *ASD*	0	-0.1	-0.1
	ZSD vs *ASA*	-0.3	0	0
	ZSA vs *ASA*	0.4	0.36	0.36
	ZSD vs *ZSA*	0	0	0
Delay scaling parameter r_τ		2.4	1.5	1.5
XPR [dB]	μ_{XPR}	8	4	4
	σ_{XPR}	4	3	3
Number of clusters N		15	14	14
Number of rays per cluster M		20	20	20
Cluster *DS* (c_{DS}) in [ns]		max(0.25, 6.5622 -3.4084 log10(fc))	max(0.25, 6.5622 -3.4084 log10(f_c))	max(0.25, 6.5622 -3.4084 log10(f_c))
Cluster *ASD* (c_{ASD}) in [deg]		2.08	1.33	1.33
Cluster *ASA* (c_{ASA}) in [deg]		5	10	10
Cluster *ZSA* (c_{ZSA}) in [deg]		7	7	7
Per cluster shadowing std ζ [dB]		3	3	3
Correlation distance in the horizontal plane [m]	DS	6	40	40
	ASD	15	30	30
	ASA	20	30	30
	SF	40	50	50
	K	10	N/A	N/A

Scenarios		SMa		
		LOS	NLOS	O2I
	ZSA	15	50	50
	ZSD	15	50	50

f_c is carrier frequency in GHz; d_{2D} is BS-UT distance in km.

NOTE 1: *DS* = rms delay spread, *ASD* = rms azimuth spread of departure angles, *ASA* = rms azimuth spread of arrival angles, *ZSD* = rms zenith spread of departure angles, *ZSA* = rms zenith spread of arrival angles, *SF* = shadow fading, and *K* = Ricean K-factor.

NOTE 2: The sign of the shadow fading is defined so that positive SF means more received power at UT than predicted by the path loss model.

NOTE 3: The following notation for mean (μ_{lgX}=mean{$\log_{10}$(X) }) and standard deviation (σ_{lgX}=std{$\log_{10}$(X) }) is used for logarithmized parameters X.

NOTE 4: Void.

NOTE 5: For all considered scenarios the AOD/AOA distributions are modelled by a wrapped Gaussian distribution, the ZOD/ZOA distributions are modelled by a Laplacian distribution and the delay distribution is modelled by an exponential distribution.

Table 7.5-7: ZSD and ZOD offset parameters for UMa

Scenarios		LOS	NLOS
ZOD spread (ZSD) lgZSD=$\log_{10}$(ZSD/1°)	μ_{lgZSD}	max[-0.5, -2.1(d_{2D}/1000) -0.01 (h_{UT} - 1.5)+0.75]	max[-0.5, -2.1(d_{2D}/1000) -0.01(h_{UT} - 1.5)+0.9]
	σ_{lgZSD}	0.40	0.49
ZOD offset	$\mu_{offset,ZOD}$	0	$e(f_c)$-10^{$a(f_c)$ $\log_{10}$(max($b(f_c)$, d_{2D})) +$c(f_c)$ -0.07(h_{UT}-1.5)}

Note: For NLOS ZOD offset:
$a(f_c)$ = 0.208$\log_{10}(f_c)$- 0.782;
$b(f_c)$ = 25;
$c(f_c)$ = -0.13$\log_{10}(f_c)$+2.03;
$e(f_c)$ = 7.66$\log_{10}(f_c)$-5.96.

Table 7.5-8: ZSD and ZOD offset parameters for UMi – Street Canyon

Scenarios		LOS	NLOS
ZOD spread (ZSD) lgZSD=$\log_{10}$(ZSD/1°)	μ_{lgZSD}	max[-0.21, -14.8(d_{2D}/1000) + 0.01|h_{UT}-h_{BS}| + 0.83]	max[-0.5, -3.1(d_{2D}/1000) + 0.01 max(h_{UT}-h_{BS},0) +0.2]
	σ_{lgZSD}	0.35	0.35
ZOD offset	$\mu_{offset,ZOD}$	0	-10^{-1.5$\log_{10}$(max(10, d_{2D}))+3.3}

Table 7.5-9: ZSD and ZOD offset parameters for RMa

Scenarios		LOS	NLOS	O2I
ZOD spread (ZSD) lgZSD=$\log_{10}$(ZSD/1°)	μ_{lgZSD}	max[-1, -0.17(d_{2D}/1000) -0.01(h_{UT} - 1.5) + 0.22]	max[-1, -0.19(d_{2D}/1000) -0.01(h_{UT} - 1.5) + 0.28]	max[-1, -0.19(d_{2D}/1000) -0.01(h_{UT} - 1.5) + 0.28]
	σ_{lgZSD}	0.34	0.30	0.30
ZOD offset	$\mu_{offset,ZOD}$	0	arctan((35 - 3.5)/d_{2D}) -arctan((35 - 1.5)/d_{2D})	arctan((35 - 3.5)/d_{2D}) -arctan((35 - 1.5)/d_{2D})

Table 7.5-10: ZSD and ZOD offset parameters for Indoor-Office

Scenarios		LOS	NLOS
ZOD spread (ZSD) lgZSD=$\log_{10}$(ZSD/1°)	μ_{lgZSD}	-1.43 $\log_{10}$(1+ f_c)+2.228	1.08
	σ_{lgZSD}	0.13 $\log_{10}$(1+f_c)+0.30	0.36
ZOD offset	$\mu_{offset,ZOD}$	0	0

Table 7.5-11: ZSD and ZOD offset parameters for InF

Scenarios		LOS	NLOS
ZOD spread (ZSD) lgZSD=$\log_{10}$(ZSD/1°)	μ_{lgZSD}	1.35	1.2
	σ_{lgZSD}	0.35	0.55

ZOD offset	$\mu_{\text{offset,ZOD}}$	0	0

Table 7.5-12: ZSD and ZOD offset parameters for SMa

Scenarios		LOS	NLOS	O2I
ZOD spread (ZSD) lgZSD=$\log_{10}$(ZSD/1°)	μ_{lgZSD}	0.14	0.14	0.14
	σ_{lgZSD}	0.16	0.16	0.16
ZOD offset	$\mu_{\text{offset,ZOD}}$	0	$\begin{cases} \text{atan}\left(\frac{h_{\text{BS}}-h_{\text{cl}}}{d_{\text{2D}}}\right)-\text{atan}\left(\frac{h_{\text{BS}}-h_{\text{UT}}}{d_{\text{2D}}}\right) & h_{\text{UT}}<h_{\text{cl}} \\ 0 & h_{\text{UT}}\geq h_{\text{cl}} \end{cases}$ h_{cl}= 3.5	

Notes for Tables 7.5-7, 7.5-8, 7.5-9, 7.5-10, 7.5-11, 7.5-12:

NOTE 1: f_c is center frequency in GHz; d_{2D} is BS-UT distance in m.

NOTE 2: h_{BS} and h_{UT} are antenna heights in m for BS and UT **respectively.**

NOTE 3: The following notation for mean (μ_{lgX}=mean{$\log_{10}$(X) }) and standard deviation (σ_{lgX}=std{$\log_{10}$(X)}) is used for logarithmized parameters X**.**

NOTE 4: For frequencies below 6 GHz, use f_c = 6 when determining the values of the frequency-dependent ZSD and ZOD offset parameters in Table 7.5-7 and 7.5-10

NOTE 5: The ZSD parameters for O2I links are the same parameters that are used for outdoor links, depending on the LOS condition of the outdoor link part in Tables 7.5-7 and 7.5-8.

7.6 Additional modelling components

7.6.0 Introduction of additional modelling components

The additional modelling components in this clause are to support advanced simulations, such as simulations with very large arrays and large bandwidth, simulations affected by oxygen absorption (frequencies between 53 and 67 GHz), simulations in which spatial consistency is important (e.g. high number of closely located user), simulations of mobility, simulations of blockage effects, simulations of absolute time of arrival, simulations of dual mobility, simulations that include sources of EM interference, simulations of devices embedded in machinery or enclosures, simulations of near-field channel effects (i.e. characteristics of spherical wavefront), simulations of spatial non-stationarity (i.e. antenna element-wise power variation), simulation of number of cluster variability, and simulation of polarization power variability. These modelling components affect some of the steps between Step 1 and Step 12 in Clause 7.5.

These extensions are computationally more expensive and might not be required in all evaluation cases.

7.6.1 Oxygen absorption

Oxygen absorption loss is applied to the cluster responses generated in Step 11 in Clause 7.5. The additional loss, $OL_n(f_c)$ for cluster n at centre frequency f_c is modelled as:

$$OL_n(f_c) = \frac{\alpha(f_c)}{1000} \cdot (d_{3D} + c \cdot (\tau_n + \tau_\Delta)) \text{ [dB]} \quad (7.6\text{-}1)$$

where:

- $\alpha(f_c)$ is frequency dependent oxygen loss [dB/km] characterized in Table 7.6.1-1;
- c is the speed of light [m/s]; and d_{3D} is the distance [m];
- τ_n is the n-th cluster delay [s] in Step 11 in Clause 7.5;

- τ_Δ is 0 in the LOS case and min(τ'_n) otherwise, where min(τ'_n) is the minimum delay in Step 5.

For centre frequencies not specified in this table, the frequency dependent oxygen loss $\alpha(f_c)$ is obtained from a linear interpolation between two loss values corresponding to the two adjacent centre frequencies of the centre frequency f_c.

Table 7.6.1-1 Frequency dependent oxygen loss $\alpha(f)$ [dB/km]

f in [GHz]	0-52	53	54	55	56	57	58	59	60	61	62	63	64	65	66	67	68-100
α(f) in [dB/km]	0	1	2.2	4	6.6	9.7	12.6	14.6	15	14.6	14.3	10.5	6.8	3.9	1.9	1	0

For large channel bandwidth, first transform the time-domain channel response of each cluster (all rays within one cluster share common oxygen absorption loss for simplicity) into frequency-domain channel response, and apply the oxygen absorption loss to the cluster's frequency-domain channel response for frequency $f_c + \Delta f$ within the considered bandwidth. The oxygen loss, $OL_n(f_c+\Delta f)$ for cluster n at frequency $f_c+\Delta f$ is modelled as:

$$OL_n(f_c+\Delta f) = \frac{\alpha(f_c+\Delta f)}{1000}\cdot(d_{3D}+c\cdot(\tau_n+\tau_\Delta)) \quad \text{[dB]} \qquad (7.6\text{-}2)$$

where:

- $\alpha(f_c+\Delta f)$ is the oxygen loss (dB/km) at frequency $f_c+\Delta f$ characterized in Table 7.6.1-1. Note that Δf is in [-B/2, B/2], where B is the bandwidth. Linear interpolation is applied for frequencies not provided in Table 7.6.1-1.

The final frequency-domain channel response is obtained by the summation of frequency-domain channel responses of all clusters.

Time-domain channel response is obtained by the reverse transform from the obtained frequency-domain channel response.

7.6.2 Large bandwidth and large antenna array

7.6.2.1 Modelling of the propagation delay

The modelling in this clause applies only when the bandwidth B is greater than c/D Hz, where

- D is the maximum antenna aperture in either azimuth or elevation (m)
- c is the speed of light (m/s)

Each ray within a cluster for a given u (Rx) and s (Tx) has unique time of arrival (TOA). The channel coefficient generation step (Step 11 in Clause 7.5) is updated to model individual rays. In this case, the channel response of ray m in cluster n for a link between Rx antenna u and Tx antenna s at delay τ at time t is given by:

$$H^{\text{NLOS}}_{u,s,n,m}(t;\tau) = \sqrt{P_{n,m}}\begin{bmatrix} F_{rx,u,\theta}(\theta_{n,m,ZOA},\phi_{n,m,AOA}) \\ F_{rx,u,\phi}(\theta_{n,m,ZOA},\phi_{n,m,AOA}) \end{bmatrix}^T \begin{bmatrix} \exp(j\Phi^{\theta\theta}_{n,m}) & \sqrt{\kappa_{n,m}^{-1}}\exp(j\Phi^{\theta\phi}_{n,m}) \\ \sqrt{\kappa_{n,m}^{-1}}\exp(j\Phi^{\phi\theta}_{n,m}) & \exp(j\Phi^{\phi\phi}_{n,m}) \end{bmatrix}$$
$$\begin{bmatrix} F_{tx,s,\theta}(\theta_{n,m,ZOD},\phi_{n,m,AOD}) \\ F_{tx,s,\phi}(\theta_{n,m,ZOD},\phi_{n,m,AOD}) \end{bmatrix} \exp\left(\frac{j2\pi(\hat{r}^T_{rx,n,m}.\bar{d}_{rx,u})}{\lambda(f)}\right)\exp\left(\frac{j2\pi(\hat{r}^T_{tx,n,m}.\bar{d}_{tx,s})}{\lambda(f)}\right) \qquad (7.6\text{-}3)$$
$$\cdot\exp\left(j2\pi\frac{\hat{r}^T_{rx,n,m}.\bar{v}}{\lambda_0}t\right)\delta(\tau-\tau_{n,m})$$

with $\lambda(f)$ is the wavelength on frequency $f \in \left[f_c-\frac{B}{2}, f_c+\frac{B}{2}\right]$, which can be implemented by user's own method. The delay (TOA) for ray m in cluster n for a link between Rx antenna u and Tx antenna s is given by:

$$\tau_{u,s,n,m} = \tau_{n,m} - \tfrac{1}{c}\hat{r}_{rx,n,m}^{T}.\bar{d}_{rx,u} - \tfrac{1}{c}\hat{r}_{tx,n,m}^{T}.\bar{d}_{tx,s} \quad (7.6\text{-}4)$$

Note that Equation (7.6-3) only considers the delays $\tau_{n,m}$ intentionally. If unequal ray powers are considered, $P_{n,m}$ are generated according to Clause 7.6.2.2. Otherwise, ray powers are equal within a cluster, i.e., $P_{n,m} = P_n / M$ for all m.
Note: this model is developed assuming plane wave propagation.

7.6.2.2 Modelling of intra-cluster angular and delay spreads

With large antenna arrays or large bandwidths, the angle and/or delay resolution can be larger than what the fast fading model in Clause 7.5 is designed to support. To model this effect, the following modifications to Step 7 in Clause 7.5 can be optionally used.

1. The offset angles α_m in (7.5-13), (7.5-18) and (7.5-20) are generated independently per cluster and ray using:

$$\alpha_{n,m,\{\mathrm{AOA,AOD,ZOA,ZOD}\}} \sim \mathrm{unif}(-2,2) \quad (7.6\text{-}5)$$

where $\mathrm{unif}(a,b)$ denotes the continuous uniform distribution in the interval $[a,b]$. These random variables may further be modelled as spatially consistent with correlation distance equal to the cluster-specific random variable correlation distance of Table 7.6.3.1-2.

2. The relative delay of *m*-th ray is given by $\tau'_{n,m} = \tau''_{n,m} - \min\left(\left\{\tau''_{n,i}\right\}_{i=1}^{M}\right)$, where *n* is the cluster index, $\tau''_{n,m} \sim \mathrm{unif}(0, 2c_{\mathrm{DS}})$, the cluster DS c_{DS} is given in Table 7.5-6. These random variables may further be modelled as spatially consistent with correlation distance equal to the cluster-specific random variable correlation distance of Table 7.6.3.1-2. In this case, the sub-cluster mapping according to (7.5-26) and Table 7.5-5 shall not be applied. The delays to be used in Equation (7.6-3) are given by $\tau_{n,m} = \tau_n + \tau'_{n,m}$.

3. Ray powers are determined unequally by the following process:

The power of *m*-th ray in *n*-th cluster is given by $P_{n,m} = P_n \cdot \dfrac{P'_{n,m}}{\sum_{m=1}^{M} P'_{n,m}}$ for *m* = 1,…,*M*, where

$$P'_{n,m} = \exp\left(-\frac{\tau'_{n,m}}{c_{\mathrm{DS}}}\right)\exp\left(-\frac{\sqrt{2}\left|\alpha_{n,m,\mathrm{AOA}}\right|}{c_{\mathrm{ASA}}}\right)\exp\left(-\frac{\sqrt{2}\left|\alpha_{n,m,\mathrm{AOD}}\right|}{c_{\mathrm{ASD}}}\right) \cdot \exp\left(-\frac{\sqrt{2}\left|\alpha_{n,m,\mathrm{ZOA}}\right|}{c_{\mathrm{ZSA}}}\right)\exp\left(-\frac{\sqrt{2}\left|\alpha_{n,m,\mathrm{ZOD}}\right|}{c_{\mathrm{ZSD}}}\right) \quad (7.6\text{-}6)$$

and c_{DS}, c_{ASA}, c_{ASD}, and c_{ZSA} are respectively the intra-cluster delay spread and the corresponding intra-cluster angular spread that are given in Table 7.5-6. The cluster zenith spread of departure is given by

$$c_{\mathrm{ZSD}} = \frac{3}{8}10^{\mu_{\mathrm{lgZSD}}}, \quad (7.6\text{-}7)$$

with μ_{lgZSD} being defined in Tables 7.5-7, 7.5-8, 7.5-9, 7.5-10 and 7.5-11.

4. The number of rays per cluster shall be calculated as follows:

$$M = min\{max(M_t M_{\mathrm{AOD}} M_{\mathrm{ZOD}}, M_{\mathrm{min}}), M_{\mathrm{max}}\} \quad (7.6\text{-}8)$$

where:

- $M_t = \lceil 4kc_{\mathrm{DS}}B \rceil$
- $M_{\mathrm{AOD}} = \left\lceil 4kc_{\mathrm{ASD}} \frac{\pi \cdot D_h}{180 \cdot \lambda} \right\rceil$
- $M_{\mathrm{ZOD}} = \left\lceil 4kc_{\mathrm{ZSD}} \frac{\pi \cdot D_v}{180 \cdot \lambda} \right\rceil$
- $M_{\min}$ can be chosen based on the mean of dominant rays across all clusters for a specific frequency and deployment scenario. For example, the number of dominant rays in a cluster is defined as the minimum number of rays that contain 95% of the total cluster power, when the rays in a cluster are sorted in descending order of power. The default value of $M_{\min} = 20$ is assumed.
- $M_{\max}$ is the upper limit of M, and it should be selected by the user of channel model based on the trade-off between simulation complexity and accuracy.
- D_h and D_v are the array size in m in horizontal and vertical dimension, B is bandwidth in Hz, c_{ASD} and c_{ZSD} are the cluster spreads in degrees, and λ is the wavelength.
- k is a "sparseness" parameter with value 0.5.

It is noted that each MPC may have different AOD, ZOD, and delay.

7.6.3 Spatial consistency

7.6.3.1 Spatial consistency procedure

A new procedure, namely *a spatial consistency procedure*, can be used for both cluster-specific and ray-specific random variables to be generated in various channel generation steps in Clause 7.5, so that they are spatially consistent for drop-based simulations. Alternatively, this can be used together with Procedure B described in Clause 7.6.3.2 for spatially consistent mobility simulations.

The procedure can be considered as a 2D random process (in the horizontal plane) given the UT locations based on the parameter-specific correlation distance values for spatial consistency, specified in Table 7.6.3.1-2. The cluster specific random variables include:

- Cluster specific random delay in Step 5;
- Cluster specific shadowing in Step 6; and
- Cluster specific offset for AOD/AOA/ZOD/ZOA in Step 7.
- Cluster specific sign for AOD/AOA/ZOD/ZOA in Step 7.
- Optionally in case of large bandwidth as described in Clause 7.6.2.2 the procedure may apply as well for the parameters of rays within a cluster.

The procedure shall apply to each cluster before sorting the delay. Cluster specific sign for AOD/AOA/ZOD/ZOA in Step 7 shall be kept unchanged per simulation drop even if UT position changes during simulation. The ray specific random variables include:

- Random coupling of rays in Step 8;
- XPR in Step 9; and
- Random phase in Step 10.

The random coupling of rays in Step 8 and the intra-cluster delays in Step 11 shall be kept unchanged per simulation drop even if UT position changes during simulation.

Table 7.6.3.1-2 Correlation distance for spatial consistency

Correlation distance in [m]	RMa			UMi			UMa			SMa			Indoor	InF
	LOS	NLOS	O2I	LOS	NLOS	O2I	LOS	NLOS	O2I	LOS	NLOS	O2I		
Cluster and ray specific random variables	50	60	15	12	15	15	40	50	15	40	50	15	10	10
LOS/NLOS state	60			50			50			50			10	$d_{clutter}/2$
Indoor/outdoor state	50			50			50			50			N/A	N/A

7.6.3.2 Spatially-consistent UT/BS mobility modelling

For mobility simulation enhancement, two alternative spatial consistency procedures – Procedure A and Procedure B – are described as follows. The procedures presented below consider the downlink direction same as in Clause 7.5.

Procedure A:

For $t_0 = 0$ when a UT/BS is dropped into the network, spatially consistent powers/delays/angles of clusters are generated according to Clause 7.6.3.1.

The updated distance of UT/BS should be limited within 1 meter, i.e. when $v \cdot \Delta t < 1$ m, and the updated procedure in the following should take the closest realization instead of $t_0 = 0$. In case the absolute time of arrival modeling of clause 7.6.9 is simultaneously used, the update distance should be the minimum of 1 meter and $d_{3D}/10$.

At $t_k = t_{k-1} + \Delta t$, update channel cluster power/delay/angles based on UT/BS channel cluster power/delay/angles, moving speed moving direction and UT position at t_{k-1}.

Cluster delay is updated as:

$$\tilde{\tau}_n(t_k) = \begin{cases} \tilde{\tau}_n(t_{k-1}) - \frac{\hat{r}_{\mathrm{rx},n}(t_{k-1})^T \bar{v}_{\mathrm{rx}}(t_{k-1}) + \hat{r}_{\mathrm{tx},n}(t_{k-1})^T \bar{v}_{\mathrm{tx}}(t_{k-1})}{c} \Delta t & \text{for } k > 0 \\ \tau_n(t_0) + \tau_\Delta(t_0) + \frac{d_{3D}(t_0)}{c} & \text{for } k = 0 \end{cases} \quad (7.6\text{-}9)$$

where

c is the speed of light in [m/s];

$\bar{v}_{\mathrm{tx}}(t_k)$ and $\bar{v}_{\mathrm{rx}}(t_k)$ are the BS and UTvelocity vectors respectively, with $\|\overline{v}_{tx}(t_k)\|_2 = v_{tx}$ and $\|\overline{v}_{rx}(t_k)\|_2 = v_{rx}$;

$d_{3D}(t_0)$ is the 3D distance between Rx antenna and Tx antenna at t_0 in [m];

$\tau_n(t_0)$ are the cluster delays in [s] as in Step 11 in Clause 7.5;

$\tau_\Delta(t_0) = \begin{cases} 0 & \text{for LOS} \\ \min\left(\{\tau'_n\}_{n=1}^N\right) & \text{for NLOS} \end{cases}$, where τ'_n are the delays from Equation (7.5-1). In case the absolute time of arrival modelling of clause 7.6.9 is simultaneously used, $\tau_\Delta(t_0) = \begin{cases} 0 & \text{for LOS} \\ \Delta\tau & \text{for NLOS} \end{cases}$ where $\Delta\tau$ is determined according to clause 7.6.9.

Also,

$$\hat{r}_{rx,n}\left(t_{k-1}\right)=\begin{bmatrix}\sin\left(\theta_{n,\mathrm{ZOA}}\left(t_{k-1}\right)\right)\cos\left(\phi_{n,\mathrm{AOA}}\left(t_{k-1}\right)\right)\\ \sin\left(\theta_{n,\mathrm{ZOA}}\left(t_{k-1}\right)\right)\sin\left(\phi_{n,\mathrm{AOA}}\left(t_{k-1}\right)\right)\\ \cos\left(\theta_{n,\mathrm{ZOA}}\left(t_{k-1}\right)\right)\end{bmatrix} \quad (7.6\text{-}10)$$

where $\theta_{n,ZOA}$ and $\phi_{n,AOA}$ are cluster specific zenith and azimuth angles of arrival.

$$\hat{r}_{\mathrm{tx},n}(t_{k-1})=\begin{bmatrix}\sin\left(\theta_{n,\mathrm{ZOD}}(t_{k-1})\right)\cos\left(\phi_{n,\mathrm{AOD}}(t_{k-1})\right)\\ \sin\left(\theta_{n,\mathrm{ZOD}}(t_{k-1})\right)\sin\left(\phi_{n,\mathrm{AOD}}(t_{k-1})\right)\\ \cos\left(\theta_{n,\mathrm{ZOD}}(t_{k-1})\right)\end{bmatrix} \quad (7.6\text{-}10aa)$$

where $\theta_{n,\mathrm{ZOD}}$ and $\phi_{n,\mathrm{AOD}}$ are the cluster specific zenith and azimuth angles of departure.

After updating the delays according to equation (7.6-9), the delays over the mobility range are normalized. Equation (7.5-2) of the fast fading model is replaced by

$$\tau_n(t_k)=\tilde{\tau}_n(t_k)-\min\left(\{\tilde{\tau}_n(t_k)\}_{n=1}^{N}\right) \quad (7.6\text{-}10a)$$

in which t_k covers the entire duration of the mobility model.

Cluster powers are updated as in Step 6 using the cluster delays from Equation (7.6-10a).
Cluster departure angles ($\theta_{n,\mathrm{ZOD}}$ and $\phi_{n,\mathrm{AOD}}$) and arrival angles ($\theta_{n,\mathrm{ZOA}}$ and $\phi_{n,\mathrm{AOA}}$) are updated using a cluster-wise transformation of the UT/BS velocity vector given by

$$\vec{v}'_{n,\mathrm{rx}}(t_k)=\begin{cases}\vec{v}_{\mathrm{rx}}(t_k)-\vec{v}_{\mathrm{tx}}(t_k) & \text{for LOS}\\ R_{n,\mathrm{rx}}\cdot\vec{v}_{\mathrm{rx}}(t_k)-\vec{v}_{\mathrm{tx}}(t_k) & \text{for NLOS}\end{cases} \quad (7.6\text{-}10b)$$

$$\vec{v}'_{n,\mathrm{tx}}(t_k)=\begin{cases}\vec{v}_{\mathrm{tx}}(t_k)-\vec{v}_{\mathrm{rx}}(t_k) & \text{for LOS}\\ R_{n,\mathrm{tx}}\cdot\vec{v}_{\mathrm{tx}}(t_k)-\vec{v}_{\mathrm{rx}}(t_k) & \text{for NLOS}\end{cases} \quad (7.6\text{-}10c)$$

with

$$R_{n,\mathrm{rx}}=R_Z\left(\phi_{n,\mathrm{AOD}}(t_k)+\pi\right)\cdot R_Y\left(\frac{\pi}{2}-\theta_{n,\mathrm{ZOD}}(t_k)\right)\cdot\begin{bmatrix}1&0&0\\0&X_n&0\\0&0&1\end{bmatrix}\cdot R_Y\left(\frac{\pi}{2}-\theta_{n,\mathrm{ZOA}}(t_k)\right)\cdot R_Z\left(-\phi_{n,\mathrm{AOA}}(t_k)\right),$$

and

$$R_{n,\mathrm{tx}}=R_Z\left(-\phi_{n,\mathrm{AOD}}(t_k)\right)\cdot R_Y\left(\frac{\pi}{2}-\theta_{n,\mathrm{ZOD}}(t_k)\right)\cdot\begin{bmatrix}1&0&0\\0&X_n&0\\0&0&1\end{bmatrix}\cdot R_Y\left(\frac{\pi}{2}-\theta_{n,\mathrm{ZOA}}(t_k)\right)\cdot R_Z\left(\phi_{n,\mathrm{AOA}}(t_k)+\pi\right),$$

where $R_Y(\beta)$ and $R_Z(\alpha)$ being the rotation matrices around y-axis and z-axis as defined in Equation (7.1-2). Random variable $X_n\in\{1,-1\}$ is sampled from a uniform distribution on a NLOS cluster basis and is not changed during the UT mobility within a drop. The cluster specific decorrelation distances are 60m, 15m, 50m and 10m for RMa, UMi, UMa and Indoor scenarios, respectively.

Now, the departure and arrival angles in radians are updated as:

$$\phi_{n,\mathrm{AOD}}(t_k)=\phi_{n,\mathrm{AOD}}(t_{k-1})+\frac{\vec{v}'_{n,\mathrm{rx}}(t_{k-1})^T\hat{\phi}\left(\theta_{n,\mathrm{ZOD}}(t_{k-1}),\phi_{n,\mathrm{AOD}}(t_{k-1})\right)}{c\cdot\tilde{\tau}_n(t_{k-1})\sin\left(\theta_{n,ZOD}(t_{k-1})\right)}\Delta t \quad (7.6\text{-}11)$$

$$\theta_{n,\mathrm{ZOD}}(t_k)=\theta_{n,\mathrm{ZOD}}(t_{k-1})+\frac{\vec{v}'_{n,\mathrm{rx}}(t_{k-1})^T\hat{\theta}\left(\theta_{n,\mathrm{ZOD}}(t_{k-1}),\phi_{n,\mathrm{AOD}}(t_{k-1})\right)}{c\cdot\tilde{\tau}_n(t_{k-1})}\Delta t \quad (7.6\text{-}12)$$

and

$$\phi_{n,\mathrm{AOA}}(t_k) = \phi_{n,\mathrm{AOA}}(t_{k-1}) + \frac{\vec{v}'_{n,\mathrm{tx}}(t_{k-1})^T \hat{\phi}\left(\theta_{n,\mathrm{ZOA}}(t_{k-1}), \phi_{n,\mathrm{AOA}}(t_{k-1})\right)}{c \cdot \tilde{\tau}_n(t_{k-1}) \sin\left(\theta_{n,\mathrm{ZOA}}(t_{k-1})\right)} \Delta t \quad (7.6\text{-}13)$$

$$\theta_{n,\mathrm{ZOA}}(t_k) = \theta_{n,\mathrm{ZOA}}(t_{k-1}) + \frac{\vec{v}'_{n,\mathrm{tx}}(t_{k-1})^T \hat{\theta}\left(\theta_{n,\mathrm{ZOA}}(t_{k-1}), \phi_{n,\mathrm{AOA}}(t_{k-1})\right)}{c \cdot \tilde{\tau}_n(t_{k-1})} \Delta t, \quad (7.6\text{-}14)$$

with $\hat{\theta}(\theta,\phi)$ and $\hat{\phi}(\theta,\phi)$ being the spherical unit vectors defined in Equations (7.1-13) and (7.1-14).

Procedure B:

In procedure B, spatial or time evolution of the channel is obtained by generating channel realizations separately for all links to different Rx positions using Steps 1-12 of Clause 7.5 together with the spatially consistent procedure of Clause 7.6.3.1. In the case of mobility these positions may be a function of time along one or more Rx trajectories. Furthermore, to ensure that the spatial or time evolution of delays and angles are within reasonable limits, Steps 5, 6, and 7 in Clause 7.5 should be replaced by the below procedure.

Note: For implementation purposes, LSPs and SSPs may be interpolated within the coherence length or time of the respective parameter.

Step 5: Generate cluster delays τ_n, with $n \in [1, N]$.

N delays are drawn randomly from a uniform distribution.

$$\tau'_n \sim \mathrm{unif}\left(0, 2 \cdot 10^{\mu_{\mathrm{lgDS}} + \sigma_{\mathrm{lgDS}}}\right) \quad (7.6\text{-}15)$$

Normalise the delays by subtracting the minimum delay: $\tau_n = \tau'_n - \min(\tau'_n)$. The autocorrelation distance for τ'_n is $2c \cdot 10^{\mu_{\mathrm{lgDS}} + \sigma_{\mathrm{lgDS}}}$.

In the case of LOS, set the delay of the first cluster τ_1 to 0.

Step 6: Generate N arrival angles and departure angles for both azimuth and elevation using (7.6-16) instead of (7.5-9) and (7.5-14).

$$\phi'_{n,\mathrm{AOA}} \sim 2 \cdot 10^{\mu_{\mathrm{lgASA}} + \sigma_{\mathrm{lgASA}}} \mathrm{unif}(-1,1) \quad (7.6\text{-}16)$$

with $n \in [1, N]$. This step is repeated independently for AOD, AOA, ZOD, and ZOA with corresponding maximum angles for the uniform distribution. In case of LOS, set the angles of the first cluster ($\phi'_{1,\mathrm{AOA}}$, etc) to 0.

The autocorrelation distances are $2c \cdot 10^{\mu_{\mathrm{lgDS}} + \sigma_{\mathrm{lgDS}}}$ for AOD, and ZOD, while they are fixed to 50m for AOA, and ZOA.

Offset angles etc are applied in the modified Step 7b below after cluster powers have been calculated.

Step 7: Generate cluster powers P_n

Cluster powers are calculated assuming a single slope exponential power profile and Laplacian angular power profiles. The cluster powers are determined by

$$P'_n = \exp\left(\frac{-\tau'_n}{\mathrm{DS}}\right) \exp\left(\frac{-\sqrt{2}\left|\phi'_{n,\mathrm{AOA}}\right|}{\mathrm{ASA}}\right) \exp\left(\frac{-\sqrt{2}\left|\phi'_{n,\mathrm{AOD}}\right|}{\mathrm{ASD}}\right) \cdot \exp\left(\frac{-\sqrt{2}\left|\theta'_{n,\mathrm{ZOA}}\right|}{\mathrm{ZSA}}\right) \exp\left(\frac{-\sqrt{2}\left|\theta'_{n,\mathrm{ZOD}}\right|}{\mathrm{ZSD}}\right) \cdot 10^{\frac{-Z_n}{10}} \quad (7.6\text{-}17)$$

where $Z_n \sim N(0, \zeta^2)$ (autocorrelation distance same as for shadow fading) is the per cluster shadowing term in [dB]. Delay spread DS and angular spreads ASA, ASD, ZSA, ZSD are generated in Step 4 of Clause 7.5. Normalize the cluster powers so that the sum of all cluster powers is equal to one, i.e.,

$$P_n = \frac{P'_n}{\sum_{n=1}^{N} P'_n} \tag{7.6-17a}$$

In the case of LOS condition, substitute DS with $\sqrt{1+K_R/2} \cdot \mathrm{DS}$ and { ASA, ASD, ZSA, ZSD } with { $\sqrt{1+K_R} \cdot \mathrm{ASA}$, $\sqrt{1+K_R} \cdot \mathrm{ASD}$, $\sqrt{1+K_R} \cdot \mathrm{ZSA}$, $\sqrt{1+K_R} \cdot \mathrm{ZSD}$ } respectively to preserve the delay and angular spreads. K_R is the Ricean K-factor as generated in Step 4 converted to linear scale. Furthermore, an additional specular component is added to the first cluster. Power of the single LOS ray is:

$$P_{1,LOS} = \frac{K_R}{K_R + 1} \tag{7.6-17b}$$

and the cluster powers are not normalized as in equation (7.6-17a), but:

$$P_n = \frac{1}{K_R + 1} \frac{P'_n}{\sum_{n=1}^{N} P'_n} + \delta(n-1) P_{1,LOS} \tag{7.6-17c}$$

where δ(.) is Dirac's delta function.

Assign the power of each ray within a cluster as P_n / M, where M is the number of rays per cluster.

Step 7b: Apply offset angles

The ray AOA angles are determined by

$$\phi_{n,m,\mathrm{AOA}} = \phi'_{n,\mathrm{AOA}} + \phi_{LOS,\mathrm{AOA}} + c_{ASA}\alpha_m \tag{7.6-17d}$$

where $\phi_{\mathrm{LOS,AOA}}$ is the LOS direction defined in the network layout description, see Step1c.

The generation of AOD ($\phi_{n,m,AOD}$) follows a procedure similar to AOA as described above.

The ZOA angles are determined by

$$\theta_{n,m,\mathrm{ZOA}} = \phi'_{n,\mathrm{ZOA}} + \bar{\theta}_{ZOA} + c_{ZSA}\alpha_m \tag{7.6-17e}$$

where $\bar{\theta}_{ZOA} = 90^0$ if the BS-UT link is O2I and $\bar{\theta}_{ZOA} = \theta_{LOS,ZOA}$ otherwise. The LOS direction is defined in the network layout description, see Step1c.

The ZOA angles are determined by

$$\theta_{n,m,\mathrm{ZOD}} = \phi'_{n,\mathrm{ZOD}} + \theta_{LOS,ZOD} + \mu_{offset,ZOD} + (3/8)(10^{\mu_{\mathrm{lgZSD}}})\alpha_m \tag{7.6-17f}$$

where μ_{lgZSD} is the mean of the ZSD log-normal distribution.

Some of the delay and angle spreads and standard deviations used in equations (7.6-15) and (7.6-16) may be frequency-dependent. In the case of multi-frequency simulations according to Clause 7.6.5, the largest value among all the

simulated frequencies should be used in (7.6-15) and (7.6-16) so that the cluster and ray delays and angles (but not the powers or the resulting delay or angular spreads) are the same for all frequencies.

7.6.3.3 LOS/NLOS, indoor states and O2I parameters

The LOS state can be determined according to the spatial consistency procedure for random variables as mentioned in Clause 7.6.3.1, by comparing a realization of a random variable generated with distance-dependent LOS probability. If the realization is less than the LOS probability, the state is LOS; otherwise NLOS. Decision of LOS and NLOS status should be used in Step 2 in Clause 7.5 if this advanced simulation is performed.

The same procedure can be applied for determining the indoor state, with the indoor probability instead of the LOS probability.

The correlation distance for LOS state and indoor/outdoor is specified in Table 7.6.3.1-2.

The indoor distance can be modeled as the minimum of two spatially consistent uniform random variables within (0, 25) meters with correlation distance 25m.

Note in case the UT is in an indoor state, the pathloss model changes and a penetration loss is considered. For details on the model, see Clause 7.4.3. Here, the focus is on modelling aspects with respect to spatial consistency. As described in Clause 7.4.3, the penetration loss deviation σ_p represents variations within and between buildings of the same type. For spatial consistency this can be modeled as a spatially consistent random variable with correlation distance 10m, see Clause 7.6.3.1. The "building type" is determined using a spatially consistent uniform random variable with correlation distance 50 m. The building type is determined by comparing the random variable with P_1, where P_1 is the probability of the building type with low loss penetration. If the realization of the random variable is less than P_1, the building type is low loss; otherwise the building type is high loss.

The cluster-specific and ray-specific random variables as defined in Clause 7.6.3.1 on the same floor are generated in the spatial consistency modelling; otherwise, these variables across different floors are uncorrelated.

In case there is a transition from LOS to NLOS due to UT mobility, there will be a hard transition in the channel response. This is because pathloss and LS parameters are different for these states, leading automatically to very different channel realizations. To circumvent such hard transitions the optional soft LOS state can be considered to determine the PL and the channel impulse responses containing characteristics of both LOS and NLOS. Soft LOS state $\mathrm{LOS}_{\mathrm{soft}}$ is generated by floating numbers between 0 (NLOS) and 1 (LOS) in the spatial consistency modelling. The value of $\mathrm{LOS}_{\mathrm{soft}}$ is determined by

$$\mathrm{LOS}_{\mathrm{soft}} = \frac{1}{2} + \frac{1}{\pi}\arctan\left(\sqrt{\frac{20}{\lambda}}\left(G + F\left(d\right)\right)\right), \tag{7.6-18}$$

where:

- G is a spatially consistent Gaussian random variable with correlation distance according to Table 7.6.3.1-2;
- $F\left(d\right) = \sqrt{2}\mathrm{erf}^{-1}\left(2\,\mathrm{Pr}_{\mathrm{LOS}}\left(d\right) - 1\right)$; and
- $\mathrm{Pr}_{\mathrm{LOS}}\left(d\right)$ is the distance dependent LOS probability function.

After $\mathrm{LOS}_{\mathrm{soft}}$ is obtained, Steps 2-12 of the channel coefficient generation described in Clause 7.5 are performed twice, once with the propagation condition in Step 2 set as LOS and once with the propagation condition in Step 2 set as NLOS. The resulting channel coefficients are denoted as H^{LOS} and H^{NLOS} respectively, where H^{LOS} is generated with the LOS path loss formula and channel model parameters while is H^{NLOS} generated using the NLOS path loss formula and channel model parameters. The channel matrix H with soft LOS state is determined from a linear combination of H^{LOS} and H^{NLOS} as:

$$H\left(\mathrm{LOS}_{\mathrm{soft}}\right) = H^{\mathrm{LOS}}\mathrm{LOS}_{\mathrm{soft}} + H^{\mathrm{NLOS}}\sqrt{1 - \mathrm{LOS}_{\mathrm{soft}}^{2}} \tag{7.6-19}$$

It is noted that soft indoor/outdoor states are not modelled in this TR. Thus the model does not support transitions between indoor/outdoor states in mobility simulations.

7.6.3.4 Applicability of spatial consistency

According to the characteristics of different cluster specific parameters and ray specific parameters, the following types on spatial consistency are defined:

- Site-specific: parameters for different BS-UT links are uncorrelated, but the parameters for links from co-sited sectors to a UT are correlated.
- All-correlated: BS-UT links are correlated.

In Table 7.6.3.4-1, correlation type for each large scale parameter, cluster specific parameter and ray specific parameter is clarified.

Table 7.6.3.4-1: Correlation type among TRPs

Parameters	Correlation type
Delays	Site-specific
Cluster powers	Site-specific
AOA/ZOA/AOD/ZOD offset	Site-specific
AOA/ZOA/AOD/ZOD sign	Site-specific
Random coupling	Site-specific
XPR	Site-specific
Initial random phase	Site-specific
LOS/NLOS states	Site-specific
Blockage (Model A)	All-correlated
O2I penetration loss	All-correlated
Indoor distance	All-correlated
Indoor states	All-correlated

Spatial consistency is not modelled in the following situations:

- Different link types, e.g., outdoor LOS, outdoor NLOS or O2I
- UE locates on different floors

Table 7.6.3.4-2, lists conditions in which each large scale parameter, cluster specific parameter and ray specific parameter is assumed not spatially correlated.

Table 7.6.3.4-2: Conditions when parameters are not spatially correlated.

Parameters	Uncorrelated states
Delays	Outdoor LOS/outdoor NLOS/O2I (different floors)
Cluster powers	Outdoor LOS/outdoor NLOS/O2I (different floors)
AOA/ZOA/AOD/ZOD offset	Outdoor LOS/outdoor NLOS/O2I (different floors)
AOA/ZOA/AOD/ZOD sign	Outdoor LOS/outdoor NLOS/O2I (different floors)
Random coupling	Outdoor LOS/outdoor NLOS/O2I (different floors)
XPR	Outdoor LOS/outdoor NLOS/O2I (different floors)
Initial random phase	Outdoor LOS/outdoor NLOS/O2I (different floors)
Blockage	Outdoor/O2I (different floors)
Standard deviation for O2I penetration loss	Different building types, i.e., high/low loss

7.6.4 Blockage

Blockage modelling is an add-on feature to the channel model. The method described in the following applies only when this feature is turned on. In addition, the temporal variability of the blockage modelling parameters is on-demand basis. It is also noted that the modelling of the blockage does not change LOS/NLOS state of each link.

When blockage model is applied, the channel generation in Clause 7.5 should have several additional steps between Step 9 and 10 as illustrated in Figure 7.6.4-1.

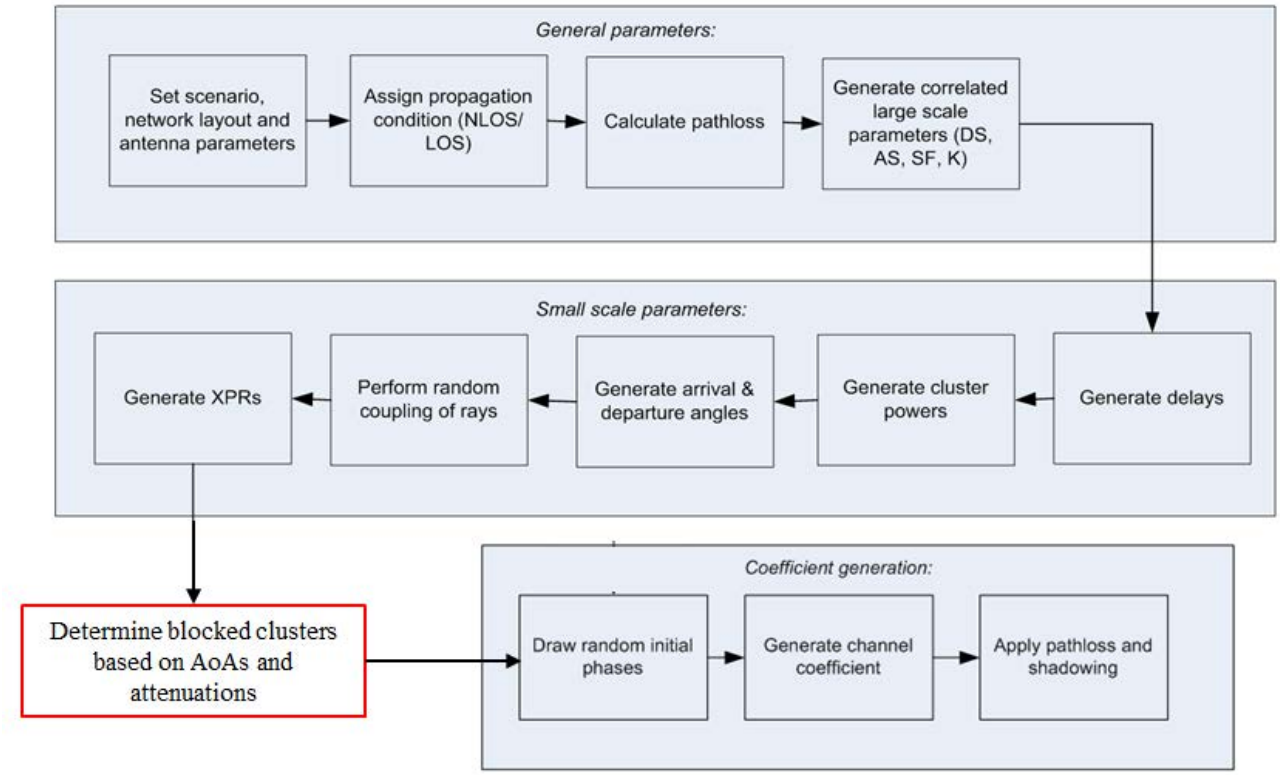

Figure.7.6.4-1 Channel generation procedure with blockage model

Two alternative models (Model A and Model B) are provided for the blockage modelling. Both approaches have their own use cases. Model A is applicable when a generic and computationally efficient blockage modelling is desired. Model B is applicable when a specific and more realistic blocking modelling is desired.

7.6.4.1 Blockage model A

Model A adopts a stochastic method for capturing human and vehicular blocking.

Step a: Determine the number of blockers.

Multiple 2-dimensional (2D) angular blocking regions, in terms of centre angle, azimuth and elevation angular span are generated around the UT. There is one self-blocking region, and K_{block} = 4 non-self-blocking regions, where K_{block} may be changed for certain scenarios (e.g., higher blocker density). Note that the self-blocking component of the model is important in capturing the effects of human body blocking.

Step b: Generate the size and location of each blocker.

For self-blocking, the blocking region in UT LCS is defined in terms of elevation and azimuth angles, ($\theta'_{\text{sb}}, \phi'_{\text{sb}}$) and azimuth and elevation angular span (x_{sb} , y_{sb}).

$$\left\{(\theta',\phi')\middle|\left(\theta'_{\text{sb}}-\frac{y_{\text{sb}}}{2}\le\theta'\le\theta'_{\text{sb}}+\frac{y_{\text{sb}}}{2},\phi'_{\text{sb}}-\frac{x_{\text{sb}}}{2}\le\phi'\le\phi'_{\text{sb}}+\frac{x_{\text{sb}}}{2}\right)\right\} \quad (7.6\text{-}20)$$

where the parameters are described in Table 7.6.4.1-1.

Table 7.6.4.1-1: Self-blocking region parameters.

	ϕ'_{sb}	x_{sb}	θ'_{sb}	y_{sb}
Portrait mode	260º	120º	100º	80º
Landscape mode	40º	160º	110º	75º

For non-self-blocking k = 1, …, 4, the blocking region in GCS is defined by

$$\left\{(\theta,\phi)\middle|\left(\theta_k-\frac{y_k}{2}\le\theta\le\theta_k+\frac{y_k}{2},\phi_k-\frac{x_k}{2}\le\phi\le\phi_k+\frac{x_k}{2}\right)\right\} \tag{7.6-21}$$

where the parameters are described in Table 7.6.4.1-2, as well as the distance r between the UT and the blocker.

Table 7.6.4.1-2: Blocking region parameters.

Blocker index (k = 1, …, 4)	ϕ_k	x_k	θ_k	y_k	r
InH scenario	Uniform in [0º, 360º]	Uniform in [15º, 45º]	90º	Uniform in [5º, 15º]	2 m
UMi, UMa, SMa, RMa scenarios	Uniform in [0º, 360º]	Uniform in [5º, 15º]	90º	5º	10 m

Step c: Determine the attenuation of each cluster due to blockers.

The attenuation of each cluster due to self-blocking corresponding to the centre angle pair (θ'_{sb}, ϕ'_{sb}), is 30 dB provided that $\left|\phi'_{\text{AOA}}-\phi'_{\text{sb}}\right|<\frac{x_{\text{sb}}}{2}$ and $\left|\theta'_{\text{ZOA}}-\theta'_{\text{sb}}\right|<\frac{y_{\text{sb}}}{2}$. Otherwise, the attenuation is 0 dB.

The attenuation of each cluster due to the non-self-blocking regions (k=1, …, 4) is given by

$$L_{\text{dB}}=-20\log_{10}\left(1-\left(F_{A_1}+F_{A_2}\right)\left(F_{Z_1}+F_{Z_2}\right)\right) \tag{7.6-22}$$

provided that $\left|\phi_{\text{AOA}}-\phi_k\right|<x_k$ and $\left|\theta_{\text{ZOA}}-\theta_k\right|<y_k$. Otherwise, the attenuation is 0 dB. The terms in the above equation are given as

$$F_{A_1|A_2|Z_1|Z_2}=\frac{\tan^{-1}\left(\pm\frac{\pi}{2}\sqrt{\frac{\pi}{\lambda}r\left(\frac{1}{\cos\left(A_1\,|\,A_2\,|\,Z_1\,|\,Z_2\right)}-1\right)}\right)}{\pi} \tag{7.6-23}$$

where

$$A_1=\phi_{\text{AOA}}-\left(\phi_k+\frac{x_k}{2}\right), \tag{7.6-24}$$

$$A_2=\phi_{\text{AOA}}-\left(\phi_k-\frac{x_k}{2}\right), \tag{7.6-25}$$

$$Z_1=\theta_{\text{ZOA}}-\left(\theta_k+\frac{y_k}{2}\right), \tag{7.6-26}$$

$$Z_2=\theta_{\text{ZOA}}-\left(\theta_k-\frac{y_k}{2}\right). \tag{7.6-27}$$

In the above formula for $F_{A_1|A_2|Z_1|Z_2}$, λ is the wavelength. The appropriate signs ($\pm$)within the $\tan^{-1}$ term are described in Table 7.6.4.1-3.

Table 7.6.4.1-3: Description of signs

	$-y_k < \theta_{\text{ZOA}} - \theta_k \le -\frac{y_k}{2}$	$-\frac{y_k}{2} < \theta_{\text{ZOA}} - \theta_k \le \frac{y_k}{2}$	$\frac{y_k}{2} < \theta_{\text{ZOA}} - \theta_k \le y_k$
$\frac{x_k}{2} < \phi_{\text{AOA}} - \phi_k \le x_k$	(-, +) for (A_1, A_2) (+, -) for (Z_1, Z_2)	(-, +) for (A_1, A_2) (+, +) for (Z_1, Z_2)	(-, +) for (A_1, A_2) (-, +) for (Z_1, Z_2)
$-\frac{x_k}{2} < \phi_{\text{AOA}} - \phi_k \le \frac{x_k}{2}$	(+, +) for (A_1, A_2) (+, -) for (Z_1, Z_2)	(+, +) for (A_1, A_2) (+, +) for (Z_1, Z_2)	(+, +) for (A_1, A_2) (-, +) for (Z_1, Z_2)
$-x_k < \phi_{\text{AOA}} - \phi_k \le -\frac{x_k}{2}$	(+, -) for (A_1, A_2) (+, -) for (Z_1, Z_2)	(+, -) for (A_1, A_2) (+, +) for (Z_1, Z_2)	(+, -) for (A_1, A_2) (-, +) for (Z_1, Z_2)

Step d: Spatial and temporal consistency of each blocker.

The centre of the blocker is generated based on a uniformly distributed random variable, which is temporally and spatially consistent. The two-dimensional autocorrelation function $R(\Delta_x, \Delta_t)$ can be described with sufficient accuracy by the exponential function

$$R(\Delta_x, \Delta_t) = \exp\left(-\left(\frac{|\Delta_x|}{d_{\text{corr}}} + \frac{|\Delta_t|}{t_{\text{corr}}}\right)\right) \quad (7.6\text{-}28)$$

The spatial correlation distance d_{corr} for the random variable determining the centre of the blocker is given in Table 7.6.4.1-4 for different scenarios.

Table 7.6.4.1-4: Spatial correlation distance for different scenarios.

Spatial correlation distance d_{corr} in [m] for the random variable determining the centre of the blocker	UMi/UMa/SMa/RMa			InH	
	LOS	NLOS	O2I	LOS	NLOS
	10	10	5	5	5

The correlation time is defined by $t_{\text{corr}} = d_{\text{corr}}/v$, where v is the speed of the moving blocker.

Note: The rectangular blocker description is chosen for self-blocking region with the specific choices of (θ'_{sb}, ϕ'_{sb}) assumed here. Generalization of this description to other choices should be done with care as the rectangular description may not be accurate.

7.6.4.2 Blockage model B

Model B adopts a geometric method for capturing e.g., human and vehicular blocking.

Step a: Determine blockers

A number, K_{block}, of blockers are modelled as rectangular screens that are physically placed on the map. Each screen has the dimension by height (h_k) and width (w_k), with the screen centre at coordinate (x_k, y_k, z_k).

Note:

- The number of blockers (K_{block}), their vertical and horizontal extensions (h_k and w_k), locations (x_k, y_k, z_k), density, and movement pattern (if non-stationary) are all simulation assumptions, to allow different blocking scenarios to be constructed depending on the need of the particular simulation study.

  Recommended parameters for typical blockers are provided in Table 7.6.4.2-5.

- The blocking effect diminishes with increasing distance to the blocker. For implementation purposes it may be sufficient to consider only the K_{block} nearest blockers or the blockers closer than some distance from a specific UT.

Table 7.6.4.2-5: Recommended blocker parameters

	Typical set of blockers	Blocker dimensions	Mobility pattern
Indoor; Outdoor; InF	Human	Cartesian: w=0.3m; h=1.7m	Stationary or up to 3 km/h
Outdoor	Vehicle	Cartesian: w=4.8m; h=1.4m	Stationary or up to 100 km/h
InF	AGV	Cartesian: w=3m; h=1.5m	Up to 30 km/h
InF	Industrial robot	Cartesian: w=2m; h=0.2m	Up to 3 m/s

Step b: Determine the blockage attenuation per sub-path

Attenuation caused by each blocker to each sub-path is modelled using a simple knife edge diffraction model and is given by

$$L_{\mathrm{dB}} = -20\log_{10}\left(1-\left(F_{h_1}+F_{h_2}\right)\left(F_{w_1}+F_{w_2}\right)\right) \tag{7.6-29}$$

where F_{h_1}, F_{h_2} and F_{w_1}, F_{w_2} account for knife edge diffraction at the four edges, and are given by

$$F_{h_1|h_2|w_1|w_2} = \begin{cases} \dfrac{\tan^{-1}\left(\pm\dfrac{\pi}{2}\sqrt{\dfrac{\pi}{\lambda}\left(\mathrm{D1}_{h_1|h_2|w_1|w_2}+\mathrm{D2}_{h_1|h_2|w_1|w_2}-r\right)}\right)}{\pi} & \text{, for direct path in LOS} \\ \dfrac{\tan^{-1}\left(\pm\dfrac{\pi}{2}\sqrt{\dfrac{\pi}{\lambda}\left(\mathrm{D1}_{h_1|h_2|w_1|w_2}-r'\right)}\right)}{\pi} & \text{, for all other paths} \end{cases} \tag{7.6-30}$$

where λ is the wave length. As shown in Figure 7.6.4.2-2, $\mathrm{D1}_{h_1|h_2|w_1|w_2}$ are the projected (onto the side and top view planes) distances between the receiver and four edges of the corresponding blocker, and $\mathrm{D2}_{h_1|h_2|w_1|w_2}$ are the projected (onto the side and top view planes) distances between the transmitter and four edges of the corresponding blocker. The side view plane is perpendicular to the horizontal ground plane. The top view is perpendicular to the side view. For each cluster, the blocker screen is rotated around its centre such that the arrival direction of the corresponding path is always perpendicular to the screen. It should be noted that different rotations are required for each individual sub-path. Meanwhile, the base and top edges of the screens are always parallel to the horizontal plane. As the screen is perpendicular to each sub-path, r is the distance between the transmitter and receiver for the direct path in LOS, and r' is the distance between the blocker screen and receiver, projected onto the incoming sub-path direction, for all the other (NLOS) paths. In the equation of $F_{h_1|h_2|w_1|w_2}$, the plus and minus signs are determined in such a way that, as shown in Figure 7.6.4.2-2,

- if the sub-path (terminated at the receiver or transmitter) does not intersect the screen in side view, minus sign is applied for the shortest path among $\mathrm{D1}_{h_1}$ and $\mathrm{D1}_{h_2}$ in the NLOS case ($\mathrm{D1}_{h_1}+\mathrm{D2}_{h_1}$ and $\mathrm{D1}_{h_2}+\mathrm{D2}_{h_2}$ in the LOS case) and plus sign is applied for the other edge.

- if the sub-path (terminated at the receiver or transmitter) does not intersect the screen in top view, minus sign is applied for the shortest path among $D1_{w_1}$ and $D1_{w_2}$ in the NLOS case ($D1_{w_1}+D2_{w_1}$ and $D1_{w_2}+D2_{w_2}$ for the LOS case) and plus sign is applied for the other edge.
- if the sub-path intersects the screen plus signs are applied for both edges.

For the case of multiple screens the total loss is given by summing the losses of each contributing screen in dB units.

The model according to option B is consistent in time, frequency and space, and is more appropriate to be used for simulations with arbitrarily designated blocker density.

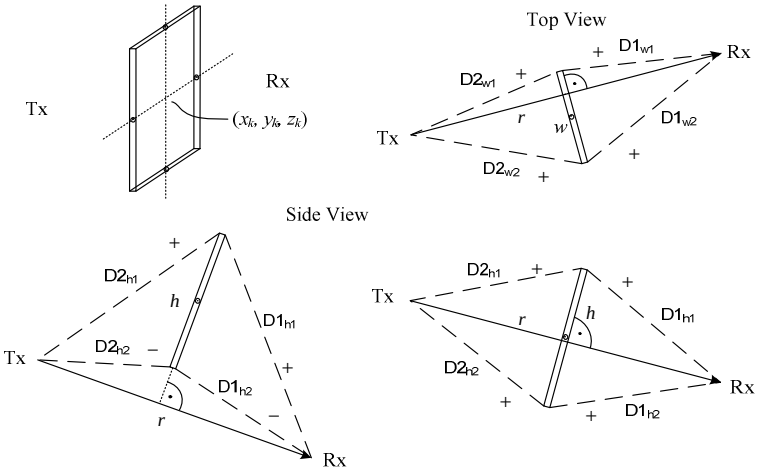

Figure 7.6.4.2-2(a): Illustration of the geometric relation among blocker, receiver and transmitter for the LOS path

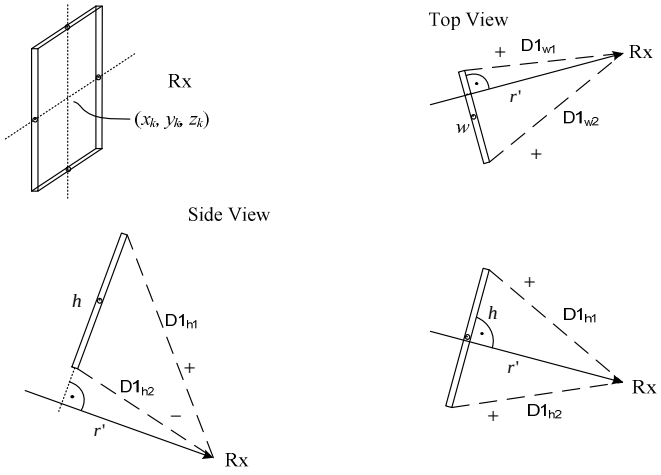

Figure 7.6.4.2-2(b): Illustration of the geometric relation between blocker and receiver for NLOS paths

7.6.5 Correlation modelling for multi-frequency simulations

This clause describes how to generate parameters to reflect correlation across different frequencies for a BS-UT link, for simulations involved with multiple frequencies.

For those simulations, the steps in Clause 7.5 should be revised according to the following:

- The parameters generated in Step 1 are the same for all the frequencies, except for antenna patterns, array geometries, system center frequency and bandwidth.
- Propagation conditions generated in Step 2 are the same for all the frequencies. It is noted that soft LOS states may be different due to frequency dependent function.
- The parameters generated in Step 4 are the same for all the frequencies, except for possibly frequency-dependent scaling of e.g. delay spread and angular spreads according to the LSP tables. I.e. let x be a random variable drawn from a Gaussian distribution: x ~ N(0,1). Then the delay spread at frequency f is DS(f)= 10^(μ_{lgDS}(f) + σ_{lgDS}(f)·x), where the same value of x is used for all frequencies. A corresponding procedure applies to each of the angular spreads.
- The cluster delays and angles resulting from Steps 5-7 are the same for all frequency bands
- Per-cluster shadowing Z_n in Step 6 are independently generated for the frequency bands.
- Cluster powers in Step 6 may be frequency-dependent.
- Steps 8-11 are independently applied for the frequency bands.

In addition, when blockage is modeled according to Clause 7.6.4, the positions of blockers are the same across all the frequencies.

Note: The requirements above may not be fully aligned with the behavior of the model according to Clause 7.5, since cluster delays and angles will be frequency-dependent in scenarios where the DS or AS is frequency-dependent. The procedure below may alternatively be used to ensure that cluster delays and angles are frequency-independently generated.

7.6.5.1 Alternative channel generation method

The alternative method replaces Steps 5-7 in Clause 7.5 with the below Steps 5'-7'. The inputs to the alternative method are the delay and angular spreads determined according to Step 4 at an anchor frequency, e.g. 2 GHz: DS_0, ASD_0, ASA_0, ZSD_0, ZSA_0, the delay and angular spreads determined according to Step 4 at a frequency of interest: DS, ASD, ASA, ZSD, ZSA, and the number of clusters *N* from Table 7.5-6.

Step 5': Generate nominal delays τ'_n and angles $\phi'_{AOD,n}$, $\phi'_{AOA,n}$, $\theta'_{ZOD,n}$, $\theta'_{ZOA,n}$.

Generate *N* delays from a single-sided exponential distribution with zero mean and standard deviation of $r\mathrm{DS}_0$, according to $\tau'_n = -r\mathrm{DS}_0 \ln(X_n)$ with $X_n \sim \mathrm{unif}(0,1)$.

Generate *N* AODs from a wrapped Gaussian distribution with zero mean and standard deviation of $r\mathrm{ASD}_0$, according to $\phi'_{AOD,n} = \arg(\exp(-jr\mathrm{ASD}_0 Y_n))$ with $Y_n \sim N(0,1)$.

Generate *N* AOAs from a wrapped Gaussian distribution with zero mean and standard deviation of $r\mathrm{ASA}_0$, according to $\phi'_{AOA,n} = \arg(\exp(-jr\mathrm{ASA}_0 Z_n))$ with $Z_n \sim N(0,1)$.

Generate *N* ZODs from a wrapped Laplacian distribution with zero mean and standard deviation of $r\mathrm{ZSD}_0$, according to $\theta'_{ZOD,n} = \arg(\exp(-jr\mathrm{ZSD}_0 \,\mathrm{sgn}(V_n - 0.5)\ln(1-2|V_n - 0.5|)/\sqrt{2}))$ with $V_n \sim \mathrm{unif}(0,1)$.

Generate *N* ZOAs from a wrapped Laplacian distribution with zero mean and standard deviation of $r\mathrm{ZSA}_0$, according to $\theta'_{ZOA,n} = \arg(\exp(-jr\mathrm{ZSA}_0 \,\mathrm{sgn}(W_n - 0.5)\ln(1-2|W_n - 0.5|)/\sqrt{2}))$ with $W_n \sim \mathrm{unif}(0,1)$.

r is a proportionality factor, r=1.5. The principal value of the arg function should be used, e.g. (-180,180).

In case of LOS, set $\tau_1' = 0$, $\phi_{\mathrm{AOD},1}' = 0$, $\phi_{\mathrm{AOA},1}' = 0$, $\theta_{\mathrm{ZOD},1}' = 0$, and $\theta_{\mathrm{ZOA},1}' = 0$.

Step 6': Generate cluster powers P_n.

Generate cluster powers as

$$P_n' = \exp\left(-\tau_n' g_{\mathrm{DS}} - \left(\frac{\phi_{\mathrm{AOD},n}' g_{\mathrm{ASD}}}{\sqrt{2}}\right)^2 - \left(\frac{\phi_{\mathrm{AOA},n}' g_{\mathrm{ASA}}}{\sqrt{2}}\right)^2 - \sqrt{2}\left|\theta_{\mathrm{ZOD},n}'\right| g_{\mathrm{ZSD}} - \sqrt{2}\left|\theta_{\mathrm{ZOA},n}'\right| g_{\mathrm{ZSA}}\right) \cdot 10^{-Q_n/10} \quad (7.6.30a)$$

where $Q_n \sim N\left(0, \zeta^2\right)$ is the per cluster shadowing term in [dB] and

$$g_{\mathrm{DS}} = \frac{\max\left(r \cdot \mathrm{DS}_0 - \mathrm{DS}, 0\right)}{\mathrm{DS} \cdot r \cdot \mathrm{DS}_0} \quad (7.6.30b)$$

$$g_{\mathrm{ASD}} = \frac{\sqrt{\max\left(\left(r \cdot \mathrm{ASD}_0\right)^2 - \mathrm{ASD}^2, 0\right)}}{\mathrm{ASD} \cdot r \cdot \mathrm{ASD}_0} \quad (7.6.30c)$$

$$g_{\mathrm{ASA}} = \frac{\sqrt{\max\left(\left(r \cdot \mathrm{ASA}_0\right)^2 - \mathrm{ASA}^2, 0\right)}}{\mathrm{ASA} \cdot r \cdot \mathrm{ASA}_0} \quad (7.6.30d)$$

$$g_{\mathrm{ZSD}} = \frac{\max\left(r \cdot \mathrm{ZSD}_0 - \mathrm{ZSD}, 0\right)}{\mathrm{ZSD} \cdot r \cdot \mathrm{ZSD}_0} \quad (7.6.30e)$$

$$g_{\mathrm{ZSA}} = \frac{\max\left(r \cdot \mathrm{ZSA}_0 - \mathrm{ZSA}, 0\right)}{\mathrm{ZSA} \cdot r \cdot \mathrm{ZSA}_0} \quad (7.6.30f)$$

Normalize the cluster powers so that the sum of all cluster powers is equal to one, i.e.,

$$P_n = \frac{P_n'}{\sum_{n=1}^{N} P_n'} \quad (7.6.30g)$$

or, in the case of LOS, so that

$$P_n = \frac{1}{1+K_R}\frac{P_n'}{\sum_{n=1}^{N} P_n'} + \frac{K_R}{1+K_R}\delta(n-1) \quad (7.6.30h)$$

where K_R is the K-factor converted to linear scale.

Step 7': Generate delays τ_n and angles $\phi_{\mathrm{AOD},n}$, $\phi_{\mathrm{AOA},n}$, $\theta_{\mathrm{ZOD},n}$, $\theta_{\mathrm{ZOA},n}$.

$$\tau_n = \begin{cases} \tau_n' & \text{, for NLOS} \\ \sqrt{1+\frac{K_R}{2}}\,\tau_n' & \text{, for LOS} \end{cases} \quad (7.6.30i)$$

$$\phi_{n,m,\mathrm{AOA}} = \begin{cases} \phi'_{n,\mathrm{AOA}} + \phi_{\mathrm{LOS,AOA}} + c_{\mathrm{ASA}}\alpha_m & \text{, for NLOS} \\ \sqrt{1+K_R}\,\phi'_{n,\mathrm{AOA}} + \phi_{\mathrm{LOS,AOA}} + c_{\mathrm{ASA}}\alpha_m & \text{, for LOS} \end{cases} \quad (7.6.30j)$$

$$\phi_{n,m,\mathrm{AOD}} = \begin{cases} \phi'_{n,\mathrm{AOD}} + \phi_{\mathrm{LOS,AOD}} + c_{\mathrm{ASD}}\alpha_m & \text{, for NLOS} \\ \sqrt{1+K_R}\,\phi'_{n,\mathrm{AOD}} + \phi_{\mathrm{LOS,AOD}} + c_{\mathrm{ASD}}\alpha_m & \text{, for LOS} \end{cases} \quad (7.6.30k)$$

$$\theta_{n,m,\mathrm{ZOA}} = \begin{cases} \theta'_{n,\mathrm{ZOA}} + \theta_{\mathrm{LOS,ZOA}} + c_{\mathrm{ZSA}}\alpha_m & \text{, for NLOS} \\ \sqrt{1+K_R}\,\theta'_{n,\mathrm{ZOA}} + \theta_{\mathrm{LOS,ZOA}} + c_{\mathrm{ZSA}}\alpha_m & \text{, for LOS} \end{cases} \quad (7.6.30l)$$

$$\theta_{n,m,\mathrm{ZOD}} = \begin{cases} \theta'_{n,\mathrm{ZOD}} + \theta_{\mathrm{LOS,ZOD}} + c_{\mathrm{ZSD}}\alpha_m & \text{, for NLOS} \\ \sqrt{1+K_R}\,\theta'_{n,\mathrm{ZOD}} + \theta_{\mathrm{LOS,ZOD}} + c_{\mathrm{ZSD}}\alpha_m & \text{, for LOS} \end{cases} \quad (7.6.30m)$$

Repeat Steps 6'-7' for each frequency of interest, reusing the delays and angles from Step 5' for all frequencies.

Note: The resulting delay and angular spreads of channels generated with this alternative method will be similar but not identical to when using Steps 5-7 in Clause 7.5.

7.6.6 Time-varying Doppler shift

The Doppler shift generally depends on the time evolution of the channel as it is defined as the derivative of the channels phase over time. It can be the result from Tx, Rx, or scatterer movement. The more general form of the exponential Doppler term as used in Equation (7.5-22) is given by

$$\exp\left(j2\pi \int_{t_0}^{t} \frac{\hat{r}_{rx,n,m}^{T}(\tilde{t}) \cdot \vec{v}(\tilde{t})}{\lambda_0} d\tilde{t} \right). \quad (7.6\text{-}31)$$

Here, $\hat{r}_{rx,n,m}(t)$ is the normalized vector that points into the direction of the incoming wave as seen from the Rx at time t. $\vec{v}(t)$ denotes the velocity vector of the Rx at time t, while t_0 denotes a reference point in time that defines the initial phase, e.g. $t_0 = 0$.

Note that Equation (7.5-22) only holds for time-invariant Doppler shift, i.e. $\hat{r}_{rx,n,m}^{T}(t) \cdot \vec{v}(t) = \hat{r}_{rx,n,m}^{T} \cdot \vec{v}$.

7.6.7 UT rotation

UT rotation modelling is an add-on feature. When modelled, Step 1 in Clause 7.5 shall consider UT rotational motion.

Step 1:

Add: h) Give rotational motion of UT in terms of its bearing angle, downtilt angle and slant angle.

7.6.8 Explicit ground reflection model

In case the ground reflection shall be modelled explicitly, Equation (7.5-30) has to be replaced by

$$H_{u,s}^{\mathrm{LOS}}(\tau,t)=\sqrt{\frac{1}{K_R+1}}H_{u,s}^{\mathrm{NLOS}}(\tau-\tau_{\mathrm{LOS}},t) + \sqrt{\frac{K_R}{K_R+1}}\left(H_{u,s,1}^{\mathrm{LOS}}(t)\delta(\tau-\tau_{\mathrm{LOS}})+\frac{d_{3\mathrm{D}}}{\mathrm{d}_{\mathrm{GR}}}H_{u,s}^{\mathrm{GR}}(t)\delta(\tau-\tau_{\mathrm{GR}})\right) \tag{7.6-32}$$

with the delays for the ground reflected and the LOS paths being defined by their lengths, according to the Tx-Rx separation $d_{2\mathrm{D}}$ and the Tx and Rx heights h_{tx} and h_{rx} respectively, as

$$\tau_{\mathrm{GR}}=\frac{d_{\mathrm{GR}}}{c}=\frac{\sqrt{(h_{\mathrm{tx}}+h_{\mathrm{rx}})^2+d_{2\mathrm{D}}^2}}{c}, \tag{7.6-33}$$

and

$$\tau_{\mathrm{LOS}}=\frac{d_{3\mathrm{D}}}{c}=\frac{\sqrt{(h_{\mathrm{tx}}-h_{\mathrm{rx}})^2+d_{2\mathrm{D}}^2}}{c}. \tag{7.6-34}$$

The channel coefficient for the ground reflected path is given by

$$H_{u,s}^{\mathrm{GR}}(t)=\begin{bmatrix}F_{\mathrm{rx},u,\theta}(\theta_{\mathrm{GR,ZOA}},\phi_{\mathrm{GR,AOA}})\\F_{\mathrm{rx},u,\phi}(\theta_{\mathrm{GR,ZOA}},\phi_{\mathrm{GR,AOA}})\end{bmatrix}^T\begin{bmatrix}R_{\parallel}^{\mathrm{GR}}&0\\0&-R_{\perp}^{\mathrm{GR}}\end{bmatrix}\begin{bmatrix}F_{\mathrm{tx},s,\theta}(\theta_{\mathrm{GR,ZOD}},\phi_{\mathrm{GR,AOD}})\\F_{\mathrm{tx},s,\phi}(\theta_{\mathrm{GR,ZOD}},\phi_{\mathrm{GR,AOD}})\end{bmatrix} \cdot\exp\left(-j2\pi\frac{d_{\mathrm{GR}}}{\lambda_0}\right)\exp\left(j2\pi\frac{\hat{r}_{\mathrm{rx,GR}}^T.\bar{d}_{\mathrm{rx},u}}{\lambda_0}\right)\exp\left(j2\pi\frac{\hat{r}_{\mathrm{tx,GR}}^T.\bar{d}_{\mathrm{tx},s}}{\lambda_0}\right)\exp\left(j2\pi\frac{\hat{r}_{\mathrm{rx,GR}}^T.\bar{v}}{\lambda_0}t\right) \tag{7.6-35}$$

with the normalized vectors pointing towards the ground reflection point from the Tx

$$\hat{r}_{\mathrm{tx,GR}}=e_r(\theta_{\mathrm{GR,ZOD}},\phi_{\mathrm{GR,AOD}})=\begin{bmatrix}\sin\theta_{\mathrm{GR,ZOD}}\cos\phi_{\mathrm{GR,AOD}}\\\sin\theta_{\mathrm{GR,ZOD}}\sin\phi_{\mathrm{GR,AOD}}\\\cos\theta_{\mathrm{GR,ZOD}}\end{bmatrix} \tag{7.6-36}$$

and from the Rx side

$$\hat{r}_{\mathrm{rx,GR}}=e_r(\theta_{\mathrm{GR,ZOA}},\phi_{\mathrm{GR,AOA}})=\begin{bmatrix}\sin\theta_{\mathrm{GR,ZOA}}\cos\phi_{\mathrm{GR,AOA}}\\\sin\theta_{\mathrm{GR,ZOA}}\sin\phi_{\mathrm{GR,AOA}}\\\cos\theta_{\mathrm{GR,ZOA}}\end{bmatrix}. \tag{7.6-37}$$

The angles for the ground reflected path are given by the geometry assuming a flat surface with its normal pointing into z-direction. The angles at the Tx side can be determined by

$$\theta_{\mathrm{GR,ZOD}}=180^\circ-\mathrm{atan}\left(\frac{d_{2\mathrm{D}}}{h_{\mathrm{rx}}+h_{\mathrm{tx}}}\right) \tag{7.6-37a}$$

$$\phi_{\mathrm{GR,AOD}}=\phi_{\mathrm{LOS,AOD}} \tag{7.6-37b}$$

and at the Rx side by

$$\theta_{\mathrm{GR,ZOA}}=\theta_{\mathrm{GR,ZOD}} \tag{7.6-37c}$$

$$\phi_{\mathrm{GR,AOA}}=\phi_{\mathrm{GR,AOD}}+180^\circ. \tag{7.6-37d}$$

The reflection coefficients for parallel and perpendicular polarization on the ground, cf. [21], are given by

$$R_{\parallel}^{\mathrm{GR}} = \frac{\frac{\varepsilon_{\mathrm{GR}}}{\varepsilon_0}\cos\left(\theta_{\mathrm{GR,ZOD}}\right) + \sqrt{\frac{\varepsilon_{\mathrm{GR}}}{\varepsilon_0} - \sin^2\left(\theta_{\mathrm{GR,ZOD}}\right)}}{\frac{\varepsilon_{\mathrm{GR}}}{\varepsilon_0}\cos\left(\theta_{\mathrm{GR,ZOD}}\right) - \sqrt{\frac{\varepsilon_{\mathrm{GR}}}{\varepsilon_0} - \sin^2\left(\theta_{\mathrm{GR,ZOD}}\right)}}, \tag{7.6-38}$$

and

$$R_{\perp}^{\mathrm{GR}} = \frac{\cos\left(\theta_{\mathrm{GR,ZOD}}\right) + \sqrt{\frac{\varepsilon_{\mathrm{GR}}}{\varepsilon_0} - \sin^2\left(\theta_{\mathrm{GR,ZOD}}\right)}}{\cos\left(\theta_{\mathrm{GR,ZOD}}\right) - \sqrt{\frac{\varepsilon_{\mathrm{GR}}}{\varepsilon_0} - \sin^2\left(\theta_{\mathrm{GR,ZOD}}\right)}}, \tag{7.6-39}$$

with the complex relative permittivity of the ground material given by

$$\frac{\varepsilon_{\mathrm{GR}}}{\varepsilon_0} = \varepsilon_r - j\frac{\sigma}{2\pi f_c \varepsilon_0}. \tag{7.6-40}$$

The electric constant ε_0 is given by 8.854187817... × 10^{-12} F·m^{-1}.

For applicable frequency ranges, the real relative permittivity can be modelled by

$$\varepsilon_r = a_\varepsilon \cdot \left(\frac{f_c}{10^9}\right)^{b_\varepsilon}, \tag{7.6-41}$$

while the conductivity in [S/m] may be modelled by

$$\sigma = c_\sigma \cdot \left(\frac{f_c}{10^9}\right)^{d_\sigma}, \tag{7.6-42}$$

with f_c being the center frequency in Hz.

A selection of material properties from [19] is given below. Since the simplified models for conductivity and relative permittivity are only applicable for frequencies between 1 and 10 GHz, Figure 7.6.8-1 presents curves up to 100 GHz at least for very, medium dry and wet ground, cf. [20].

Table 7.6.8-1 Material properties [19]

Material class	Relative permittivity		Conductivity		Frequency range in [GHz]
	a_ε	b_ε	c_σ	d_σ	
Concrete	5.31	0	0.0326	0.8095	1-100
Brick	3.75	0	0.038	0	1-10
Plasterboard	2.94	0	0.0116	0.7076	1-100
Wood	1.99	0	0.0047	1.0718	0.001-100
Floorboard	3.66	0	0.0044	1.3515	50-100
Metal	1	0	10^7	0	1-100
Very dry ground	3	0	0.00015	2.52	1-10
Medium dry ground	15	−0.1	0.035	1.63	1-10
Wet ground	30	−0.4	0.15	1.30	1-10

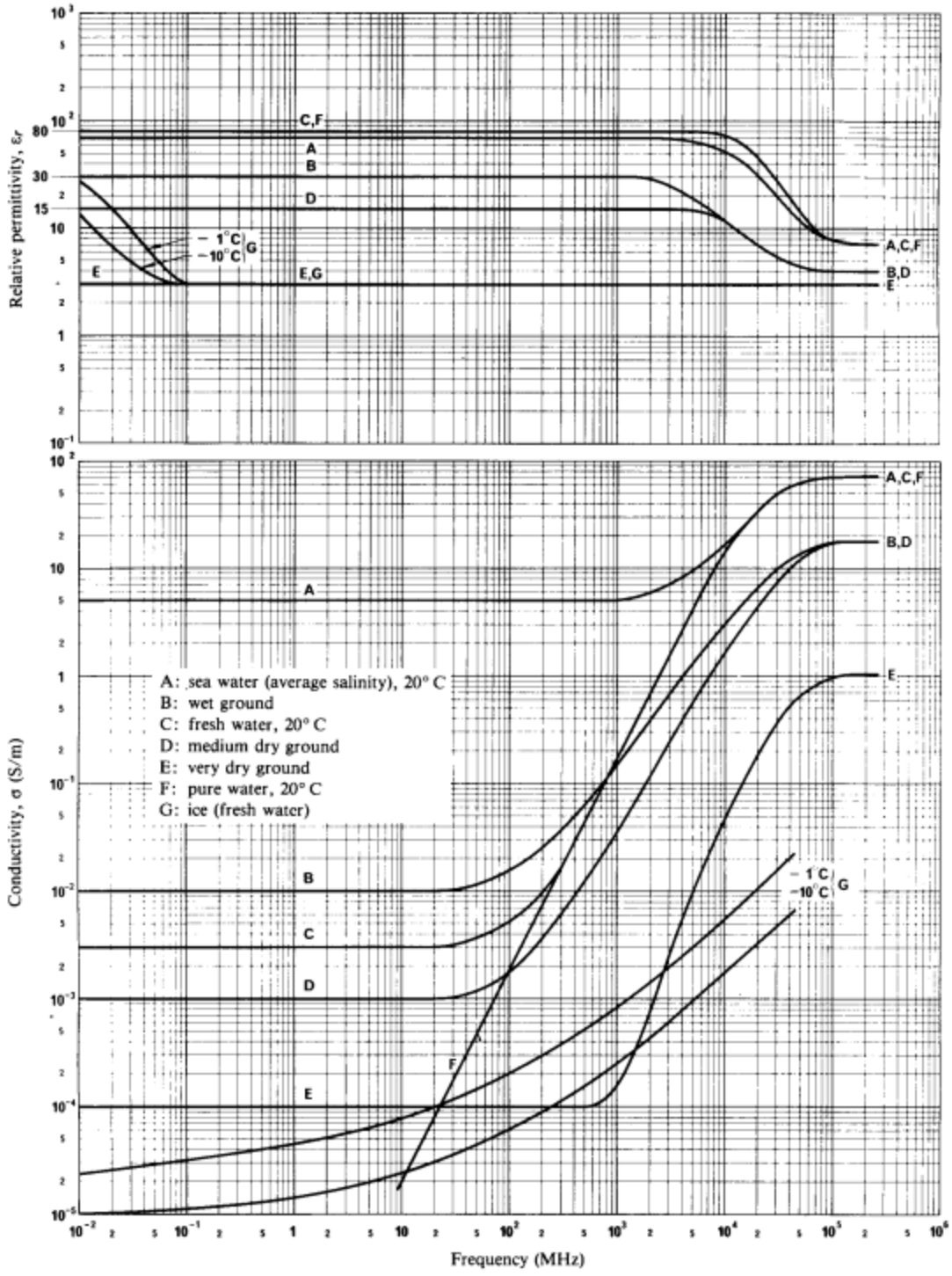

Figure 7.6.8-1: Relative permittivity and conductivity as a function of frequency [20]

7.6.9 Absolute time of arrival

To support simulations in which absolute time of arrival is important, the propagation time delay due to the total path length is considered in step 11 of the fast fading model as follows. The impulse response in NLOS is determined using equation (7.6-43) instead of (7.5-27) and the impulse response in LOS is determined using equation (7.6-44) instead of (7.5-30), where c is the speed of light. $\Delta\tau$ is generated from a lognormal distribution with parameters according to Table 7.6.9-1. $\Delta\tau$ is generated independently for links between the same UT and different BS sites. For InF and InH scenarios, the excess delay in NLOS, $\Delta\tau$, should further be upper bounded by $2L/c$, where L is the largest dimension of the factory hall and office room, i.e. L = max(length, width, height). For UMi-Street Canyon, UMa, SMa, and RMa scenarios, the excess delay is not upper bounded.

$$H_{u,s}^{NLOS}(\tau,t)=\sum_{n=1}^{2}\sum_{i=1}^{3}\sum_{m\in R_i}H_{u,s,n,m}^{NLOS}(t)\delta\left(\tau-\tau_{n,i}-\frac{d_{3D}}{c}-\Delta\tau\right)+\sum_{n=3}^{N}H_{u,s,n}^{NLOS}(t)\delta\left(\tau-\tau_n-\frac{d_{3D}}{c}-\Delta\tau\right) \quad (7.6.-43)$$

$$H_{u,s}^{LOS}(\tau,t)=\sqrt{\frac{1}{K_R+1}}H_{u,s}^{NLOS}(\tau,t)+\sqrt{\frac{K_R}{K_R+1}}H_{u,s,1}^{LOS}(t)\delta(\tau-\tau_1-d_{3D}/c). \quad (7.6-44)$$

where, in LOS case,

$$H_{u,s}^{NLOS}(\tau,t)=\sum_{n=1}^{2}\sum_{i=1}^{3}\sum_{m\in R_i}H_{u,s,n,m}^{NLOS}(t)\delta\left(\tau-\tau_{n,i}-\frac{d_{3D}}{c}\right)+\sum_{n=3}^{N}H_{u,s,n}^{NLOS}(t)\delta\left(\tau-\tau_n-\frac{d_{3D}}{c}\right) \quad (7.6-44a)$$

Table 7.6.9-1: Parameters for the absolute time of arrival model in NLOS

Scenarios		InH	InF-SL, InF-DL	InF-SH, InF-DH	UMi	UMa	RMa	SMa
$lg\Delta\tau$ $= log_{10}(\Delta\tau/1s)$	$\mu_{lg\Delta\tau}$	-8.6	-7.5	-7.5	-7.5	-7.4	-8.33	-7.702
	$\sigma_{lg\Delta\tau}$	0.1	0.4	0.4	0.5	0.2	0.26	0.4
Correlation distance in the horizontal plane [m]		10	6	11	15	50	50	50

7.6.10 Dual mobility

To support simulations that involve dual Tx and Rx mobility or scatterer mobility, the Doppler frequency component in the channel coefficient generation in step 11 in clause 7.5 should be updated as follows.

For the LOS path, the Doppler frequency is given by

$$\boldsymbol{v_{n,m}}=\frac{\hat{\boldsymbol{r}}_{\boldsymbol{rx,n,m}}^{T}\cdot\bar{\boldsymbol{v}}_{\boldsymbol{rx}}+\hat{\boldsymbol{r}}_{\boldsymbol{tx,n,m}}^{T}\cdot\bar{\boldsymbol{v}}_{\boldsymbol{tx}}}{\boldsymbol{\lambda_0}} \quad (7.6-45)$$

where $\hat{\boldsymbol{r}}_{\boldsymbol{rx,n,m}}$ and $\hat{\boldsymbol{r}}_{\boldsymbol{tx,n,m}}$ are defined in (7.5-23) and (7.5-24) respectively, and

$$\bar{v}_{rx}=v_{rx}\begin{bmatrix}\sin\theta_{v,rx}\cos\phi_{v,rx} & \sin\theta_{v,rx}\sin\phi_{v,rx} & \cos\theta_{v,rx}\end{bmatrix}^T$$

$$\bar{v}_{tx}=v_{tx}\begin{bmatrix}\sin\theta_{v,tx}\cos\phi_{v,tx} & \sin\theta_{v,tx}\sin\phi_{v,tx} & \cos\theta_{v,tx}\end{bmatrix}^T$$

For all other paths, the Doppler frequency component is given by:

$$\boldsymbol{v_{n,m}}=\frac{\hat{\boldsymbol{r}}_{\boldsymbol{rx,n,m}}^{T}\cdot\bar{\boldsymbol{v}}_{\boldsymbol{rx}}+\hat{\boldsymbol{r}}_{\boldsymbol{tx,n,m}}^{T}\cdot\bar{\boldsymbol{v}}_{\boldsymbol{tx}}+2\boldsymbol{\alpha_{n,m}D_{n,m}}}{\boldsymbol{\lambda_0}} \quad (7.6-46)$$

where $D_{n,m}$ is a random variable from $-v_{scatt}$ to v_{scatt}, $\alpha_{n,m}$ is a random variable of Bernoulli distribution with mean p, and v_{scatt} is the maximum speed of the clutter. Parameter p determines the proportion of mobile scatterers and can thus be selected to appropriately model statistically larger number of mobile scatterers (higher p) or statistically smaller number of mobile scatterers (e.g. in case of a completely static environment: **p**=0 results in all scatteres having zero speed). A typical value of p is 0.2.

7.6.11 Sources of EM interference

When the simulation includes sources of EM interference in industrial scenarios, the channel(s) between the interferer(s) and the BS or UT should be modeled using the appropriate sub-scenario(s), e.g. clutter-embedded or elevated Tx or Rx and low or high clutter density. Characterization of EM interference sources is out of the scope of this TR.

7.6.12 Embedded devices

To simulate devices that are embedded inside machinery or enclosures, an additional loss parameter $L_{embedded}$ is added to the path loss in step 12. The additional path loss parameter $L_{embedded}$ to embedded devices is left as a simulation assumption, where it may be formulated e.g. as a value or range, or derived using a methodology similar to the building penetration loss in clause 7.4.3.1.

7.6.13 Near-field channel model

The near-field channel model is to support the simulations that involve the impacts of the spherical wavefront from the perspective of antenna array.

To model the antenna element-wise channel parameters, in the Step 11 in Clause 7.5, the following updates are considered to generate the channel impulse response:

For the NLOS channel impulse response, determine the NLOS channel coefficient for the two strongest clusters, say *n* = 1 and 2, instead of the equation (7.5-28) and for the N – 2 weakest clusters, say n = 3, 4,…, N, using $H_{u,s,n}^{NLOS}(t) = \sum_{m=1}^{M} H_{u,s,n,m}^{NLOS}(t)$ instead of equation (7.5-22).

- To model the antenna element-wise phase at TRP side, the NLOS channel coefficient, $H_{u,s,n,m}^{NLOS}(t)$, is given by:

$$H_{u,s,n,m}^{NLOS}(t) = \sqrt{\frac{P_n}{M}} \begin{bmatrix} F_{rx,u,\theta}(\theta_{n,m,ZOA}, \phi_{n,m,AOA}) \\ F_{rx,u,\phi}(\theta_{n,m,ZOA}, \phi_{n,m,AOA}) \end{bmatrix}^T \begin{bmatrix} exp(j\Phi_{n,m}^{\theta\theta}) & \sqrt{k_{n,m}^{-1}} exp(j\Phi_{n,m}^{\theta\phi}) \\ \sqrt{k_{n,m}^{-1}} exp(j\Phi_{n,m}^{\phi\theta}) & exp(j\Phi_{n,m}^{\phi\phi}) \end{bmatrix} \begin{bmatrix} F_{tx,s,\theta}(\theta_{n,m,ZOD}, \phi_{n,m,AOD}) \\ F_{tx,s,\phi}(\theta_{n,m,ZOD}, \phi_{n,m,AOD}) \end{bmatrix}$$

$$exp\left(j2\pi \frac{d_{1,n,m} - \|d_{1,n,m} \cdot \hat{r}_{tx,n,m} - \bar{d}_{tx,s}\|}{\lambda_0}\right) exp\left(j2\pi \frac{\hat{r}_{rx,n,m}^T \cdot \bar{d}_{rx,u}}{\lambda_0}\right) exp\left(j2\pi \frac{\hat{r}_{rx,n,m}^T \cdot \bar{v}}{\lambda_0} t\right) \quad (7.6\text{-}47)$$

where, the $\hat{r}_{tx,n,m}$ is the spherical unit vector with azimuth departure angle and elevation departure angle for ray m of cluster n. $\bar{d}_{tx,s}$ is the vector pointing from reference point to transmit antenna element s, wherein the reference point is the physical center of the antenna array/center at Tx side. The $d_{1,n,m}$ is the distance calculated as:

$$d_{1,n,m} = \begin{cases} s_{TRP,n} * \left(d_{3D} + \Delta\tau * \mathrm{c} + \tau_{n,i} * \mathrm{c}\right), \text{for the two strongest clusters, say } n = 1 \text{ and } 2 \\ s_{TRP,n} * \left(d_{3D} + \Delta\tau * \mathrm{c} + \tau_n * \mathrm{c}\right), \text{for the N} - 2 \text{ weakest clusters, say n} = 3, 4, \ldots, \mathrm{N} \end{cases},$$

where the d_{3D} refers to the 3D distance between reference point at TRP and UT side. The $\Delta\tau$ refers to the excess delay, which is only applicable when it's not in LOS case, and generated according to the Clause 7.6.9, otherwise $\Delta\tau$ is assumed to be 0. The $\tau_{n,i}$ refers to the delay of *i*-th sub-cluster mapping to the rays defined in Table 7.5-5. The ray index, *m*, should be determined based on the sub-cluster information in Table 7.5-5. For the $s_{TRP,n}$, if the nth cluster is one of the k_1 strongest cluster, $s_{TRP,n} = 1$, otherwise $s_{TRP,n}$ is generated according to the $Beta(\alpha, \beta)$. The corresponding value of k_1 and Beta distribution is defined in Table 7.6-13-1, respectively.

Table 7.6-13-1: Parameters for Uma, Umi, Indoor-Office and Indoor-Factory

Scenarios		UMa	UMi	InH	InF
k_1		2	2	4	4
Beta distribution	α	1.93	1.53	1.25	1.38
	β	1.33	1.42	1.27	1.26

Optionally,

- To model the antenna element-wise phase at UT side additionally, the $H_{u,s,n,m}^{NLOS}(t)$ is given by:

$$H_{u,s,n,m}^{NLOS}(t) = \sqrt{\frac{P_n}{M}} \begin{bmatrix} F_{rx,u,\theta}(\theta_{n,m,ZOA}, \phi_{n,m,AOA}) \\ F_{rx,u,\phi}(\theta_{n,m,ZOA}, \phi_{n,m,AOA}) \end{bmatrix}^T \begin{bmatrix} exp(j\Phi_{n,m}^{\theta\theta}) & \sqrt{k_{n,m}^{-1}} exp(j\Phi_{n,m}^{\theta\phi}) \\ \sqrt{k_{n,m}^{-1}} exp(j\Phi_{n,m}^{\phi\theta}) & exp(j\Phi_{n,m}^{\phi\phi}) \end{bmatrix} \begin{bmatrix} F_{tx,s,\theta}(\theta_{n,m,ZOD}, \phi_{n,m,AOD}) \\ F_{tx,s,\phi}(\theta_{n,m,ZOD}, \phi_{n,m,AOD}) \end{bmatrix}$$

$$\exp\left(j2\pi \frac{d_{2,n,m} - \|d_{2,n,m} \cdot \hat{r}_{rx,n,m} - \bar{d}_{rx,u}\|}{\lambda_0}\right) \exp\left(j2\pi \frac{d_{1,n,m} - \|d_{1,n,m} \cdot \hat{r}_{tx,n,m} - \bar{d}_{tx,s}\|}{\lambda_0}\right) \exp\left(\mathrm{j}2\pi \frac{\hat{r}_{rx,n,m}^T \cdot \bar{v}}{\lambda_0} \mathrm{t}\right) \quad (7.6\text{-}48)$$

where $\hat{r}_{rx,n,m}$ is the spherical unit vector with azimuth arrival angle and elevation arrival angle for ray m of cluster n. $\bar{d}_{rx,u}$ is the vector pointing from reference point to receive antenna element u, wherein the reference point is the physical center of the antenna array/center at Rx side. The $d_{2,n,m}$ is the distance calculated as:

$$d_{2,n,m} = \begin{cases} s_{UE,n} * \left(d_{3D} + \Delta\tau * \mathrm{c} + \tau_{n,i} * \mathrm{c}\right), \text{for the two strongest clusters, say } n = 1 \text{ and } 2 \\ s_{UE,n} * \left(d_{3D} + \Delta\tau * \mathrm{c} + \tau_{n} * \mathrm{c}\right), \text{for the N} - 2 \text{ weakest clusters, say n} = 3, 4, \ldots, \mathrm{N}' \end{cases}$$

where $s_{UE,n} = 1$, if the nth cluster is one of the k_1 strongest cluster, otherwise $s_{UE,n} = 1 - s_{TRP,n}$. Note that it is assumed that only single non-specular interaction along with specular reflection(s) is considered in the propagation channel and most of the sources of non-specular interaction are assumed to be a point scatterer or diffractions.

- To model the antenna element-wise antenna field patterns additionally, the $H_{u,s,n,m}^{NLOS}(t)$ is given by:

$$H_{u,s,n,m}^{NLOS}(t) = \sqrt{\frac{P_n}{M}} \begin{bmatrix} F_{rx,u,\theta}\left(\theta_{n,m,ZOA,u}, \phi_{n,m,AOA,u}\right) \\ F_{rx,u,\phi}\left(\theta_{n,m,ZOA,u}, \phi_{n,m,AOA,u}\right) \end{bmatrix}^T \begin{bmatrix} exp\left(j\Phi_{n,m}^{\theta\theta}\right) & \sqrt{k_{n,m}^{-1}} exp\left(j\Phi_{n,m}^{\theta\phi}\right) \\ \sqrt{k_{n,m}^{-1}} exp\left(j\Phi_{n,m}^{\phi\theta}\right) & exp\left(j\Phi_{n,m}^{\phi\phi}\right) \end{bmatrix} \begin{bmatrix} F_{tx,s,\theta}\left(\theta_{n,m,ZOD,s}, \phi_{n,m,AOD,s}\right) \\ F_{tx,s,\phi}\left(\theta_{n,m,ZOD,s}, \phi_{n,m,AOD,s}\right) \end{bmatrix}$$

$$\exp\left(j2\pi \frac{d_{2,n,m} - \left\|d_{2,n,m} \cdot \hat{r}_{rx,n,m} - \bar{d}_{rx,u}\right\|}{\lambda_0}\right) \exp\left(j2\pi \frac{d_{1,n,m} - \left\|d_{1,n,m} \cdot \hat{r}_{tx,n,m} - \bar{d}_{tx,s}\right\|}{\lambda_0}\right) \exp\left(\mathrm{j}2\pi \frac{\hat{r}_{rx,n,m}^T \cdot \bar{v}}{\lambda_0} \mathrm{t}\right) \quad (7.6\text{-}49)$$

where $\theta_{n,m,ZOA,u}$ and $\phi_{n,m,AOA,u}$ are the antenna element-wise elevation arrival angles and azimuth arrival angles, respectively, for ray *m* of cluster *n* for receive antenna element *u*, and $\theta_{n,m,ZOD,s}$ and $\phi_{n,m,AOD,s}$ are the antenna element-wise elevation departure angles and azimuth departure angles, respectively, for ray *m* of cluster *n* for transmit antenna element *s*.

In the LOS channel impulse response, determine the LOS channel coefficient as:

- To model the antenna element-wise phase, the equation (7.5-29) in Clause 7.5 is replaced by:

$$H_{u,s,1}^{LOS}(t) = \begin{bmatrix} F_{rx,u,\theta}\left(\theta_{LOS,ZOA}, \phi_{LOS,AOA}\right) \\ F_{rx,u,\phi}\left(\theta_{LOS,ZOA}, \phi_{LOS,AOA}\right) \end{bmatrix}^T \begin{bmatrix} 1 & 0 \\ 0 & -1 \end{bmatrix} \begin{bmatrix} F_{tx,s,\theta}\left(\theta_{LOS,ZOD}, \phi_{LOS,AOD}\right) \\ F_{tx,s,\phi}\left(\theta_{LOS,ZOD}, \phi_{LOS,AOD}\right) \end{bmatrix}$$

$$\exp\left(-\mathrm{j}2\pi \frac{\mathrm{d_{3D}}}{\lambda_0}\right) \exp\left(-\mathrm{j}2\pi \frac{\left|\vec{\mathrm{r}}_{\mathrm{u,s}}\right| - \mathrm{d_{3D}}}{\lambda_0}\right) \exp\left(\mathrm{j}2\pi \frac{\hat{\mathrm{r}}_{\mathrm{rx,LOS}}^{\mathrm{T}} \cdot \bar{\mathrm{v}}}{\lambda_0} \mathrm{t}\right) \quad (7.6\text{-}50)$$

where, the $\vec{r}_{u,s}$ refers to the vector determined by the location of the uth antenna element at receiver and the sth antenna element at transmitter. The d_{3D} refers to the 3D distance between reference point at TRP and UT side, wherein the the reference point is the physical center of the antenna array/center of the device.

Optionally,

- To model the element-wise antenna field patterns additionally, the equation (7.5-29) in Clause 7.5 is replaced by:

$$H_{u,s,1}^{LOS}(t) = \begin{bmatrix} F_{rx,u,\theta}\left(\theta_{LOS,ZOA,u,s}, \phi_{LOS,AOA,u,s}\right) \\ F_{rx,u,\phi}\left(\theta_{LOS,ZOA,u,s}, \phi_{LOS,AOA,u,s}\right) \end{bmatrix}^T \begin{bmatrix} 1 & 0 \\ 0 & -1 \end{bmatrix} \begin{bmatrix} F_{tx,s,\theta}\left(\theta_{LOS,ZOD,u,s}, \phi_{LOS,AOD,u,s}\right) \\ F_{tx,s,\phi}\left(\theta_{LOS,ZOD,u,s}, \phi_{LOS,AOD,u,s}\right) \end{bmatrix}$$

$$\exp\left(-\mathrm{j}2\pi \frac{\mathrm{d_{3D}}}{\lambda_0}\right) \exp\left(-\mathrm{j}2\pi \frac{\left|\vec{\mathrm{r}}_{\mathrm{u,s}}\right| - \mathrm{d_{3D}}}{\lambda_0}\right) \exp\left(\mathrm{j}2\pi \frac{\hat{\mathrm{r}}_{\mathrm{rx,LOS}}^{\mathrm{T}} \cdot \bar{\mathrm{v}}}{\lambda_0} \mathrm{t}\right) \quad (7.6\text{-}51)$$

where $\theta_{LOS,ZOA,u,s}$, $\phi_{LOS,AOA,u,s}$, $\theta_{LOS,ZOD,u,s}$, $\phi_{LOS,AOD,u,s}$ are the respective antenna element-wise elevation arrival angles, azimuth arrival angles, elevation departure angles and azimuth departure angles of LOS path between the transmit antenna element s and receive antenna element u.

7.6.14 Spatial non-stationarity channel model

7.6.14.1 Spatial non-stationarity channel model at TRP side

7.6.14.1.1 Introduction

The spatial non-stationarity (SNS) channel model is to support the simulations that involve the impacts of the antenna element-wise power variation at TRP. Two alternative models (i.e., Physical blocker-based Model and Stochastic based Model) are provided for the SNS modelling.

From the perspective of the simulation requirements:

- The physical blocker-based model can be considered for simulation where physical accuracy and consistency are desired.
- The stochastic based model can be considered for simulation where computational efficient SNS modelling is desired.

From the perspective of the model mechanism:

- To reflect the SNS phenomenon due to partial blockage, the physical blocker-based model can be considered in simulation.
- To reflect the SNS phenomenon due to incomplete scattering, the stochastic based model can be considered in simulation.

The stochastic based model is recommended to be used in the simulation except for the case where it is not applicable.

7.6.14.1.2 Physical blocker-based Model

To model the antenna element-wise power variation at TRP side for each UT, the following additional steps between Step 9 and 10 in Clause 7.5 are introduced to calculate the antenna element-wise power variation, i.e., for NLOS cluster, $L_{dB,u,n,m}^{NLOS}$ if the TRP is the receiver or $L_{dB,s,n,m}^{NLOS}$ if the TRP is the transmitter, and $L_{dB,u,s,1}^{LOS}$ for LOS ray.

Step I: Determine blockers

The number of blockers (K), their vertical and horizontal extensions ($h_k$and w_k), locations (x_k,y_k,z_k) are determined according to 'Step a' in the Clause 7.6.4.2:

Note:

- Recommended parameters for typical blockers are provided in Table 7.6.14.1.1-1.
- The blocking effect diminishes with increasing distance to the blocker. For implementation purposes it may be sufficient to consider only the K nearest blockers from a BS.

Table 7.6.14.1.1-1: Blocker parameters

	Typical set of blockers	Blocker dimensions	Mobility pattern
Indoor; Outdoor; InF	Human	Cartesian: w=0.3m; h=1.7m	Stationary or up to 3 km/h
Outdoor	Vehicle	Cartesian: w=4.8m; h=1.4m	Stationary or up to 100 km/h
InF	AGV	Cartesian: w=3m; h=1.5m	Up to 30 km/h
InF	Industrial robot	Cartesian: w=2m; h=0.2m	Up to 3 m/s
Outdoor	Billboard	Cartesian: w=2.4m; h=3.6m	Stationary
Outdoor	Street lamp	Cartesian: w=0.4m; h=0.8m	Stationary
Outdoor	Building edge	Cartesian: w=50 m; h=20 m	Stationary
Indoor	Pillar	Cartesian: w=0.3m; h=3m	Stationary

Step II: Determine the antenna element-wise power variation per ray for each element

The antenna element-wise power variation caused by each blocker to the *m*th ray of *n*th cluster for each element is modelled using a simple knife edge diffraction model and is given by:

$$L_{dB,u,n,m}^{NLOS} \text{ or } L_{dB,s,n,m}^{NLOS} \text{ or } L_{dB,u,s,1}^{LOS} = \begin{cases} -20log_{10}(1-(F_{h_1}+F_{h_2})(F_{w_1}+F_{w_2})), \\ -20\log_{10}(0.5-F), \text{if blocker is building edge} \end{cases} \quad (7.6\text{-}52)$$

where F represents one of F_{h_1}, F_{h_2}, F_{w_1}, and F_{w_2} which account for knife edge diffraction at the four edges, and are given by equation (7.6-30) in Clause 7.6.4.2 by assuming that:

- $D1_{h_1|h_2|w_1|w_2}$ are the projected (onto the side and top view planes) distances between the uth antenna element at receiver and four edges of the corresponding blocker, and $D2_{h_1|h_2|w_1|w_2}$ are the projected (onto the side and top view planes) distances between the sth antenna element at transmitter and four edges of the corresponding blocker.

- The side view plane is perpendicular to the horizontal ground plane. The top view is perpendicular to the side view.

- For each cluster and each element at BS side, the blocker screen is rotated around its centre such that the arrival (if the BS is receiver)/or departure (if the BS is transmitter) direction of the corresponding path is always perpendicular to the screen. It should be noted that different rotations are required for each individual ray and each antenna element. Meanwhile, the base and top edges of the screens are always parallel to the horizontal plane. As the screen is perpendicular to each ray, r is the distance between the uth antenna element at receiver and the sth antenna element at transmitter for the direct path in LOS, and r' is the distance between the blocker screen and the uth antenna element at receiver or the sth antenna element at transmitter, projected onto the incoming ray direction, for all the other (NLOS) paths.

Step III: Apply the antenna element-wise power variation in coefficient generation

The antenna element-wise power variation is considered in the Step 11 for coefficient generation in Clause 7.5 with following:

- For the NLOS cluster, the channel coefficients $H_{u,s,n}^{NLOS}(t)$ are calculated according to the equation (7.5-28) in Clause 7.5 by applying the $L_{dB,u,n,m}^{NLOS}$ or $L_{dB,s,n,m}^{NLOS}$.

- In the LOS case, the LOS channel coefficient $H_{u,s,1}^{LOS}(t)$ is calculated according to the equation (7.5-29) in Clause 7.5 by applying the $L_{dB,u,s,1}^{LOS}$ for LOS path.

7.6.14.1.3 Stochastic based Model

To model the antenna element-wise power variation at TRP side for each UT, the following additional steps between Step 9 and 10 in Clause 7.5 are introduced to calculate the antenna element-wise power attenuation factor, i.e., $\alpha_{u,n}$ if the TRP is the receiver or $\alpha_{s,n}$ if the TRP is the transmitter.

Step I: Determine the visibility limiting condition for the *n*th cluster of UT

For the *n*th cluster, the cluster is assumed to be impacted by the visibility limitation, if the $x_n < Pr_{sns}$, where the x_n is generated per cluster using:

$$x_n \sim unif(0,1). \tag{7.6-53}$$

The Pr_{sns} is generated per UT using the truncated normal distribution,

$$Pr_{sns} = N(\mu, \sigma^2). \tag{7.6-54}$$

where $0 \leq Pr_{sns} \leq 1$, which is defined in Table 7.6.14.1.2-1.

Table 7.6.14.1.2-1: Parameters for Pr_{sns}

	RMa	SMa	UMa	UMi	InH	InF
μ	0.14	0.24	0.56	0.49	0.31	0.32
σ	0.08	0.07	0.20	0.18	0.08	0.06

Step II: Generate the visibility region (VR)

For the *n*th cluster which is assumed to be impacted by the visibility limitation, the visibility region is generated as a rectangle region with dimension $a * b$ by using:

$$a \sim \text{unif}(V_n * W, W), \tag{7.6-55}$$

$$b = V_n * H * W / a, \tag{7.6-56}$$

where H is the height of TRP antenna array (i.e., in vertical direction) and W is the width of antenna array (i.e., in horizontal direction). The V_n is generated as:

$$V_n = A * \mathrm{e}^{-\frac{\max(P_n) - P_n}{R}} + B + \delta. \tag{7.6-57}$$

where P_n refers to the power of cluster generated by (7.5-6) in dB scale. In the case of LOS condition, the LOS path is considered as an additional cluster, and the power ratio of the LOS path to NLOS clusters follows the Ricean K-factor generated in Clause 7.5. The parameters A, B, R, and δ are defined in Table 7.6.14.1.2-2.

Table 7.6.14.1.2-2: Parameters for *A*, *B*, *R*, and δ

Parameters		RMa	SMa	UMa	UMi	InH	InF
A		0.16	0.06	0.15	0.12	0	0
B		0.74	0.56	0.45	0.48	0.6	0.57
R		60	23	33	50	NA	NA
δ	μ	0	0	0	0	0	0
$N(\mu, \sigma^2)$	σ^2	0.0016	0.0013	0.0015	0.001	0.0011	0.002

Each visibility region is assumed to be randomly located at one of the corners of TRP antenna array (i.e., reference conrner), which is determined by the following conditions:

- The probability of VR located at either left or right part of antenna array in horizontal domain is 0.5.
- The probability of VR located at either upper or lower part of antenna array in vertical domain is 0.5.

Step III: Determine the antenna element-wise power attenuation factor

For the *n*th cluster which is assumed not to be impacted by the visibility limitation, the $\alpha_{u,n} = 1$ or $\alpha_{s,n} = 1$.

For the *n*th cluster which is assumed to be impacted by the visibility limitation, the $\alpha_{u,n} = \alpha_{i,n}$ or $\alpha_{s,n} = \alpha_{i,n}$.

$$\alpha_{i,n} = \begin{cases} 1 & , |x_i - x_{0,n}| \le a, |y_i - y_{0,n}| \le b \\ e^{\left(\frac{-|x_i - x_{a,n}|}{D_n}\right) \cdot C} & , |x_i - x_{0,n}| > a, |y_i - y_{0,n}| \le b \\ e^{\left(\frac{-|y_i - y_{b,n}|}{D_n}\right) \cdot C} & , |x_i - x_{0,n}| \le a, |y_i - y_{0,n}| > b \\ e^{\left(\frac{-\sqrt{(x_i - x_{a,n})^2 + (y_i - y_{b,n})^2}}{D_n}\right) \cdot C} & , others \end{cases} \quad (7.6\text{-}58)$$

where, $D_n = \sqrt{(x_{A,n} - x_{a,n})^2 + (y_{B,n} - y_{b,n})^2}$, $(x_{A,n}, y_{B,n})$ is the coordinate of the other corner of the antenna array on the diagonal with reference corner $(x_{0,n}, y_{0,n})$, and $(x_{a,n}, y_{b,n})$ is the coordinate of the other corner of the visibility region on the diagonal with reference corner $(x_{0,n}, y_{0,n})$. The (x_i, y_i) denotes the coordinate of the antenna element i. C is the roll-off factor between the visible and invisible regions and defined in Table 7.6.14.1.2-3.

Table 7.6.14.1.2-3: Parameters for *C*

	UMa/UMi/RMa/SMa/InF/InH
C	13

Step IV: Apply the antenna element-wise power attenuation factor in coefficient generation

The antenna element-wise power variation is considered in the Step 11 for coefficient generation in Clause 7.5 with following:

- For the NLOS cluster, the channel coefficients $H_{u,s,n}^{NLOS}(t)$ are calculated according to the equation (7.5-28) in Clause 7.5 by applying the $\sqrt{\alpha_{u,n}}$ or $\sqrt{\alpha_{s,n}}$.
- In the LOS case, the LOS channel coefficient $H_{u,s,1}^{LOS}(t)$ is calculated according to the equation (7.5-29) in Clause 7.5 by applying the $\sqrt{\alpha_{u,1}}$ or $\sqrt{\alpha_{s,1}}$ for LOS path.

7.6.14.2 Spatial non-stationarity channel model at UT side

The spatial non-stationarity (SNS) channel model is to support the simulations that involve the impacts of the antenna element-wise power variation at UT.

The ratio of UT with impact of SNS is 90% and for each UT, the probability of each usage scenario is defined in Table 7.6.14.2-1:

Table 7.6.14.2-1: The probability of each scenario

Usage scenario	One hand grip	Dual hand grip	Head and one hand grip
Probability	58%	29%	13%

The antenna element-wise power variation at UT side, i.e., $L_{dB,u}^{UT}$ if the UT is receiver or $L_{dB,s}^{UT}$ if the UT is transmitter, is defined in Table 7.6.14.2-2 for each candidate antenna location in Clause 7.3.

Table 7.6.14.2-2: The power attenuation for each candidate antenna location

Antenna index	Power attenuation (dB)								
	One hand grip			Dual hand grip			Head and one hand grip		
	Below 1 GHz	1 - 8.4 GHz	14.5 - 15.5 GHz	Below 1 GHz	1 - 8.4 GHz	14.5 - 15.5 GHz	Below 1 GHz	1 - 8.4 GHz	14.5 - 15.5 GHz
1	-	0.7	1.0	-	11.0	3.8	-	3.7	4.0
2	-	4.1	2.4	-	1.1	3.8	-	4.6	3.7
3	-	3.3	3.8	-	10.5	3.8	-	4.3	3.3
4	13.6	7.2	3.6	5.8	5.6	2.6	15.1	7.8	3.3
5	-	10.8	3.8	-	1.5	1.0	-	11.7	3.3
6	-	9.1	2.4	-	1.4	1.0	-	10.1	3.7
7	-	0.7	1.0	-	1.3	1.0	-	2.9	4.0
8	2.4	0.6	1.0	5.6	6.2	2.6	4.9	4.2	4.0
NOTE 1: For below 1GHz, the model is only applicable for 2-antenna system with antenna location index 4 and 8. NOTE 2: The selection of number of antenna and antenna index will be determined as part of the assumption for simulation.									

The antenna element-wise power variation is applied in the Step 11 for coefficient generation in Clause 7.5.

7.6.15 Number of cluster variability model

The number of clusters observed in real-world deployments can vary due to one or more factors, including but not limited to the propagation environment, carrier frequency, bandwidth, and spatial resolution. To capture this variability in simulations, the number of clusters for each link can be chosen between a closed range of [D_1, D_2]. The values of D_1 and D_2 are provided in Table 7.6.15-1. The selection of the number of clusters for each link is determined by the user of the model. The selected number of clusters for each link replaces the number of clusters *N* in Table 7.5.6-Part 1 and 7.5.6-Part 2. A similar framework for modeling the variability in number of clusters is also adopted in the METIS channel model [6].

Table 7.6.15-1: Range of number of clusters

Scenarios	LOS	NLOS	O2I
UMi-Street Canyon	D_1: 6 D_2: 12	D_1: 6 D_2: 19	D_1: 6 D_2: 12
UMa	D_1: 10 D_2: 12	D_1: 15 D_2: 20	D_1: 10 D_2: 12
Indoor-office	D_1: 7 D_2: 15	D_1: 6 D_2: 19	N/A

7.6.16 Polarization power variability model

To support simulation of polarization power variability, the polarization variability powers $\eta_{\theta\theta}$, $\eta_{\theta\phi}$, $\eta_{\phi\theta}$ and $\eta_{\phi\phi}$ for each ray *m* of each cluster *n* is generated and applied to NLOS channel coefficients. The equation (7.5-22) and equation (7.5-28) are replaced by equation (7.6-59) and (7.6-60), respectively, to enable polarization power variability.

$$H_{u,s,n}^{\mathrm{NLOS}}(t) = \sqrt{\frac{P_n}{M}} \sum_{m=1}^{M} \begin{bmatrix} F_{rx,u,\theta}\left(\theta_{n,m,ZOA}, \phi_{n,m,AOA}\right) \\ F_{rx,u,\phi}\left(\theta_{n,m,ZOA}, \phi_{n,m,AOA}\right) \end{bmatrix}^T \begin{bmatrix} \sqrt{\eta_{n,m.\theta\theta}} \exp\left(j\Phi_{n,m}^{\theta\theta}\right) & \sqrt{\eta_{n,m,\theta\phi}\kappa_{n,m}^{-1}} \exp\left(j\Phi_{n,m}^{\theta\phi}\right) \\ \sqrt{\eta_{n,m,\phi\theta}\kappa_{n,m}^{-1}} \exp\left(j\Phi_{n,m}^{\phi\theta}\right) & \sqrt{\eta_{n,m,\phi\phi}} \exp\left(j\Phi_{n,m}^{\phi\phi}\right) \end{bmatrix}$$

$$\begin{bmatrix} F_{tx,s,\theta}\left(\theta_{n,m,ZOD}, \phi_{n,m,AOD}\right) \\ F_{tx,s,\phi}\left(\theta_{n,m,ZOD}, \phi_{n,m,AOD}\right) \end{bmatrix} \exp\left(\frac{j2\pi\left(\hat{r}_{rx,n,m}^{T} \cdot \bar{d}_{rx,u}\right)}{\lambda_0}\right) \exp\left(\frac{j2\pi\left(\hat{r}_{tx,n,m}^{T} \cdot \bar{d}_{tx,s}\right)}{\lambda_0}\right) \exp\left(j2\pi \frac{\hat{r}_{rx,n,m}^{T} \cdot \bar{v}}{\lambda_0} t\right), \quad (7.6\text{-}59)$$

$$H_{u,s,,n,m}^{\mathrm{NLOS}}(t) = \sqrt{\frac{P_n}{M}} \begin{bmatrix} F_{rx,u,\theta}\left(\theta_{n,m,ZOA}, \phi_{n,m,AOA}\right) \\ F_{rx,u,\phi}\left(\theta_{n,m,ZOA}, \phi_{n,m,AOA}\right) \end{bmatrix}^{T} \begin{bmatrix} \sqrt{\eta_{n,m.\theta\theta}} \exp\left(j\Phi_{n,m}^{\theta\theta}\right) & \sqrt{\eta_{n,m,\theta\phi}\kappa_{n,m}^{-1}} \exp\left(j\Phi_{n,m}^{\theta\phi}\right) \\ \sqrt{\eta_{n,m,\phi\theta}\kappa_{n,m}^{-1}} \exp\left(j\Phi_{n,m}^{\phi\theta}\right) & \sqrt{\eta_{n,m,\phi\phi}} \exp\left(j\Phi_{n,m}^{\phi\phi}\right) \end{bmatrix}$$

$$\begin{bmatrix} F_{tx,s,\theta}\left(\theta_{n,m,ZOD}, \phi_{n,m,AOD}\right) \\ F_{tx,s,\phi}\left(\theta_{n,m,ZOD}, \phi_{n,m,AOD}\right) \end{bmatrix} \exp\left(\frac{j2\pi\left(\hat{r}_{rx,n,m}^{T} \cdot \bar{d}_{rx,u}\right)}{\lambda_0}\right) \exp\left(\frac{j2\pi\left(\hat{r}_{tx,n,m}^{T} \cdot \bar{d}_{tx,s}\right)}{\lambda_0}\right) \exp\left(j2\pi \frac{\hat{r}_{rx,n,m}^{T} \cdot \bar{v}}{\lambda_0} t\right), \quad (7.6\text{-}60)$$

where $Q_{n,m,\{\theta\theta,\theta\phi,\phi\theta,\phi\phi\}}$ is a Normal distributed random variable with mean 0 and variance 3^2, $N(0, 3^2)$, independently drawn for each ray, cluster, and polarization component, and used to generate polarization variability powers $\eta_{\theta\theta}$, $\eta_{\theta\phi}$, $\eta_{\phi\theta}$ and $\eta_{\phi\phi}$ based on following equations:

$$\eta'_{n,m,\{\theta\theta,\theta\phi,\phi\theta,\phi\phi\}} = 10^{Q_{n,m,\{\theta\theta,\theta\phi,\phi\theta,\phi\phi\}}/10}, \quad (7.6\text{-}61)$$

$$\eta_{n,m,\{\theta\theta,\theta\phi,\phi\theta,\phi\phi\}} = \eta'_{n,m,\{\theta\theta,\theta\phi,\phi\theta,\phi\phi\}} \frac{2+2\kappa_{n,m}^{-1}}{\eta'_{n,m,\theta\theta}+\eta'_{n,m,\phi\phi}+\eta'_{n,m,\theta\phi}\kappa_{n,m}^{-1}+\eta'_{n,m,\phi\theta}\kappa_{n,m}^{-1}}. \quad (7.6\text{-}62)$$

NOTE: Polarization power variability model is at least applicable for Model-2 of the antenna polarization modelling.

7.7 Channel models for link-level evaluations

7.7.1 Clustered Delay Line (CDL) models

The CDL models are defined for the full frequency range from 0.5 GHz to 100 GHz with a maximum bandwidth of 2 GHz. CDL models can be implemented by e.g., coefficient generation Step 10 and Step 11 in Clause 7.5 or generating TDL model using spatial filter from Clause 7.7.4. Three CDL models, namely CDL-A, CDL-B and CDL-C are constructed to represent three different channel profiles for NLOS while CDL-D and CDL-E are constructed for LOS, the parameters of which can be found respectively in Table 7.7.1-1, Table 7.7.1-2 , Table 7.7.1-3, Table 7.7.1-4 and Table 7.7.1-5.

Each CDL model can be scaled in delay so that the model achieves a desired RMS delay spread, according to the procedure described in Clause 7.7.3. Each CDL model can also be scaled in angles so that the model achieves desired angle spreads, according to the procedure described in Clause 7.7.5.1.

For LOS channel models, the K-factor of CDL-D and CDL-E can be set to a desired value following the procedure described in Clause 7.7.6.

For modelling effect of beamforming in a simplified way, a brick-wall window can be applied to a delay-scaled CDL model. The power shall be normalized after applying the window. A TDL model for simplified evaluations can be obtained from the CDL model, according to this method.

The following step by step procedure should be used to generate channel coefficients using the CDL models.

Step 1: Generate departure and arrival angles

Generate arrival angles of azimuth using the following equation

$$\phi_{n,m,\mathrm{AOA}} = \phi_{n,\mathrm{AOA}} + c_{\mathrm{ASA}}\alpha_m, \quad (7.7\text{-}0a)$$

Where $\phi_{n,\mathrm{AOA}}$ is the cluster AOA and c_{ASA} is the cluster-wise rms azimuth spread of arrival angles (cluster ASA) in Tables 7.7.1.1 – 7.7.1.5 below, and α_m denotes the ray offset angles within a cluster given by Table 7.5-3. If angular

scaling according to Clause 7.7.5.1 is used, this is applied to the ray angles $\phi_{n,m,\mathrm{AOA}}$. The generation of AOD ($\phi_{n,m,\mathrm{AOD}}$), ZSA ($\theta_{n,m,\mathrm{ZOA}}$), and ZSD ($\theta_{n,m,\mathrm{ZOD}}$) follows a procedure similar to AOA as described above.

Step 2: Coupling of rays within a cluster for both azimuth and elevation

Couple randomly AOD angles $\phi_{n,m,\mathrm{AOD}}$ to AOA angles $\phi_{n,m,\mathrm{AOA}}$ within a cluster *n*. Couple randomly ZOD angles $\theta_{n,m,\mathrm{ZOD}}$ with ZOA angles $\theta_{n,m,\mathrm{ZOA}}$using the same procedure. Couple randomly AOD angles $\phi_{n,m,\mathrm{AOD}}$ with ZOD angles $\theta_{n,m,\mathrm{ZOD}}$within a cluster *n*.

Step 3: Generate the cross polarization power ratios

Generate the cross polarization power ratios (XPR) κ for each ray *m* of each cluster *n* as

$$\kappa_{n,m} = 10^{X/10}, \tag{7.7-0b}$$

where *X* is the per-cluster XPR in dB from Tables 7.7.1.1 – 7.7.1.5.

Step 4: Coefficient generation

Follow the same procedure as in Steps 10 and 11 in Clause 7.5, with the exception that all clusters are treated as "weaker cluster", i.e. no further sub-clusters in delay should be generated. Additional clusters representing delay spread of the stronger clusters are already provided in Tables 7.7.1.1 – 7.7.1.5.

Table 7.7.1-1. CDL-A

Cluster #	Normalized delay	Power in [dB]	AOD in [°]	AOA in [°]	ZOD in [°]	ZOA in [°]
1	0.0000	-13.4	-178.1	51.3	50.2	125.4
2	0.3819	0	-4.2	-152.7	93.2	91.3
3	0.4025	-2.2	-4.2	-152.7	93.2	91.3
4	0.5868	-4	-4.2	-152.7	93.2	91.3
5	0.4610	-6	90.2	76.6	122	94
6	0.5375	-8.2	90.2	76.6	122	94
7	0.6708	-9.9	90.2	76.6	122	94
8	0.5750	-10.5	121.5	-1.8	150.2	47.1
9	0.7618	-7.5	-81.7	-41.9	55.2	56
10	1.5375	-15.9	158.4	94.2	26.4	30.1
11	1.8978	-6.6	-83	51.9	126.4	58.8
12	2.2242	-16.7	134.8	-115.9	171.6	26
13	2.1718	-12.4	-153	26.6	151.4	49.2
14	2.4942	-15.2	-172	76.6	157.2	143.1
15	2.5119	-10.8	-129.9	-7	47.2	117.4
16	3.0582	-11.3	-136	-23	40.4	122.7
17	4.0810	-12.7	165.4	-47.2	43.3	123.2
18	4.4579	-16.2	148.4	110.4	161.8	32.6
19	4.5695	-18.3	132.7	144.5	10.8	27.2
20	4.7966	-18.9	-118.6	155.3	16.7	15.2
21	5.0066	-16.6	-154.1	102	171.7	146
22	5.3043	-19.9	126.5	-151.8	22.7	150.7
23	9.6586	-29.7	-56.2	55.2	144.9	156.1
Per-Cluster Parameters						
Parameter	c_{ASD} in [°]	c_{ASA} in [°]	c_{ZSD} in [°]	c_{ZSA} in [°]	XPR in [dB]	
Value	5	11	3	3	10	

Table 7.7.1-2. CDL-B

Cluster #	Normalized delay	Power in [dB]	AOD in [°]	AOA in [°]	ZOD in [°]	ZOA in [°]
1	0.0000	0	9.3	-173.3	105.8	78.9
2	0.1072	-2.2	9.3	-173.3	105.8	78.9
3	0.2155	-4	9.3	-173.3	105.8	78.9
4	0.2095	-3.2	-34.1	125.5	115.3	63.3
5	0.2870	-9.8	-65.4	-88.0	119.3	59.9
6	0.2986	-1.2	-11.4	155.1	103.2	67.5
7	0.3752	-3.4	-11.4	155.1	103.2	67.5
8	0.5055	-5.2	-11.4	155.1	103.2	67.5
9	0.3681	-7.6	-67.2	-89.8	118.2	82.6
10	0.3697	-3	52.5	132.1	102.0	66.3
11	0.5700	-8.9	-72	-83.6	100.4	61.6
12	0.5283	-9	74.3	95.3	98.3	58.0
13	1.1021	-4.8	-52.2	103.7	103.4	78.2
14	1.2756	-5.7	-50.5	-87.8	102.5	82.0
15	1.5474	-7.5	61.4	-92.5	101.4	62.4
16	1.7842	-1.9	30.6	-139.1	103.0	78.0
17	2.0169	-7.6	-72.5	-90.6	100.0	60.9
18	2.8294	-12.2	-90.6	58.6	115.2	82.9
19	3.0219	-9.8	-77.6	-79.0	100.5	60.8
20	3.6187	-11.4	-82.6	65.8	119.6	57.3
21	4.1067	-14.9	-103.6	52.7	118.7	59.9
22	4.2790	-9.2	75.6	88.7	117.8	60.1
23	4.7834	-11.3	-77.6	-60.4	115.7	62.3
Per-Cluster Parameters						
Parameter	c_{ASD} in [°]	c_{ASA} in [°]	c_{ZSD} in [°]	c_{ZSA} in [°]	XPR in [dB]	
Value	10	22	3	7	8	

Table 7.7.1-3. CDL-C

Cluster #	Normalized delay	Power in [dB]	AOD in [°]	AOA in [°]	ZOD in [°]	ZOA in [°]
1	0	-4.4	-46.6	-101	97.2	87.6
2	0.2099	-1.2	-22.8	120	98.6	72.1
3	0.2219	-3.5	-22.8	120	98.6	72.1
4	0.2329	-5.2	-22.8	120	98.6	72.1
5	0.2176	-2.5	-40.7	-127.5	100.6	70.1
6	0.6366	0	0.3	170.4	99.2	75.3
7	0.6448	-2.2	0.3	170.4	99.2	75.3
8	0.6560	-3.9	0.3	170.4	99.2	75.3
9	0.6584	-7.4	73.1	55.4	105.2	67.4
10	0.7935	-7.1	-64.5	66.5	95.3	63.8
11	0.8213	-10.7	80.2	-48.1	106.1	71.4
12	0.9336	-11.1	-97.1	46.9	93.5	60.5
13	1.2285	-5.1	-55.3	68.1	103.7	90.6
14	1.3083	-6.8	-64.3	-68.7	104.2	60.1
15	2.1704	-8.7	-78.5	81.5	93.0	61.0
16	2.7105	-13.2	102.7	30.7	104.2	100.7
17	4.2589	-13.9	99.2	-16.4	94.9	62.3
18	4.6003	-13.9	88.8	3.8	93.1	66.7
19	5.4902	-15.8	-101.9	-13.7	92.2	52.9
20	5.6077	-17.1	92.2	9.7	106.7	61.8
21	6.3065	-16	93.3	5.6	93.0	51.9
22	6.6374	-15.7	106.6	0.7	92.9	61.7
23	7.0427	-21.6	119.5	-21.9	105.2	58
24	8.6523	-22.8	-123.8	33.6	107.8	57

Per-Cluster Parameters					
Parameter	c_{ASD} in [°]	c_{ASA} in [°]	c_{ZSD} in [°]	c_{ZSA} in [°]	XPR in [dB]
Value	2	15	3	7	7

Table 7.7.1-4. CDL-D.

Cluster #	Cluster PAS	Normalized Delay	Power in [dB]	AOD in [°]	AOA in [°]	ZOD in [°]	ZOA in [°]
1	Specular(LOS path)	0	-0.2	0	-180	98.5	81.5
	Laplacian	0	-13.5	0	-180	98.5	81.5
2	Laplacian	0.035	-18.8	89.2	89.2	85.5	86.9
3	Laplacian	0.612	-21	89.2	89.2	85.5	86.9
4	Laplacian	1.363	-22.8	89.2	89.2	85.5	86.9
5	Laplacian	1.405	-17.9	13	163	97.5	79.4
6	Laplacian	1.804	-20.1	13	163	97.5	79.4
7	Laplacian	2.596	-21.9	13	163	97.5	79.4
8	Laplacian	1.775	-22.9	34.6	-137	98.5	78.2
9	Laplacian	4.042	-27.8	-64.5	74.5	88.4	73.6
10	Laplacian	7.937	-23.6	-32.9	127.7	91.3	78.3
11	Laplacian	9.424	-24.8	52.6	-119.6	103.8	87
12	Laplacian	9.708	-30.0	-132.1	-9.1	80.3	70.6
13	Laplacian	12.525	-27.7	77.2	-83.8	86.5	72.9

Per-Cluster Parameters					
Parameter	c_{ASD} in [°]	c_{ASA} in [°]	c_{ZSD} in [°]	c_{ZSA} in [°]	XPR in [dB]
Value	5	8	3	3	11

Table 7.7.1-5. CDL-E.

Cluster #	Cluster PAS	Normalized Delay	Power in [dB]	AOD in [°]	AOA in [°]	ZOD in [°]	ZOA in [°]
1	Specular (LOS path)	0.000	-0.03	0	-180	99.6	80.4
	Laplacian	0.000	-22.03	0	-180	99.6	80.4
2	Laplacian	0.5133	-15.8	57.5	18.2	104.2	80.4
3	Laplacian	0.5440	-18.1	57.5	18.2	104.2	80.4
4	Laplacian	0.5630	-19.8	57.5	18.2	104.2	80.4
5	Laplacian	0.5440	-22.9	-20.1	101.8	99.4	80.8
6	Laplacian	0.7112	-22.4	16.2	112.9	100.8	86.3
7	Laplacian	1.9092	-18.6	9.3	-155.5	98.8	82.7
8	Laplacian	1.9293	-20.8	9.3	-155.5	98.8	82.7
9	Laplacian	1.9589	-22.6	9.3	-155.5	98.8	82.7
10	Laplacian	2.6426	-22.3	19	-143.3	100.8	82.9
11	Laplacian	3.7136	-25.6	32.7	-94.7	96.4	88
12	Laplacian	5.4524	-20.2	0.5	147	98.9	81
13	Laplacian	12.0034	-29.8	55.9	-36.2	95.6	88.6
14	Laplacian	20.6419	-29.2	57.6	-26	104.6	78.3
Per-Cluster Parameters							
Parameter	c_{ASD} in [°]		c_{ASA} in [°]	c_{ZSD} in [°]	c_{ZSA} in [°]	XPR in [dB]	
Value	5		11	3	7	8	

7.7.2 Tapped Delay Line (TDL) models

The TDL models for simplified evaluations, e.g., for non-MIMO evaluations, are defined for the full frequency range from 0.5 GHz to 100 GHz with a maximum bandwidth of 2 GHz.

Three TDL models, namely TDL-A, TDL-B and TDL-C, are constructed to represent three different channel profiles for NLOS while TDL-D and TDL-E are constructed for LOS, the parameters of which can be found respectively in Table 7.7.2-1, Table 7.7.2-2 , Table 7.7.2-3, Table 7.7.2-4 and Table 7.7.2-5.

The Doppler spectrum for each tap is characterized by a classical (Jakes) spectrum shape and a maximum Doppler shift f_D where $f_D = |\bar{v}| / \lambda_0$. Due to the presence of a LOS path, the first tap in TDL-D and TDL-E follows a Ricean fading distribution. For those taps the Doppler spectrum additionally contains a peak at the Doppler shift $f_S = 0.7\, f_D$ with an amplitude such that the resulting fading distribution has the specified K-factor.

Each TDL model can be scaled in delay so that the model achieves a desired RMS delay spread, according to the procedure described in Clause 7.7.3.

For LOS channel models, the K-factor of TDL-D and TDL-E can be set to a desired value following the procedure described in Clause 7.7.6.

Table 7.7.2-1. TDL-A

Tap #	Normalized delay	Power in [dB]	Fading distribution
1	0.0000	-13.4	Rayleigh
2	0.3819	0	Rayleigh
3	0.4025	-2.2	Rayleigh
4	0.5868	-4	Rayleigh
5	0.4610	-6	Rayleigh
6	0.5375	-8.2	Rayleigh
7	0.6708	-9.9	Rayleigh
8	0.5750	-10.5	Rayleigh
9	0.7618	-7.5	Rayleigh
10	1.5375	-15.9	Rayleigh
11	1.8978	-6.6	Rayleigh
12	2.2242	-16.7	Rayleigh
13	2.1718	-12.4	Rayleigh
14	2.4942	-15.2	Rayleigh
15	2.5119	-10.8	Rayleigh
16	3.0582	-11.3	Rayleigh
17	4.0810	-12.7	Rayleigh
18	4.4579	-16.2	Rayleigh
19	4.5695	-18.3	Rayleigh
20	4.7966	-18.9	Rayleigh
21	5.0066	-16.6	Rayleigh
22	5.3043	-19.9	Rayleigh
23	9.6586	-29.7	Rayleigh

Table 7.7.2-2. TDL-B

Tap #	Normalized delay	Power in [dB]	Fading distribution
1	0.0000	0	Rayleigh
2	0.1072	-2.2	Rayleigh
3	0.2155	-4	Rayleigh
4	0.2095	-3.2	Rayleigh
5	0.2870	-9.8	Rayleigh
6	0.2986	-1.2	Rayleigh
7	0.3752	-3.4	Rayleigh
8	0.5055	-5.2	Rayleigh
9	0.3681	-7.6	Rayleigh
10	0.3697	-3	Rayleigh
11	0.5700	-8.9	Rayleigh
12	0.5283	-9	Rayleigh
13	1.1021	-4.8	Rayleigh
14	1.2756	-5.7	Rayleigh
15	1.5474	-7.5	Rayleigh
16	1.7842	-1.9	Rayleigh
17	2.0169	-7.6	Rayleigh
18	2.8294	-12.2	Rayleigh
19	3.0219	-9.8	Rayleigh
20	3.6187	-11.4	Rayleigh
21	4.1067	-14.9	Rayleigh
22	4.2790	-9.2	Rayleigh
23	4.7834	-11.3	Rayleigh

Table 7.7.2-3. TDL-C

Tap #	Normalized delays	Power in [dB]	Fading distribution
1	0	-4.4	Rayleigh
2	0.2099	-1.2	Rayleigh
3	0.2219	-3.5	Rayleigh
4	0.2329	-5.2	Rayleigh
5	0.2176	-2.5	Rayleigh
6	0.6366	0	Rayleigh
7	0.6448	-2.2	Rayleigh
8	0.6560	-3.9	Rayleigh
9	0.6584	-7.4	Rayleigh
10	0.7935	-7.1	Rayleigh
11	0.8213	-10.7	Rayleigh
12	0.9336	-11.1	Rayleigh
13	1.2285	-5.1	Rayleigh
14	1.3083	-6.8	Rayleigh
15	2.1704	-8.7	Rayleigh
16	2.7105	-13.2	Rayleigh
17	4.2589	-13.9	Rayleigh
18	4.6003	-13.9	Rayleigh
19	5.4902	-15.8	Rayleigh
20	5.6077	-17.1	Rayleigh
21	6.3065	-16	Rayleigh
22	6.6374	-15.7	Rayleigh
23	7.0427	-21.6	Rayleigh
24	8.6523	-22.8	Rayleigh

Table 7.7.2-4. TDL-D.

Tap #	Normalized delay	Power in [dB]	Fading distribution
1	0	-0.2	LOS path
	0	-13.5	Rayleigh
2	0.035	-18.8	Rayleigh
3	0.612	-21	Rayleigh
4	1.363	-22.8	Rayleigh
5	1.405	-17.9	Rayleigh
6	1.804	-20.1	Rayleigh
7	2.596	-21.9	Rayleigh
8	1.775	-22.9	Rayleigh
9	4.042	-27.8	Rayleigh
10	7.937	-23.6	Rayleigh
11	9.424	-24.8	Rayleigh
12	9.708	-30.0	Rayleigh
13	12.525	-27.7	Rayleigh
NOTE: The first tap follows a Ricean distribution with a K-factor of K_1 = 13.3 dB and a mean power of 0dB.			

Table 7.7.2-5. TDL-E.

Tap #	Normalized delay	Power in [dB]	Fading distribution
1	0	-0.03	LOS path
	0	-22.03	Rayleigh
2	0.5133	-15.8	Rayleigh
3	0.5440	-18.1	Rayleigh
4	0.5630	-19.8	Rayleigh
5	0.5440	-22.9	Rayleigh
6	0.7112	-22.4	Rayleigh
7	1.9092	-18.6	Rayleigh
8	1.9293	-20.8	Rayleigh
9	1.9589	-22.6	Rayleigh
10	2.6426	-22.3	Rayleigh
11	3.7136	-25.6	Rayleigh
12	5.4524	-20.2	Rayleigh
13	12.0034	-29.8	Rayleigh
14	20.6519	-29.2	Rayleigh
NOTE: The first tap follows a Ricean distribution with a K-factor of K_1 = 22 dB and a mean power of 0dB.			

7.7.3 Scaling of delays

The RMS delay spread values of both CDL and TDL models are normalized and they can be scaled in delay so that a desired RMS delay spread can be achieved. The scaled delays can be obtained according to the following equation:

$$\tau_{n,\text{scaled}} = \tau_{n,\text{model}} \cdot \text{DS}_{\text{desired}} \quad (7.7\text{-}1)$$

in which

$\tau_{n,\text{model}}$ is the normalized delay value of the *n*th cluster in a CDL or a TDL model

$\tau_{n,\text{scaled}}$ is the new delay value (in [ns]) of the *n*th cluster

$\text{DS}_{\text{desired}}$ is the wanted delay spread (in [ns])

The example scaling parameters are selected according to Table 7.7.3-1 where the values have been chosen such that the RMS delay spreads span the range observed in measurements corresponding to the typical 5G evaluation scenarios. For information purposes, examples of such RMS delay spreads for the different scenarios are given in Table 7.7.3-2 where the "short-delay profile" corresponds to the median RMS delay spread for LOS scenarios, while "normal-delay profile" and "long-delay profile" correspond to the median and the 90th percentile RMS delay spread for NLOS scenarios according to the channel parameters in Table 7.5-6. It can therefore be understood that a particular RMS delay spread in Table 7.7.3-1 may occur in any scenario; however certain values may be more likely in some scenarios than in others.

The example parameters given in Table 7.7.3-1 does not preclude the use of other scaling values if this is found appropriate, for instance if additional scenarios are introduced or if e.g. the effect of beamforming needs to be captured in a TDL. Both of these examples can potentially result in an increased range of experienced RMS delay spreads.

Table 7.7.3-1. Example scaling parameters for CDL and TDL models.

Model	$\text{DS}_{\text{desired}}$
Very short delay spread	10 ns
Short delay spread	30 ns
Nominal delay spread	100 ns
Long delay spread	300 ns
Very long delay spread	1000 ns

Table 7.7.3-2. Scenario specific scaling factors - for information only

Proposed Scaling Factor $DS_{desired}$ in [ns]		Frequency [GHz]						
		2	6	15	28	39	60	70
Indoor office	Short-delay profile	20	16	16	16	16	16	16
	Normal-delay profile	39	30	24	20	18	16	16
	Long-delay profile	59	53	47	43	41	38	37
UMi Street-canyon	Short-delay profile	65	45	37	32	30	27	26
	Normal-delay profile	129	93	76	66	61	55	53
	Long-delay profile	634	316	307	301	297	293	291
UMa	Short-delay profile	93	93	85	80	78	75	74
	Normal-delay profile	363	363	302	266	249	228	221
	Long-delay profile	1148	1148	955	841	786	720	698
RMa & RMa O2I	Short-delay profile	32	32	N/A	N/A	N/A	N/A	N/A
	Normal-delay profile	37	37	N/A	N/A	N/A	N/A	N/A
	Long-delay profile	153	153	N/A	N/A	N/A	N/A	N/A
UMi / UMa O2I	Normal-delay profile	240						
	Long-delay profile	616						

7.7.4 Spatial filter for generating TDL channel model

The TDL models described in Clause 7.7.2 are generated from the CDL models assuming ideal isotropic antennas at both Tx and Rx. It is also possible to generate TDL models by assuming non-isotropic antennas like directive horn antennas or array antennas.

The basic idea to generate a TDL model based on a filtered CDL model is shown in Figure 7.7.4-1 below.

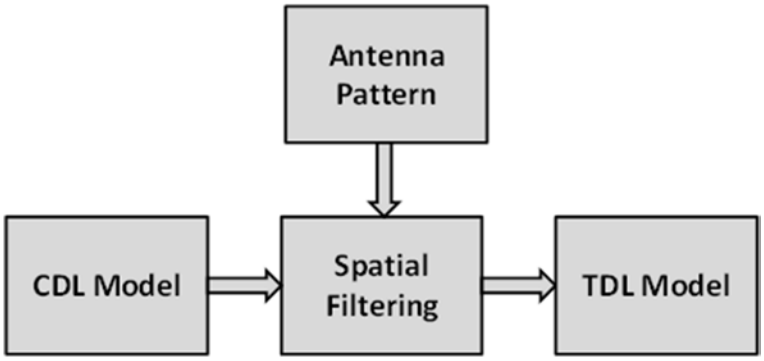

Figure 7.7.4-1 The basic idea for filtering the CDL model to TDL model.

7.7.4.1 Exemplary filters/antenna patterns

Note that any filter/pattern can be applied on a CDL to derive a TDL for evaluating directional algorithms.

Example 1: Isotropic pattern

$$A'_{\{tx,rx\}}(\theta',\phi')=1 \tag{7.7-2}$$

Example 2: Rectangular mask

$$A'_{\{tx,rx\}}(\theta',\phi',\mathrm{BW})=\begin{cases}1, & |\theta'-90°|\le\frac{\mathrm{BW}}{2}\ \&\ |\phi'|\le\frac{\mathrm{BW}}{2}\\ 0, & \text{otherwise.}\end{cases} \tag{7.7-3}$$

with BW denotes beamwidth.

Example 3: Simplified antenna pattern given in [ITU-R M.2135]

Figure 7.7.4-2 Simplified antenna pattern [ITU-R M.2135].

7.7.4.2 Generation procedure

1. The following steps are needed to generate tapped delay line (TDL) models:Choose a CDL model (e.g. CDL-A). Note that the models may be scaled according to Clause 7.7.5.1 prior to the filtering in order to represent different angular spreads.
2. Choose spatial filters A'_{tx} and A'_{rx} defined in LCS
3. Transform the spatial filter into GCS to obtain A_{tx} and A_{rx} such that the pointing direction (θ_p, ϕ_p) is centered within the filter. The pointing direction may be defined
   a. by the dominant path $(\theta_P, \phi_P) = (\theta_i, \phi_i)$ with $i = \text{argmax}_n\left(P_n^{\text{CDL}}\right)$, where P_n^{CDL} denotes the CDL cluster power values
   b. Or an arbitrary direction
4. Calculate TDL cluster power values P_n^{TDL} given the following equation

$$P_n^{\text{TDL}} = P_n^{\text{CDL}} A_{rx}\left(\theta_{n,\text{ZOA}}, \phi_{n,\text{AOA}}\right) A_{tx}\left(\theta_{n,\text{ZOD}}, \phi_{n,\text{AOD}}\right) \quad (7.7\text{-}4)$$

7.7.5 Extension for MIMO simulations

Extended MIMO link-level channel models can be constructed according to two alternative methods described in the following.

7.7.5.1 CDL extension: Scaling of angles

The angle values of CDL models are fixed, which is not very suitable for MIMO simulations for several reasons; The PMI statistics can become biased, and a fixed precoder may perform better than open-loop and on par with closed-loop or reciprocity beamforming. Furthermore, a CDL only represents a single channel realization. The predefined angle values in the CDL models can be generalized by introducing angular translation and scaling. By translation, mean angle $\mu_{\phi,model}$ can be changed to $\mu_{\phi,desired}$ and angular spread AS_{model} can be changed to match $AS_{desired}$ by scaling. The translated and scaled ray angles can be obtained according to the following equation:

$$\phi_{n,m,scaled} = \phi_{n,scaled} + c_{\{ASA,ASD,ZSA,ZSD\}}\alpha_m \quad (7.7\text{-}5)$$

$$\phi_{LOS,scaled} = \phi_{LOS,intermediate} - \mu_{\phi,intermediate} + \mu_{\phi,desired} \quad (7.7\text{-}5a)$$

$$\phi_{n,intermediate} = s \cdot \text{WrapTo180}\left(\phi_{n,model} - \mu_{\phi,model}\right) \quad (7.7\text{-}5b)$$

$$\phi_{LOS,intermediate} = s \cdot \mathrm{WrapTo180}\left(\phi_{LOS,model} - \mu_{\phi,model}\right) \quad (7.7\text{-}5c)$$

$$\phi_{n,scaled} = \phi_{n,intermediate} - \mu_{\phi,intermediate} + \mu_{\phi,desired} \quad (7.7\text{-}5d)$$

in which:

- $\mu_{\phi,model}$ is the cluster mean angle calculated using Annex A.4 with $\phi_{n,model}$ and $\phi_{LOS,model}$ as the input cluster angles,
- $\mu_{\phi,intermediate}$ is the intermediate cluster mean angle calculated using Annex A.4 with $\phi_{n,intermediate}$ and $\phi_{LOS,intermediate}$ as input cluster angles,
- s is a scale factor chosen to change the distribution of the angles based on calculation in Annex A.5. Table 7.7.5.1-1 shows required scale factor for typical desired angular spread values for AOD, AOD, ZOA, and ZOD,
- $\phi_{n,\mathrm{model}}$ is the tabulated CDL cluster angle,
- AS_{model} is the rms cluster angular spread of the tabulated CDL including the offset ray angles, calculated using the angular spread definition in Annex A.3,
- $\mu_{\phi,desired}$ is the desired cluster mean angle,
- $AS_{desired}$ is the desired rms cluster angular spread,
- $\phi_{n,\mathrm{scaled}}$ is the scaled CDL cluster angle of the *n*th cluster,
- $\phi_{n,m,scaled}$ is the resulting scaled ray angle that corresponds to *m*th subpath angle of *n*th cluster,
- $c_{\{ASA,ASD,ZSA,ZSD\}}$ is the cluster-wise RMS angular spread of either custer ASA, ASD, ZSA, or ZSD from Table 7.7.1-1, 7.7.1-2, 7.7.1-3, 7.7.1-4, and 7.7.1-5,
- α_m is the offset angles from Table 7.5-3,
- $WrapTo180(\cdot)$ is a function which wraps an azimuth angle to the half-open interval (-180, 180].

Table 7.7.5.1-1: Scale factor values for each CDL model

CDL Type	Desired AOD Spread (°)	Scale Factor (AOD)	Desired AOA Spread (°)	Scale Factor (AOA)	Desired ZOA Spread (°)	Scale Factor (ZOA)	Desired ZOD Spread (°)	Scale Factor (ZOD)
CDL-A	5	0.0680	30	0.3531	5	0.2397	1	0.0352
	10	0.1360	45	0.5268	10	0.4802	3	0.1056
	15	0.2041	60	0.6981	15	0.7225	5	0.1761
	25	0.3405						
CDL-B	5	0.1238	30	0.5417	5	0.6519	1	0.1940
	10	0.2475	45	0.8081	10	1.3018	3	0.5822
	15	0.3710	60	1.0709	15	1.9480	5	0.9705
	25	0.6168						
CDL-C	5	0.1281	30	0.4307	5	0.6476	1	0.3643
	10	0.2568	45	0.6447	10	1.2971	3	1.0929
	15	0.3864	60	0.8585	15	1.9504	5	1.8219
	25	0.6513						
CDL-D	5	0.3231	30	9.8888	5	4.3268	1	0.4477
	10	0.6652	45	N/A	10	8.8868	3	1.3469
	15	1.0594	60	N/A	15	14.0344	5	2.2579
	25	5.8637						
CDL-E	5	0.3950	30	2.9733	5	6.9195	1	0.9714
	10	0.8009	45	N/A	10	14.8378	3	2.9180
	15	1.2330	60	N/A	15	27.2849	5	4.8774
	25	2.3627				0.2397		

NOTE: Values of Table 7.7.5.1-1 were computed based on scaling factor calculation method described in Annex A.5.

Alternatively, for CDL-D and CDL-E, if maintaining the LOS angle is desired, the translated and scaled ray angles can be obtained according to the following equation instead of using equation (7.7-5) and (7.7-5a):

$$\phi_{n,m,scaled} = \phi_{n,scaled} + c_{\{ASA,ASD,ZSA,ZSD\}}\alpha_m \quad (7.7\text{-}6)$$

$$\phi_{LOS,scaled} = \phi_{LOS,\text{model}} \quad (7.7\text{-}6a)$$

$$\phi_{n,scaled} = \phi_{n,intermediate} - \phi_{LOS,\text{intermediate}} + \phi_{LOS,\text{model}} \quad (7.7\text{-}6b)$$

in which:

- $\phi_{LOS,\text{model}}$ is the LOS path angle of the model,
- $\phi_{n,\text{scaled}}$ is the scaled CDL cluster angle of the *n*th cluster.

The angular scaling is applied on the cluster angles including offsets from the tabulated cluster angles. Typical angular spreads for different scenarios can be obtained from the system-level model.

Example scaling values are:

- AOD spread (ASD) for each CDL model: {5, 10, 15, 25} degrees.
- AOA spread (ASA) for each CDL model: {30, 45, 60} degrees.
- ZOA spread (ZSA) for each CDL model: {5, 10, 15} degrees.
- ZOD spread (ZSD) for each CDL model: {1, 3, 5} degrees.

The angular scaling and translation can be applied to some or all of the azimuth and zenith angles of departure and arrival.

Note: The azimuth angles may need to be wrapped around to be within [0, 360] degrees, while the zenith angles may need to be clipped to be within [0, 180] degrees.

7.7.5.2 TDL extension: Applying a correlation matrix

The TDLs and the spatial-filtered TDLs can be used with the correlation matrices for MIMO link-level simulations. Typical correlation parameters can be derived from 1) delay & angular scaled CDLs with antenna array assumptions, 2) system-level model with antenna array assumptions, or 3) by selecting extreme cases, e.g. uncorrelated, highly correlated etc. For example, these following options can be considered:

1) Zero correlation (IID channel coefficients) can be used for any number of antenna elements
2) The correlation matrix construction method from TS36.101/104 [15][16] can be used for linear and planar (single- or dual-polarized) arrays.
    - Other correlation parameters α, β, γ than those specified in TS36.101/104 [15][16] and extensions to larger antenna arrays can be considered. For typical scenarios, α and β will be in the range 0-1
        - A representative set of values is {0,0.7,0.9,0.99}

Note: This approach can be applied to TDLs derived from spatially filtered CDLs to emulate hybrid BF system

Note: Other methodologies could also be developed, e.g.

- extending the TS36.101/104 [15][16] procedure to planar arrays or more elements
- using CDLs in combination with array assumptions to derive per-tap correlation matrices as in [17].
- using the system-level model in combination with array assumptions to derive per-tap or per-channel correlation matrices

7.7.6 K-factor for LOS channel models

For the LOS channel models of CDL/TDL-D and CDL/TDL-E, the K-factor values may be changed by the user. Mean and standard deviation of K-factor values can be found in Table 7.5-6, although other values may also be used.

If the K-factor of a model shall be changed to K_{desired} [dB], the cluster powers for the Laplacian clusters (in case of CDL) or the tap powers for the Rayleigh fading taps (in case of TDL) are determined by

$$P_{n,\text{scaled}} = P_{n,\text{model}} - K_{\text{desired}} + K_{\text{model}}, \quad (7.7.6\text{-}1)$$

where $P_{n,\text{scaled}}$ and $P_{n,\text{model}}$ denote the scaled and the model path power (as given in the tables) of tap/cluster n. The model's K-factor K_{mode} is defined as

$$K_{\text{model}} = P_{1,\text{model}}^{\text{LOS}} - 10\log_{10}\left(\sum_{n=1}^{N} 10^{P_{n,\text{model}}/10}\right). \quad (7.7.6\text{-}2)$$

After scaling the powers, the delay spread needs to be re-normalized. This is done through the two steps below.

1) Calculate the actual RMS delay spread after the K-factor adjustment.
2) Divide the delays by that value to obtain DS = 1.

7.8 Channel model calibration

7.8.1 Large scale calibration

For large scale calibration, fast fading is not modeled. The calibration parameters can be found in Table 7.8-1. The calibration results based on TR 38.900 V14.0.0 can be found in R1-165974.

Table 7.8-1: Simulation assumptions for large scale calibration

Parameter	Values
Scenarios	UMa, UMi-Street Canyon, Indoor-office (open office)
Sectorization	3 sectors per cell site: 30, 150 and 270 degrees 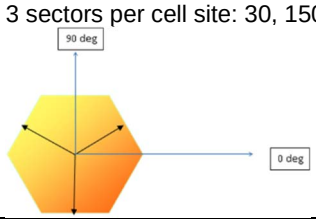
BS antenna configurations	$M_g = N_g = 1$; (M,N,P) = (10, 1, 1), $d_V = 0.5\lambda$
BS port mapping	The 10 elements are mapped to a single CRS port
BS antenna electrical downtilting	102 degrees for UMa and UMi Street Canyon 110 degrees for indoor
Antenna virtualization	DFT precoding according to TR 36.897 with application of panning and tilting angles
BS Tx power	44 dBm for UMi-Street Canyon, 49 for UMa at 6GHz 35 dBm at 30GHz and 70 GHz for UMa and UMi-Street canyon 24 dBm for Indoor for all carrier frequencies
Bandwidth	20MHz for 6GHz, and 100MHz for 30GHz and 70 GHz
UT antenna configurations	1 element (vertically polarized), Isotropic antenna gain pattern
Handover margin (for calibration)	0dB
UT distribution	Following TR36.873 for UMa and UMi, (3D dropping) uniform dropping for indoor with minimum distance (2D) of 0 m
UT attachment	Based on pathloss considering LOS angle
UT noise figure	9 dB
Fast fading channel	Fast fading channel is not modelled
O2I penetration loss	50% low loss and 50% high loss
Carrier Frequency	6 GHz, 30 GHz, 70GHz
Wrapping method for UMa and UMi	geographical distance based wrapping (mandatory) radio distance (optional)
Metrics	1) Coupling loss – serving cell (based on LOS pathloss)
	2) Geometry (based on LOS pathloss) with and without white noise

Additional calibration parameters can be found in Table 7.8-1A. It is assumed that parameters from Table 7.8-1 is used if unspecified by the additional calibration parameters in Table 7.8-1A. In addition, calibration of UMa and UMi-Street Canyon at 6 GHz carrier frequency using simulation assumptions in Table 7.8-1 with updated channel modeling is part of the additional calibration. The calibration results based on additional calibration parameters can be found in R1-2506406.

Table 7.8-1A: Simulation assumptions for large scale calibration

Parameter	Values
Scenarios	UMa, UMi-Street Canyon, SMa
Carrier Frequency	7 GHz
BS antenna downtilting	Mechanical downtilt of 95 degrees for SMa for ISD = 1299m Mechanical downtilt of 92 degrees for SMa for ISD = 1732m Electrical downtilt in Table 7.8-1 for UMa and UMi-Street Canyon
BS antenna configurations	$M_g = N_g = 1$; (M,N,P) = (10, 1, 1), $d_V = 0.5\lambda$
BS port mapping	$M_p = 1$, $N_p = 1$, i.e., 10 elements are mapped to a single port M_p and N_p are the number of vertical, horizontal TXRUs within a panel and polarization
BS Tx power	49 dBm for SMa
Bandwidth	20 MHz
UT distribution	For SMa, 20% of UT outdoor, 80% of UT indoor. Among indoor UT, 90% of indoor UT are within residential buildings, and 10% of indoor UT in commercial buildings. Indoor UTs are uniformly distributed across all floors for a building type.
LOS probability	For SMa, 0% vegetation
O2I penetration loss	For SMa, Low-loss A model
O2I car penetration loss	For SMa, non-metallic car window
Wrapping method	For UMa, UMi-Street Canyon, SMa: - geographical distance based wrapping (mandatory) - radio distance (optional)

7.8.2 Full calibration

The calibration parameters for full calibration including the fast fading modelling can be found in Table 7.8-2. Unspecified parameters in Table 7.8-2 are the same as those in Table 7.8-1. When P=2, X-pol (+/-45 degree) is used for BS antenna configuration 1 and X-pol (0/+90 degree) is used for UT antenna configuration. The calibration results based on TR 38.900 V14.0.0 can be found in R1-165975.

Table 7.8-2: Simulation assumptions for full calibration

Parameter	Values
Scenarios	UMa, UMi-street Canyon, Indoor-office (open office)
Carrier Frequency	6 GHz, 30 GHz, 60GHz, 70GHz
Bandwidth	20MHz for 6GHz, and 100MHz for 30GHz, 60 GHz and 70 GHz
BS Tx power	44 dBm for UMi-Street Canyon, 49 for UMa at 6GHz 35 dBm at 30GHz, 60 GHz and 70 GHz for UMa and UMi-Street canyon 24 dBm for Indoor for all carrier frequencies
BS antenna configurations	Config 1: M = 4,N = 4,P = 2, M_g = 1, N_g = 2, $d_H = d_V = 0.5\lambda$, $d_{H,g} = d_{V,g} = 2.5\lambda$ … calibration metrics 1), 2), 3) are calibrated Config 2: $M_g = N_g = 1$, M = N = 2, P = 1 … calibration metrics 1), 2), 4) are calibrated
BS port mapping	Config 1: all 16 elements for each polarization on each panel are mapped to a single CRS port; panning angles of the two subarrays: (0,0) degs; same downtilt angles as used for the large-scale calibrations Config 2: each antenna element is mapped to one CRS port
UT antenna configurations	$M_g = N_g = 1$, M = N = 1, P = 2
UT distribution	Following TR36.873 for UMa and UMi, (3D dropping) uniform dropping for indoor with minimum distance (2D) of 0 m
UT attachment	Based on RSRP (formula) from CRS port 0
Polarized antenna modelling	Model-2 in TR36.873
UT orientation	$\Omega_{UT,\alpha}$ uniformly distributed on [0,360] degree, $\Omega_{UT,\beta}$ = 90 degree, $\Omega_{UT,\gamma}$= 0 degree
UT antenna pattern	Isotropic
Metrics	1) Coupling loss – serving cell
	2) Wideband SIR before receiver without noise
	3) CDF of Delay Spread and Angle Spread (ASD, ZSD, ASA, ZSA) from the serving cell (according to circular angle spread definition of TR 25.996)
	4) CDF of largest (1st) PRB singular values (serving cell) at t=0 plotted in 10*log10 scale. CDF of smallest (2nd) PRB singular values (serving cell) at t=0 plotted in 10*log10 scale. CDF of the ratio between the largest PRB singular value and the smallest PRB singular value (serving cell) at t=0 plotted in 10*log10 scale. See note.
NOTE: The PRB singular values of a PRB are the eigenvalues of the mean covariance matrix in the PRB.	

Additional full calibration parameters can be found in Table 7.8-2A. It is assumed that parameters from Table 7.8-2 is used if unspecified by the additional full calibration parameters in Table 7.8-2A. In addition, calibration of UMa and UMi-Street Canyon at 6 GHz carrier frequency using simulation assumptions in Table 7.8-2 with updated channel modeling is part of the additional calibration. For calibration of UMa and UMi-Street Canyon at 6 GHz, the following is additionally assumed.

- SCS of 15 kHz
- UT attachment is based on RSRP (formula) from BS port 0
- BS antenna configuration 1 and 2 both apply
- UT antenna configuration, pattern, and polarization modeling are labeled as UT antenna config A

The calibration results based on additional calibration parameters can be found in R1-2506406.

Table 7.8-2A: Simulation assumptions for full calibration

Parameter	Values
Scenarios	UMa, UMi-Street Canyon, SMa
Carrier Frequency	7 GHz, (optional) 15 GHz
BS antenna downtilting	Mechanical downtilt of 95 degrees for SMa for ISD = 1299m Mechanical downtilt of 92 degrees for SMa for ISD = 1732m Electrical downtilt as in Table 7.8-1 for UMa and UMi-Street Canyon
BS antenna configurations	Config 3 for UMi, UMa, SMa at 7 GHz: $M_g = N_g = 1$, M = 8, N = 16, P = 2, $d_H = d_V = 0.5\lambda$ … calibration metrics 1), 2), 3), 4) are calibrated (optional) Config 4 for UMa at 7 and 15 GHz: $M_g = N_g = 1$, M = 64, N = 16, P = 2, $M_g = 1$, $N_g = 1$, $d_H = d_V = 0.5\lambda$ … calibration metrics 1), 2), 3), 4) are calibrated
BS Polarized antenna modelling	Model-2 in Clause 7.3.2
BS port mapping	Config 3 for UMi, UMa, SMa at 7 GHz: $M_p = 8$, $N_p = 16$, each antenna element is mapped to one port (optional) Config 4 for UMa at 7 and 15 GHz: $M_p = 16$, $N_p = 16$ M_p and N_p are the number of vertical, horizontal TXRUs within a panel and polarization
BS Tx power	49 dBm for SMa
Bandwidth	20 MHz for 7 GHz (optional) 200 MHz for 7 and 15 GHz
UT attachment	Based on RSRP (formula) from BS port 0
UT distribution	For SMa, 20% of UT outdoor, 80% of UT indoor. Among indoor UT, 90% of indoor UT are within residential buildings, and 10% of indoor UT in commercial buildings. Indoor UTs are uniformly distributed across all floors for a building type.
UT array orientation	Config B, C: $\Omega_{UT,\alpha}$ uniformly distributed on [0,360] degree, $\Omega_{UT,\beta}$ = 45 degree, $\Omega_{UT,\gamma}$= 0 degree Config D: $\Omega_{UT,\alpha}$ = 0 degree, $\Omega_{UT,\beta}$ = 0 degree, $\Omega_{UT,\gamma}$= 0 degree
UT antenna configurations	Config B for 7 GHz: 4 antenna port with single polarization for calibration based on handheld device antenna model using candidate antenna locations (1,7,3,5) as described in Clause 7.3 (optional) Config C for 15 GHz: 16 antenna port with dual polarization based on handheld device antenna model using candidate antenna locations in (1,2,3,4,5,6,7,8) as described in Clause 7.3 (only for metric 5) Config D: 8 antenna port with single polarization based on handheld device antenna model using candidate antenna locations in (1,2,3,4,5,6,7,8) as described in Clause 7.3
UT antenna pattern	Config B, C, D: Based on directional antenna for handheld UT described in Clause 7.3
UT Polarized antenna modelling	Config B, C, D: Based on directional antenna for handheld UT described in Clause 7.3
O2I penetration loss	For SMa, low-loss A model
SCS assumption	30 kHz
Additional metrics	5) Antenna field pattern of handheld UT, $F'_{u,\theta'}(\theta', \phi')$ and $F'_{u,\phi'}(\theta', \phi')$, in UT LCS using UT antenna configuration D

7.8.3 Calibration of additional features

The calibration parameters for the calibration of oxygen absorption, large bandwidth and large antenna array, spatial consistency, and blockage can be respectively found in Table 7.8-3, 7.8-4, 7.8-5, and 7.8-6. Unspecified parameters in these tables are the same as those in Tables 7.8-1 and 7.8-2. When P=2, X-pol (+/-45 degree) is used for BS antenna configuration 1 and X-pol (0/+90 degree) is used for UT antenna configuration. The calibration results based on TR 38.900 V14.0.0 can be found in R1-1700990.

The additional calibration parameters for the calibration of near field channel modeling, BS side spatial non-stationarity, and UT side spatial non-stationarity can be respectively found in Table 7.8-6A, 7.8-6B, and 7.8-6C. For the assumption on the aperture size of the antenna array, the following guidance is considered:

- Up to 1.5 m for UMa with maximum antenna elements in the array is 5k for single Polarization.
- Up to 1 m for UMi with maximum antenna elements in the array is 2.22k for single Polarization.
- Up to 0.71 m for Indoor factory with maximum antenna elements in the array is 1.12k for single Polarization.

- Up to 0.25 (for rectangular antenna array), 0.5 (for linear antenna array) m for Indoor office with maximum antenna elements in the array is 256, 80 for single Polarization, respectively.

The additional calibration results can be found in R1-2506406.

Table 7.8-3: Simulation assumptions for calibration for oxygen absorption

Parameter	Values
Scenarios	UMi-street Canyon
Carrier Frequency	60 GHz
BS antenna configurations	M = 4, N = 4, P = 2, M_g = 1, N_g = 2, $d_H = d_V$ = 0.5λ, $d_{H,g} = d_{V,g}$ = 2.5λ
BS port mapping	all 16 elements for each polarization on each panel are mapped to a single CRS port; panning angles of the two subarrays: (0,0) degs; same downtilt angles as used for the large-scale calibrations
Calibration method	Drop multiple users in the multiple cells randomly, and collect the following metrics for each user after attachment.
Metrics	1) CDF of coupling loss (serving cell) 2) Wideband SINR before receiver – determined from RSRP (formula) from CRS port 0 3) CDF of Delay Spread from the serving cell

Table 7.8-4: Simulation assumptions for calibration for large bandwidth and large antenna array

Parameter	Values
Scenarios	UMi-street Canyon
Carrier Frequency	30GHz
Bandwidth	2GHz
BS antenna configurations	M = 8, N = 8, P = 2, M_g = 1, N_g = 4, $d_H = d_V$ = 0.5λ, $d_{H,g} = d_{V,g}$ = 4λ
BS port mapping	all 64 elements for each polarization on each panel are mapped to a single CRS port; panning angles of the two subarrays: (0,0) degs; same downtilt angles as used for the large-scale calibrations
The number of rays per cluster	N_{MPC} = 40
Calibration method	Drop multiple users in the multiple cells randomly, and collect the following metrics for each user after attachment.
Metrics	1) CDF of coupling loss (serving cell) 2) Wideband SINR before receiver – determined from RSRP (formula) from CRS port 0 3) CDF of largest (1st) PRB singular values (serving cell) at t=0 plotted in 10*log10 scale

Table 7.8-5: Simulation assumptions for calibration for spatial consistency

Parameter	Values
Scenarios	UMi-street Canyon
Carrier Frequency	30 GHz
BS antenna configurations	M = 4, N = 4, P = 2, M_g = 1, N_g = 2, $d_H = d_V$ = 0.5λ, $d_{H,g} = d_{V,g}$ = 2.5λ
BS port mapping	all 16 elements for each polarization on each panel are mapped to a single CRS port; panning angles of the two subarrays: (0,0) degs; same downtilt angles as used for the large-scale calibrations
UT distribution	Following TR36.873, 3D dropping uniform dropping for indoor with minimum distance of 0 m For Config1: 100% UT indoor and in the 1st floor For Config2: 100% UT outdoor
Mobility	Config1: UT is stationary Config2: UT is moving with random direction and fixed speed, e.g., 30 km/h
Calibration method	For Config1: Drop multiple UEs in a single cell, determine all permutations of pairs of UEs, collect the variables for each pair and bin them into certain distance ranges, e.g., 1m/2m/10m, to get enough samples. Collect the following metrics 1) –6). For Config2: Drop multiple users in the single cell, and collect metric 1)-2) and 7)-9) for each user after attachment.
Metrics	1) CDF of coupling loss (serving cell) 2) Wideband SINR before receiver – determined from RSRP (formula) from CRS port 0 3) Cross-correlation coefficient of delay for the third cluster between paired UEs, see note 1 4) Cross-correlation coefficient of AOA for the third cluster between paired UEs 5) Cross-correlation coefficient of LOS/NLOS status between paired UEs 6) Cross correlation coefficient of the channel response in Step 11 on the first non-DC subcarrier in an OFDM symbol on antenna port 0 received on the first UT antenna over multiple realizations between paired UEs 7) CDF of average varying rate of power for the third cluster, see note 2 8) CDF of average varying rate of delay for the third cluster (ns) 9) CDF of average varying rate of AOA for the third cluster (degree)
NOTE 1	For the UT pair at a certain distance range, the variables collected by two UEs can be denoted as X and Y, respectively, then the cross-correlation coefficient for real number can be written as [E(XY)-E(X)E(Y)] /sqrt([E(X^2)-E(X)^2])/ sqrt([E(Y^2)-E(Y)^2]), the cross-correlation coefficient for complex number can be written as |[E(XY*)-E(X)E(Y)*]/sqrt([E(XX*)-E(X)E(X)*])/sqrt([E(YY*)-E(Y)E(Y)*])|.
NOTE 2	For the average varying rate, we assume the collecting interval, e.g., 100ms, and then get the samples for a certain UT, the varying rate can be written as the standard variance of the samples per 100ms.

Table 7.8-6: Simulation assumptions for calibration for blockage

Parameter	Values
Scenarios	UMi-street Canyon
Carrier Frequency	30 GHz
BS antenna configurations	M = 4, N = 4, P = 2, M_g = 1, N_g = 2, $d_H = d_V$ = 0.5λ, $d_{H,g} = d_{V,g}$ = 2.5λ
BS port mapping	all 16 elements for each polarization on each panel are mapped to a single CRS port; panning angles of the two subarrays: (0,0) degs; same downtilt angles as used for the large-scale calibrations
Calibration method	For Model A: Drop multiple users in the multiple cells, and collect the following metrics 1) – 3) for each user after attachment. Optional self-blocking feature is made mandatory in the Landscape mode only for calibration purposes. For Model B: Drop a BS in (0,0,30) and a UT in (100,0,1.5), Jump directly to Step 11 and replace the channel with CDL-E. Drop a blocking screen of size h=10m, w = 2m in (80,10,1.5) Move the UT from (100,0,1.5) to (100,20,1.5) in small increments. For each UT position, translate all the AODs and AOAs of CDL-E such that the specular (LOS path) of CDL-E is pointing along the direct path between the BS and UT. Collect metric 4)
Metrics	1) CDF of coupling loss (serving cell) 2) Wideband SINR before receiver – determined from RSRP (formula) from CRS port 0 3) CDF of ASA from the serving cell 4) RSRP as a function of UT position

Table 7.8-6A: Simulation assumptions for calibration for near field channel modeling

Parameter		Values
Scenarios		UMi-street canyon, Indoor-office (open office)
Sectorization		For UMi-street canyon: sectorized as described in Table 7.8-1. For indoor-office: non-sectorized, 1 BS per BS location.
Carrier Frequency		7 GHz (optional) 15 GHz
Bandwidth		20 MHz
BS antenna height		UMi-street Canyon: 10m Indoor-office: 3m
BS antenna downtilt		Electrical downtilt of 102 degrees for UMi-street canyon Mechanical downtilt of 180 degrees for indoor-office
BS Tx power		44 dBm for UMi-street canyon 24 dBm for Indoor-office
BS antenna configurations and port mapping		For UMi-street canyon scenario: Config 1 for 7 GHz: $(M, N, P, M_g, N_g; M_P, N_P) = (24, 32, 2, 1, 1; 8, 32)$, $d_H = 0.5\lambda$, $d_V = 0.7\lambda$; (optional) $(M, N, P, M_g, N_g; M_P, N_P) = (64, 16, 2, 1, 1; 16, 16)$, $d_H = d_V = 0.5\lambda$ Config 2 for 15 GHz: $(M, N, P, M_g, N_g; M_P, N_P) = (64, 16, 2, 1, 1; 8, 16)$, $d_H = d_V = 0.5\lambda$ For Indoor-office scenario for 7 GHz: $(M, N, P, M_g, N_g; M_P, N_P) = (8, 24, 2, 1, 1; 8, 8)$, $d_H = d_V = 0.5\lambda$ (optional) $(M, N, P, M_g, N_g; M_P, N_P) = (64, 16, 2, 1, 1; 16, 16)$, $d_H = d_V = 0.5\lambda$ M_p and N_p are the number of vertical, horizontal TXRUs within a panel and polarization
BS Polarized antenna modeling		Model-2 in Clause 7.3.2
UT Location	Outdoor/indoor	UMi-street canyon: 100% outdoor Indoor-office: 100% indoor
	LOS/NLOS	100% LOS
	UT antenna height	UMi-street canyon: 1.5m Indoor-office: 1m
UT antenna configurations		Config A: $M_g = N_g = 1$, $M = 2$, $N = 1$, $P = 2$, $d_H = d_V = 0.5\lambda$ Config B: 4 antenna port with single/linear polarization for calibration based on handheld device antenna model using candidate antenna locations (1,7,3,5) as described in Clause 7.3
UT antenna pattern		Isotropic
UT Polarized antenna modelling		For UT Config A: Model-2 in Clause 7.3.2 For UT Config B: following the clause 7.3
UT orientation		Config A: $\Omega_{UT,\alpha}$ uniformly distributed on [0,360] degree, $\Omega_{UT,\beta}$ = 90 degree, $\Omega_{UT,\gamma}$= 0 degree Config B: $\Omega_{UT,\alpha}$ uniformly distributed on [0,360] degree, $\Omega_{UT,\beta}$ = 45 degree, $\Omega_{UT,\gamma}$= 0 degree
Applicability of Nearfield Modeling		Component of NF channel to be considered: - Phase of Direct path - Phase of Non-direct path, applied only at the BS side (optionally)

Calibration method	Drop multiple users in the multiple cells at the fixed horizontal distance Z from the BS, and collect the metric for ~~a~~ each distance Z For UMi-street Canyon: Z = 10, 30, 50, 100 m (optional) Z = 20, 40, 80 m 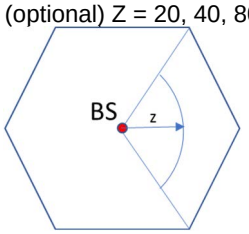 For Indoor: Z = 0, 2, 6, 10 m (optional) Z = 4, 8 m BS
Metric	CDF of the ratio between the 2nd, 3rd ,4th, ..., xth (smallest, see note 1) PRB singular value and the 1st PRB (largest) singular value (see note 2) of the serving cell at t=0 plotted in 10*log10 scale.
NOTE 1: The value of x is the minimum value of (number of BS antenna ports, number of UT antenna ports) NOTE 2: The PRB singular values of a PRB are the eigenvalues of the mean covariance matrix in the PRB.	

Table 7.8-6B: Simulation assumptions for calibration for BS side spatial non-stationarity

Parameter	Values
Scenarios	UMi-street Canyon
Carrier Frequency	7 GHz (optional) 15 GHz
Bandwidth	20 MHz
BS Antenna height	10m for UMi-Street Canyon
BS Tx power	44 dBm for UMi-Street Canyon
BS Antenna Configuration and port mapping	Config 1 for 7 GHz: $(M, N, P, M_g, N_g; M_P, N_P) = (24, 32, 2, 1, 1; 8, 32)$, $d_H = 0.5\lambda$, $d_V = 0.7\lambda$; (optional) $(M, N, P, M_g, N_g; M_P, N_P) = (64, 16, 2, 1, 1; 16, 16)$, $d_H = d_V = 0.5\lambda$ Config 2 for 15 GHz: $(M, N, P, M_g, N_g; M_P, N_P) = (64, 16, 2, 1, 1; 8, 16)$, $d_H = d_V = 0.5\lambda$ M_p and N_p are the number of vertical, horizontal TXRUs within a panel and polarization
BS Polarized antenna modeling	Model-2 in Clause 7.3.2
UT Antenna Configuration	Config 1: 4 antenna port with single/linear polarization for calibration based on handheld device antenna model using candidate antenna locations (1,7,3,5) as described in Clause 7.3
UT antenna pattern	Isotropic
UT Polarized antenna modelling	Following the Clause 7.3
UT orientation	$\Omega_{UT,\alpha}$ uniformly distributed on [0,360] degree, $\Omega_{UT,\beta}$ = 45 degree, $\Omega_{UT,\gamma}$= 0 degree
UT attachment	Based on RSRP (formula) from BS port 0
UT distribution	Following TR36.873 for UMi, (3D dropping)
Spatial non-stationarity modeling at the BS	Case 1: Spatial blocker-based approach (e.g. K = 1 per sector) Case 2: Stochastic-based approach
Metric	(1) CDF of coupling loss (serving cell). 2) CDF of the ratio between the 2nd, 3rd ,4th, ..., xth (smallest, see note 1) PRB singular value and the 1st PRB (largest) singular value (see note 2) of the serving cell at t=0 plotted in 10*log10 scale.
NOTE 1: The value of x is the minimum value of (number of BS antenna ports, number of UT antenna ports) NOTE 2: The PRB singular values of a PRB are the eigenvalues of the mean covariance matrix in the PRB.	

Table 7.8-6C: Simulation assumptions for calibration for UT side spatial non-stationarity

Parameter	Values
Scenarios	UMi-street Canyon
Carrier Frequency	7 GHz (optional) 15 GHz
Bandwidth	20 MHz
BS Antenna height	10m for UMi-Street Canyon
BS Tx power	44 dBm for UMi-Street Canyon
BS Antenna Configuration and port mapping	$(M, N, P, M_g, N_g; M_P, N_P) = (8, 16, 2, 1, 1; 8, 16)$, $dH = dV = 0.5\lambda$ M_p and N_p are the number of vertical, horizontal TXRUs within a panel and polarization
BS Polarized antenna modeling	Model-2 in Clause 7.3.2
UT Antenna Configuration	Config A for 7GHz: 4 antenna port with single polarization for calibration based on handheld device antenna model using candidate antenna locations (1, 7, 3, 5) as described in Clause 7.3 Config B for 15 GHz: 8 antenna port with single polarization based on handheld device antenna model using all candidate antenna locations (1,2,3,4,5,6,7,8) as described in Clause 7.3.
UT antenna pattern	Based on directional antenna for UT described in Clause 7.3 for each supported UT antenna configuration
UT Polarized antenna modelling	Following the Clause 7.3
UT orientation	Case with blockage: - For one-hand blockage, $\Omega_{UT,\alpha}$ = 0 – 360 deg, $\Omega_{UT,\beta}$ = 45 deg, $\Omega_{UT,\gamma}$ = 0 deg, - For dual-hand blockage, $\Omega_{UT,\alpha}$ = 0 – 360 deg, $\Omega_{UT,\beta}$ = 0 deg, $\Omega_{UT,\gamma}$ = 45 deg, - For hand and head blockage, $\Omega_{UT,\alpha}$ = 0 – 360 deg, $\Omega_{UT,\beta}$ = 90 deg, $\Omega_{UT,\gamma}$ = 0 deg, Case without blockage: - $\Omega_{UT,\alpha}$ = 0 – 360 deg, $\Omega_{UT,\beta}$ = 45 deg, $\Omega_{UT,\gamma}$ = 0 deg,
UT attachment	Based on RSRP (formula) from BS port 0
UT distribution	Following TR36.873 for UMi, (3D dropping)
Spatial non-stationarity modeling at the UT	Case 1: one hand grip Case 2: dual hand grip Case 3: head and one hand grip See note 3
Metric	CDF of coupling loss (serving cell) received per UT port CDF of the ratio between the 2nd, 3rd ,4th, ..., xth (smallest, see note 1) PRB singular value and the 1st PRB (largest) singular value (see note 2) of the serving cell at t=0 plotted in 10*log10 scale.
NOTE 1: The value of x is the minimum value of (number of BS antenna ports, number of UT antenna ports) NOTE 2: The PRB singular values of a PRB are the eigenvalues of the mean covariance matrix in the PRB. NOTE 3: For each UT, the selection of case is determined by the probability defined in Table 7.5.14-1. Probability of applying blockage for UT is 90%.	

7.8.4 Calibration of the indoor factory scenario

For the InF, the calibration parameters can be found in Table 7.8-7. The calibration results can be found in R1-1909704.

It should be noted absolute delay model had not been agreed by the deadline, so companies were not able to submit CDF of first path excess delay for serving cell.

Table 7.8-7: Simulation assumptions for large scale calibration for the indoor factory scenario

Parameter	Values
Scenario	InF-SL, InF-DL, InF-SH, InF-DH
Hall size	InF-SL: 120x60 m InF-DL: 300x150 m InF-SH: 300x150 m InF-DH: 120x60 m
Room height	10 m
Sectorization	None
BS antenna configurations	1 element (vertically polarized), Isotropic antenna gain pattern
UT antenna configurations	1 element (vertically polarized), Isotropic antenna gain pattern
Handover margin (for calibration)	0dB
BS deployment	18 BSs on a square lattice with spacing D, located D/2 from the walls. - for the small hall (L=120m x W=60m): D=20m - for the big hall (L=300m x W=150m): D=50m 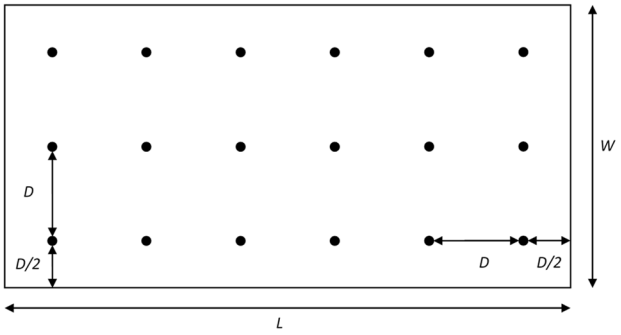 BS height = 1.5 m for InF-SL and InF-DL BS-height = 8 m for for InF-SH and InF-DH
UT distribution	uniform dropping for indoor with minimum 2D distance of 1 m UT height = 1.5 m
UT attachment	Based on pathloss
UT noise figure	9 dB
Carrier frequency	3.5 GHz, 28 GHz
Bandwidth	100 MHz
Clutter density: r	Low clutter density: 20% High clutter density: 60%
Clutter height: h_c	Low clutter density: 2 m High clutter density: 6 m
Clutter size: $d_{clutter}$	Low clutter density: 10 m High clutter density: 2 m
Metrics	1) Coupling loss – serving cell
	2) Geometry with and without noise
	3) CDF of delay spread and angle spread (ASD, ZSD, ASA, ZSA) according to the definition in Annex A.1
	4) CDF of first path excess delay for serving cell

7.9 Channel model(s) for ISAC

7.9.0 Introduction

The channel model for ISAC in Clause 7.9 is designed based on the channel model defined in the previous clauses within Clause 7 taking into account the known properties, e.g., location, Radar Cross-Section (RCS), polarization and etc. of one or more physical objects. A physical object is categorized as a sensing target (ST) or an environment object (EO). A ST is an object of interest for sensing. An EO is a non-target object with known location. Two types of EO are supported in the ISAC channel model. A first type of EO (type-1 EO) has similar characteristic as a ST and is modelled

in the same way as a ST. In the following descriptions in Clause 7.9, only the related details on ST are described, which are also applicable to type-1 EO. A second type of EO (type-2 EO, Clause 7.9.5.2) is of large size and is modelled differently from a ST.

The large scale and small scale parameters of the channel between any two of sensing transmitter (STX), ST and sensing receiver (SRX) in a sensing scenario are obtained from the Technical Reports for the same communication scenario unless updates on the parameter values are specially described. The ST is considered as a receiver or transmitter, respectively, in the determination of a reference Technical Report to generate the channel model for a STX-ST link or a ST-SRX link.

The common framework for the ISAC channel between a pair of STX and SRX is composed of a component for one or multiple target channel(s) and a component for a background channel (described in Clause 7.9.4.3 and 7.9.5.3). One or multiple STs can be modelled in the channel between one pair of STX and SRX. The target channel of ST k includes all multipath components impacted by ST k, $1 \leq k \leq K$, where K is the number of STs. The background channel includes other multipath components not belonging to any of the K target channel(s).

7.9.1 Scenarios

Sensing scenario X is defined as a scenario for sensing where STX/SRX are selected among the TRPs and UEs in the corresponding communication scenario X. X can be UMi/UMa/RMa/InH/InF/UMi-AV/UMa-AV/RMa-AV/Urban grid/Highway/High Speed Train (HST). Based on the interested type of ST, the sensing scenarios can be grouped to UAV sensing scenarios (ISAC-UAV), Automotive sensing scenarios (ISAC-Automotive), Human sensing scenarios (ISAC-Human), Automated Guided Vehicles (AGV) sensing scenarios (ISAC-AGV), and Objects creating hazards on roads/railways sensing scenarios (ISAC-Objects creating hazards on roads/railways).

The detailed sensing scenario description in this clause can be used for channel model calibration.

ISAC-UAV

In the ISAC-UAV sensing scenarios, the sensing targets are outdoor UAVs below or above the buildings in urban or rural areas. Monostatic or bistatic sensing can be performed using TRPs and/or UEs, including UEs on other UAVs. Details on ISAC-UAV scenarios are listed in Table 7.9.1-1.

Table 7.9.1-1: Evaluation parameters for UAV sensing scenarios

Parameters	Value

Applicable communication scenarios		UMi, UMa, RMa, SMa UMi-AV, UMa-AV, RMa-AV [36.777]
Sensing transmitters and receivers properties	STX/SRX Locations	STX/SRX locations are selected among the TRPs and UEs locations in the corresponding communication scenarios. see note 1
Sensing target	LOS/NLOS	LOS and NLOS
	Outdoor/indoor	Outdoor
	3D mobility	Horizontal velocity: uniform distribution between 0 and 180km/h, if horizontal velocity is not fixed to 0. Vertical velocity: 0km/h, optional {20, 40} km/h see note 2 and 3
	3D distribution	Horizontal plane: Option A: *N* targets uniformly distributed within one cell. Option B: *N* targets uniformly distributed per cell. Option C: *N* targets uniformly distributed within an area not necessarily determined by cell boundaries. *N* = {1, 2, 3, 4, 5} see note 4 Vertical plane: Option A: Uniform between 1.5m and 300m. Option B: Fixed height value chosen from {25, 50, 100, 200, 300} m assuming vertical velocity is equal to 0.
	Orientation	Random in horizontal domain
	Physical characteristics (e.g., size)	Size: Option 1: 1.6m x 1.5m x 0.7m Option 2: 0.3m x 0.4m x 0.2m
Minimum 3D distances between STX/SRX and sensing target		Min distances based on min TRP/UE distances defined in TR36.777.
Minimum 3D distance between sensing targets		Option 1: At least larger than the physical size of a target Option 2: 10 meters
NOTE 1: This may include aerial UEs for UMi-AV, UMa-AV, RMa-AV communication scenarios. In this case, other STX/SRX properties (e.g. mobility) are also taken from the corresponding communication scenario. NOTE 2: 3D mobility can be horizontal only or vertical only or a combination for each sensing target NOTE 3: time-varying velocity may be considered for future evaluations. NOTE 4: *N*=0 may be considered for the evaluation of false alarm		

ISAC-Automotive

In the ISAC-Automotive sensing scenarios, the sensing targets are passenger vehicles or trucks and buses traveling on roads and streets in urban and rural areas. Monostatic or bistatic sensing can be performed using TRPs and/or UEs, including UEs on other vehicles and roadside UEs (RSU-type UEs). Details on ISAC-Automotive scenarios are listed in Table 7.9.1-2.

Table 7.9.1-2: Evaluation parameters for Automotive sensing scenarios

Parameters		Values
Applicable communication scenarios		Highway, Urban Grid. UMi, UMa, RMa, SMa
Sensing transmitters and receivers properties		STX/SRX locations are selected among the TRPs and UEs (e.g., VRU, vehicle, RSU-type UEs) locations in the corresponding communication scenario. Additional option: ISD between TRPs of Urban Grid is 250m
Sensing target	LOS/NLOS	LOS and NLOS (including NLOSv)
	Outdoor/indoor	Outdoor
	Mobility (horizontal plane only)	Based on TR37.885 mobility for urban grid or highway scenario
	Distribution (horizontal)	Based on dropping in TR37.885 per urban grid or highway communication scenario
	Orientation	Lane direction in horizontal plane
	Physical characteristics (e.g., size)	Type 1/2 (passenger vehicle) Type 3 (truck/bus) Vehicle type distribution per TR 37.885
Minimum 3D distances between STX/SRX and sensing target		For Highway, Urban Grid - Min distances based on min TRP/UE distances defined in TR37.885 For UMi, UMa, RMa, SMa - Min distances based on min TRP/UE distances defined in TR38.901
Minimum 3D distance between sensing targets		Option 1: At least larger than the physical size of a sensing target Option 2: Fixed value, 10 m.
Environment Objects, e.g., types, characteristics, mobility, distribution, etc.		Type-2 EO for Urban Grid - up to 4 walls modelled as Type-2 EO, per building of size 413m x 230m x 20m.

ISAC-Human

In the ISAC-Human sensing scenarios, the sensing targets are children and adult persons in indoor (room, office, factory) and outdoor (urban, rural) locations. Monostatic or bistatic sensing can be performed using TRPs and/or UEs in the corresponding communication scenarios. Details on ISAC-Human scenarios are listed in Table 7.9.1-3.

Table 7.9.1-3: Evaluation parameters for Human (indoor and outdoor) sensing scenarios

Parameters		Indoor Values	Outdoor Values
Applicable communication scenarios		Indoor office, indoor factory Indoor room [TR38.808]	UMi, UMa, RMa, SMa
Sensing transmitters and receivers properties	STX/SRX Locations	STX/SRX locations are selected among the TRPs and UE locations in the corresponding communication scenario	STX/SRX locations are selected among the TRPs and UE locations in the corresponding communication scenario
	STX/SRX Mobility for UEs	Option 1: 0km/h Option 2: 3km/h Option 3: Uniform distribution between 0km/h and 3km/h	Option 1: 0km/h Option 2: 3km/h Option 3: Uniform distribution between 0km/h and 10km/h
Sensing target	LOS/NLOS	LOS and NLOS	LOS and NLOS
	Outdoor/indoor	Indoor	Outdoor
	3D mobility	Option 1: 0km/h Option 2: 3km/h Option 3: Uniform distribution between 0km/h and 3km/h (horizontal plane with random direction straight-line trajectory)	Option 1: 0km/h Option 2: 3km/h Option 3: Uniform distribution between 0km/h and 10km/h (horizontal plane with random direction straight-line trajectory)
	3D distribution	*N* targets uniformly distributed over the horizontal area of the convex hull of the TRP deployment see note 1	Option A: *N* targets uniformly distributed within one cell. Option B: *N* targets uniformly distributed per cell. Option C: *N* targets uniformly distributed within an area not necessarily determined by cell boundaries. see note 1
	Orientation	Random over the horizontal area	Random over the horizontal area
	Physical characteristics (e.g., size)	Size (Length x Width x Height): Child: 0.2m x 0.3m x 1m Adult Pedestrian: 0.5m x 0.5m x 1.75m	Size (Length x Width x Height): Child: 0.2m x 0.3m x 1m Adult Pedestrian: 0.5m x 0.5m x 1.75m
Minimum 3D distances between STX/SRX and sensing target		For TRP monostatic and TRP-TRP bistatic sensing modes, the minimum 2D distance between STX/SRX and the sensing target is 0 m For UE monostatic and UE-UE bistatic sensing modes, the minimum 2D distance between STX/SRX and the sensing target is 1 m (as specified in TR 38.858)	For TRP monostatic and TRP-TRP bistatic sensing modes, the minimum 2D distances between STX/SRX and the sensing target are 10 m for UMi scenarios and 35 m for UMa scenarios For UE monostatic and UE-UE bistatic sensing modes, the minimum 2D distance between STX/SRX and the sensing target is 1 m (as specified in TR 38.858)
Minimum 3D distance between sensing targets		Option 1: At least larger than the physical size of a sensing target Option 2: Fixed value, 1m	Option 1: At least larger than the physical size of a sensing target Option 2: Fixed value, 1m
NOTE 1: N=0 may be considered for the evaluation of false alarm			

ISAC-AGV

In the ISAC-AGV sensing scenarios, the sensing targets are automated guided vehicles (AGVs) inside a factory. Monostatic or bistatic sensing can be performed using TRPs and/or UEs in the corresponding communication scenario. Details on ISAC-AGV sensing scenarios are listed in Table 7.9.1-4.

Table 7.9.1-4: Evaluation parameters for AGV sensing scenarios

Parameters		Value
Applicable communication scenarios		InF (Table 7.8-7)
Sensing transmitters and receivers properties		STX/SRX location are selected among the TRPs and UEs location in the corresponding communication scenario STX/SRX Mobility for UEs Option 1: 0 km/h Option 2: 3km/h Option 3: Uniform distribution between 0km/h and 3km/h
Sensing target	LOS/NLOS	LOS and NLOS
	Outdoor/indoor	Indoor
	3D mobility	Horizontal velocity with random straight-line trajectory Option 1: Uniform distribution in the range of up to 30 km/h Option 2: Fixed velocities {3, 10} km/h
	3D distribution	Option A: Uniformly distributed in the convex hull of the horizontal BS deployment Option B: Uniformly distributed in horizontal plane
	Orientation	Horizontal plane only
	Physical characteristics (e.g., size)	Size Option 1: 0.5m x 1.0m x 0.5m Option 2: 1.5 m x 3.0m x 1.5 m
Minimum 3D distances between STX/SRX and sensing target		Min distances based on min TRP/UE distances defined in TR38.901
Minimum 3D distance between sensing targets		Option A: At least larger than the physical size of a target Option B: Fixed value, 5m

ISAC-Objects creating hazards on roads/railways

In the ISAC-Objects creating hazards on roads/railways sensing scenarios, the sensing targets are adult humans and children and animals in communication scenarios involving vehicles or high-speed trains. Monostatic or bistatic sensing can be performed using TRPs and/or UEs, including UEs on other vehicles and roadside UEs (RSU-type UEs). Details on ISAC- Objects creating hazards on roads/railways sensing scenarios are listed in Table 7.9.1-5.

Table 7.9.1-5: Evaluation parameters for objects creating hazards on roads/railways sensing scenarios

Parameters		Value
Applicable communication scenarios		Highway, Urban grid, HST (High Speed Train, TR 38.802) UMi, UMa, RMa, SMa
Sensing transmitters and receivers properties	STX/SRX Locations	STX/SRX locations are selected among the TRPs and UEs (e.g., VRU, vehicle, RSU-type UEs) locations in the corresponding communication scenarios. Additional option: ISD between TRPs of Urban Grid is 250 m
Sensing target	LOS/NLOS	LOS and NLOS
	Outdoor/indoor	Outdoor
	3D mobility	Horizontal velocity: up to 10 km/h for humans and animals
	3D distribution	Uniformly distributed in horizontal plane
	Orientation	Random distribution in horizontal plane
	Physical characteristics (e.g., size)	For human/pedestrians: Child: 0.2m x 0.3m x 1m Adult: 0.5m x 0.5m x 1.75m For animals: Size: 1.5m x 0.5m x 1 m
Minimum 3D distances between STX/SRX and sensing target		For Highway, Urban Grid, HST - Min. distance is based on min TRP/UE distances defined in TR37.885 and TR38.802 For UMi, UMa, RMa, SMa - Min distances based on min TRP/UE distances defined in TR38.901
Minimum 3D distance between sensing targets		Option 1: At least larger than the physical size of a sensing target Option 2: Fixed value, 10 m.
Environment objects, e.g., types, characteristics, mobility, distribution, etc.		Type-2 EO for Urban Grid - up to 4 walls modelled as Type-2 EO, per building of size 413m x 230m x 20m.

7.9.2 Physical object model

7.9.2.0 Introduction

A ST is modelled with one or multiple scattering points. Each scattering point of a ST (SPST) is used to model the total scattering effects of some adjacent scattering centres at the ST. The impact of a SPST to the channel includes at least two aspects, i.e., the RCS (Radar Cross Section, Clause 7.9.2.1) and the polarization matrix (Clause 7.9.2.2).

7.9.2.1 RCS of a sensing target

The RCS of a SPST is a scalar value defined in LCS of the ST and is dependent on both the incident angle and the scattered angle. The RCS values with same incident/scattered angles can be referred as monostatic RCS values.

The RCS related coefficient σ_{RCS} of a SPST for a pair of incident/scattered angles is composed of a first component σ_M which is included in the large-scale parameters (described in Step 15 in Clause 7.9.4.1), and a second component σ_D and third component σ_S which are both included in the small-scale parameters (described in Step 10 in Clause 7.9.4.1), i.e., $\sigma_{RCS} = \sigma_M \sigma_D \sigma_S$. σ_M is a deterministic value for the SPST. σ_D can be fixed to 1 or can be angular dependent. σ_S follows log-normal distribution. The mean $\mu_{\sigma_{S_dB}}$ and standard deviation $\sigma_{\sigma_{S_dB}}$ used to characterize $10lg(\sigma_S)$ satisfy a fixed relation.

$$\mu_{\sigma_{S_dB}} = \frac{-ln(10)}{20}\sigma^2_{\sigma_{S_dB}} \quad (7.9.2\text{-}1)$$

A first RCS model, called RCS model 1, is to characterize a ST as single SPST with component σ_D of the monostatic RCS values fixed to 1. σ_M is the mean of linear monostatic RCS values at the SPST. For UAV of small size and human with RCS model 1, the values/pattern $10lg(\sigma_M \sigma_D)$, denoted as $\sigma_{MD_dB}(\theta_{\mathrm{i}}, \phi_{\mathrm{i}}, \theta_{\mathrm{s}}, \phi_{\mathrm{s}})$, of the RCS for a SPST is deterministic based on the incident angle $(\theta_{\mathrm{i}}, \phi_{\mathrm{i}},)$ and the scattered angle $(\theta_{\mathrm{s}}, \phi_{\mathrm{s}})$.

$$\sigma_{\mathrm{MD_dB}}(\theta_{\mathrm{i}}, \phi_{\mathrm{i}}, \theta_{\mathrm{s}}, \phi_{\mathrm{s}}) = max\left(10lg(\sigma_M) - 3sin\left(\frac{\beta}{2}\right), \sigma_{\mathrm{FS}}(\theta_i, \phi_i, \theta_s, \phi_s)\right) \quad (7.9.2\text{-}2)$$

where,

- $\beta \in [0°, 180°]$. β is the bistatic angle between the incident ray and scattering ray within the plane defined by incident angle $(\theta_{\mathrm{i}}, \phi_{\mathrm{i}},)$ and scattering angle $(\theta_{\mathrm{s}}, \phi_{\mathrm{s}})$.

- $\sigma_{\mathrm{FS}}(\theta_{\mathrm{i}}, \phi_{\mathrm{i}}, \theta_{\mathrm{s}}, \phi_{\mathrm{s}})$ is for the effect of forward scattering and is set to $-\infty$.

The logarithmic values of σ_M, σ_S of the RCS values for the different STs are provided in Table 7.9.2.1-1.

Table 7.9.2.1-1: Parameters on RCS for the STs with angular independent monostatic RCS values

Sensing target	$10lg(\sigma_M)$ (dBsm)	$\sigma_{\sigma_{S_dB}}$ (dB)
UAV with small size	-12.81	3.74
Human with RCS model 1	-1.37	3.94

A second RCS model, called RCS model 2, adopts an angular dependent component σ_D of the monostatic RCS values for each SPST, and is to split a ST into single or multiple SPSTs. For UAV with large size and human, single SPST is modelled. While for vehicle and AGV, both models with single and multiple SPSTs are provided. For vehicle and AGV modelled with multiple scattering points, the recommended five scattering points are located at the front, left, back, right and roof side of the vehicle respectively. The orientation of a ST in LCS is provided as follows.

- The face of a human, the front of a vehicle, a UAV with large size or an AGV is facing the direction with azimuth angle $\phi = 0^0$ and zenith angle $\theta = 90^0$. The front of the AGV is the short edge of AGV in horizontal direction.

- The top of the ST is facing the direction with zenith angle $\theta = 0^0$.

For UAV of large size with single SPST, human with RCS model 2 with single SPST, vehicle with single/multiple SPSTs, and AGV with single/multiple SPSTs, the values/pattern $10lg(\sigma_M \sigma_D)$, denoted as $\sigma_{MD_dB}(\theta_{\mathrm{i}}, \phi_{\mathrm{i}}, \theta_{\mathrm{s}}, \phi_{\mathrm{s}})$, of the RCS for a SPST is deterministic based on the incident angle $(\theta_{\mathrm{i}}, \phi_{\mathrm{i}},)$ and the scattered angle $(\theta_{\mathrm{s}}, \phi_{\mathrm{s}})$.

$$\sigma_{\mathrm{MD_dB}}(\theta_{\mathrm{i}}, \phi_{\mathrm{i}}, \theta_{\mathrm{s}}, \phi_{\mathrm{s}}) = max\left(G_{max} - min\{-(\sigma^{V}{}_{\mathrm{dB}}(\theta) + \sigma^{H}{}_{\mathrm{dB}}(\phi)), \sigma_{max}\} - k_1 \sin\left(\frac{k_2\beta}{2}\right) + 5log_{10}\left(cos\left(\frac{\beta}{2}\right)\right), G_{max} - \sigma_{max}, \sigma_{\mathrm{FS}}(\theta_{\mathrm{i}}, \phi_{\mathrm{i}}, \theta_{\mathrm{s}}, \phi_{\mathrm{s}})\right) \quad (7.9.2\text{-}3)$$

With $\sigma^{V}{}_{dB}(\theta), \sigma^{H}{}_{dB}(\phi)$ defined by,

$$\sigma^{V}{}_{\mathrm{dB}}(\theta) = -min\left\{12\left(\frac{\theta-\theta_{center}}{\theta_{3dB}}\right)^2, \sigma_{max}\right\}$$

$$\sigma^{H}{}_{\mathrm{dB}}(\phi) = -min\left\{12\left(\frac{\phi-\phi_{center}}{\phi_{3dB}}\right)^2, \sigma_{max}\right\}$$

where,

- (θ, ϕ) are zenith angle and azimuth angle of the bisector between the incident ray with zenith angle and azimuth angle $(\theta_{\mathrm{i}}, \phi_{\mathrm{i}})$, and scattered ray with zenith angle and azimuth angle $(\theta_{\mathrm{s}}, \phi_{\mathrm{s}})$.
- $\beta \in [0°, 180°]$. β is the bistatic angle between the incident ray and scattering ray within the plane defined by incident angle $(\theta_{\mathrm{i}}, \phi_{\mathrm{i}},)$ and scattering angle $(\theta_{\mathrm{s}}, \phi_{\mathrm{s}})$.
  - $k_1 = 6.05, k_2 = 1.33$ for UAV with large size.
  - $k_1 = 0.5714, k_2 = 0.1$ for human with RCS model 2.
  - $k_1 = 6, k_2 = 1.65$ for vehicle with single/multiple SPSTs.
  - $k_1 = 12, k_2 = 1.45$ for AGV with single/multiple SPSTs.
- $\sigma_{\mathrm{FS}}(\theta_{\mathrm{i}}, \phi_{\mathrm{i}}, \theta_{\mathrm{s}}, \phi_{\mathrm{s}})$ is for the effect of forward scattering and is set to $-\infty$.

For a ST with single scattering point, $N_{sp} \geq 1$ sets of parameters $\varphi_{center}, \varphi_{3\mathrm{dB}}, \theta_{center}, \theta_{3\mathrm{dB}}, G_{max}, \sigma_{\max}$, *Range of* θ and *Range of* ϕ are defined. The bisector angle (θ, ϕ) is used to index one set from the N_{sp} sets of parameters, and determine $\sigma_{MD_dB}(\theta_{\mathrm{i}}, \phi_{\mathrm{i}}, \theta_{\mathrm{s}}, \phi_{\mathrm{s}})$ of the ST consequently. If the ST is split into N_{sp} scattering points, with each scattering point characterized by one of N_{sp} sets of parameters, $\sigma_{MD_dB}(\theta_{\mathrm{i}}, \phi_{\mathrm{i}}, \theta_{\mathrm{s}}, \phi_{\mathrm{s}})$ are respectively determined for each scattering point.

The N_{sp} sets of parameters to define $\sigma_M \sigma_D$ and the parameters σ_M, σ_S of the RCS for the different STs are provided in Table 7.9.2.1-2/3/4/5/6/7.

Table 7.9.2.1-2: Parameters on RCS for UAV with large size

	$10lg(\sigma_M\sigma_D)$ (dBsm)								$10lg(\sigma_M)$ (dBsm)	$\sigma_{\sigma_S_dB}$ (dB)
	ϕ_{center} in [°]	$\phi_{3\mathrm{dB}}$ in [°]	θ_{center} in [°]	$\theta_{3\mathrm{dB}}$ in [°]	G_{max}	$\sigma_{\max}$	Range of θ in [°]	Range of ϕ in [°]		
Left	90	7.13	90	8.68	7.43	14.30	[45,135)	[45,135)	-5.85	2.50
Back	180	10.09	90	11.43	3.99	10.86	[45,135)	[135,225)		
Right	270	7.13	90	8.68	7.43	14.30	[45,135)	[225,315)		
Front	0	14.19	90	16.53	1.02	7.89	[45,135)	[-45,45)		
Bottom	-	-	180	4.93	13.55	20.42	[135,180]	[0,360)		
Roof	-	-	0	4.93	13.55	20.42	[0,45)	[0,360)		
NOTE: When θ is in the range [0,45] or [135,180], $\sigma^{H}{}_{\mathrm{dB}}(\phi) = 0$.										

Table 7.9.2.1-3: Parameters on RCS for human with RCS model 2

	$10lg(\sigma_M\sigma_D)$ (dBsm)								$10lg(\sigma_M)$ (dBsm)	$\sigma_{\sigma_S_dB}$ (dB)
	ϕ_{center} in [°]	$\phi_{3\mathrm{dB}}$ in [°]	θ_{center} in [°]	$\theta_{3\mathrm{dB}}$ in [°]	G_{max}	$\sigma_{\max}$	Range of θ in [°]	Range of ϕ in [°]		
Front	0	216.65	90	55.7	2.14	7.7	[0,180]	[-90, 90)	-1.37	3.94
Back	180	216.65	90	55.7	2.14	7.7	[0,180]	[90,270)		

Table 7.9.2.1-4: Parameters on RCS for vehicle with single scattering point

	$10lg(\sigma_M\sigma_D)$ (dBsm)								$10lg(\sigma_M)$ (dBsm)	$\sigma_{\sigma_S_dB}$ (dB)
	ϕ_{center} in [°]	ϕ_{3dB} in [°]	θ_{center} in [°]	θ_{3dB} in [°]	G_{max}	σ_{max}	Range of θ in [°]	Range of ϕ in [°]		
Left	90	26.90	79.70	44.42	20.75	13.68	[30,180]	[45,135)	11.25	3.41
Back	180	36.32	79.65	36.73	14.56	7.50	[30,180]	[135,225)		
Right	270	26.90	79.70	44.42	20.75	13.68	[30,180]	[225,315)		
Front	0	40.54	71.75	29.13	15.52	8.45	[30,180]	[-45, 45)		
Roof	-	-	0.00	18.13	21.26	14.19	[0,30)	[0,360)		
NOTE: When θ is in the range [0, 30), $\sigma^H{}_{dB}(\phi) = 0$.										

Table 7.9.2.1-5: Parameters on RCS for vehicle with multiple scattering points

	$10lg(\sigma_M\sigma_D)$ (dBsm)								$10lg(\sigma_M)$ (dBsm)	$\sigma_{\sigma_S_dB}$ (dB)
	ϕ_{center} in [°]	ϕ_{3dB} in [°]	θ_{center} in [°]	θ_{3dB} in [°]	G_{max}	σ_{max}	Range of θ in [°]	Range of ϕ in [°]		
Left	90	26.90	79.70	44.42	20.60	20.52	[0,180]	[0,360)	11.25	3.41
Back	180	36.32	79.65	36.73	13.90	13.82	[0,180]	[0,360)		
Right	270	26.90	79.70	44.42	20.60	20.52	[0,180]	[0,360)		
Front	0	40.54	71.75	29.13	14.99	14.91	[0,180]	[0,360)		
Roof	-	-	0.00	18.13	21.12	21.05	[0,180]	[0,360)		
NOTE: For the scattering point associated with roof of the vehicle, $\sigma^H{}_{dB}(\phi) = 0$.										

Table 7.9.2.1-6: Parameters on RCS for AGV with single scattering point

	$10lg(\sigma_M\sigma_D)$ (dBsm)								$10lg(\sigma_M)$ (dBsm)	$\sigma_{\sigma_S_dB}$ (dB)
	ϕ_{center} in [°]	ϕ_{3dB} in [°]	θ_{center} in [°]	θ_{3dB} in [°]	G_{max}	σ_{max}	Range of θ in [°]	Range of ϕ in [°]		
Front	0	13.68	90	13.68	13.02	23.29	[30,180]	[-45,45)	-4.25	2.51
Left	90	15.53	75	20.03	7.33	17.60	[30,180]	[45,135)		
Back	180	12.49	90	11.89	11.01	21.28	[30,180]	[135,225)		
Right	270	15.53	75	20.03	7.33	17.60	[30,180]	[225,315)		
Roof	-	-	0	11.44	11.79	22.06	[0,30)	[0,360)		
NOTE: When θ is in the range [0,30), $\sigma^H{}_{dB}(\phi) = 0$.										

Table 7.9.2.1-7: Parameters on RCS for AGV with multiple scattering points

	$10lg(\sigma_M\sigma_D)$ (dBsm)								$10lg(\sigma_M)$ (dBsm)	$\sigma_{\sigma_S_dB}$ (dB)
	ϕ_{center} in [°]	ϕ_{3dB} in [°]	θ_{center} in [°]	θ_{3dB} in [°]	G_{max}	σ_{max}	Range of θ in [°]	Range of ϕ in [°]		
Front	0	13.68	90	13.68	13.00	30.26	[0,180]	[0,360)	-4.25	2.51
Left	90	15.53	75	20.03	7.27	24.53	[0,180]	[0,360)		
Back	180	12.49	90	11.89	10.98	28.24	[0,180]	[0,360)		
Right	270	15.53	75	20.03	7.27	24.53	[0,180]	[0,360)		
Roof	-	-	0	11.44	11.77	29.03	[0,180]	[0,360)		
NOTE: For the scattering point associated with roof of the AGV, $\sigma^H{}_{dB}(\phi) = 0$.										

7.9.2.2 Cross-polarization matrix of a sensing target

The cross-polarization matrix $CPM_{sp,i}$ of a SPST for a pair i of incident/scattered angles is defined in LCS of the ST and is generally modelled by amplitude factors $\alpha_{i,1}, \alpha_{i,2}, \beta_{i,1}, \beta_{i,2}$, and initial random phases $\{\Phi_{sp,i}^{\theta\theta}, \Phi_{sp,i}^{\theta\phi}, \Phi_{sp,i}^{\phi\theta}, \Phi_{sp,i}^{\phi\phi}\}$, i.e.,

$$CPM_{sp,i} = \begin{bmatrix} \alpha_{i,1} exp\left(j\Phi_{sp,i}^{\theta\theta}\right) & \beta_{i,1} exp\left(j\Phi_{sp,i}^{\theta\phi}\right) \\ \beta_{i,2} exp\left(j\Phi_{sp,i}^{\phi\theta}\right) & \alpha_{i,2} exp\left(j\Phi_{sp,i}^{\phi\phi}\right) \end{bmatrix} \quad (7.9.2\text{-}4)$$

For UAV, human, vehicle and AGV, $\alpha_{i,1} = \alpha_{i,2} = 1$, $\beta_{i,1} = \beta_{i,2} = \sqrt{\kappa_{sp,i}{}^{-1}}$, i.e.,

$$CPM_{sp,i} = \begin{bmatrix} exp\left(j\Phi_{sp,i}^{\theta\theta}\right) & \sqrt{\kappa_{sp,i}{}^{-1}} exp\left(j\Phi_{sp,i}^{\theta\phi}\right) \\ \sqrt{\kappa_{sp,i}{}^{-1}} exp\left(j\Phi_{sp,i}^{\phi\theta}\right) & exp\left(j\Phi_{sp,i}^{\phi\phi}\right) \end{bmatrix} \quad (7.9.2\text{-}5)$$

where,

- $\kappa_{sp,i}$ is the XPR of the pair i of incident/scattered angles. $\kappa_{sp,i}$ is randomly generated by log-normal distribution per target type defined in Table 7.9.2.2-1.
- $\left\{\Phi_{sp,i}^{\theta\theta}, \Phi_{sp,i}^{\theta\phi}, \Phi_{sp,i}^{\phi\theta}, \Phi_{sp,i}^{\phi\phi}\right\}$ is uniformly distributed within $(-\pi, \pi)$.

Table 7.9.2.2-1: Parameters on XPR (dB) for the targets

Target	μ_{XPR}	σ_{XPR}
UAV	13.75	7.07
Human	19.81	4.25
Vehicle	21.12	6.88
AGV	9.60	6.85

7.9.3 Reference channel models and required updates

A transmitter or receiver in the sensing operation can be TRP, terrestrial UE, vehicle UE, aerial UE, AGV UE or RSU-type UE. The reference TR(s) to generate the channel for each combination of transmitter and receiver for each sensing scenario are provided in Table 7.9.3-1, where the terrestrial UE, AGV are referred as terrestrial UE.

Table 7.9.3-1: Reference TRs to generate channel for ISAC

Case	Tx/Rx	Rx/Tx	Reference TR to define the channel model
1	TRP	TRP	For sensing scenario UMi/UMi-AV, UMa/UMa-AV, RMa/RMa-AV, InH, InF - TRP-TRP link of scenario UMi, UMa, InH, and InF following the option based on TR 38.901 defined in Clause A.3 of TR 38.858 - For InF, h_{UT} is changed to the same height as the BS - TRP-UE link of scenario RMa defined in Clause 7 of TR 38.901 by setting h_{UT}=35m (see note 1) For sensing scenario Highway - TRP-UE link of scenario RMa in Clause 7 of TR 38.901 by setting h_{UT}=35m for FR1(see note 1) - TRP-TRP link of scenario UMa following the option based on TR 38.901 defined in Clause A.3 of TR 38.858 for FR2 For sensing scenario Urban grid - TRP-TRP link of scenario UMa following the option based on TR 38.901 defined in Clause A.3 of TR 38.858 For sensing scenario HST - TRP-UE link of scenario RMa in Clause 7 of TR 38.901 by setting h_{UT}=35m for FR1 (see note 1) - TRP-TRP link of scenario UMa following the option based on TR 38.901 defined in Clause A.3 of TR 38.858 for FR2
2	TRP	terrestrial UE	For sensing scenario UMi/UMi-AV, UMa/UMa-AV, RMa/RMa-AV, InH, InF - TRP-UE link of scenario UMi, UMa, RMa, InH, and InF in Clause 7 of TR 38.901 For sensing scenario Highway and Urban grid - P2B link of scenario Highway and Urban grid in Clause 6 of TR 37.885 For sensing scenario HST - TRP-UE link of scenario RMa in Clause 7 of TR 38.901 for FR1 and TRP-UE link of scenario UMa in Clause 7 of TR 38.901 for FR2
3	TRP	vehicle UE	For sensing scenario Highway and Urban grid - V2B link of scenario Highway and Urban grid in Clause 6 of TR 37.885 For sensing scenario UMi, UMa, and RMa - TRP-UE link of scenario UMi, UMa, and RMa in Clause 7 of TR 38.901
4	TRP	aerial UE	For sensing scenario UMa-AV, UMi-AV, and RMa-AV - TRP-aerial UE link of scenario UMa-AV, UMi-AV, and RMa-AV in Clause Annex A and B of TR 36.777 for FR1 - Reuse the channel model of scenario UMa-AV, UMi-AV, and RMa-AV of FR1 for FR2
5	terrestrial UE	terrestrial UE	For sensing scenario UMi/UMi-AV, UMa/UMa-AV, RMa/RMa-AV, InH, InF - UE-UE link of scenario UMi, UMa, InH, and InF following the option based on TR 38.901 defined in Clause A.3 of TR 38.858 - TRP-UE link of scenario RMa defined in Clause 7 of TR 38.901 by setting h_{BS}=1.5m (see note 2) For sensing scenario Highway and Urban grid - P2P link in Clause 6 of TR 37.885 For sensing scenario HST - TRP-UE link of scenario RMa in Clause 7 of TR 38.901 by setting h_{BS}=1.5m for FR1 - UE-UE link of scenario UMa following the option based on TR 38.901 defined in Clause A.3 of TR 38.858 for FR2
6	terrestrial UE	vehicle UE	For sensing scenario UMi, UMa, RMa - UE-UE link of scenario UMi, UMa following the option based on TR 38.901 defined in Clause A.3 of TR 38.858 - TRP-UE link of scenario RMa defined in Clause 7 of TR 38.901 by setting h_{BS}=1.5m For sensing scenario Highway and Urban grid - V2P link in Clause 6 of TR 37.885
7	terrestrial UE	aerial UE	For sensing scenario UMi-AV, UMa-AV, and RMa-AV - TRP-aerial UE link of UMi-AV in Annex A and B of TR 36.777 by setting h_{BS}=1.5m for FR1 - Reuse the channel model of scenario UMa-AV, UMi-AV, and RMa-AV of FR1 for FR2 - The corresponding parameter values in FR2 are used
8	vehicle UE	vehicle UE	For sensing scenario Highway and Urban grid - V2V link of scenario Highway and Urban grid in Clause 6 of TR 37.885 For sensing scenario UMi, UMa, and RMa - UE-UE link of scenario UMi, UMa following the option based on TR 38.901 defined in Clause A.3 of TR 38.858 - TRP-UE link of scenario RMa defined in Clause 7 of TR 38.901 by setting h_{BS}=1.5m

9	aerial UE	aerial UE	For sensing scenario UMi-AV, UMa-AV, RMa-AV - TRP-aerial UE link of UMi-AV in Annex A and B of TR 36.777 by setting height of TRP equal to the height of the first aerial UE for FR1 (see note 4) - Reuse the channel model of scenario UMa-AV, UMi-AV, and RMa-AV of FR1 for FR2 - The corresponding parameter values in FR2 are used
10	TRP	RSU-type UE	Highway and Urban grid - B2R link in Clause 6 of TR 37.885
11	RSU-type UE	terrestrial UE	Highway and Urban grid - V2V link in Clause 6 of TR 37.885, with antenna height at RSU is 5m
12	RSU-type UE	RSU-type UE	Highway and Urban grid - V2V link in Clause 6 of TR 37.885, with antenna height at RSU is 5m
13	RSU-type UE	vehicle UE	Highway and Urban grid - V2V link in Clause 6 of TR 37.885, with antenna height at RSU is 5m
NOTE 1: ASA and ZSA statistics updated to be the same as ASD and ZSD; ZoD offset = 0 NOTE 2: ASD and ZSD statistics updated to be the same as ASA and ZSA NOTE 3: Indoor office scenario can be categorized into 5 sub-indoor scenarios defined in TR38.808. NOTE 4: First aerial UE height is h_{UT1}, second aerial UE height is h_{UT2}, where $abs(h_{UT1} - h_{BS}) \leq abs(h_{UT2} - h_{BS})$.			

The large scale and small scale parameters of the STX-ST link and the ST-SRX link for a sensing scenario are determined according to Table 7.9.3-1 assuming the same sensing scenario. The targets of UAV and vehicle are respectively considered as an aerial UE and vehicle UE. Other targets are considered as terrestrial UE. The proper case for each combination of STX/STX and ST are provided in Table 7.9.3-2.

Table 7.9.3-2: Channel model for STX-ST and ST-SRX link

STX/SRX	Target	Cases in Table 7.9.3-1 assuming the same sensing scenario
TRP	UAV	Case 4: TRP-Aerial UE link
	Human	Case 2: TRP- terrestrial UE link
	Vehicle	Case 3: TRP-Vehicle UE link
	AGV	Case 2: TRP- terrestrial UE link
	Object (Hazard)	Case 2: TRP- terrestrial UE link
Terrestrial UE	UAV	Case 7: terrestrial UE - Aerial UE link
	Human	Case 5: terrestrial UE- terrestrial UE link
	Vehicle	Case 6: terrestrial UE - Vehicle UE link
	AGV	Case 5: terrestrial UE- terrestrial UE link
	Object (Hazard)	Case 5: terrestrial UE- terrestrial UE link
Vehicle UE	Human	Case 6: terrestrial UE - Vehicle UE link
	Vehicle	Case 8: Vehicle UE - Vehicle UE link
	Object (Hazard)	Case 6: terrestrial UE - Vehicle UE link
Aerial UE	UAV	Case 9: Aerial UE - Aerial UE link
AGV UE	AGV	Case 5: terrestrial UE - terrestrial UE link
RSU-type UE	Human	Case 11: RSU-type UE - terrestrial UE link
	Vehicle	Case 13: RSU-type UE - vehicle UE link

The large scale and small scale parameters of the STX-SRX link, i.e., background channel for a sensing scenario are determined according to Table 7.9.3-1 assuming the same sensing scenario. The proper case for each combination of STX and SRX are provided in Table 7.9.3-3. For TRP monostatic sensing mode, a reference point (RP) is considered as a terrestrial UE. For UT monostatic sensing mode, a RP is considered as a TRP and an aerial UE is considered as a terrestrial UE.

Table 7.9.3-3: Channel model for background channel

STX/SRX	SRX/STX	Cases in Table 7.9.3-1 assuming the same sensing scenario
TRP	TRP	Case 1: TRP-TRP link
	Terrestrial UE	Case 2: TRP- terrestrial UE link
	Vehicle UE	Case 3: TRP-Vehicle UE link
	Aerial UE	Case 4: TRP-Aerial UE link
	AGV UE	Case 2: TRP- terrestrial UE link
	RSU-type UE	Case 10: TRP - RSU-type UE link
Terrestrial UE	Terrestrial UE	Case 5: terrestrial UE- terrestrial UE link
	Vehicle UE	Case 6: terrestrial UE - Vehicle UE link
	Aerial UE	Case 7: terrestrial UE - Aerial UE link
	AGV UE	Case 5: terrestrial UE - terrestrial UE link
	RSU-type UE	Case 11: RSU-type UE - terrestrial UE link
Vehicle UE	Vehicle UE	Case 8: Vehicle UE - Vehicle UE link
	RSU-type UE	Case 13: RSU-type UE - vehicle UE link
Aerial UE	Aerial UE	Case 9: Aerial UE - Aerial UE link
AGV UE	AGV UE	Case 5: terrestrial UE - terrestrial UE link
RSU-type UE	RSU-type UE	Case 12: RSU-type UE – RSU-type UE link

The following updates compared to the reference TRs are identified to generate ISAC channel.

- For human as a sensing target with a single scattering point, the height of the scattering point is 1.5 m.
- For sensing scenario RMa, UMi-AV, UMa-AV and RMa-AV, the height of a scattering point of a target is used to calculate the LOS probability and pathloss, regardless of the lower bound of h_{UT} in the reference TRs that are used to generate ISAC channel.
- For sensing scenario UMi, UMa, the height of a scattering point of a target is used to calculate the LOS probability and pathloss, regardless of the lower bound of h_{UT} in the reference TRs that are used to generate ISAC channel, except that h_{UT}=1.5 m is assumed for breakpoint distance (d_{BP}) calculation.
- For sensing scenario Urban grid, the absolute delay model of scenarios UMa in Table 7.6.9-1 are reused
- For sensing scenario highway and HST, the absolute delay model of scenarios RMa and UMa are reused for FR1 and FR2 respectively
- For sensing scenarios UMi-AV, UMa-AV and RMa-AV,
  - For the TRP-TRP link and TRP-terrestrial UE link, the absolute delay model of scenarios UMi, UMa and RMa are respectively reused.
  - For the terrestrial UE- terrestrial UE link, the terrestrial UE - aerial UE link and the aerial UE - aerial UE link, the absolute delay model of scenario UMi is reused.
  - For the TRP- aerial UE link, the absolute delay model of scenarios UMi, UMa and RMa are respectively reused.
- On Case 7 in Table 7.9.3-1, the LOS probability between an aerial UE and a terrestrial UE is generated by Table 7.9.3-4. h_{UT} is the height of the aerial UE.
- On Case 9 in Table 7.9.3-1, the LOS probability between two aerial UEs is generated by Table 7.9.3-5. h_{UT1}, h_{UT2} are the height of the two aerial UEs.

Table 7.9.3-4: LOS condition determination for Case 7

Reference scenario to determined LOS probability	Applicability range in terms of aerial UE height
UMi in Table 7.4.2-1 in TR 38.901 for sensing scenario UMi-AV/UMa-AV/RMa-AV	Sensing scenario UMi-AV, UMa-AV: $1.5m \leq h_{UT} \leq 22.5m$ Sensing scenario RMa-AV: $1.5m \leq h_{UT} \leq 10m$
UMi-AV in Table B-1 in TR 36.777 for sensing scenario UMi-AV/UMa-AV RMa-AV in Table B-1 in TR 36.777 for sensing scenario RMa-AV	Sensing scenario UMi-AV, UMa-AV: $22.5m < h_{UT} \leq 300m$ Sensing scenario RMa-AV: $10m < h_{UT} \leq 300m$

Table 7.9.3-5: LOS condition determination for Case 9

Reference scenario to determined LOS probability	Applicability range in terms of aerial UE height
UMi in Table 7.4.2-1 in TR 38.901 for sensing scenario UMi-AV/UMa-AV/RMa-AV	Sensing scenario UMi-AV, UMa-AV: $1.5m \leq h_{UT1}, h_{UT2} \leq 22.5m$ Sensing scenario RMa-AV: $1.5m \leq h_{UT1}, h_{UT2} \leq 10m$
UMi-AV in Table B-1 in TR 36.777 for sensing scenario UMi-AV/UMa-AV RMa-AV in Table B-1 in TR 36.777 for sensing scenario RMa-AV	Sensing scenario UMi-AV, UMa-AV: $22.5m < max(h_{UT1}, h_{UT2}) \leq 300m$, $1.5m \leq min(h_{UT1}, h_{UT2}) \leq 22.5m$ Sensing scenario RMa-AV: $10m < max(h_{UT1}, h_{UT2}) \leq 300m$, $1.5m \leq min(h_{UT1}, h_{UT2}) \leq 10m$
UMa-AV in Table B-1 in TR 36.777 for aerial UE height in range (22.5m, 100m] for sensing scenario UMi-AV/UMa-AV RMa-AV in Table B-1 in TR 36.777 for aerial UE height in range (10m, 40m] for sensing scenario RMa-AV	Sensing scenario UMi-AV, UMa-AV: $22.5m < h_{UT1}, h_{UT2} \leq 100m$ Sensing scenario RMa-AV: $10m < h_{UT1}, h_{UT2} \leq 40m$
LOS probability is 100%	Sensing scenario UMi-AV, UMa-AV: $100m < max(h_{UT1}, h_{UT2}) \leq 300m$, $22.5m < min(h_{UT1}, h_{UT2}) \leq 100m$ Sensing scenario RMa-AV: $40m < max(h_{UT1}, h_{UT2}) \leq 300m$, $10m < min(h_{UT1}, h_{UT2}) \leq 40m$

7.9.4 Fast fading model

7.9.4.0 Introduction

The ISAC channel between a pair of STX and SRX is composed of the target channel(s) and the background channel. A multipath component in the target channel may include stochastic generated clusters in either of or both the STX-ST link and ST-SRX link. If blockage/forward scattering between sensing targets is not considered, a propagation path from STX to SRX interacting with more than one sensing target is not modelled.

A stepwise procedure illustrated in Figure 7.9.4-1 is used to generate the channel model for ISAC referring to the procedure in Clause 7.5 with parameters derived by Table 7.9.3-2 and 7.9.3-3. Step 1 is commonly executed, followed by the respective steps for target channel (7.9.4.1) and background channel (7.9.4.2). Finally, the target channel and background channel are combined to form the final channel model for ISAC (7.9.4.3).

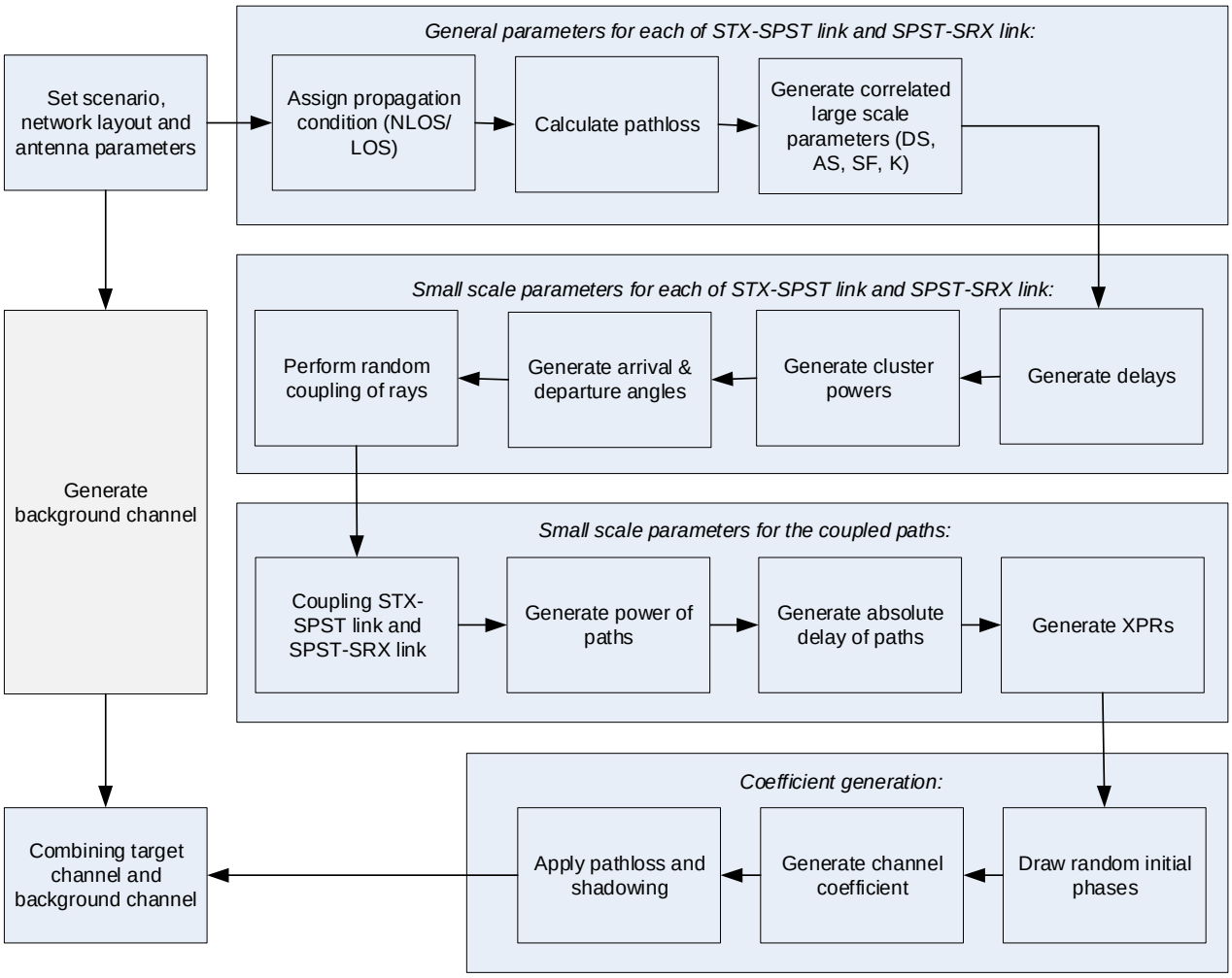

Figure 7.9.4-1 Channel coefficient generation procedure

Step 1: Set environment, network layout, and antenna array parameters

a) Choose one of the sensing scenarios (ISAC-UAV, ISAC-Automotive, ISAC-Human, ISAC-AGV, ISAC-Objects creating hazards on roads/railways) and related communication scenarios (e.g. UMa, UMi-Street Canyon, RMa, InH-Office, Urban grid, Highway, or InF). Choose a global coordinate system and define zenith angle θ, azimuth angle ϕ, and spherical basis vectors $\hat{\theta}$, $\hat{\phi}$ as shown in Figure 7.5-2.

b) Give number of STX, ST and SRX. Give the number of the SPST(s) of each ST.

c) Give 3D locations of STX and SRX, give 3D locations of SPST(s) of each ST, and determine LOS AOD ($\phi_{LOS,AOD}$), LOS ZOD ($\theta_{LOS,ZOD}$), LOS AOA ($\phi_{LOS,AOA}$), and LOS ZOA ($\theta_{LOS,ZOA}$) of each pair of STX and SPST, and each pair of SPST and SRX in the global coordinate system

d) Give STX and SRX antenna field patterns F_{rx} and F_{tx} in the global coordinate system and array geometries.

e) Give STX and SRX array orientations with respect to the global coordinate system. STX array orientation is defined by three angles $\Omega_{STX,\alpha}$ (STX bearing angle), $\Omega_{STX,\beta}$ (STX downtilt angle) and $\Omega_{STX,\gamma}$ (STX slant angle). SRX array orientation is defined by three angles $\Omega_{SRX,\alpha}$ (SRX bearing angle), $\Omega_{SRX,\beta}$ (SRX downtilt angle) and $\Omega_{SRX,\gamma}$ (SRX slant angle). Give the orientation of ST in the global coordinate system. ST orientation is defined by three angles $\Omega_{ST,\alpha}$ (ST bearing angle), $\Omega_{ST,\beta}$ (ST downtilt angle) and $\Omega_{ST,\gamma}$ (ST slant angle).

f) Give speed and direction of motion of STX, ST and SRX in the global coordinate system

g) Specify system centre frequency f_c and bandwidth B

NOTE: In case wrapping is used, each wrapping copy of a STX or SRX should be treated as a separate STX/SRX considering channel generation.

For monostatic sensing mode, a STX and a corresponding SRX are co-located, and have the same antenna field pattern, array orientations, speed and direction of motion.

7.9.4.1 Target channel

Following Step 1 in Clause 7.9.4.0, the target channels for the one or multiple STs between a pair of STX and SRX is generated using the following procedure with parameters derived by Table 7.9.3-2. It assumes a ST *k* consists of *P* scattering points indexed $p = 0,1,..P-1$, $P \geq 1$. The propagation conditions for different STX-SPST links and SPST-SRX links can be modelled by spatial consistency procedure in Clause 7.9.5.1.

Large scale parameters:

Step 2: Assign propagation condition (LOS/NLOS) for each pair of STX and SPST, and each pair of SPST and SRX according to LOS probability equation defined in reference TRs in Clause 7.9.3.

Step 3: Calculate pathloss with formulas defined in reference TRs in Clause 7.9.3 for each STX-SPST link, and each SPST-SRX link.

Step 4: For each STX-SPST link and SPST-SRX link, generate large scale parameters, e.g. delay spread (DS), angular spreads (ASA, ASD, ZSA, ZSD), Ricean K factor (K) and shadow fading (SF) taking into account cross correlation according to Table 7.5-6 and using the procedure described in clause 3.3.1 of [14] with the square root matrix$\sqrt{C_{MxM}(0)}$ being generated using the Cholesky decomposition and the following order of the large scale parameter vector: $\mathbf{s}_M = [s_{SF}, s_K, s_{DS}, s_{ASD}, s_{ASA}, s_{ZSD}, s_{ZSA}]^T$.

The LSPs for links from co-sited sectors to a STX/SPST/SRX are the same. In addition, these LSPs for the links of STX/SPST/SRX on different floors are uncorrelated.

Limit random RMS azimuth arrival and azimuth departure spread values to 104 degrees, i.e., ASA= min(ASA, 104°), ASD = min(ASD, 104°). Limit random RMS zenith arrival and zenith departure spread values to 52 degrees, i.e., ZSA = min(ZSA, 52°), ZSD = min(ZSD, 52°).

For monostatic sensing mode, the large scale parameters generated in step 2 to Step 4 are identical for a STX-SPST link and the corresponding SPST-SRX link of the same SPST.

Small scale parameters:

Step 5: Generate cluster delays

The cluster delays of cluster *n* in a STX-SPST link are generated using Step 5 of Clause 7.5, i.e., $\tau_{tx,n}^{k,p} = \tau_n$.

The cluster delays of cluster n' in the corresponding SPST-SRX link of the same SPST are generated using Step 5 of Clause 7.5 by replacing subscript *n* with *n'*, i.e., $\tau_{rx,n'}^{k,p} = \tau_{n'}$.

Step 6: Generate cluster powers.

The cluster power of cluster *n* in a STX-SPST link are generated using Step 6 of Clause 7.5, i.e., $P_{tx,n}^{k,p} = P_n$.

The cluster power of cluster n' in the corresponding SPST-SRX link of the same SPST are generated using Step 6 of Clause 7.5 by replacing subscript *n* with *n'*, i.e., $P_{rx,n'}^{k,p} = P_{n'}$.

Step 7: Generate arrival angles and departure angles for both azimuth and elevation.

The arrival angles and departure angles for both azimuth and elevation of a cluster *n* in a STX-SPST link are generated using Step 7 of Clause 7.5, i.e., $\phi_{tx,n,m,AOA}^{k,p} = \phi_{n,m,AOA}$, $\phi_{tx,n,m,AOD}^{k,p} = \phi_{n,m,AOD}$, $\theta_{tx,n,m,ZOA}^{k,p} = \theta_{n,m,ZOA}$, $\theta_{tx,n,m,ZOD}^{k,p} = \theta_{n,m,ZOD}$.

The arrival angles and departure angles for both azimuth and elevation of a cluster *n'* in the corresponding SPST-SRX link of the same SPST are generated using Step 7 of Clause 7.5 by replacing subscript *n, m* with *n', m'*, i.e., $\phi_{rx,n',m',AOA}^{k,p} = \phi_{n',m',AOA}$, $\phi_{rx,n',m',AOD}^{k,p} = \phi_{n',m',AOD}$, $\theta_{rx,n',m',ZOA}^{k,p} = \theta_{n',m',ZOA}$, $\theta_{rx,n',m',ZOD}^{k,p} = \theta_{n',m',ZOD}$.

For monostatic sensing mode, $\tau_{tx,n}^{k,p}$, $P_{tx,n}^{k,p}$, $\phi_{tx,n,m,AOA}^{k,p}$, $\phi_{tx,n,m,AOD}^{k,p}$, $\theta_{tx,n,m,ZOA}^{k,p}$, $\theta_{tx,n,m,ZOD}^{k,p}$ are respectively equal to $\tau_{rx,n'}^{k,p}$, $P_{rx,n'}^{k,p}$, $\phi_{rx,n',m',AOD}^{k,p}$, $\phi_{rx,n',m',AOA}^{k,p}$, $\theta_{rx,n',m',ZOD}^{k,p}$, $\theta_{rx,n',m',ZOA}^{k,p}$ in Step 5-7, if $n = n'$ and if applicable $m = m'$.

Step 8: Coupling of rays within a cluster for both azimuth and elevation.

The rays within a cluster *n* for both azimuth and elevation in a STX-SPST link are coupled using Step 8 of Clause 7.5.

The rays within a cluster *n'* for both azimuth and elevation in the corresponding SPST-SRX link of the same SPST are coupled using Step 8 of Clause 7.5 by replacing subscript *n, m* with *n', m'*.

For monostatic sensing mode, the same ray-coupling way applies to both the STX-SPST link and the SPST-SRX link.

Step 9: Coupling of rays for a STX-SPST link and the corresponding SPST-SRX link of the same SPST.

In the STX-SPST link, a LOS ray is represented by $n = 0, m = 0$, while a NLOS ray *m* of a stochastic cluster *n* is represented by $n > 0, m > 0$. In the SPST-SRX link, a LOS ray is represented by $n' = 0, m' = 0$, while a NLOS ray *m'* of a stochastic cluster *n'* is represented by $n' > 0, m' > 0$. A ray in the STX-SPST link and a ray in the corresponding SPST-SRX link that are coupled to each other construct a path.

The LOS ray (if present) in the STX-SPST link is coupled with the LOS ray (if present) in the SPST-SRX link. The resulting path is never dropped. Further, a set R_0 of paths are generated which include the coupled rays as follows.

- The LOS ray in the STX-SPST link (if present) is coupled with each NLOS ray in the SPST-SRX link.
- Each NLOS ray in the STX-SPST link is coupled with the LOS ray (if present) in the SPST-SRX link.
- The NLOS rays in the STX-SPST link are coupled with the NLOS rays in the SPST-SRX link. Two options for the coupling are recommended with other methods for complexity reduction up to company choice.
  - Option 1: Each NLOS ray in the STX-SPST link is coupled with each NLOS ray in the SPST-SRX link.
  - Option 2: The NLOS rays in the STX-SPST link are 1-by-1 randomly coupled with the NLOS rays in the ST-SRX link. If the number of rays in the two links M1, M2 are not equal, min(M1, M2) rays are randomly selected in the link with larger number of rays in the coupling operation.

Step 10: Obtain the power for all generated paths

The power of a path (k, p, n', m', n, m) is given by

$$P_{n',m',n,m}^{k,p} = \sigma_{D,n',m',n,m}^{k,p} min\left(\sigma_{S,n',m',n,m'}^{k,p}, 10^{\left(\mu_{\sigma_{S_dB}} + 3\sigma_{\sigma_{S_dB}}\right)/10}\right) P_{rx,n',m'}^{k,p} P_{tx,n,m}^{k,p} \qquad (7.9.4\text{-}1)$$

where, $\sigma_{D,n',m',n,m}^{k,p}$, $\sigma_{S,n',m',n,m}^{k,p}$ are the second and third component of RCS at the SPST *p* for a path are derived by the incident angle, i.e., AOA ($\phi_{tx,n,m,AOA}^{k,p}$), ZOA ($\theta_{tx,n,m,ZOA}^{k,p}$) of the ray in the STX-SPST link and the scattered angle, i.e., AOD ($\phi_{rx,n',m',AOD}^{k,p}$), ZOD ($\theta_{rx,n',m',ZOD}^{k,p}$) of the ray in the SPST-SRX link, referring to the RCS model defined in Clause

7.9.2.1 for the SPST. $\sigma^{k,p}_{S,n',m',n,m}$ is independently determined for each path of a SPST of the same ST and of the different STs. $\sigma^{k,p}_{S,n',m',n,m}$ of a path of a SPST keeps unchanged until it is updated. For monostatic sensing mode, $\sigma^{k,p}_{S,n',m',n,m}$ is equal to $\sigma^{k,p}_{S,n,m,n',m'}$ if $n = n'$ and $m = m'$.

NOTE: The transformation between GCS and LCS for the incident/scattered angles is necessary to determine the RCS at the SPST p. $P^{k,p}_{rx,n',m'}$, $P^{k,p}_{tx,n,m}$ are respectively the ray power in the SPST-SRX link and the STX-SPST link.

- If the STX-SPST link is in LOS condition,
  - for a LOS ray, $P^{k,p}_{tx,0,0} = \frac{K^{k,p}_{tx,R}}{K^{k,p}_{tx,R}+1}$, where $K^{k,p}_{tx,R}$ is the Ricean K-factor of the STX-SPST link.
  - for a NLOS ray *m* of a stochastic cluster *n*, $P^{k,p}_{tx,n,m} = \frac{1}{K^{k,p}_{tx,R}+1}\frac{P^{k,p}_{tx,n}}{M}$, where *M* is number of rays per cluster
- If the STX-SPST link is not in LOS condition,
  - for a NLOS ray m of a stochastic cluster n, $P^{k,p}_{tx,n,m} = \frac{P^{k,p}_{tx,n}}{M}$.
- If the SPST-SRX link is in LOS condition,
  - for a LOS ray, $P^{k,p}_{rx,0,0} = \frac{K^{k,p}_{rx,R}}{K^{k,p}_{rx,R}+1}$. $K^{k,p}_{rx,R}$ is the Ricean K-factor of the SPST-SRX link.
  - for a NLOS ray m' of a stochastic cluster n', $P^{k,p}_{rx,n',m'} = \frac{1}{K^{k,p}_{rx,R}+1}\frac{P^{k,p}_{rx,n'}}{M}$.
- If the SPST-SRX link is not in LOS condition,
  - for a NLOS ray m' of a stochastic cluster n', $P^{k,p}_{rx,n',m'} = \frac{P^{k,p}_{rx,n'}}{M}$.

A path with power less than X dB compared to the maximum power among all paths in set R_0 is dropped. The value of X can be up to -25 and -40 respectively for Option 1 and Option 2 in Step 9. The value X is up to company choice. The set of remaining paths (k, p, n', m', n, m) after path dropping is denoted as set *R*. The path that couples the LOS ray in the STX-SPST link and the LOS ray in the SPST-SRX link, if present, is included in set R.

Step 11: Obtain the absolute delay for each path in set *R*

The absolute delay of a path (k, p, n', m', n, m) is given by

$$\tau^{k,p}_{n',m',n,m} = \tau^{k,p}_{rx,n',m'} + d^{k,p}_{rx,3D}/c + \Delta\tau^{k,p}_{rx} + \tau^{k,p}_{tx,n,m} + d^{k,p}_{tx,3D}/c + \Delta\tau^{k,p}_{tx} \quad (7.9.4\text{-}2)$$

where, for the LOS ray in the STX-SPST link, if present, $\tau^{k,p}_{tx,0,0} = 0$. For the LOS ray in the SPST-SRX link, if present, $\tau^{k,p}_{rx,0,0} = 0$. $d^{k,p}_{tx,3D}$ is the 3D distance between STX and SPST *p*. $d^{k,p}_{rx,3D}$ is the 3D distance between SPST *p* and SRX. $\Delta\tau^{k,p}_{rx}$, $\Delta\tau^{k,p}_{tx}$ values are generated separately for NLOS rays in the SPST-SRX link and the STX-SPST link according to Table 7.6.9-1 in Clause 7.6.9. For the two strongest clusters in each of the STX-SPST link and SPST-SRX link, $\tau^{k,p}_{rx,n',m'}$ and $\tau^{k,p}_{tx,n,m}$ of sub-clusters are revised according to equation (7.5-26).

For monostatic sensing mode, $\Delta\tau^{k,p}_{rx}$ is equal to $\Delta\tau^{k,p}_{tx}$. $\Delta\tau^{k,p}_{rx}$, $\Delta\tau^{k,p}_{tx}$ are set to 0 for the LOS ray, if present, in the SPST-SRX link and the STX-SPST link.

Step 12: Generate the cross polarization power ratios for paths in set *R*.

The cross polarization power ratios for each ray *m* of a cluster *n* in a STX-SPST link is generated using Step 9 of Clause 7.5, i.e., $\kappa_{tx,n,m}^{k,p}=\kappa_{n,m}$.

The cross polarization power ratios for each ray *m'* of a cluster *n'* in a SPST-SRX link is generated using Step 9 of Clause 7.5 by replacing subscript *n, m* with *n'*, *m'*, i.e., $\kappa_{rx,n',m'}^{k,p} = \kappa_{n',m'}$.

For monostatic sensing mode, $\kappa_{tx,n,m}^{k,p}$ is equal to $\kappa_{rx,n',m'}^{k,p}$ if $n = n'$ and $m = m'$.

Generate the cross polarization power ratios (XPR) $\kappa_{n',m',m,n}^{k,p}$ for each path (k, p, n', m', n, m) in set R at SPST *p*. XPR is log-Normal distributed. Draw XPR values as

$$\kappa_{n',m',m,n}^{k,p} = 10^{X_{n',m',m,n}^{k,p}/10}, \quad (7.9.4\text{-}3)$$

where $X_{n',m',m,n}^{k,p} \sim N(\mu_{\mathrm{XPR}}, \sigma_{\mathrm{XPR}}^2)$ is Gaussian distributed with μ_{XPR} and σ_{XPR} from Table 7.9.2.2. Note: $X_{n,m}$ is independently drawn for each path in set R. $\kappa_{n',m',m,n}^{k,p}$ is independently determined for each path of a SPST of the same ST and of the different STs. $\kappa_{n',m',m,n}^{k,p}$ of a path of a SPST keeps unchanged until it is updated.

The outcome of Steps 1-12 shall be identical for all the links from co-sited sectors to a STX/ST/SRX.

Coefficient generation:

Step 13: Draw initial random phases for paths in set *R*.

The random initial phases for each ray *m* of a cluster *n* in a STX-ST link is generated using Step 9 of Clause 7.5, i.e., $\left\{\Phi_{tx,n,m}^{k,p,\theta\theta}, \Phi_{tx,n,m}^{k,p,\theta\phi}, \Phi_{tx,n,m}^{k,p,\phi\theta}, \Phi_{tx,n,m}^{k,p,\phi\phi}\right\} = \left\{\Phi_{n,m}^{\theta\theta}, \Phi_{n,m}^{\theta\phi}, \Phi_{n,m}^{\phi\theta}, \Phi_{n,m}^{\phi\phi}\right\}$

The random initial phases for each ray *m'* of a cluster *n'* in a ST-SRX link is generated using Step 9 of Clause 7.5 by replacing subscript *n, m* with *n'*, *m'*, i.e., $\left\{\Phi_{rx,n',m'}^{k,p,\theta\theta}, \Phi_{rx,n',m'}^{k,p,\theta\phi}, \Phi_{rx,n',m'}^{k,p,\phi\theta}, \Phi_{rx,n',m'}^{k,p,\phi\phi}\right\} = \left\{\Phi_{n',m'}^{\theta\theta}, \Phi_{n',m'}^{\theta\phi}, \Phi_{n',m'}^{\phi\theta}, \Phi_{n',m'}^{\phi\phi}\right\}$.

For monostatic sensing mode, $\Phi_{tx,n,m}^{k,p,\theta\theta}, \Phi_{tx,n,m}^{k,p,\theta\phi}, \Phi_{tx,n,m}^{k,p,\phi\theta}, \Phi_{tx,n,m}^{k,p,\phi\phi}$ are respectively equal to $\Phi_{rx,n',m'}^{k,p,\theta\theta}, \Phi_{rx,n',m'}^{k,p,\phi\theta}$, $\Phi_{rx,n',m'}^{k,p,\theta\phi}, \Phi_{rx,n',m'}^{k,p,\phi\phi}$ if $n = n'$ and $m = m'$.

Draw random initial phases $\left\{\Phi_{n',m',m,n}^{k,p,\theta\theta}, \Phi_{n',m',m,n}^{k,p,\theta\phi}, \Phi_{n',m',m,n}^{k,p,\phi\theta}, \Phi_{n',m',m,n}^{k,p,\phi\phi}\right\}$ for each path (k, p, n', m', n, m) in set *R* at SPST *p* and for four different polarisation combinations (θθ, θϕ, ϕθ, ϕϕ). The distribution for initial phases is uniform within (-π, π). $\left\{\Phi_{n',m',m,n}^{k,p,\theta\theta}, \Phi_{n',m',m,n}^{k,p,\theta\phi}, \Phi_{n',m',m,n}^{k,p,\phi\theta}, \Phi_{n',m',m,n}^{k,p,\phi\phi}\right\}$ are independently determined for each path of a SPST of the same ST and of the different STs. $\left\{\Phi_{n',m',m,n}^{k,p,\theta\theta}, \Phi_{n',m',m,n}^{k,p,\theta\phi}, \Phi_{n',m',m,n}^{k,p,\phi\theta}, \Phi_{n',m',m,n}^{k,p,\phi\phi}\right\}$ of a path of a SPST keeps unchanged until it is updated.

Step 14: Generate channel coefficients for paths in set *R* for each receiver and transmitter element pair *u*, *s*.

The channel coefficient for a path (k, p, n', m', n, m) in set *R* is generated by

$$H_{u,s,n',m',n,m}^{k,p}(t) = \sqrt{P_{n',m',n,m}^{k,p}} \begin{bmatrix} F_{rx,u,\theta}\left(\theta_{rx,n',m',ZOA}^{k,p}, \phi_{rx,n',m',AOA}^{k,p}\right) \\ F_{rx,u,\phi}\left(\theta_{rx,n',m',ZOA}^{k,p}, \phi_{rx,n',m',AOA}^{k,p}\right) \end{bmatrix}^T \frac{CPM_{rx,n',m'}^{k,p} CPM_{n',m',n,m}^{k,p} CPM_{tx,n,m}^{k,p}}{\sqrt{(|d^{\theta\theta}|^2 + |d^{\phi\phi}|^2)/2}}$$

$$\cdot \begin{bmatrix} F_{tx,s,\theta}\left(\theta_{tx,n,m,ZOD}^{k,p}, \phi_{tx,n,m,AOD}^{k,p}\right) \\ F_{tx,s,\phi}\left(\theta_{tx,n,m,ZOD}^{k,p}, \phi_{tx,n,m,AOD}^{k,p}\right) \end{bmatrix} exp\left(j2\pi \frac{\hat{r}_{rx,k,p,n',m'}^T(t).\bar{d}_{rx,u} + \hat{r}_{tx,k,p,n,m}^T(t).\bar{d}_{tx,s}}{\lambda_0}\right) exp\left(j2\pi \int_{t_0}^{t} f_{D,n',m',n,m}^{k,p}(\tilde{t})d\tilde{t}\right) \quad (7.9.4\text{-}4)$$

with the Doppler frequency $f_{D,n',m',n,m}^{k,p}(t)$ defined as

$$f_{D,n',m',n,m}^{k,p}(t) = \frac{\hat{r}_{rx,k,p,n',m'}^{T}(t)\tilde{v}_{rx}(t)+\hat{r}_{k,p,n',m'}^{T}(t)\tilde{v}_{k,p}(t)}{\lambda_0} + \frac{\hat{r}_{tx,k,p,n,m}^{T}(t)\tilde{v}_{tx}(t)+\hat{r}_{k,p,n,m}^{T}(t)\tilde{v}_{k,p}(t)}{\lambda_0} \quad (7.9.4\text{-}5)$$

where,

- $CPM_{n',m',n,m}^{k,p}$ is the polarization matrix of the SPST *p*.

$$CPM_{n',m',n,m}^{k,p} = \begin{bmatrix} exp\left(j\Phi_{n',m',n,m}^{k,p,\theta\theta}\right) & \sqrt{\kappa_{n',m',n,m}^{k,p\ -1}}\, exp\left(j\Phi_{n',m',n,m}^{k,p,\theta\phi}\right) \\ \sqrt{\kappa_{n',m',n,m}^{k,p\ -1}}\, exp\left(j\Phi_{n',m',n,m}^{k,p,\phi\theta}\right) & exp\left(j\Phi_{n',m',n,m}^{k,p,\phi\phi}\right) \end{bmatrix} \quad (7.9.4\text{-}6)$$

$CPM_{n,m,n',m'}^{k,p} = \left[CPM_{n',m',n,m}^{k,p}\right]^T$ if paths (k,p,n,m,n',m') and (k,p,n',m',n,m) are in set R for mono-static sensing mod.

- $CPM_{tx,n,m}^{k,p}$ is the polarization matrix of the ray in the STX-SPST link.
  - for the LOS ray, if present, $CPM_{tx,0,0}^{k,p} = \begin{bmatrix} 1 & 0 \\ 0 & -1 \end{bmatrix}$
  - for NLOS ray generated by stochastic cluster,

$$CPM_{tx,n,m}^{k,p} = \begin{bmatrix} exp\left(j\Phi_{tx,n,m}^{k,p,\theta\theta}\right) & \sqrt{\kappa_{tx,n,m}^{k,p\ -1}}\, exp\left(j\Phi_{tx,n,m}^{k,p,\theta\phi}\right) \\ \sqrt{\kappa_{tx,n,m}^{k,p\ -1}}\, exp\left(j\Phi_{tx,n,m}^{k,p,\phi\theta}\right) & exp\left(j\Phi_{tx,n,m}^{k,p,\phi\phi}\right) \end{bmatrix} \quad (7.9.4\text{-}7)$$

- $CPM_{rx,n',m'}^{k,p}$ is the polarization matrix of the ray in the SPST-SRX link.
  - for the LOS ray, if present, $CPM_{rx,0,0}^{k,p} = \begin{bmatrix} 1 & 0 \\ 0 & -1 \end{bmatrix}$
  - for NLOS ray generated by stochastic cluster,

$$CPM_{rx,n',m'}^{k,p} = \begin{bmatrix} exp\left(j\Phi_{rx,n',m'}^{k,p,\theta\theta}\right) & \sqrt{\kappa_{rx,n',m'}^{k,p\ -1}}\, exp\left(j\Phi_{rx,n',m'}^{k,p,\theta\phi}\right) \\ \sqrt{\kappa_{rx,n',m'}^{k,p\ -1}}\, exp\left(j\Phi_{rx,n',m'}^{k,p,\phi\theta}\right) & exp\left(j\Phi_{rx,n',m'}^{k,p,\phi\phi}\right) \end{bmatrix} \quad (7.9.4\text{-}8)$$

- $d^{\theta\theta}, d^{\phi\phi}$ are the two elements in the main diagonal of combined matrix $CPM_{rx,n',m'}^{k,p} CPM_{n',m',n,m}^{k,p} CPM_{tx,n,m}^{k,p}$
- $\hat{r}_{rx,k,p,n',m'}^{T}$ is the spherical unit vector at receiver for the link from SRX to SPST *p* of ST *k*, given by

$$\hat{r}_{rx,k,p,n',m'} = \begin{bmatrix} sin\theta_{rx,n',m',ZOA}^{k,p} cos\phi_{rx,n',m',AOA}^{k,p} \\ sin\theta_{rx,n',m',ZOA}^{k,p} sin\phi_{rx,n',m',AOA}^{k,p} \\ cos\theta_{rx,n',m',ZOA}^{k,p} \end{bmatrix} \quad (7.9.4\text{-}9)$$

- $\hat{r}_{tx,k,p,n,m}^{T}$ is the spherical unit vector at transmitter for the link from STX to SPST *p* of ST *k*, given by

$$\hat{r}_{tx,k,p,n,m} = \begin{bmatrix} sin\theta_{tx,n,m,ZOD}^{k,p} cos\phi_{tx,n,m,AOD}^{k,p} \\ sin\theta_{tx,n,m,ZOD}^{k,p} sin\phi_{tx,n,m,AOD}^{k,p} \\ cos\theta_{tx,n,m,ZOD}^{k,p} \end{bmatrix} \quad (7.9.4\text{-}10)$$

- $\hat{r}_{k,p,n',m'}^{T}$ is the spherical unit vector at the scattering point for the link from SPST *p* of ST *k* to SRX, given by

$$\hat{r}_{k,p,n',m'} = \begin{bmatrix} sin\theta^{k,p}_{rx,n',m',ZOD} cos\phi^{k,p}_{rx,n',m',AOD} \\ sin\theta^{k,p}_{rx,n',m',ZOD} sin\phi^{k,p}_{rx,n',m',AOD} \\ cos\theta^{k,p}_{rx,n',m',ZOD} \end{bmatrix} \quad (7.9.4\text{-}11)$$

- $\hat{r}^{T}_{k,p,n,m}$ is the spherical unit vector at the scattering point for the link from SPST p of ST k to STX, given by

$$\hat{r}_{k,p,n,m} = \begin{bmatrix} sin\theta^{k,p}_{tx,n,m,ZOA} cos\phi^{k,p}_{tx,n,m,AOA} \\ sin\theta^{k,p}_{tx,n,m,ZOA} sin\phi^{k,p}_{tx,n,m,AOA} \\ cos\theta^{k,p}_{tx,n,m,ZOA} \end{bmatrix} \quad (7.9.4\text{-}12)$$

- $\bar{v}_{rx}(t)$, $\bar{v}_{tx}(t)$ are respectively the velocity of SRX, STX.
- $\bar{v}_{k,p}(t)$ is the velocity of SPST p of ST k, $\bar{v}_{k,p}(t) = \bar{v}_{ma,k}(t) + \bar{v}_{mi,k,p}(t)$, where $\bar{v}_{ma,k}(t)$ is the velocity of the ST k, $\bar{v}_{mi,k,p}(t)$ is velocity due to micro motion of SPST p of ST k.
- t_0 denotes a reference point in time that defines the initial phase, e.g., $t_0 = 0$.

The channel impulse response of SPST p of ST k is given by

$$H^{k,p}_{u,s}(\tau, t) = \sum_{(n',m',n,m)\in R} H^{k,p}_{u,s,n',m',n,m}(t)\, \delta\left(\tau - \tau^{k,p}_{n',m',n,m}\right) \quad (7.9.4\text{-}13)$$

Step 15: Apply pathloss, shadowing, the first component of RCS for the channel coefficients.

The target channel for ST k, $H^{(k)}_{u,s}(\tau, t)$ is formed by summing the channel coefficients of the P SPST respectively scaled by the pathloss, shadowing and the first component of RCS σ_M of the P SPST.

$$H^{(k)}_{u,s}(\tau, t) = \sum_p \left(10^{-\left(PL_{tx,k,p}+PL_{rx,k,p}+SF_{tx,k,p}+SF_{rx,k,p}\right)/20} \cdot \sqrt{\frac{4\pi\sigma^{k,p}_M}{\lambda_0{}^2}} \cdot H^{(k,p)}_{u,s}(\tau, t) \right) \quad (7.9.4\text{-}14)$$

where,

- $PL_{tx,k,p}$ is the pathloss of the STX-SPST link.
- $PL_{rx,k,p}$ is the pathloss of the SPST-SRX link.
- $SF_{tx,k,p}$ is the shadow fading of the STX-SPST link.
- $SF_{rx,k,p}$ is the shadow fading of the SPST-SRX link.
- $\sigma^{k,p}_M$ is the first component of RCS for the SPST p of ST k, referring to the RCS model defined in Clause 7.9.2.1.
- $p = 0,1,..P-1$, P is the total number of SPST of the ST k.

7.9.4.2 Background channel

For TRP-TRP, TRP-UE, UE-TRP and UE-UE bistatic sensing modes, following Step 1 in Clause 7.9.4.0, the background channel between a pair of STX and SRX is generated using Step 2 to Step12 of Clause 7.5 with parameters derived by Table 7.9.3-3. The absolute time of arrival in clause 7.6.9 is applied. The resulting channel is denoted as $H^{bk}_{u,s}(\tau, t)$.

For TRP monostatic and UE monostatic sensing modes, the background channel between a pair of STX and SRX is generated using the following steps after Step 1 in Clause 7.9.4.0.

Step 2: Generate 3 reference points (RPs) for the STX/SRX.

Draw the 2D distance between the STX/SRX and each RP and the height of each RP respectively $\mathrm{G}(\alpha_d, \beta_d) + c_d$ and $\mathrm{G}(\alpha_h, \beta_h) + c_h$ with parameters defined in Table 7.9.4.2-1/2, where the UT in Table 7.9.4.2-2 Part-1 refers to any of terrestrial UE, vehicle UE, AGV UE and RSU-type UE, and the UT in Table 7.9.4.2-2 Part-2 refers to an aerial UE. Note that $\mathrm{G}(\alpha_d, \beta_d)$ and $\mathrm{G}(\alpha_h, \beta_h)$ are random values generated by the shape-rate parameterized Gamma distribution $f(x|\alpha, \beta) = \frac{\beta^\alpha}{\Gamma(\alpha)} x^{\alpha-1} e^{-\beta x}$. With uniform distribution within range$(-\pi, \pi]$, draw the LOS AOD ($\phi_{LOS,AOD}$) between the STX/SRX and the first RP. The LOS AOD is further rotated by $\frac{2}{3}\pi$ and $\frac{4}{3}\pi$ to respectively derive the LOS AOD from the STX/SRX to the second and third RPs. Consequently, the 3D location of each RP can be calculated.

- Determine LOS ZOD ($\theta_{LOS,ZOD}$) of the STX/SRX and each RP in the global coordinate system.
- Set each RP the same antenna field patterns F_{rx} in the global coordinate system and array geometries as the STX/SRX.
- Set each RP the same array orientations with respect to the global coordinate system, i.e., $\Omega_{RP,\alpha}$ (RP bearing angle), $\Omega_{RP,\beta}$ (RP downtilt angle) and $\Omega_{RP,\gamma}$ (RP slant angle) as the STX/SRX.
- Set each RP the same velocity as the STX/SRX.

NOTE: Distributions of height and distance of RPs are not subject to geographical constraints on TRP and UT for the corresponding deployment scenario.

Step 3: Assign NLOS propagation condition to the channel between the STX/SRX and each of the 3 RPs. Note: O2I is not applicable.

Step 4: Generate the channel between the STX/SRX and each of the 3 RPs using Step 3 to Step12 of Clause 7.5 and Clause 7.6.10 with parameters derived by Table 7.9.3-3, with updates as follows.

- In Step 7 of Clause 7.5, the arrival angles $\phi_{n,m,AOA}$, $\theta_{n,m,ZOA}$ are respectively equal to the departure angles $\phi_{n,m,AOD}$, $\theta_{n,m,ZOD}$. The rays in a cluster with $\theta_{n,m,ZOA}$ less than 50, 80 and 90 degrees respectively for scenario UMi, UMa and RMa are dropped. The dropping is not applicable to other sensing scenarios.
- Step 8 of Clause 7.5 is not applicable, except that the random coupling of AOD angles $\phi_{n,m,AOD}$ with ZOD angles $\theta_{n,m,ZOD}$ within a cluster n or within a sub-cluster in the case of two strongest clusters. Apply the same coupling in the corresponding arrival angles $\phi_{n,m,AOA}$, $\theta_{n,m,ZOA}$.
- The absolute time of arrival in clause 7.6.9 is applied with d_{3D}/c replaced by $max\left(\frac{d_{3D} - \sqrt{c_d^2 + (c_h - h_{TX})^2}}{c}, 0\right)$, where h_{TX} is the height of the STX/SRX. Three $\Delta\tau$ are independently generated and respectively applied to the 3 channels between the STX/SRX and the 3 RPs.

NOTE: In the UT monostatic sensing in UMa and UMi scenario, the ZOD offset should be set as 0.

Step 5: Generate the background channel for the STX/SRX

The background channel for the STX/SRX $H_{u,s}^{bk}(\tau, t)$ is formed by summing the 3 channels between STX/SRX and the 3 RPs after applying the respective pathloss and shadowing.

$$H_{u,s}^{bk}(\tau, t) = \sum_{r=0}^{2} 10^{-\left(PL_{rx,tx}^{bk,r} + SF_{rx,tx}^{bk,r}\right)/20} \cdot H_{u,s}^{bk,r}(\tau, t) \quad (7.9.4\text{-}15)$$

where,

- $PL_{rx,tx}^{bk,r}$ is the pathloss between the STX/SRX and the RP with index r.
- $SF_{rx,tx}^{bk,r}$ is the shadow fading between the STX/SRX and the RP with index r.

Table 7.9.4.2-1: Parameters of background channel for TRP monostatic sensing

Sensing scenarios		UMi	UMa / Urban grid / Highway(FR2) / HST(FR2)	RMa / Highway(FR1) / HST(FR1)	Indoor office	Indoor Factory
Distance (m)	α_d	6.1996	10.3370	6.2025	4.236	0.039836
	β_d	0.1558	0.1317	0.0391	0.19255	0.179783
	c_d	15.2697	68.7778	1.2940	4.99	1.130020
Height (m)	α_h	12.0487	16.2253	0.0007	1.3293	0.283447
	β_h	2.3261	1.9218	5.0146	0.1442	0.435965
	c_h	0.0157	2.6142	0.0522	-13.19	-17.043530

Table 7.9.4.2-2 Part-1: Parameters of background channel for UT monostatic sensing

Sensing scenarios		UMi	UMa / Urban grid / Highway(FR2) / HST(FR2)	RMa / Highway(FR1) / HST(FR1)	Indoor office	Indoor Factory
Distance (m)	α_d	10.0220	2.9072	10.2421	4.3733	0.231418
	β_d	1.2522	0.1031	0.0526	0.4457	0.128133
	c_d	11.0040	3.8471	3.3131	4.6302	2.004903
Height (m)	α_h	3.0487	1.6640	0.3175	0.2974	0.462968
	β_h	1.9128	1.6215	1.4150	0.4103	0.281526
	c_h	0.1785	-1.4205	1.5906	2.9711	-16.921515

Table 7.9.4.2-2 Part-2: Parameters of background channel for UT monostatic sensing

Sensing scenarios		UMi-AV	UMa-AV	RMa-AV
Distance (m)	α_d	$0.0156h + 5.5399$	$0.83 + 0.00015h$	$4.423 + 0.001926h$
	β_d	$40.4517/(h + 254.6318)$	$1/(536.305 + 1.0279h)$	$1/(3.8467 + 0.6547h)$
	c_d	$0.0140h + 15.1184$	$13.824 + 0.03085h$	$3.864 + 0.1538h$
Height (m)	α_h	$0.0123h + 11.9569$	$0.9054 - 0.0001117h$	$1.4231 + 0.00192h$
	β_h	$17.8047/(h - 0.2202)$	$1/(38.672 - 0.04658h)$	$1/(1.7157 - 0.00538h)$
	c_h	$0.0532h - 0.0120$	$25.4898 - 0.02398h$	$2.6541 - 0.003851h$
NOTE: h is the height of the aerial UE.				

7.9.4.3 Combining target channel and background channel

The channel model for ISAC for a pair of STX and STX is the sum of the target channel(s) and the background channel generated in Clause 7.9.4.1 and 7.9.4.2, i.e.,

$$H_{u,s}^{ISAC}(\tau, t) = \sum_k H_{u,s}^{(k)}(\tau, t) + H_{u,s}^{bk}(\tau, t). \quad (7.9.4\text{-}16)$$

7.9.5 Additional modelling components

7.9.5.0 Introduction

Similar to Clause 7.6, the additional modelling components in this clause are to support advanced simulations, such as simulations in which spatial consistency is important, simulations that include known type-2 EO, simulations that need adjusting the sum power of the target channel and the background channel, simulations of moving scatterers, simulation with impacts of lower power clusters in the background channels, and simulations of blockage effects of ST.

These extensions are computationally more expensive and might not be required in all evaluation cases.

7.9.5.1 Spatial consistency

The spatial consistency procedure is used to generate the random variables for the STX-SPST links, the SPST-SRX links and the background channels, so that they are spatial consistent.

For sensing scenario UMi-AV, UMa-AV and RMa-AV, the 2D random process (in the horizontal plane) can be extended to a 3D random process within each applicability range in terms of aerial UE height (defined in 36.777). The correlation distance is equal to the horizontal correlation distance defined in the previous clauses within Clause 7. The random coupling of NLOS rays of Option 2 in Step 9 in Clause 7.9.4.1 shall be kept unchanged per simulation drop even if STX/ST/SRX position(s) changes during simulation.

The spatial consistency procedures in Clause 7.6.3 are reused to handle the links between TRPs and STs/UTs. RSU-type UE is considered as a TRP in the spatial consistency procedures. The spatial consistency procedures in Clause 7.6.3 applies to the links between UT and UT/SPSTs (denoted as UT-UT/SPST links), with a new correlation type for the large scale parameter, cluster specific parameters and ray specific parameters of the links.

- Link-correlated: parameters of any two links of UT-UT/SPST links are correlated, subjected to correlation distance.
- All-correlated: all UT-UT/SPST links are correlated.

In Table 7.9.5.1-1, the correlation type for each parameter of the new spatial consistency procedure is clarified.

Table 7.9.5.1-1: Correlation type among UT-UT/SPST links

Parameters	Correlation type
Delays	Link-correlated
Cluster powers	Link-correlated
AOA/ZOA/AOD/ZOD offset	Link-correlated
AOA/ZOA/AOD/ZOD sign	Link-correlated
Random coupling	Link-correlated
XPR	Link-correlated
Initial random phase	Link-correlated
LOS/NLOS states	Link-correlated
Blockage (Model A)	All-correlated
O2I penetration loss	All-correlated
Indoor distance	All-correlated
Indoor states	All-correlated

Spatial consistency is not modelled among STX-SPST links, the SPST-SRX links and the background channels in the following situations:

- Different link types, e.g., outdoor LOS, outdoor NLOS or O2I, as defined in Table 7.6.3.4-2.
- UE locates on different floors, as defined in Table 7.6.3.4-2.
- Background channel for monostatic sensing mode, and any link (STX-SPST link, SPST-SRX link, background channel) for bistatic sensing mode.
- Links associated with different non-co-located TRPs, e.g. TRP1-ST/UT/TRP and TRP2-ST/UT/TRP.
- Links that are generated referring to channel models with parameter values of different communication scenarios.
- The background channels for UT monostatic sensing across different UTs or across different RPs for the same UT.
- Between TRP-target/UT link and target/UT-UT link for sensing scenario UMi, InH and InF.
- Between TRP-TRP link and any other links for ISAC channel.
- The background channels for TRP monostatic sensing across different TRPs or across different RPs for the same TRP.

The spatial consistency across the links between STX/SRX and multiple SPSTs of a ST are modelled as if the multiple SPSTs are multiple STs.

7.9.5.2 Type-2 environment object

A type-2 EO, e.g., wall, is modelled as a surface with finite size. A ray specularly reflected by a type-2 EO can be modelled in the STX-SPST link, SPST-SRX link and optionally in the background channel, if a specular reflection point can be found within the surface of the type-2 EO.

A general procedure to generated small scale parameters of a type-2 EO, e.g., a wall, is provided assuming the incident ray comes from Tx and the scattered ray arrives at Rx.

Step A: Check whether a ray specularly reflected by a type-2 EO needs to be modelled or not for the pair of Tx and Rx

The type-2 EO can be described by a plane equation perpendicular to the ground.

$$Ax + By = \mathrm{D}, x \in [x_{left,} x_{right}], y \in [y_{left,} y_{right}], z \in [z_{left,} z_{right}] \quad (7.9.5\text{-}1)$$

D is real number. [A, B, 0] is the normal vector of the plane, which points to the same direction as the orientation of the type-2 EO. The location of Tx and Rx is denoted as $[x_{tx}, y_{tx}, z_{tx}]$ and $[x_{rx}, y_{rx}, z_{rx}]$.

The location of reflection point $[x_w, y_w, z_w]$ is determined as follows.

$$x_w = x_{tx'} + \frac{(x_{rx} - x_{tx'})(\mathrm{D} - Ax_{tx'} - By_{tx'})}{A(x_{rx} - x_{tx'}) + B(y_{rx} - y_{tx'})} \quad (7.9.5\text{-}2)$$

$$y_w = y_{tx'} + \frac{(y_{rx} - y_{tx'})(\mathrm{D} - Ax_{tx'} - By_{tx'})}{A(x_{rx} - x_{tx'}) + B(y_{rx} - y_{tx'})} \quad (7.9.5\text{-}3)$$

$$z_w = z_{tx'} + \frac{(z_{rx} - z_{tx'})(\mathrm{D} - Ax_{tx'} - By_{tx'})}{A(x_{rx} - x_{tx'}) + B(y_{rx} - y_{tx'})} \quad (7.9.5\text{-}4)$$

where, $[x_{tx'}, y_{tx'}, z_{tx'}]$ is the location of the reflection image of Tx relative to the plane. $x_{tx'} = x_{tx} - \frac{2A(Ax_{tx} + By_{tx} - D)}{A^2 + B^2}$. $y_{tx'} = y_{tx} - \frac{2B(Ax_{tx} + By_{tx} - D)}{A^2 + B^2}$. $z_{tx'} = z_{tx}$.

If $x_w \in [x_{left,} x_{right}], y_w \in [y_{left,} y_{right}], z_w \in [z_{left,} z_{right}]$, the reflection point is on the surface of the type-2 EO, otherwise, there is no reflection ray in the Tx-Rx link due to the type-2 EO.

Step B: Generate parameters of the ray specularly reflected by a type-2 EO if the reflection point is on the surface of the type-2 EO

The 3D distance from the Tx to the reflection point then to the Rx d_{EO} is

$$d_{EO} = \sqrt{(x_{tx'} - x_{rx})^2 + (y_{tx'} - y_{rx})^2 + (z_{tx'} - z_{rx})^2} \quad (7.9.5\text{-}5)$$

The ZoD and AoD from Tx to the reflection point are derived based on the location of Tx and reflection point.

$$\theta_{EO,ZOD} = \arccos\left(\frac{z_w - z_{tx}}{\sqrt{(x_w - x_{tx})^2 + (y_w - y_{tx})^2 + (z_w - z_{tx})^2}}\right) \quad (7.9.5\text{-}6)$$

$$\phi_{EO,AOD} = atan2(y_w - y_{tx}, x_w - x_{tx}) \quad (7.9.5\text{-}7)$$

The ZoA and AoA from Rx to the reflection point are derived based on the location of Rx and reflection point.

$$\theta_{EO,ZOA} = \arccos\left(\frac{z_w - z_{rx}}{\sqrt{(x_w - x_{rx})^2 + (y_w - y_{rx})^2 + (z_w - z_{rx})^2}}\right) \quad (7.9.5\text{-}8)$$

$$\phi_{EO,AOA} = atan2(y_w - y_{rx}, x_w - x_{rx}) \quad (7.9.5\text{-}9)$$

The effective polarization matrix of the type-2 EO reflection ray is given by

$$CPM_{EO} = \begin{bmatrix} \cos\gamma_2 & -\sin\gamma_2 \\ \sin\gamma_2 & \cos\gamma_2 \end{bmatrix} \begin{bmatrix} R_{\parallel} & 0 \\ 0 & -R_{\perp} \end{bmatrix} \begin{bmatrix} \cos\gamma_1 & \sin\gamma_1 \\ -\sin\gamma_1 & \cos\gamma_1 \end{bmatrix} \quad (7.9.5\text{-}10)$$

where,

- $\gamma_1 = \mathrm{atan2}\left(-e_{\theta_{EO,ZOD}} n_{plane}, e_{\phi_{EO,AOD}} n_{plane}\right)$. n_{plane} represents the normal vector of the incident plane. $n_{plane} = v_{tx \to w} \times v_{w \to rx}$, in which $v_{tx \to w} = [x_w - x_{tx}, y_w - y_{tx}, z_w - z_{tx}]$ and $v_{w \to rx} = [x_{rx} - x_w, y_{rx} -$

$y_w, z_{rx} - z_w]$. $e_{\theta_{EO,ZOD}}$ represents the spherical basis vector of incident ray in vertical direction. $e_{\theta_{EO,ZOD}} = \left[cos\,\theta_{EO,ZOD}\,cos\,\phi_{EO,AOD}, cos\,\theta_{EO,ZOD}\,sin\,\phi_{EO,AOD}, -sin\,\theta_{EO,ZOD}\right]^T$. $e_{\phi_{EO,AOD}}$ represents the spherical basis vector of incident ray in horizontal direction. $e_{\phi_{EO,AOD}} = \left[-sin\,\varphi_{EO,AOD}, cos\,\varphi_{EO,AOD}, 0\right]^T$.

- $\gamma_2 = \text{atan2}\left(e_{\theta_{EO,ZOA}} n_{plane}, -e_{\phi_{EO,AOA}} n_{plane}\right)$. $e_{\theta_{EO,ZOA}}$ represents the polar basis vector of scattering ray in vertical direction. $e_{\phi_{EO,AOA}}$ represents the spherical basis vector of scattering ray in horizontal direction. $e_{\theta_{EO,ZOA}} = \left[cos\,\theta_{EO,ZOA}\,cos\,\phi_{EO,AOA}, cos\,\theta_{EO,ZOA}\,sin\,\phi_{EO,AOA}, -sin\,\theta_{EO,ZOA}\right]^T$. $e_{\phi_{EO,AOA}} = \left[-sin\,\phi_{EO,AOA}, cos\,\phi_{EO,AOA}, 0\right]^T$.

- The formula 7.6-38 and 7.6-39 of reflection coefficients $R_{//}$ and $R_{\perp}$ in Clause 7.6.8 can be reused with modified incidence angle. The incidence angle θ_{EO} is the angle between the incident vector from Tx to the reflected point and the normal vector of the type-2 EO, which is

$$\theta_{EO} = \arccos\left(\frac{(x_w - x_{tx})A + (y_w - y_{tx})B}{\sqrt{A^2+B^2}\sqrt{(x_w - x_{tx})^2 + (y_w - y_{tx})^2 + (z_w - z_{tx})^2}}\right) \quad (7.9.5\text{-}11)$$

The reflection coefficients for parallel and perpendicular polarization are given by

$$R_{//} = \frac{\frac{\varepsilon_{EO}}{\varepsilon_0} cos(\theta_{EO}) + \sqrt{\frac{\varepsilon_{EO}}{\varepsilon_0} - sin^2(\theta_{EO})}}{\frac{\varepsilon_{EO}}{\varepsilon_0} cos(\theta_{EO}) - \sqrt{\frac{\varepsilon_{EO}}{\varepsilon_0} - sin^2(\theta_{EO})}} \quad (7.9.5\text{-}12)$$

$$R_{\perp} = \frac{cos(\theta_{EO}) + \sqrt{\frac{\varepsilon_{EO}}{\varepsilon_0} - sin^2(\theta_{EO})}}{cos(\theta_{EO}) - \sqrt{\frac{\varepsilon_{EO}}{\varepsilon_0} - sin^2(\theta_{EO})}} \quad (7.9.5\text{-}13)$$

When a type-2 EO is deployed in the simulation area, the following modification to the ISAC channel generation in Clause 7.9.4, 7.9.4.1 and 7.9.4.2 can be applied.

1. In Step 1 in Clause 7.9.4.0,

   b) Give number of type-2 EO, additionally.

   c) Give 3D locations of type-2 EO in the global coordinate system, additionally.

   e) Give the orientation of type-2 EO in the global coordinate system, additionally. The type-2 EO orientation is defined by three angles $\Omega_{EO,\alpha}$ (type-2 EO bearing angle), $\Omega_{EO,\beta}$ (type-2 EO downtilt angle) and $\Omega_{EO,\gamma}$ (type-2 EO slant angle).

   NOTE: In case wrapping is used, each wrapping copy of a type-2 EO should be treated as a separate type-2EO considering channel generation.

2. In Step 2 in Clause 7.9.4.1,

Two options are provided to determine the LOS condition of a STX-SPST link and a SPST-SRX link.

- Option 1: If a type-2 EO blocks the LOS ray of a link, the LOS probability of the link is equal to 0, and otherwise use the LOS probability equation defined in reference TRs in Clause 7.9.3 to determine propagation condition (LOS/NLOS) of the link.

- Option 2: no change to Step 2 in Clause 7.9.4.1.

NOTE: The same option is used to determine the LOS condition of a STX-SPST link, a SPST-SRX link and the background channel.

3. Between Step 8 and 9 in Clause 7.9.4.1, insert one step to generate NLOS rays specularly reflected by type-2 EO, if present.

In a STX-SPST link, the general procedure to model a type-2 EO as described above is executed by substitute Tx with the STX and Rx with the SPST. A NLOS ray specularly reflected by a type-2 EO, if present, is represented by $n = 0, m > 0$. $d_{tx,EO,m}^{k,p} = d_{EO}, \theta_{tx,0,m,ZOA}^{k,p} = \theta_{EO,ZOA}, \phi_{tx,0,m,AOA}^{k,p} = \phi_{EO,AOA}, \theta_{tx,0,m,ZOD}^{k,p} = \theta_{EO,ZOD}, \phi_{tx,0,m,AOD}^{k,p} = \phi_{EO,AOD}$, $CPM_{tx,0,m}^{k,p} = CPM_{EO}$.

In a SPST-SRX link, the general procedure to model a type-2 EO as described above is executed by substitute Tx with the SPST and Rx with the SRX. A NLOS ray specularly reflected by a type-2 EO, if present, is represented by $n' = 0, m' > 0$. $d_{rx,EO,m'}^{k,p} = d_{EO}, \theta_{rx,0,m',ZOA}^{k,p} = \theta_{EO,ZOA}, \phi_{rx,0,m',AOA}^{k,p} = \phi_{EO,AOA}, \theta_{rx,0,m',ZOD}^{k,p} = \theta_{EO,ZOD}, \phi_{rx,0,m',AOD}^{k,p} = \phi_{EO,AOD}$, $CPM_{rx,0,m'}^{k,p} = CPM_{EO}$.

4. In Step 9 in Clause 7.9.4.1,

The following paths are generated and added to set R_0.

- A NLOS ray specularly reflected by type-2 EO, if present in the SPST-SRX link is coupled with a NLOS ray specularly reflected by type-2 EO, if present in the STX-SPST link
- A NLOS ray specularly reflected by type-2 EO, if present in the SPST-SRX link is coupled with any LOS ray (if present) and NLOS rays of stochastic clusters in the STX-SPST link
- A NLOS ray specularly reflected by type-2 EO, if present in the STX-SPST link is coupled with any LOS ray (if present) and NLOS rays of stochastic clusters in the SPST-SRX link

5. In Step 10 in Clause 7.9.4.1,

$P_{rx,0,m'}^{k,p}, P_{tx,0,m}^{k,p}$ for a NLOS ray specularly reflected by a type-2 EO, if present, in the SPST-SRX link and the STX-SPST link is determined as follows.

- If the STX-SPST link is in LOS condition, $P_{tx,0,m}^{k,p} = \left(\frac{d_{tx,3D}^{k,p}}{d_{tx,EO,m}^{k,p}}\right)^2$
- If the STX-SPST link is not in LOS condition, $P_{tx,0,m}^{k,p} = 10^{\left(-PL_{tx,k,p}^{LOS}+PL_{tx,k,p}\right)/10} \cdot \left(\frac{d_{tx,3D}^{k,p}}{d_{tx,EO,m}^{k,p}}\right)^2$, where $PL_{tx,k,p}^{LOS}$ is the pathloss of STX-SPST link assuming LOS condition.
- If the SPST-SRX link is in LOS condition, $P_{rx,0,m'}^{k,p} = \left(\frac{d_{rx,3D}^{k,p}}{d_{rx,EO,m'}^{k,p}}\right)^2$
- If the SPST-SRX link is not in LOS condition, $P_{rx,0,m'}^{k,p} = 10^{\left(-PL_{rx,k,p}^{LOS}+PL_{rx,k,p}\right)/10} \cdot \left(\frac{d_{rx,3D}^{k,p}}{d_{rx,EO,m'}^{k,p}}\right)^2$, where $PL_{rx,k,p}^{LOS}$ is the pathloss of SPST-SRX link assuming LOS condition.

6. In Step 11 in Clause 7.9.4.1,

For a NLOS ray specularly reflected by a type-2 EO in the STX-SPST link, if present, $\tau_{tx,n,m}^{k,p} + d_{tx,3D}^{k,p}/c$ is replaced by $d_{tx,EO,m}^{k,p}/c$, and $\Delta\tau_{tx}^{k,p}$ is set to 0.

For a NLOS ray specularly reflected by a type-2 EO in the SPST-SRX link, if present, $\tau_{rx,n',m'}^{k,p} + d_{rx,3D}^{k,p}/c$ is replaced by $d_{rx,EO,m'}^{k,p}/c$, and $\Delta\tau_{rx}^{k,p}$ is set to 0.

7. The outcome of Steps 1-12 in Clause 7.9.4.1 shall be identical for all the links from co-sited sectors to a STX/ST/EO/SRX.

8. In Clause 7.9.4.2, if a type-2 EO is modelled in the background channel between a pair of STX and SRX, the general procedure to model a type-2 EO as described above is executed by substitute Tx with the STX and Rx with the SRX.

7.9.5.3 Power normalization across target channel and background channel

To combine the target channel and the background channel, power normalization can be applied to keep the same/similar channel power as the background channel without sensing target.

7.9.5.4 Doppler of mobile scatterers

To support scatterer mobility, the Doppler frequency component $f_{D,n',m',n,m}^{k,p}(t)$ in the channel coefficient generation in step 14 in clause 7.9.4.1 should be updated as follows.

$$f_{D,n',m',n,m}^{k,p}(t) = \frac{\hat{r}_{rx,k,p,n',m'}^{T}(\tilde{t})\tilde{v}_{rx}(\tilde{t}) + \hat{r}_{k,p,n',m'}^{T}(\tilde{t})\tilde{v}_{k,p}(\tilde{t}) + 2\alpha_{rx,n',m'}^{k,p} D_{rx,n',m'}^{k,p}}{\lambda_0} + \frac{\hat{r}_{tx,k,p,n,m}^{T}(\tilde{t})\tilde{v}_{tx}(\tilde{t}) + \hat{r}_{k,p,n,m}^{T}(\tilde{t})\tilde{v}_{k,p}(\tilde{t}) + 2\alpha_{tx,n,m}^{k,p} D_{tx,n,m}^{k,p}}{\lambda_0} \quad (7.9.5\text{-}14)$$

where,

- $D_{rx,n',m'}^{k,p}$ is a random variable from $-v_{scatt}$ to v_{scatt}, and v_{scatt} is the maximum speed of the clutter. $\alpha_{rx,n',m'}^{k,p}$ is a random variable of Bernoulli distribution with mean p' if $n' > 0$, otherwise $\alpha_{rx,n',m'}^{k,p} = 0$. Parameter p' determines the proportion of mobile scatterers and can thus be selected to appropriately model statistically larger number of mobile scatterers (higher p') or statistically smaller number of mobile scatterers (e.g. in case of a completely static environment: p'=0 results in all scatterers having zero speed).
- $D_{tx,n,m}^{k,p}$ is a random variable from $-v_{scatt}$ to v_{scatt}, and v_{scatt} is the maximum speed of the clutter. $\alpha_{tx,n,m}^{k,p}$ is a random variable of Bernoulli distribution with mean p if $n > 0$, otherwise $\alpha_{tx,n,m}^{k,p} = 0$. Parameter p determines the proportion of mobile scatterers and can thus be selected to appropriately model statistically larger number of mobile scatterers (higher p) or statistically smaller number of mobile scatterers (e.g. in case of a completely static environment: p=0 results in all scatterers having zero speed).

7.9.5.5 Lower power clusters

In addition to the clusters/rays in background channel generated in Clause 7.9.4.2, more clusters/rays using NLOS propagation condition can be generated between a sensing Tx and a sensing Rx for bi-static sensing or between a sensing Tx and a reference point r, where r=0, 1, 2 for mono-static sensing to simulate the weak rays in the background channel. The following procedure is applicable for bistatic sensing or for monostatic sensing.

Step 1: Generate a first background channel $H_{u,s}^{bk1}(\tau, t)$ for bi-static sensing and $H_{u,s}^{bk1,r}(\tau, t)$ for reference point r for mono-static sensing according to Clause 7.9.4.2.

Step 2: Generate a second background channel $H_{u,s}^{bk2}(\tau, t)$ for bi-static sensing and $H_{u,s}^{bk2,r}(\tau, t)$ for reference point *r* for mono-static sensing according to Clause 7.9.4.2 including utilizing the same DS, ASA, ASD, ZSA, ZSD, C_θ, C_ϕ as used for the first step, if applicable, with the following revised parameters: 1) The number of clusters (N in Clause 7.5) is increased to 360; 2) The number of ray per cluster (M in Clause 7.5) is reduced to 1; 3) If LOS condition is assumed in Step 1, use NLOS condition to generate DS, ASA, ASD, ZSA, and ZSD values.

Step 3: The power of the clusters/rays in the second background channel is scaled down by $P_{max}^{(S1)} 10^{\frac{G}{10}}$, and is added to the first background channel, where, $G = -25$ dB, $P_{max}^{(S1)}$ is the maximum power of the NLOS clusters in the first background channel for bi-static sensing and $P_{max}^{(S1,r)}$ is the maximum power of the NLOS clusters for reference point *r* in the first background channel. The final background channel $H_{u,s}^{bk}(\tau, t)$ is 7.9.5-15a for bi-static sensing mode and 7.9.5-15b for mono-static sensing.

$$H_{u,s}^{bk}(\tau,t) = H_{u,s}^{bk1}(\tau,t) + \sqrt{P_{max}^{(S1)}\ 10^{\frac{G}{10}}} \cdot H_{u,s}^{bk2}(\tau,t) \quad (7.9.5\text{-}15a)$$

$$H_{u,s}^{bk}(\tau,t) = H_{u,s}^{bk1}(\tau,t) + \sum_{r=0}^{2} \sqrt{P_{max}^{(S1,r)}\ 10^{\frac{G}{10}}} \cdot H_{u,s}^{bk2,r}(\tau,t) \quad (7.9.5\text{-}15b)$$

7.9.5.6 Blockage

The blockage models in Clause 7.6.4 can be reused as an optional feature to model the blocking effects in the ISAC channel including the blockage due to the ST(s). The blockage of ST(s) can be applied to the LOS/NLOS rays in the background channel of the ST(s). The blockage of a first ST can be applied to the LOS/NLOS rays in the STX-ST and ST-SRX link of a second ST. The location, orientation and size of the ST as a blocker is known before applying the blockage models.

7.9.6 Channel model calibration

7.9.6.1 Large scale calibration

For the purposes of large scale calibration without fast fading modelling for sensing targets UAV, human, automotive and AGV, the following calibration parameters are respectively provided in Table 7.9.6.1-1/2/3/4. Unspecified parameters in Table 7.9.6.1-2/3/4 are the same as those in Table 7.9.6.1-1. The calibration results based on TR 38.901 V19.0.0 can be found in R1-2509126.

Table 7.9.6.1-1: Simulation assumptions for large scale calibration for UAV sensing targets

Parameters	Values
Scenario	UMa-AV
Sensing mode	TRP monostatic, TRP-TRP bistatic, TRP-UE bistatic, UE-UE bistatic
Target type	UAV of small size (0.3m x 0.4m x 0.2m)
Sectorization	Single 360-degree sector can be assumed
Carrier Frequency	FR1: 6 GHz FR2: 30 GHz
BS antenna configurations	Single dual-pol isotropic antenna
BS Tx power	FR1: 56dBm FR2: 41dBm
Bandwidth	FR1: 100MHz FR2: 400MHz
BS noise figure	FR1: 5dB FR2: 7dB
UT antenna configurations	Single dual-pol isotropic antenna; (M,N,P,Mg,Ng;Mp,Np) = (1,1,2,1,1;1,1)
UT noise figure	FR1: 9dB FR2: 10dB
UT height	1.5m for terrestrial UTs,
UT Tx power	23dBm
UT Distribution	- The overall number of UTs is 30 uniformly distributed in the center cell. - All of the UTs are either terrestrial UTs or aerial UTs, all outdoors. - Vertical distribution of aerial UE: Fixed height value of 200 m. - FR1 is assumed for aerial UE.
Sensing target distribution	1 target uniformly distributed (across multiple drops) within the center cell. Vertical distribution: Fixed height value of 200 m.
Component σ_M of the RCS for each scattering point	-12.81 dBsm
Minimum 3D distances between STX/SRX and sensing target	10 m
Wrapping Method	No wrapping method is used if interference is not modelled, otherwise geographical distance based wrapping
Coupling loss for target channel	power scaling factor (pathloss, shadow fading, and RCS component σ_M included): $L_{TX-SPST-RX} = PL_{dB}(d_1) + PL_{dB}(d_2) + 10lg\left(\frac{c^2}{4\pi f^2}\right) - 10lg(\sigma_{RCS,A}) + SF_{dB,1} + SF_{dB,2}$
STX/SRX selection	Best N = 4 STX-SRX pairs to be selected for the target. see note 1
Metrics	Coupling loss for target channel Coupling loss for background channel (in case of monostatic sensing, this is the coupling loss between Tx and one reference point) see note 2
NOTE 1: Based on the STX-SRX pairs with the smallest power scaling factor of the target channel. NOTE 2: CDFs can be separately generated for target channel, background channel.	

Table 7.9.6.1-2. Simulation assumptions for large scale calibration for Human sensing targets

Parameters	Indoor Values	Outdoor Values
Scenario	Indoor office 12 sectors per 120m * 50m * 3m ISD = 20m InF-SH Hall size: L=300 x W=150 m Room height: 10m 18 BSs on a square lattice with spacing D, located D/2 from the walls. - D=50m 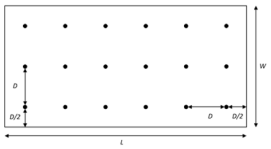	UMa (ISD = 500m), UMi (ISD= 200m)
Sensing mode	TRP monostatic, TRP-TRP bistatic, TRP-UE bistatic, UE-UE bistatic, UE monostatic	
Target type	Adult Pedestrian: 0.5m x 0.5m x 1.75m. See note.	
BS Tx power	FR1: 24dBm FR2: 23dBm	FR1: 56dBm FR2: 41dBm
UT height	1m	1.5m
UT Distribution	Per Table 7.8-1 Indoor-Office Number of UTs: 20	Per Table 7.8-1. Number of UTs/cell: 10
Sensing target distribution	100% indoor, 1 target uniformly distributed (across multiple drops) over the convex hull of the TRP deployment	100% outdoor. 1 target uniformly distributed (across multiple drops) within the center cell.
Component σ_M of the RCS for each scattering point	-1.37 dBsm	
Minimum 3D distances between STX/SRX and sensing target	For TRP monostatic and TRP-TRP bistatic sensing modes, the minimum 2D distance between STX/SRX and the sensing target is 0 m For UE monostatic and UE-UE bistatic sensing modes, the minimum 2D distance between STX/SRX and the sensing target is 1 m (as specified in TR 38.858)	For TRP monostatic and TRP-TRP bistatic sensing modes, the minimum 2D distances between STX/SRX and the sensing target are 10 m for UMi scenarios and 35 m for UMa scenarios For UE monostatic and UE-UE bistatic sensing modes, the minimum 2D distance between STX/SRX and the sensing target is 1 m (as specified in TR 38.858)
Wrapping Method	N/A	No wrapping method is used if interference is not modelled, otherwise geographical distance based wrapping
NOTE: Height of scattering point 1.5m		

Table 7.9.6.1-3. Simulation assumptions for large scale calibration for Automotive sensing targets

Parameters	Values
Scenario	For FR1: - Urban Grid (ISD=500m, BS height=25m) - Highway (ISD=1732m, BS height=35m) For FR2: - Urban Grid (ISD=250m, BS height=25m) - Highway (ISD=500m, BS height=25m) For Urban Grid ISD =250m - The layout is configured as follows: - Red triangles: BS with 250m ISD, 18 BSs are located. 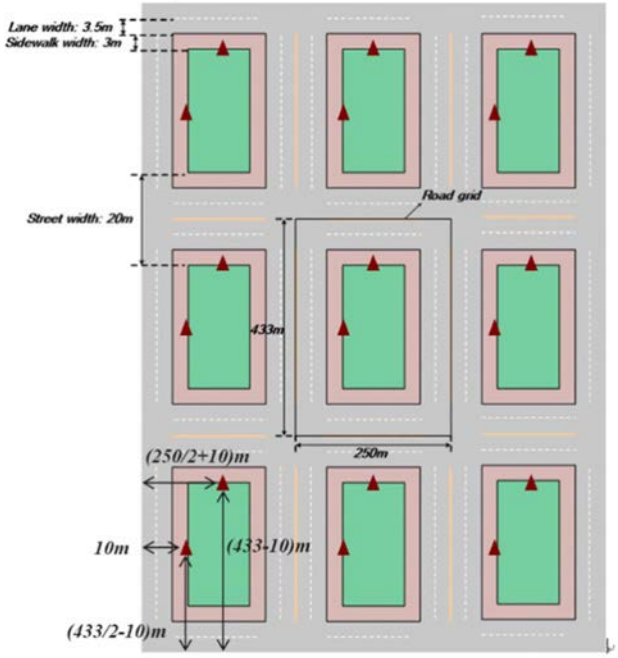
Sensing mode	TRP monostatic, TRP-TRP bistatic, TRP-UE bistatic, UE-UE bistatic, UE monostatic
Target type	Vehicle type 2 [TR37.885]
UT height	1.5m for pedestrian type UE 5m for RSU type UE 1.6m for vehicle type UE

UT Distribution	For Highway:
	- Vehicle Type UT distribution follows vehicle UE dropping as in Clause 6.1.2 from TR37.885.
	- RSU-type UTs are uniformly allocated with 100m spacing in the middle of the freeway as per TR37.885.
	For Urban grid:
	- Vehicle Type UT distribution follows vehicle UE dropping as in Clause 6.1.2 from TR37.885.
	- Pedestrian type UT, the dropping using equally spaced along the sidewalk with a fixed inter-pedestrian X m dropped per TR37.885
	  - Total number of pedestrian UEs is 16 in the centre grid.
	  - Pedestrian UE is in the middle of the sidewalk
	  - The inter-pedestrian UE distance (m) (i.e., X) is calculated by ‘A/(16*N)’, where ‘A’ is the total length of sidewalk where the pedestrian UEs are dropped under the assumption of ‘N’ road grids (i.e., ‘{(250m – 17m) + (433m – 17m)} * 2 * N’).
	  - N=1;
	- RSU-type UT: the dropping is at the center of intersection per TR37.885.
	see note 1

Sensing target distribution	Per TR37.885: - Option A - Vehicle type distribution: 100% vehicle type 2. - Clustered dropping is not used. - Highway: one target uniformly distributed (across multiple drops) within the simulation region. Vehicle speed is 140 km/h in all the lanes as baseline. - Urban Grid: one target is uniformly distributed (across multiple drops) within the center road grid. Vehicle speed is 60 km/h in all the lanes as baseline. see note 2
Component σ_M of the RCS for each scattering point	11.25 dBsm
Minimum 3D distances between STX/SRX and sensing target	Min distances based on min TRP/UE distances defined in TR37.885
Wrapping Method	No wrapping method is used if interference is not modelled, otherwise geographical distance based wrapping. As defined in urban grid/highway scenario
STX/SRX selection	Best N = 4 STX-SRX pairs to be selected for the target, with the following exceptions for Highway for FR1: - For TRP-TRP monostatic sensing, N=2 - For TRP-TRP bistatic sensing, N=1
NOTE 1: A single UT type is used per calibration, e.g., pedestrian type UT, RSU type UT, or vehicle type UTPer TR37.885 NOTE 2: A vehicle with size L*W*H can be dropped with 5 scattering points (front/left/right/back/roof), respectively with locations (L/2,0,H/2), (0,W/2,H/2), (0,-W/2,H/2), (-L/2,0,H/2) and (0,0,H) in LCS. A vehicle with size L*W*H can be dropped with 1 scattering point with location (0,0,H/2) in LCS. In the case of vehicle with 5 scattering points, spatial consistency is enabled with the following assumptions: - The correlation for LOS/NLOS condition of the 5 points is assumed equal to 1. LOS/NLOS condition can be calculated based on the distance of the STX/SRX to the centroid of the ST, then apply the LOS/NLOS condition to each of the 5 points. - The correlation for stochastic cluster paths of the 5 points is assumed equal to 1. The stochastic cluster paths can be calculated between the STX/SRX and the centroid of the ST, then the stochastic cluster paths are added to each of the 5 points.	

Table 7.9.6.1-4. Simulation assumptions for large scale calibration for AGV sensing targets

Parameters	Values
Scenario	InF: 18 TRPs per the big hall: L = 300 m x W = 150 m 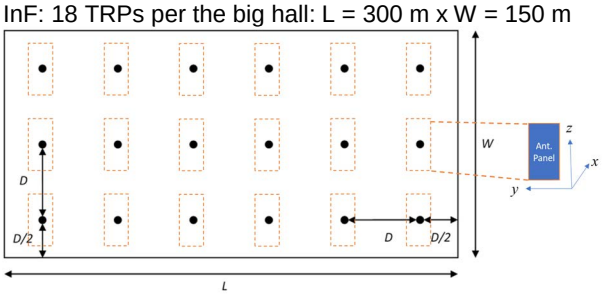 - X-axis is pointing down to the floor - The antenna array is mounted in the Y-Z plane with boresight along the X-axis - The X-axis/Y-axis/Z-axis refer to LCS - 8 m for high BS scenario
Sensing mode	TRP monostatic, TRP-TRP bistatic, TRP-UE bistatic, UE-UE bistatic, UE monostatic
Target type	Option 1: 0.5m x 1.0m x 0.5m
BS Tx power	FR1: 24dBm FR2: 23dBm
UT height	1.5m
UT Distribution	Per Table 7.8-7 Indoor Factory. Number of UTs: 30
Sensing target distribution	100% indoor, 1 target uniformly distributed (across multiple drops) over the convex hull of the TRP deployment
Component σ_M of the RCS for each scattering point	-4.25 dBsm see note
NOTE: For calibration purposes, other value(s) are not precluded,	

7.9.6.2 Full calibration

For the purpose of full calibration including the fast fading modelling for sensing scenarios UAV, human, automotive and AGV, the calibration parameters are respectively provided in Table 7.9.6.2-1/2/3/4. Unspecified parameters in the tables are the same as those in Table 7.9.6.1-1/2/3/4 for the same sensing target. If still not specified, the parameters in Table 7.9.6.2-1 are used. The calibration results based on TR 38.900 V19.0.0 can be found in R1-2509126.

Table 7.9.6.2-1: Simulation assumptions for full calibration for UAV sensing targets

Parameters	Values
Scenario	UMa-AV
Sensing mode	TRP monostatic, TRP-TRP bistatic, TRP-UE bistatic, UE-UE bistatic
Target type	UAV of small size (0.3m x 0.4m x 0.2m)
RCS for each scattering point	Component σ_M: -12.81 dBsm Component σ_D: 0 dB Component σ_S: 3.74 dB for standard deviation The same values are used for monostatic RCS and bistatic RCS
Fast fading model	TR 36.777 Annex B.1.3
(u, std) for XPR of target	Mean 13.75 dB, deviation 7.07 dB
The power threshold for path dropping after concatenation for target channel	-40 dB
Coupling loss for target channel	By definition, need to consider all direct and indirect paths. The following parameters are included in the calculation: - power scaling factor (pathloss, shadow fading, and RCS component σ_M included) - for small scale RCS σ_D/σ_S and power of rays in Tx-target/target-Rx links ($P^{k,p}_{n',m',n,m}$), STX/SRX antenna pattern, 3 polarization matrixes, i.e., $\sqrt{P^{k,p}_{n',m',n,m}}\begin{bmatrix}F_{rx,u,\theta}\left(\theta^{k,p}_{rx,n',m',ZOA},\phi^{k,p}_{rx,n',m',AOA}\right)\\F_{rx,u,\phi}\left(\theta^{k,p}_{rx,n',m',ZOA},\phi^{k,p}_{rx,n',m',AOA}\right)\end{bmatrix}^T \frac{CPM^{k,p}_{rx,n',m'}\,CPM^{k,p}_{n',m',n,m}\,CPM^{k,p}_{tx,n,m}}{\sqrt{(\lvert d11\rvert^2+\lvert d22\rvert^2)/2}} \cdot \begin{bmatrix}F_{tx,s,\theta}\left(\theta^{k,p}_{tx,n,m,ZOD},\phi^{k,p}_{tx,n,m,AOD}\right)\\F_{tx,s,\phi}\left(\theta^{k,p}_{tx,n,m,ZOD},\phi^{k,p}_{tx,n,m,AOD}\right)\end{bmatrix}$
Absolute delay	The model of UMa scenario defined in Table 7.6.9-1 is reused for UMa-AV for all sensing modes.
Metrics	Coupling loss for target channel Coupling loss for background channel (in case of monostatic sensing, this is the linear sum of coupling losses between STX/SRX and all reference points) See note. CDF of Delay Spread and Angle Spread (ASD, ZSD, ASA, ZSA). For monostatic sensing mode: delay spread and angle spread of the background channel is calculated separately for each reference point. Definition of Delay Spread is similar to the definition of angle spread in Annex A of TR 25.996, Definition of Angle Spread can ref to Annex A of TR 25.996.
NOTE: CDFs can be separately generated for target channel, background channel	

Table 7.9.6.2-2: Simulation assumptions for full calibration for Human sensing targets

Parameters	Indoor Values	Outdoor Values
Scenario	As specified in Table 7.9.6.1-2	As specified in Table 7.9.6.1-2
Sensing mode	TRP monostatic, TRP-TRP bistatic, TRP-UE bistatic, UE-UE bistatic, UE monostatic	
Target type	Adult Pedestrian: 0.5m x 0.5m x 1.75m see note	
UT Distribution	Per Table 7.8-2 Indoor-Office Number of UTs: 20	Per Table 7.8-2 Number of UTs/cell: 10
RCS for each scattering point	Component σ_M: -1.37 dBsm Component σ_D: 0 dB Component σ_S: 3.94 dB The same values are used for monostatic RCS and bistatic RCS	Component σ_M: -1.37 dBsm Component σ_D: 0 dB Component σ_S: 3.94 dB The same values are used for monostatic RCS and bistatic RCS
Fast fading model	For BS to UE link: Follow the procedure defined in TR38.901 For BS to target link: Follow the procedure defined in TR38.901 for target to UE link: Follow the procedure defined in 38.858	For BS to UE link: Follow the procedure defined in TR38.901 For BS to target link: Follow the procedure defined in TR38.901 for target to UE link: Follow the procedure defined in 38.858
(u, std) for XPR of target	(19.81, 4.25) dB	(19.81, 4.25) dB
Absolute delay	The model of InH, InF-SH scenarios defined in Table 7.6.9-1.	The model of UMa/UMi scenario defined in Table 7.6.9-1.
NOTE: Height of scattering point 1.5m		

Table 7.9.6.2-3: Simulation assumptions for full calibration for Automotive sensing targets

Parameters	Values
Scenario	As specified in Table 7.9.6.1-3
Sensing mode	TRP monostatic, TRP-TRP bistatic, TRP-UE bistatic, UE-UE bistatic, UE monostatic
Target type	Vehicle type 2 [TR37.885]
RCS for each scattering point	Based on the RCS model in Clause 7.9.2.1.
Fast fading model (full calibration)	Procedures based on 37.885
(u, std) for XPR of target	(21.12, 6.88) dB.
Absolute delay	The model of UMa scenario defined in Table 7.6.9-1 is reused for Highway (FR2)/Urban Grid for all sensing modes. The model of RMa scenario defined in Table 7.6.9-1 is reused for Highway (1732m ISD) for all sensing modes.

Table 7.9.6.2-4: Simulation assumptions for full calibration for AGV sensing targets

Parameters	Values
Scenario	As specified in Table 7.9.6.1-4
Sensing mode	TRP monostatic, TRP-TRP bistatic, TRP-UE bistatic, UE-UE bistatic, UE monostatic
Target type	Option 1: 0.5m x 1.0m x 0.5m
RCS for each scattering point	The values/pattern of component $\sigma_M \sigma_D$ are generated by Table 7.9.2.1-6 The same values are used for monostatic RCS and bistatic RCS
Fast fading model (Full calibration)	For BS to UE link: Follow the procedure defined in TR38.901 For BS to target link: Follow the procedure defined in TR38.901 for target to UE link: Follow the procedure defined in TR 38.858
(u, std) for XPR of target	(9.60, 6.85) dB
Absolute delay	The model of InF scenario defined in Table 7.6.9-1 is reused for all sensing modes.

7.9.6.3 Calibration of additional features

The calibration parameters for the calibration of spatial consistency and type-2 EO can be respectively found in Table 7.9.6.3-1/2. Unspecified parameters in these tables are the same as those in Tables 7.9.6.1-2/3 and Tables 7.9.6.2-2/3. The calibration results based on TR 38.900 V19.0.0 can be found in R1-2509126.

Table 7.9.6.3-1: Simulation assumptions for calibration of spatial consistency

Parameter	Values
Scenario	Urban grid, Indoor office
Cell layout	Urban grid: ISD = 500m, the same layout with 37.885 Indoor office: Office size (WxLxH): 120mx50mx3m, ISD=20m (refer to TR 38.901)
Sensing mode	TRP- pedestrian UE bistatic in urban grid and TRP-UE bistatic in indoor office
Polarized antenna model	Model-2 in clause 7.3.2 in TR 38.901
Scattering point	Single point
Calibration link and calibration method	- Calibration link: same target associated to different UT as following figure 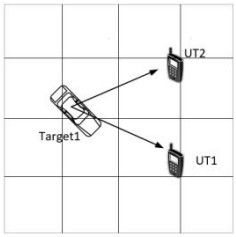 - Calibration method Step1: In single drop simulation, drop one Target and multiple UTs. Step2: Generate the channel of each link based on Target level spatial consistency method. Step3: Determine Target-UT groups based on the distance between UTs. Step4: Bin all the link pairs into certain distance groups, e.g., - 0m <= the location distance of link pair < 1m -> 0m group - 1m <= the location distance of link pair < 2m -> 1m group - 2m <= the location distance of link pair < 3m -> 2m group - 3m <= the location distance of link pair < 4m -> 3m group … - (N)m <= the location distance of pair < (N+1)m -> (N)m group (see note 2) Step5: Calculate the correlation coefficient metric of each distance groups. Step6: Draw the x-y cure, where x=0, …, N, y= correlation coefficient metric related to (x)m group
ST and UT distribution	- Urban grid one target is uniformly dropped within the center grid in the outside lane with length of 433m, the UT is distributed by a uniform distribution distance of [0,1]m in the walk road where is in the same street with the target. As following figure. 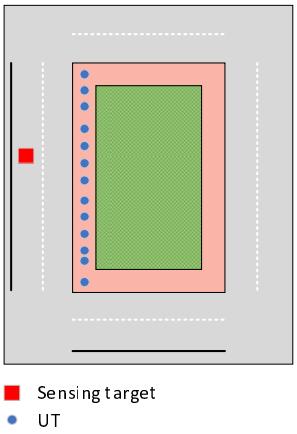 see note 3 - Indoor office 1 Target is uniform dropped in office region 10 UTs are dropped uniformly per cell, i.e., totally 120 UTs are uniformly dropped in office region.
Metrics	Cross-correlation coefficient of delay for the third cluster of channel between link pairs. Cross-correlation coefficient of AOA (for UT) for the third cluster of channel between link pairs. Cross-correlation coefficient of LOS/NLOS status of channel between link pairs(only for indoor office scenario).

NOTE 1:	Other necessary but unspecified parameters in this table are the same as those in the table for urban grid scenario calibration and indoor office scenario calibration.
NOTE 2:	N is at least twice the maximum correlation distance associated with the channel parameters in the scenario
NOTE 3:	The ST-UT link only consider LOS condition discarding NLOSv condition.

Table 7.9.6.3-2: Simulation assumptions for calibration of type-2 EO

Parameter	Values
Scenario	Urban grid
Cell layout	For FR1: ISD = 500m, the layout is defined as below: The BSs are placed at the top of buildings at one corner. Specifically, the road grids shall be shifted by $(\frac{\mathrm{ISD}}{3}-10, \frac{\sqrt{3}}{2}*\frac{\mathrm{ISD}}{3}-10)$ m in horizontal plane, or the BSs are shifted by $(-\frac{\mathrm{ISD}}{3}+10, -\frac{\sqrt{3}}{2}*\frac{\mathrm{ISD}}{3}+10)$m in horizontal plane equivalently. 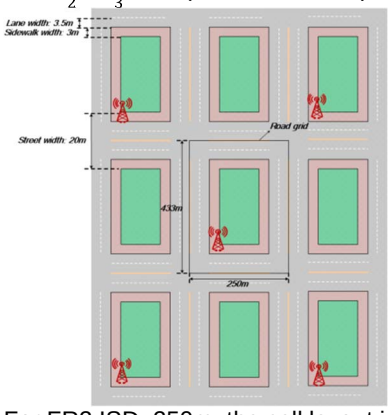 For FR2 ISD=250m, the cell layout is as that specified in Table 7.9.6.1-3
Sensing mode	TRP- pedestrian UE bistatic TRP- RSU type UE bistatic TRP monostatic TRP-TRP bistatic RSU type UE - RSU type UE bistatic (optional)
EO deployment	9 buildings with size 413m x 230m x 20m illustrated by the green blocks as in the figure shown in the row of cell layout.
ST distribution	one target is uniformly distributed (across multiple drops) within the center of the outside lane of the grid.

UT distribution	- For pedestrian UT
	  - Pedestrian type UE, the dropping using equally spaced along the sidewalk with a fixed inter-pedestrian X m dropped per TR37.885.
	  - Total number of pedestrian UEs is 16 in the centre grid.
	  - Pedestrian UE is in the middle of the sidewalk
	  - The inter-pedestrian UE distance (m) (i.e., X) is calculated by 'A/(16*N)', where 'A' is the total length of sidewalk where the pedestrian UEs are dropped under the assumption of 'N' road grids (i.e., '{(250m – 17m) + (433m – 17m)} * 2 * N').
	  - N=1;
	- For RSU type UT
	  - The dropping is at the center of intersection per TR37.885.

EM-parameters	Refer to the row for concrete in Table 7.6.8-1
Metrics	CDF curves: - Full coupling loss: calculate the coupling loss for each Tx-EO-ST-LOS-Rx and Tx-LOS-ST-EO-Rx rays. - CDF of the Delay. - CDF of the AoA, AoD, ZoA, ZoD.
NOTE:	Other necessary but unspecified parameters in this table are the same as those in the table for urban grid scenario calibration.

8 Map-based hybrid channel model (Alternative channel model methodology)

Map-based hybrid model is composed of a deterministic component following, e.g., METIS work [6] and a stochastic component following mainly the model described in clause 7. The channel model methodology described in this clause is an alternative to the methodology specified in clause 7, and can be used if:

- The system performance is desired to be evaluated or predicted with the use of digital map to take into account the impacts from environmental structures and materials.

The map-based hybrid model defined in this clause is not calibrated and can be used per company basis.

8.1 Coordinate system

The same coordinate system as defined in Clause 7.1 is applied.

8.2 Scenarios

The same scenarios as in Clause 7.2 can be applied.

8.3 Antenna modelling

The same antenna modelling as defined in Clause 7.3 can be applied.

8.4 Channel generation

The radio channels are created using the deterministic ray-tracing upon a digitized map and emulating certain stochastic components according to the statistic parameters listed in Tables 7.5-6 to 7.5-11 [Note: Not all parameters listed in these tables are used in hybrid model]. The channel realizations are obtained by a step-wise procedure illustrated in Figure 8.4-1 and described below. In the following steps, downlink is assumed. For uplink, arrival and departure parameters have to be swapped.

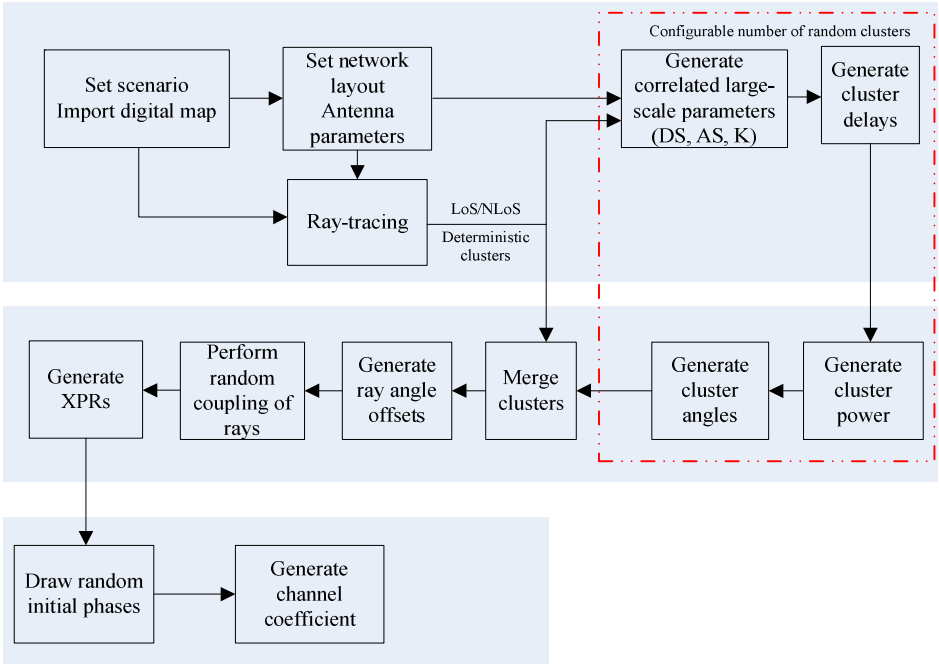

Figure 8.4-1: Channel coefficient generation procedure

Step-wise procedure:

Step 1: Set environment and import digitized map accordingly

a) Choose scenario. Choose a global coordinate system and define zenith angle θ, azimuth angle ϕ, and spherical basis vectors $\hat{\theta}$, $\hat{\phi}$ as shown in Figure 7.5-2.

b) Import digitized map according to the chosen scenario. The digitized map should at least contain the following information:

- The 3D geometric information for each of major structures involving with buildings or rooms. The external building walls and internal room walls are represented by surfaces and identified by the coordinates of the vertices on each wall.
- The material and thickness of each wall as well as the corresponding electromagnetic properties including permittivity and conductivity.
- Random small objects in certain scenarios (e.g, UMi outdoor)

The format of digitized map, including additional information besides above-mentioned, is per implementation wise and out of scope of this description.

Step 2: Set network layout, and antenna array parameters

a) Give number of BS and UT.

b) Give 3D locations of BS and UT, and calculate LOS AOD ($\phi_{LOS,AOD}$), LOS ZOD ($\theta_{LOS,ZOD}$), LOS AOA ($\phi_{LOS,AOA}$), LOS ZOA ($\theta_{LOS,ZOA}$) of each BS and UT in the global coordinate system

c) Give BS and UT antenna field patterns F_{rx} and F_{tx} in the global coordinate system and array geometries

d) Give BS and UT orientations with respect to the global coordinate system. BS array orientation is defined by three angles $\Omega_{BS,\alpha}$ (BS bearing angle), $\Omega_{BS,\beta}$ (BS downtilt angle) and $\Omega_{BS,\gamma}$ (BS slant angle). UT orientation is defined by three angles $\Omega_{UT,\alpha}$ (UT bearing angle), $\Omega_{UT,\beta}$ (UT downtilt angle) and $\Omega_{UT,\gamma}$ (UT slant angle). Give rotational motion of UT in terms of its bearing angle, downtilt angle and slant angle if UT rotation is modelled.

e) Give speed and direction of motion of UT in the global coordinate system for virtual motion.

f) Give system centre frequency/frequencies and bandwidth(s) for each of BS-UT links

If the bandwidth (denoted as B) is greater than *c/D* Hz, where *c* is the speed of light and *D* is the maximum antenna aperture in either azimuth or elevation, the whole bandwidth is split into K_B equal-sized frequency bins, where $K_B \geq \left\lceil \frac{B}{c/D} \right\rceil$ is a per-implementation parameter taking into account the channel constancy as well as other potential evaluation needs, and the bandwidth of each frequency bin is $\Delta B = \frac{B}{K_B}$. Within *k*-th frequency bin, the channel power attenuation, phase rotation, Doppler are assumed constant, whose corresponding values are calculated based on the centre frequency of *k*-th frequency bin $f_k = f_c - \frac{K_B - 2k + 1}{2}\Delta B$ for $1 \leq k \leq K_B$, where f_c is the centre frequency of the corresponding BS-UT link.

Step 3: Apply ray-tracing to each pair of link ends (i.e., end-to-end propagation between pair of Tx/Rx arrays).

a) Perform geometric calculations in ray-tracing to identify propagation interaction types, including LOS, reflections, diffractions, penetrations and scattering (in case the digitized map contains random small objects), for each propagation path. In general, some maximum orders of different interaction types can be set.

- The theoretical principles and procedures of geometric tracing calculations can be found in [6]~[10][12]. This description does not intend to mandate new concepts and/or procedures to the conventional ray-tracing algorithms; on the other hand, the implementation-based variations aiming to reduce computation complexity are allowed within limits of acceptable calibration tolerances.

- The same geometric calculation is shared among all K_B frequency bins.

b) Perform electric field calculations over propagation path, based on identified propagation interaction types (LOS, reflection, diffraction, penetration and scattering) and centre frequencies of frequency bins.

The details of electric field calculation can be found in [6]~[13].

The modelling algorithms in geometry and electric field calculations for different propagation interactions are summarized in the table below.

Table 8.4-1 Principles applied in ray-tracing

	Geometry calculation	Electric field calculation
LOS	Free space LOS	Friis equation [11]
Reflection	Snell's law with image-based method [7]	Fresnel equation [7]
Diffraction	Fermat's principle [12]	UTD [13]
Penetration	Snell's law for transmission through slab [8]	Fresnel equation [7]
Scattering (upon small objects)	Isotropic scattering [6]	RCS-based scattering coefficient [6]

Note: For reasons of simplicity and simulation speed, the maximum order of reflection on a path without diffraction is configurable from {1,2,3}; the maximum order of diffraction on a path without reflection is configurable from {1,2}; the path containing both reflection and diffraction has 1-order reflection and 1-order diffraction, besides any potential penetrations; and the maximum order of penetration on a path is configurable, with the recommended value equal to 5.

The outputs from Step 3 should at least contain following for each pair of link ends:

- the LOS/NLOS flag to indicate whether a LOS propagation mechanism exists;

- the number of deterministic propagation paths L_{RT} (also referred as deterministic clusters in Step 8. To avoid the unnecessary computation complexity, these L_{RT} deterministic paths only include those paths whose powers are higher than 25dB below the maximum deterministic path power, where the path power is denoted as $P_{l_{RT}}^{RT,real}$ and defined below);

- for each deterministic path (l_{RT} -th path sorted in ascending order of path delay):
  - the flag indicating whether the deterministic path is generated with scattering upon random small objects;
  - the normalized path delay $\tau_{l_{RT}}^{RT} = \tau'_{l_{RT}} - \min_{l_{RT}}\left(\tau'_{l_{RT}}\right)$ and the first arrival absolute delay $\min_{l_{RT}}\left(\tau'_{l_{RT}}\right)$ (with $\tau'_{l_{RT}}$ to be the real absolute propagation delay of the path);
  - angles of arrival and departure [$\phi_{l_{RT},AOA}^{RT}$, $\theta_{l_{RT},ZOA}^{RT}$, $\phi_{l_{RT},AOD}^{RT}$, $\theta_{l_{RT},ZOD}^{RT}$];
  - the power $P_{l_{RT},k}^{RT,real}$ for k-th frequency bin, and the path power $P_{l_{RT}}^{RT,real} = \frac{1}{K_B}\sum_{k=1}^{K_B} P_{l_{RT},k}^{RT,real}$
  - the XPR $\kappa_{l_{RT}}^{RT}$ of the path, where $\kappa_{l_{RT}}^{RT} = \frac{1}{K_B}\sum_{k=1}^{K_B} \kappa_{l_{RT},k}^{RT}$ with $\kappa_{l_{RT},k}^{RT}$ being the XPR for k-th frequency bin.
  - to support for true motion, i.e. the case when a trajectory is specified for UT, a path ID is associated for each deterministic path. The same ID is associated for a path across a number of UT locations as far as 1) it has same interaction types in the same order and 2) its interactions occur in same walls or other surfaces.

  The L_{RT} deterministic paths are sorted by normalized path delay ($\tau_{l_{RT}}^{RT}$) in ascending order. That is to say, τ_1^{RT} = 0.

  If L_{RT} =0 for a pair of link ends, the channel gain for this pair of link ends is assumed to be zero and the remaining steps are skipped with none of random cluster.

Step 4: Generate large scale parameters e.g. delay spread, angular spreads and Ricean K factor for random clusters.

The generation of large scale parameters takes into account cross correlation according to Table 7.5-6 and uses the procedure described in Clause 3.3.1 of [14] with the square root matrix $\sqrt{C_{MxM}(0)}$ being generated using the Cholesky decomposition and the following order of the large scale parameter vector: $\mathbf{s}_M = [s_{K,}\ s_{DS},\ s_{ASD},\ s_{ASA,}\ s_{ZSD,}\ s_{ZSA}]^T$. Limit random RMS azimuth arrival and azimuth departure spread values to 104 degrees, i.e., ASA= min(ASA ,104°), ASD = min(ASD ,104°). Limit random RMS zenith arrival and zenith departure spread values to 52 degrees, i.e., ZSA = min(ZSA,52°), ZSD = min(ZSD,52°). For the parameter selection from Table 7.5-6, the LOS/NLOS condition determined in Step 3 is applied.

Step 5: Generate delays (denoted as { τ^{RC} }) for random clusters.

Delays are drawn randomly according to the exponential delay distribution

$$\tau'_n = -\mu_\tau^{RC}\ln\left(X_n\right) \tag{8.4-1}$$

where $\mu_\tau^{RC} = \max\left\{\mu_\tau, \frac{1}{L_{RT}}\sum_{l_{RT}=1}^{L_{RT}}\tau_{l_{RT}}^{RT}\right\}$, X_n ~ uniform(0,1), and cluster index n = 0,…, L'_{RC} with L'_{RC} to be configurable. A recommended value for L'_{RC} is the number of clusters given in Table 7.5-6.

$\mu_\tau = r_\tau \mathrm{DS} + \frac{L_{RT}}{L'_{RC}+1}\left(r_\tau \mathrm{DS} - \frac{1}{L_{RT}}\sum_{l_{RT}=1}^{L_{RT}}\tau_{l_{RT}}^{RT}\right)$, where r_τ is the delay distribution proportionality factor given in Table 7.5-6.

Normalise the delays by subtracting the minimum delay and sort the normalised delays to ascending order:

$$\tau_n = \mathrm{sort}\left(\tau'_n - \min\left(\tau'_n\right)\right)/C_\tau \tag{8.4-2}$$

where C_τ is the additional scaling of delays to compensate for the effect of LOS peak addition to the delay spread, and is depending on the heuristically determined Ricean K-factor [dB] as generated in Step 4:

$$C_\tau = \begin{cases} 0.7705 - 0.0433K + 0.0002K^2 + 0.000017K^3 & \text{LOS condition} \\ 1 & \text{NLOS condition} \end{cases} \quad (8.4\text{-}3)$$

For the delay used in cluster power generation in Step 6, the scaling factor C_τ is always 1.

The *n*-th random cluster is removed if *n=0* or $\left|\tau_n - \tau_{l_{RT}}^{RT}\right| < \tau_{th}$ for any of $1 \le l_{RT} \le L_{RT}$, where τ_{th} is given by $\tau_{th} = \mu_\tau^{RC} \cdot \ln\left(\frac{1}{1-p_0}\right)$, and p_0 is the configurable probability for cluster inter-arrival interval to be less than τ_{th}. For example, set p_0 =0.2 to obtain τ_{th}=0.223μ_τ^{RC}.

Denote τ_n^{RC} for $1 \le n \le L_{RC}$ as the delays of the L_{RC} random clusters that remain after the cluster removal.

As an add-on feature, the absolute time of arrival of a cluster is derived as:

- $\tau'_{l_{RT}}$, if the cluster is the l_{RT}-th deterministic path obtained in Step 3 for $1 \le l_{RT} \le L_{RT}$;
- $\min_{l_{RT}}\left(\tau'_{l_{RT}}\right) + \tau_n^{RC}$, if the cluster is the n-th random cluster for $1 \le n \le L_{RC}$.

Step 6: Generate powers (denoted as $P_i^{RC,real}$ for $1 \le i \le L_{RC}$) for random clusters.

Cluster powers for the random clusters are calculated assuming a single slope exponential power delay profile. First, the virtual powers (denoted as $P_i^{RC,virtual}$ for $1 \le i \le L_{RC}$) of random clusters and virtual powers (denoted as $P_j^{RT,virtual}$ for $1 \le j \le L_{RT}$) of deterministic clusters are calculated as following.

Denote:

$$V_i^{RC} = \exp\left(-\tau_i^{RC}\frac{r_\tau - 1}{r_\tau \mathrm{DS}}\right) \cdot 10^{\frac{-Z_{i,RC}}{10}} \quad (8.4\text{-}4)$$

$$V_j^{RT} = \exp\left(-\tau_j^{RT}\frac{r_\tau - 1}{r_\tau \mathrm{DS}}\right) \cdot 10^{\frac{-Z_{j,RT}}{10}} \quad (8.4\text{-}5)$$

where $Z_{i,RC}$ and $Z_{j,RT}$ are the per cluster shadowing terms in [dB] and meet distribution of $N(0, \zeta^2)$. Then,

$$P_i^{RC,virtual} = \frac{1}{A+1} \cdot \frac{V_i^{RC}}{\sum_{i=1}^{L_{RC}} V_i^{RC} + \sum_{j=1}^{L_{RT}} V_j^{RT}} \quad (8.4\text{-}6)$$

$$P_j^{RT,virtual} = \frac{1}{A+1} \cdot \frac{V_j^{RT}}{\sum_{i=1}^{L_{RC}} V_i^{RC} + \sum_{j=1}^{L_{RT}} V_j^{RT}} + \frac{A}{A+1} \cdot \delta(j-1) \quad (8.4\text{-}7)$$

In the case of LOS condition, A=K_R with K_R being the Ricean *K*-factor obtained in Step 4 and converted to linear scale; otherwise, *A=0*. The real power (including effects of pathloss) per random cluster in *k*-th frequency bin is given by

$$P_{i,k}^{RC,real} = \frac{\sum_{j=1}^{L_{RT}} P_{j,k}^{RT,real}}{\sum_{j=1}^{L_{RT}} P_{j}^{RT,virtual}} \cdot P_{i}^{RC,virtual} \tag{8.4-8}$$

for $1 \le i \le L_{RC}$ and $1 \le k \le K_B$. Similar to path power of deterministic cluster, the path power of *i*-th random cluster is calculated as

$$P_{i}^{RC,real} = \frac{1}{K_B} \sum_{k=1}^{K_B} P_{i,k}^{RC,real} . \tag{8.4-9}$$

Step 7: Generate arrival angles and departure angles for both azimuth and elevation, for each random cluster.

For azimuth angles of the n-th random cluster:

The composite PAS in azimuth of all random clusters is modelled as wrapped Gaussian (see Table 7.5-6). The AOAs are determined by applying the inverse Gaussian function with input parameters $P_n^{RC,real}$ and RMS angle spread ASA

$$\phi'_{n,AOA} = \frac{2(\mathrm{ASA}/1.4)\sqrt{-\ln\left(P_n^{RC,real} \Big/ \max_{i,j}\left(P_i^{RC,real}, P_j^{RT,real}\right)\right)}}{C_\phi} \tag{8.4-10}$$

with constant C_ϕ defined as

$$C_\phi = \begin{cases} C_\phi^{\mathrm{NLOS}} \cdot \left(1.1035 - 0.028K - 0.002K^2 + 0.0001K^3\right) & \text{, for LOS} \\ C_\phi^{\mathrm{NLOS}} & \text{, for NLOS} \end{cases} \tag{8.4-11}$$

where C_ϕ^{NLOS} is defined as a scaling factor related to the total number of clusters and is given in Table 7.5-2.

In the LOS case, constant C_ϕ also depends on the Ricean K-factor *K* in [dB], as generated in Step 4. Additional scaling of the angles is required to compensate for the effect of LOS peak addition to the angle spread.

Assign positive or negative sign to the angles by multiplying with a random variable X_n with uniform distribution to the discrete set of {1,–1}, and add component $Y_n \sim N\left(0, (\mathrm{ASA}/7)^2\right)$ to introduce random variation

$$\phi_{n,AOA} = X_n \phi'_{n,AOA} + Y_n + \phi_{center,AOA} \tag{8.4-12}$$

where $\phi_{center,AOA}$ is calculated as

$$\phi_{center,AOA} = \arg\left(\sum_{l=1}^{L_{RT}} P_l^{RT,real} \cdot \exp\left(j\phi_{l,AOA}^{RT}\right)\right) \tag{8.4-13}$$

Note that $\phi_{l,AOA}^{RT}$ shall be given in radians here.

The generation of AOD ($\phi_{n,AOD}$) follows a procedure similar to AOA as described above.

For zenith angles of the n-th random cluster:

The generation of ZOA assumes that the composite PAS in the zenith dimension of all random clusters is Laplacian (see Table 7.5-6). The ZOAs are determined by applying the inverse Laplacian function with input parameters $P_n^{RC,real}$ and RMS angle spread ZSA

$$\theta'_{n,ZOA} = -\frac{\mathrm{ZSA}\ln\left(P_n^{RC,real} \Big/ \max_{i,j}\left(P_i^{RC,real}, P_j^{RT,real}\right)\right)}{C_\theta} \tag{8.4-14}$$

with C_θ defined as

$$C_\theta = \begin{cases} C_\theta^{\mathrm{NLOS}} \cdot \left(1.3086 + 0.0339K - 0.0077K^2 + 0.0002K^3\right) & \text{, for LOS} \\ C_\theta^{\mathrm{NLOS}} & \text{, for NLOS} \end{cases}, \tag{8.4-15}$$

where C_θ^{NLOS} is a scaling factor related to the total number of clusters and is given in Table 7.5-4.

In the LOS case, constant C_θ also depends on the Ricean K-factor K in [dB], as generated in Step 4. Additional scaling of the angles is required to compensate for the effect of LOS peak addition to the angle spread.

Assign positive or negative sign to the angles by multiplying with a random variable X_n with uniform distribution to the discrete set of {1,–1}, and add component $Y_n \sim N\left(0, (\mathrm{ZSA}/7)^2\right)$ to introduce random variation

$$\theta_{n,ZOA} = X_n\theta'_{n,ZOA} + Y_n + \bar{\theta}_{ZOA} \tag{8.4-16}$$

where $\bar{\theta}_{ZOA} = 90^0$ if the UT is located indoors and $\bar{\theta}_{ZOA} = \theta_{center,ZOA}$ if the UT is located outdoors, where $\theta_{center,ZOA}$ is calculated as

$$\theta_{center,ZOA} = \arg\left(\sum_{l=1}^{L_{RT}} P_l^{RT,real} \cdot \exp\left(j\theta_{l,ZOA}^{RT}\right)\right) \tag{8.4-17}$$

Note that $\theta_{l,ZOA}^{RT}$ shall be given in radians here.

The generation of ZOD follows the same procedure as ZOA described above except equation (8.4-16) is replaced by

$$\theta_{n,ZOD} = X_n\theta'_{n,ZOD} + Y_n + \theta_{center,ZOD} + \mu_{offset,ZOD} \tag{8.4-18}$$

where variable X_n is with uniform distribution to the discrete set of {1,–1}, $Y_n \sim N\left(0, (\mathrm{ZSD}/7)^2\right)$, $\mu_{offset,ZOD}$ is given in Tables 7.5-7 to 7.5-11.

Step 8: Merge deterministic clusters and random clusters.

First, remove any deterministic or random cluster with less than -25 dB power compared to max{ $P_j^{RT,real}$, $P_i^{RC,real}$ } for all $1 \le j \le L_{RT}$ and $1 \le i \le L_{RC}$. Then, simply put the remaining deterministic clusters and random clusters into single set of clusters, and meanwhile maintain an attribute for each cluster to indicate whether the cluster is a deterministic cluster or a random cluster.

Step 9: Generate ray delays and ray angle offsets inside each cluster, where the cluster can be either random or deterministic.

Denote *M* as the number of rays per cluster, where *M=1* if the cluster corresponds to n=1 in the LOS case, otherwise the value of *M* is given in Table 7.5-6.

When $K_B = 1$*:*

The relative delay of *m*-th ray within *n*-th cluster is given by $\tau'_{n,m} = 0$ for *m* = 1,…,*M*.

The azimuth angle of arrival (AOA) for the *m*-th ray in *n*-th cluster is given by

$$\phi_{n,m,AOA} = \phi_{n,AOA} + c_{ASA}\alpha_m \tag{8.4-19}$$

where c_{ASA} is the cluster-wise rms azimuth spread of arrival angles (cluster ASA) in Table 7.5-6, and offset angle α_m is given in Table 7.5-3. $\phi_{n,AOA}$ equals to the AOA angle output from Step 3 if *n*-th cluster is deterministic cluster, and equals to the AOA angle (8.4-12) in Step 7 if *n*-th cluster is random cluster.

The generation of AOD ($\phi_{n,m,AOD}$) follows a procedure similar to AOA as described above.

The zenith angle of arrival (ZOA) for the *m*-th ray in *n*-th cluster is given by

$$\theta_{n,m,ZOA} = \theta_{n,ZOA} + c_{ZSA}\alpha_m \tag{8.4-20}$$

where c_{ZSA} is the cluster-wise rms spread of ZOA (cluster ZOA) in Table 7.5-6, and offset angle α_m is given in Table 7.5-3. Assuming that $\theta_{n,m,ZOA}$ is wrapped within [0, 360°], if $\theta_{n,m,ZOA} \in [180°, 360°]$, then $\theta_{n,m,ZOA}$ is set to $(360° - \theta_{n,m,ZOA})$. $\theta_{n,ZOA}$ equals to the ZOA angle output from Step 3 if *n*-th cluster is deterministic cluster, and equals to the ZOA angle (8.4-16) in Step 7 if *n*-th cluster is random cluster.

The zenith angle of departure (ZOD) for the *m*-th ray in *n*-th cluster is given by

$$\theta_{n,m,ZOD} = \theta_{n,ZOD} + (3/8)(10^{\mu_{\text{lgZSD}}})\alpha_m \tag{8.4-21}$$

where μ_{lgZSD} is the mean of the ZSD log-normal distribution. $\theta_{n,ZOD}$ equals to the ZOD angle output from Step 3 if *n*-th cluster is deterministic cluster, and equals to the ZOD angle (8.4-18) in Step 7 if *n*-th cluster is random cluster.

When $K_B > 1$*:*

The relative delay of *m*-th ray within *n*-th cluster is given by $\tau'_{n,m} = \text{sort}\left(\tau''_{n,m} - \min_{1 \le m \le M}\left\{\tau''_{n,m}\right\}\right)$ that are sorted in ascending order, where $\tau''_{n,m} \sim \text{unif}\left(0, 2c_{\text{DS}}\right)$, with the cluster delay spread as given in Table 7.5-6. $\text{unif}(a,b)$ denotes the continuous uniform distribution on the interval $[a,b]$. Note that $\tau''_{n,m}$ shall be the independently generated.

The azimuth angles (AOA and AOD) and zenith angles (ZOA and ZOD) for the *m*-th ray in *n*-th cluster in each frequency bin is given by

$$\begin{aligned}
\phi_{n,m,AOA} &= \phi_{n,AOA} + \phi'_{n,m,AOA} \\
\phi_{n,m,AOD} &= \phi_{n,AOD} + \phi'_{n,m,AOD} \\
\theta_{n,m,ZOA} &= \theta_{n,ZOA} + \theta'_{n,m,ZOA} \\
\theta_{n,m,ZOD} &= \theta_{n,ZOD} + \theta'_{n,m,ZOD}
\end{aligned} \tag{8.4-22}$$

for m = 1,…,M, where $\phi_{n,\{AOA|AOD\}}$ and $\theta_{n,\{ZOA|ZOD\}}$ equal to the {AOA,AOD} and {ZOA, ZOD} angle outputs from Step 3 if n-th cluster is deterministic cluster, and equal to the {AOA,AOD} and {ZOA, ZOD} angle in Step 7 if n-th cluster is random cluster; and

$$\begin{aligned}\phi'_{n,m,AOA} &\sim 2c_{\text{ASA}}\,\text{unif}\left(-1,1\right)\\ \phi'_{n,m,AOD} &\sim 2c_{\text{ASD}}\,\text{unif}\left(-1,1\right)\\ \theta'_{n,m,ZOA} &\sim 2c_{\text{ZSA}}\,\text{unif}\left(-1,1\right)\\ \theta'_{n,m,ZOD} &\sim 2c_{\text{ZSD}}\,\text{unif}\left(-1,1\right)\end{aligned} \tag{8.4-23}$$

with the respective cluster angular spreads as given in Tables 7.5-6 to 7.5-11.

Assuming that $\theta_{n,m,ZOA}$ is wrapped within [0, 360°], if $\theta_{n,m,ZOA} \in [180°, 360°]$, then $\theta_{n,m,ZOA}$ is set to $(360° - \theta_{n,m,ZOA})$.

Step 10: Generate power of rays in each cluster, where coupling of rays within a cluster for both azimuth and elevation could be needed.

Given $P_{n,k}$ as the real power in k-th frequency bin for the n-th cluster (either deterministic or random) obtained from Step 8,

When $K_B = 1$*:*

Couple randomly AOD angles $\phi_{n,m,AOD}$ to AOA angles $\phi_{n,m,AOA}$ within a cluster n. Couple randomly ZOD angles $\theta_{n,m,ZOD}$ with ZOA angles $\theta_{n,m,ZOA}$ using the same procedure. Couple randomly AOD angles $\phi_{n,m,AOD}$ with ZOD angles $\theta_{n,m,ZOD}$ within a cluster n.

The power of m-th ray in n-th cluster and in k-th frequency bin is given by $P_{n,m,k} = P_{n,k} / M$ for m = 1,…,M.

When $K_B > 1$*:*

The power of m-th ray in n-th cluster and in k-th frequency bin is given by $P_{n,m,k} = P_{n,k} \cdot \dfrac{P'_{n,m}}{\sum_{m=1}^{M} P'_{n,m}}$ for m = 1,…,M, where

$$\begin{aligned}P'_{n,m} = &\exp\left(-\frac{\tau'_{n,m}}{c_{\text{DS}}}\right)\exp\left(-\frac{\sqrt{2}\left|\phi'_{n,m,AOA}\right|}{c_{\text{ASA}}}\right)\exp\left(-\frac{\sqrt{2}\left|\phi'_{n,m,AOD}\right|}{c_{\text{ASD}}}\right)\\ &\cdot\exp\left(-\frac{\sqrt{2}\left|\theta'_{n,m,ZOA}\right|}{c_{\text{ZSA}}}\right)\exp\left(-\frac{\sqrt{2}\left|\theta'_{n,m,ZOD}\right|}{c_{\text{ZSD}}}\right)\end{aligned} \tag{8.4-24}$$

and c_{DS}, c_{ASA}, c_{ASD}, and c_{ZSA} are respectively the intra-cluster delay spread and the corresponding intra-cluster angular spreads that are given in Table 7.5-6. The cluster zenith spread of departure is given by

$$c_{\text{ZSD}} = \frac{3}{8}10^{\mu_{\text{lgZSD}}}, \tag{8.4-25}$$

with μ_{lgZSD} being defined in Tables 7.5-7, 7.5-8, 7.5-9, 7.5-10 and 7.5-11.

Step 11: Generate XPRs

Generate the cross polarization power ratios (XPR) κ for each ray *m* of each cluster *n*. XPR is log-Normal distributed. Draw XPR values as

$$\kappa_{n,m} = 10^{X_{n,m}/10} \tag{8.4-26}$$

where $X_{n,m} \sim N(\mu_{\text{XPR}}, \sigma^2_{\text{XPR}})$ is Gaussian distributed with σ_{XPR} given from Table 7.5-6. If *n*-th cluster is a deterministic cluster, $\mu = 10\log_{10} \kappa^{RT}_{l_{RT}}$; otherwise, $\mu = \mu_{\text{XPR}}$ is given in Table 7.5-6.

Note: $X_{n,m}$ is independently drawn for each ray and each cluster.

Step 12: Draw initial random phases

Draw random initial phase $\left\{\Phi^{\theta\theta}_{n,m}, \Phi^{\theta\phi}_{n,m}, \Phi^{\phi\theta}_{n,m}, \Phi^{\phi\phi}_{n,m}\right\}$ for each ray *m* of each cluster *n* and for four different polarisation combinations ($\theta\theta$, $\theta\phi$, $\phi\theta$, $\phi\phi$). The distribution for initial phases is uniform within ($-\pi$,π).

In the LOS case, calculate an initial phase $\Phi_{LOS} = -2\pi\, d_{3D}/\lambda_0$ for both $\theta\theta$ and $\phi\phi$ polarisations, where d_{3D} is the 3D distance between transmitter and receiver and $\lambda_0 = c/f_c$ is the wavelength of the modelled propagation link.

Step 13: Generate channel coefficients for each cluster *n* and each receiver and transmitter element pair *u*, *s*.

In case of NLOS, the channel coefficients of ray *m* in cluster *n* for a link between Rx antenna *u* and Tx antenna *s* at time *t* in *k*-th frequency bin can be calculated as

$$\begin{aligned} H_{u,s,n,m,k}(t) = & \begin{bmatrix} F_{rx,u,\theta}(\theta_{n,m,ZOA}, \phi_{n,m,AOA}) \\ F_{rx,u,\phi}(\theta_{n,m,ZOA}, \phi_{n,m,AOA}) \end{bmatrix}^T \begin{bmatrix} \exp(j\Phi^{\theta\theta}_{n,m}) & \sqrt{\kappa^{-1}_{n,m}}\exp(j\Phi^{\theta\phi}_{n,m}) \\ \sqrt{\kappa^{-1}_{n,m}}\exp(j\Phi^{\phi\theta}_{n,m}) & \exp(j\Phi^{\phi\phi}_{n,m}) \end{bmatrix} \\ & \cdot \begin{bmatrix} F_{tx,s,\theta}(\theta_{n,m,ZOD}, \phi_{n,m,AOD}) \\ F_{tx,s,\phi}(\theta_{n,m,ZOD}, \phi_{n,m,AOD}) \end{bmatrix} \cdot \exp\left(j2\pi \frac{f_k}{c} \left(\hat{r}^T_{rx,n,m} . \bar{d}_{rx,u} + \hat{r}^T_{tx,n,m} . \bar{d}_{tx,s} \right) \right) \\ & \cdot \left(\sqrt{P_{n,m,k}} \cdot 10^{\frac{-(OL_{n,m}(f_k) + BL_{n,m}(f_k,t))}{20}} \right) \exp\left(j2\pi \frac{f_k}{c} \hat{r}^T_{rx,n,m} . \bar{v} t \right) \end{aligned} \tag{8.4-27}$$

where $F_{rx,u,\theta}$ and $F_{rx,u,\phi}$ are the receive antenna element *u* field patterns in the direction of the spherical basis vectors, $\hat{\theta}$ and $\hat{\phi}$ respectively, $F_{tx,s,\theta}$ and $F_{tx,s,\phi}$ are the transmit antenna element *s* field patterns in the direction of the spherical basis vectors, $\hat{\theta}$ and $\hat{\phi}$ respectively. The delay (TOA) for ray *m* in cluster *n* for a link between Rx antenna *u* and Tx antenna *s* is given by:

$$\tau_{u,s,n,m} = \tau_n + \tau'_{n,m} - \tfrac{1}{c}\hat{r}^T_{rx,n,m} . \bar{d}_{rx,u} - \tfrac{1}{c}\hat{r}^T_{tx,n,m} . \bar{d}_{tx,s} \tag{8.4-28}$$

For the *m*-th ray within *n*-th cluster, $\hat{r}_{rx,n,m}$ is the spherical unit vector with azimuth arrival angle $\phi_{n,m,AOA}$ and elevation arrival angle $\theta_{n,m,ZOA}$, given by

$$\hat{r}_{rx,n,m} = \begin{bmatrix} \sin\theta_{n,m,ZOA}\cos\phi_{n,m,AOA} \\ \sin\theta_{n,m,ZOA}\sin\phi_{n,m,AOA} \\ \cos\theta_{n,m,ZOA} \end{bmatrix} \tag{8.4-29}$$

$\hat{r}_{tx,n,m}$ is the spherical unit vector with azimuth departure angle $\phi_{n,m,AOD}$ and elevation departure angle $\theta_{n,m,ZOD}$, given by

$$\hat{r}_{tx,n,m} = \begin{bmatrix} \sin\theta_{n,m,ZOD}\cos\phi_{n,m,AOD} \\ \sin\theta_{n,m,ZOD}\sin\phi_{n,m,AOD} \\ \cos\theta_{n,m,ZOD} \end{bmatrix} \quad (8.4\text{-}30)$$

Also, $\bar{d}_{rx,u}$ is the location vector of receive antenna element *u* and $\bar{d}_{tx,s}$ is the location vector of transmit antenna element *s*, $\kappa_{n,m}$ is the cross polarisation power ratio in linear scale. If polarisation is not considered, the 2x2 polarisation matrix can be replaced by the scalar $\exp(j\Phi_{n,m})$ and only vertically polarised field patterns are applied.

The Doppler frequency component is calculated from the arrival angles (AOA, ZOA), and the UT velocity vector $\bar{v}$ with speed *v*, travel azimuth angle ϕ_v, elevation angle θ_v and is given by

$$\bar{v} = v.[\sin\theta_v\cos\phi_v \quad \sin\theta_v\sin\phi_v \quad \cos\theta_v]^T, \quad (8.4\text{-}31)$$

In case of LOS, the channel coefficient is calculated in the same way as in (8.4-27) except for n=1:

$$H_{u,s,n=1,k}(t) = \begin{bmatrix} F_{rx,u,\theta}(\theta_{LOS,ZOA},\phi_{LOS,AOA}) \\ F_{rx,u,\phi}(\theta_{LOS,ZOA},\phi_{LOS,AOA}) \end{bmatrix}^T \begin{bmatrix} \exp(j\Phi_{LOS}) & 0 \\ 0 & -\exp(j\Phi_{LOS}) \end{bmatrix} \begin{bmatrix} F_{tx,s,\theta}(\theta_{LOS,ZOD},\phi_{LOS,AOD}) \\ F_{tx,s,\phi}(\theta_{LOS,ZOD},\phi_{LOS,AOD}) \end{bmatrix} \quad (8.4\text{-}32)$$
$$\cdot \exp\left(j2\pi \frac{f_k}{c}\left(\hat{r}^T_{rx,LOS}.\bar{d}_{rx,u} + \hat{r}^T_{tx,LOS}.\bar{d}_{tx,s}\right)\right).\left(\sqrt{P_{1,k}}\cdot 10^{\frac{-(OL_{n,m=1}(f_k)+BL_{n,m=1}(f_k,t))}{20}}\right)\exp\left(j2\pi \frac{f_k}{c}\hat{r}^T_{rx,LOS}.\bar{v}t\right)$$

where the corresponding delay (TOA) for cluster *n*=1 for a link between Rx antenna *u* and Tx antenna *s* is given by $\tau_{u,s,n=1} = \tau_n - \frac{1}{c}\hat{r}^T_{rx,LOS}.\bar{d}_{rx,u} - \frac{1}{c}\hat{r}^T_{tx,LOS}.\bar{d}_{tx,s}$.

In (8.4-27) and (8.4-32), the oxygen absorption loss, $OL_{n,m}(f)$, for each ray *m* in cluster *n* at carrier frequency *f* is modelled as

$$OL_{n,m}(f) = \alpha(f)/1000 \cdot c \cdot \left[\tau_n + \tau'_{n,m} + \min_{l_{RT}}\left(\tau'_{l_{RT}}\right)\right] \text{ [dB]} \quad (8.4\text{-}33)$$

where:

- $\alpha(f)$ is the frequency dependent oxygen loss per distance (dB/km) characterized in Clause 7.6.1;
- *c* is speed of light (m/s); and
- τ_n is the delay (s) obtained from Step 3 for deterministic clusters and from Step 5 for random clusters. $\min_{l_{RT}}\left(\tau'_{l_{RT}}\right)$ is from the output of Step 3.

In (8.4-27) and (8.4-32), blockage modelling is an add-on feature. If the blockage model is applied, the blockage loss, $BL_{n,m}(f,t)$ in unit of dB, for each ray *m* in cluster *n* at carrier frequency *f* and time *t* is modelled in the same way as given in Clause 7.6.4; otherwise $BL_{n,m}(f,t)$=0dB for all *f* and *t*.

Annex A:
Further parameter definitions

A.1 Calculation of angular spread

Based on the circular standard deviation in directional statistics, the following expression for the angular spread AS in radians is proposed

$$\mathrm{AS} = \sqrt{-2\,ln\left(\left|\frac{\sum_{n=1}^{N}\sum_{m=1}^{M} exp\left(j\varphi_{n,m}\right)P_{n,m}}{\sum_{n=1}^{N}\sum_{m=1}^{M} P_{n,m}}\right|\right)} \quad \text{(A-1)}$$

where $P_{n,m}$ is the power for the *m*th subpath of the *n*th path and $\varphi_{n,m}$ is the subpaths angle (either AOA, AOD, ZOA, ZOD) given in radians.

A.2 Calculation of mean angle

The power weighted mean angle is given by

$$\mu_{\varphi} = arg\left\{\sum_{n=1}^{N}\sum_{m=1}^{M} exp\left(j\varphi_{n,m}\right) P_{n,m}\right\} \quad \text{(A-2)}$$

where $P_{n,m}$ is the power for the *m*th subpath of the *n*th path and $\varphi_{n,m}$ is the subpaths angle (either AOA, AOD, ZOA, ZOD) given in radians.

A.3 Calculation of cluster angular spread

The cluster angular spread in degrees is given by

$$\mathrm{AS} = \frac{180}{\pi}\sqrt{-2\,ln\left(\left|\frac{exp\left(\frac{j\pi}{180}\varphi_{LOS}\right)P_{LOS}+\sum_{n=1}^{N} exp\left(\frac{j\pi}{180}\varphi_{n}\right)P_{n}}{P_{LOS}+\sum_{n=1}^{N} P_{n}}\right|\right)} \quad \text{(A-3)}$$

where P_n is the power for the *n*th cluster path, φ_n is the cluster path angle (either AOA, AOD, ZOA, ZOD) given in degrees, P_{LOS} is the power for the LOS path, and φ_{LOS} is the LOS path angle (either AOA, AOD, ZOA, ZOD) given in degrees. If LOS path does not exist, $P_{LOS} = 0$ is assumed.

A.4 Calculation of cluster mean angle

The power weighted cluster mean angle in degrees is given by

$$\mu_{\varphi} = \frac{180}{\pi} arg\left\{exp\left(\frac{j\pi}{180}\varphi_{LOS}\right) P_{LOS} + \sum_{n=1}^{N} exp\left(\frac{j\pi}{180}\varphi_{n}\right) P_{n}\right\} \quad \text{(A-4)}$$

where $arg\{z\}$ is the angle in radians measured from the positive real axis to the line joining the origin and complex value z, P_n is the power for the *n*th cluster path, φ_n is the cluster path angle (either AOA, AOD, ZOA, ZOD) given in degrees, P_{LOS} is the power for the LOS path, and φ_{LOS} is the LOS path angle (either AOA, AOD, ZOA, ZOD) given in degrees. If LOS path does not exist, $P_{LOS} = 0$ is assumed.

A.5 Calculation of scaling factor for changing CDL model angular spread

The following expression for the computing scaling factor, s, to achieve a specific angular spread, AS, in degrees is given by

$$s = \min_{x \geq 0}\{x: AS(x) = AS_{desired}\} \quad \text{(A-5)}$$

$$AS(x) = \frac{180}{\pi}\sqrt{-2\,ln\left(\left|\frac{exp\left(jx\cdot\frac{\pi}{180}WrapTo180(\varphi_{LOS})\right)P_{LOS}+\sum_{n=1}^{N}exp\left(jx\cdot\frac{\pi}{180}WrapTo180(\varphi_n)\right)P_n}{P_{LOS}+\sum_{n=1}^{N}P_n}\right|\right)} \quad \text{(A-6)}$$

where P_n is the power for the *n*th cluster path, φ_n is the input cluster path angle (either AOA, AOD, ZOA, ZOD) given in degrees, P_{LOS} is the power for the input LOS path, and φ_{LOS} is the input LOS path angle (either AOA, AOD, ZOA, ZOD) given in degrees. If input LOS path does not exist, $P_{LOS} = 0$ is assumed.

Annex B:
Change history

Change history							
Date	**Meeting**	**TDoc**	**CR**	**Rev**	**Cat**	**Subject/Comment**	**New version**
2017-02	RAN1#88	R1-1703641				Skeleton TR based on TR 38.900 v14.2.0, adding new changes (from R1-1701231, R1-1701406, R1-1701410, R1-1701411, R1-1701412, R1-1701413, R1-1701414, R1-1701416, R1-1701417 and R1-1701425) to have a TR applicable for the frequency range 0.5 to 100 GHz	0.0.1
2017-02	RAN1#88	R1-1704145				Adding new agreements (from R1-1702701, R1-1703635, R1-1703873, R1-1703358, R1-1702703, R1-1703637, R1-1703354, R1-1703458, R1-1703647, R1-1701936) and reflecting comments from RAN1 e-mail discussions [88-17].	0.1.0
2017-02	RAN#75	RP-170394				Submitted to RAN for information	1.0.0
2017-03	RAN#75	RP-170737				Add TR number further to the approval of revised SID in RP-170379. Submitted to RAN for one step approval	1.0.1
2017-03	RAN#75					MCC clean-up – Further to RAN#75 decision, TR goes under change control as Rel-14	14.0.0
2017-06	RAN#76	RP-171208	0001	-	F	Correction on site specific effective height for TR38.901	14.1.0
2017-06	RAN#76	RP-171208	0003	-	F	Correction for LOS probability	14.1.0
2017-06	RAN#76	RP-171208	0004	-	F	Correction for scaling factor for ZOD generation	14.1.0
2017-06	RAN#76	RP-171208	0005	-	F	Correction for modelling of intra-cluster angular and delay spreads	14.1.0
2017-06	RAN#76	RP-171208	0007	-	F	TR38.901_CR_LCS_Radiation_Field_Notation	14.1.0
2017-06	RAN#76	RP-171208	0008	-	F	TR38.901_CR_Mean_angle_definition	14.1.0
2017-06	RAN#76	RP-171208	0009	-	F	TR38.901_CR_O2I_penetration_loss	14.1.0
2017-06	RAN#76	RP-171208	0010	1	F	TR38.901_CR_Correction_on_Rural_LSP	14.1.0
2017-06	RAN#76	RP-171208	0011	1	F	Clarification for spatial consistency procedure	14.1.0
2017-06	RAN#76	RP-171208	0013	-	F	TR38.901_CR_Scenarios_in_Simulation_Assumptions	14.1.0
2017-06	RAN#76	RP-171208	0014	-	F	TR38.901_CR_TDL_Spatial_Filter	14.1.0
2017-06	RAN#76	RP-171208	0015	-	F	Correction of spatial-consistency UE mobility modelling Procedure A	14.1.0
2017-07						MCC: UMa LOS probability in Table 7.4-2 is made fully visible	14.1.1
2017-09	RAN#77	RP-171648	0016	-	F	Correction on the formula of Annex A	14.2.0
2017-09	RAN#77	RP-171648	0018	2	F	Correction on cross polarization power ratios in TR 38.901	14.2.0
2017-09	RAN#77	RP-171648	0019	1	F	TR38.901_CR_Spatially-consistent_UT_modelling	14.2.0
2017-09	RAN#77	RP-171648	0020	1	F	TR38.901_CR_Calibraiton_Results	14.2.0
2017-12	RAN#78	RP-172687	0022	-	F	Correction on 3D-InH channel model in TR 38.901	14.3.0
2018-06	SA#80	-	-	-	-	Update to Rel-15 version (MCC)	15.0.0
2019-09	RAN#85	RP-191944	0023	-	B	Addition of indoor industrial channel model – version created in error – withdrawn	15.1.0
2019-10	RAN#85	RP-191944	0023	-	B	Addition of indoor industrial channel model – creation of rel-16 report	16.0.0
2019-12	RAN#86	RP-192629	0024	-	F	CR to TR 38.901 for remaining open issues in IIOT channel modelling	16.1.0
2022-03	SA#95-e					Update to Rel-17 version (MCC)	17.0.0
2023-12	RAN#102	RP-233727	0025	-	F	CR correcting scaling of angles for CDL model and a figure reference	17.1.0
2024-03	SA#103	-	-	-	-	Update to Rel-18 version (MCC)	**18.0.0**
2025-06	RAN#108	RP-251566	0026	-	B	Introduction of Rel-19 7-24 GHz channel model enhancements	19.0.0
2025-06	RAN#108	RP-251567	0027	-	B	CR to introduce channel model for ISAC	19.0.0
2025-09	RAN#109	RP-252622	0028	-	F	Correction of channel modeling enhancements for 7 - 24 GHz	19.1.0
2025-09	RAN#109	RP-252623	0029	-	F	CR to incorporate new agreements on ISAC CM	19.1.0
2025-12	RAN#110	RP-253012	0031	-	F	CR to incorporate new agreements on ISAC CM	19.2.0
2025-12	RAN#110	RP-253011	0032	-	F	CR on Handheld UT Polarized Antenna Model	19.2.0
2025-12	RAN#110	RP-253012	0033	-	F	CR to incorporate new agreements on ISAC CM	19.2.0
2025-12	RAN#110	RP-253031	0035	-	A	CR on UL and DL reciprocity modelling	19.2.0
2025-12	RAN#110	RP-253017	0036	-	F	Correction of Rel-19 enhancements for channel modeling for 7-24 GHz	19.2.0
2026-03	RAN#111	RP-260166	0038	-	F	CR to incorporate new agreements on ISAC CM	19.3.0

History

Version	Date	Status
V19.1.0	October 2025	Publication
V19.2.0	February 2026	Publication
V19.3.0	April 2026	Publication